HOT CORROSION OF SOME INDUSTRIALLY IMPORTANT STEELS AND SUPERALLOYS

SUMMARY
AND
CONCLUSION

A THESIS SUBMITTED FOR THE DEGREE OF

Doctor of Philosophy

IN

CHEMISTRY

BY

NAUSHA ASRAR

M. Sc., M. Phil (Alig)

DEPARTMENT OF CHEMISTRY
ALIGARH MUSLIM UNIVERSITY
ALIGARH

NOV. 1983

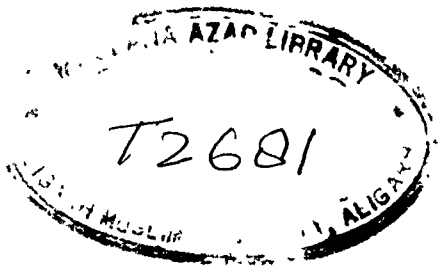
AZAD LIBRARY
T2681

SUMMARY AND CONCLUSIONS

SUMMARY

The studies presented in this thesis deal with the hot corrosion behaviour of stainless steels (viz. AISI 303 and 321) and nickel-base superalloys (viz. Inconel-600, Inconel-800, Monel-400, Nimonic-105, Nickel-200 and B-1900). Low temperature hot corrosion behaviour of some of the nickel-base superalloys have also been studied in presence of Na_2SO_4-$NiSO_4$ mixture.

Chapter I, part I describes some aspects of hot corrosion. Recent studies carried out on hot corrosion of nickel and cobalt superalloys, and iron-base alloys with special reference to the effect of salt and alloy compositions, have been referred. Various mechanisms, proposed to explain hot corrosion attack, are discussed in reasonable details.

Chapter I, part II presents a literature survey pertaining to oxidation behaviour of iron and iron-base alloys and discusses important contributions made to the oxidation chemistry of iron-base alloys.

Chapter II describes hot corrosion behaviour of sensitized and unsensitized steels in presence of Na_2SO_4.

Hot corrosion behaviour of sensitized (AISI 321) and

unsensitized (AISI 303) steels has been studied in presence of Na_2SO_4 of varying thicknesses at 800 and 1000°C. At 800°C, both the steels show highest oxidation rates at a certain salt concentration which is 4.0 and 9.5 mg/cm^2 for AISI 321 and AISI 303 steels, respectively followed by a gradual decrease in oxidation rates with increasing salt concentration.

At 1000°C, there is a linear relationship existing between amount of salt deposited and oxidation rate — the oxidation rate increases with increasing salt deposition. Initially unsensitized steel has higher oxidation rate than the sensitized steel but when the salt deposition exceeds by 3.5 mg/cm^2 the oxidation rate of sensitized steel becomes higher than the unsensitized steel.

Initially a sulfidation reaction is favoured. With the consumption of sulfur, there is an increase in oxygen activity; Cr_2O_3 is converted into chromate, Na_2CrO_4 dissolves in the melt and precipitated as Cr_2O_3 at the salt/gas interface due to low a_{Na_2O}. The sulfidation and fluxing reactions are represented as follows:

I $\quad Cr_2O_3 + 3Na_2SO_4 \longrightarrow Cr_2S_3 + 3Na_2O + 6O_2$

II $\quad Cr_2O_3 + 2Na_2O + \frac{3}{2}O_2 \longrightarrow 2Na_2CrO_4$

III $\quad FeO + Na_2SO_4 \longrightarrow FeS + Na_2O + 2O_2$

IV $Na_2O + FeO \longrightarrow Na_2FeO_2$

V $NiO + Na_2SO_4 \longrightarrow NiS + Na_2O + 2O_2$

VI $Na_2O + NiO \longrightarrow Na_2NiO_2$

VII $2FeO + \frac{1}{2}O_2 \longrightarrow Fe_2O_3$

At lower temperature (600°C) reactions I to VII proceed only to a limited extent and once a compact oxide layer is formed beneath the Na_2SO_4 coating the oxidation rate falls gradually and Na_2SO_4 acts only as a protective barrier.

At higher temperature (1000°C) same mechanism will be followed but the aggressiveness of the melt increases with increasing salt deposition. In addition, the following reactions are likely to occur, the complex species NiO_2^{--}, CrO_4^{--} and FeO_2^{--} are likely to be precipitated as NiO, Cr_2O_3 and FeO, respectively at the salt/air interface.

VIII $4Cr + 3Na_2SO_4(l) \longrightarrow Cr_2O_3 + 3Na_2O + Cr_2S_3 + 3O_2$

IX $Cr + Na_2O + 3O \longrightarrow Na_2CrO_4$

X $4Fe + Na_2SO_4 \longrightarrow FeS + 2FeO + Na_2FeO_2$

Sensitised AISI 321 steel oxidises at a much faster rate than unsensitized AISI 303 steel when relatively large amount of salt is deposited on the alloy. Due to rapid oxidation at this temperature a Cr-depleted zone is esta-

blished in the matrix and TiC is now subjected to be attacked by Na_2SO_4:

XI $$TiC + Na_2SO_4 \longrightarrow TiO_2 + Na_2O + S + CO$$

TiO_2 is either concentrated at the alloy/oxide interface or present as oxide dispersion in the matrix. Release of sulfur, CO and Na_2O further enhances the oxidation rates.

The observed scale morphologies are consistent with the proposed mechanism. Sulfides or sulfospinels form inner scales and oxides forming outer scales. Internal sulfidation is invariably observed. The sensitised steels are more aggressively attacked as indicated by the presence of thicker porous scales and more intense penetration of the salt into the matrix.

Chapter III contains the results of a hot corrosion study carried out on AISI 303 and AISI 321 steels in presence of Na_2SO_4 or transition metal sulfates, viz. $NiSO_4$, $CoSO_4$ and $Cr_2(SO_4)_3$ or their mixtures, at 800 and 1000°C. At 800°C, steels coated either with transition metal salt or its mixture with Na_2SO_4 show relatively heavy weight losses with increasing salt deposition. The weight losses are usually higher in steels coated with salt mixture than

coated with bare salt. The continuing weight losses with increasing transition metal salt on the steel can be attributed to the fact that inner chromium oxide scales initially formed on the alloy remain intact and probably do not interact with decomposition products of metallic sulfates, e.g. oxides(s), SO_2(g) and O_2(g). The gaseous products escape resulting in weight losses:

XII $\quad NiSO_4 \longrightarrow NiO + SO_2 + \frac{1}{2}O_2$

XIII $\quad CoSO_4 \longrightarrow CoO + SO_2 + \frac{1}{2}O_2$

XIV $\quad Cr_2(SO_4)_3 \longrightarrow Cr_2O_3 + 3SO_2 + \frac{3}{2}O_2$

At 800°C, the Na_2SO_4-$CoSO_4$ and Na_2SO_4-$NiSO_4$ coated steels show much higher oxidation rates than the corresponding Na_2SO_4-$Cr_2(SO_4)_3$ steel due to the formation of low temperature eutectics (Na_2SO_4-$CoSO_4$: 575°C and Na_2SO_4-$NiSO_4$: 671°C). The liquidus phase breaks the protective chromia film and the alloy oxidizes at a much higher oxidation rate.

The weight losses in Na_2SO_4-$Cr_2(SO_4)_3$ coated steel may be attributed to the following reactions:

XV $\quad Cr_2O_3(s) + 2Na_2SO_4(l) + \frac{1}{2}O_2 \longrightarrow 2Na_2CrO_4(l) + 2SO_2(g)$

XVI $FeO(s) + Na_2SO_4(l) \longrightarrow Na_2FeO_2(l) + SO_2(g) + \frac{1}{2}O_2(g)$

At 1000°C, both steels show increasing oxidation rates with increasing salt/mixture deposition till a maxima is reached; this is followed by weight losses on further increase in salt deposition. The transition metal sulfate coated on the steel at this temperature is likely to decompose into oxide (XII to XIV) and sulfide (XVII to XIX) at the air/salt and oxide/salt interfaces, respectively.

XVII $Cr_2(SO_4)_3 \longrightarrow Cr_2S_3 + 6O_2$

XVIII $CoSO_4 \longrightarrow CoS + 2O_2$

XIX $NiSO_4 \longrightarrow NiS + 2O_2$

In case of $Cr_2(SO_4)_3$ coated steel reaction XVII seems to proceed only to a limited extent and XIV is likely to be predominant throughout the oxidation. This is shown by relatively lower oxidation rates and the presence of compact and adhered chromia scales. In $CoSO_4$ coated steels, CoS formed at the oxide/salt interface (XVIII) may undergo following reactions which are thermodynamically feasible:

XX $CoS + Cr_2O_3 \longrightarrow 3CoO + Cr_2S_3$

XXI $CoS + FeO \longrightarrow CoO + FeS$

} Oxide/salt interface

XXII $FeS.Cr_2S_3 \longrightarrow FeS + Cr_2S_3$) Oxide/salt interface

XXIII $CoS + 2O_2 \longrightarrow CoSO_4$) Gas/salt interface

No CoS was detected in the scales and observed morphology is consistent with the proposed reactions.

In $NiSO_4$ coated steel, NiS formed (XIX) accumulates beneath the Cr_2O_3 scales and may undergo the following reaction:

XXIV $3NiS + Cr_2O_3 \longrightarrow 3NiO + Cr_2S_3$

There is a possibility of penetration of NiS through oxide scale and its interaction with Ni in the substrate to form low melting Ni-NiS eutectic. When the S-activity at the oxide/salt interface is sufficiently lowered due to formation of sulfide, the sulfides get oxidised to NiO and Cr_2O_3 and sulfur thus released produces internal sulfidation. Cr_2S_3 as internal sulfide particles along with NiS were actually found in the matrix.

During oxidation of $Cr_2(SO_4)_3 + Na_2SO_4$ coated steels at 1000°C reactions XIV and XV will undergo at the air/salt interface in the initial stages.

XV $Na_2SO_4 \rightleftharpoons Na_2O + S + \frac{3}{2}O_2$

In the propagation stage, there will be sufficient S poten-

tial to form FeS and Cr_2S_3. The culmination of sulfidation reactions at the oxide/salt interface will increase the oxygen activity and resulting in the oxidation of sulfides into respective oxides and the sulfur released is available for internal sulfidation. The oxides are likely to get fluxed forming Na_2FeO_2 (IV), $Na_2Fe_2O_4$ (XXVI) and Na_2CrO_4 (II), $Na_2Cr_2O_4$ (XXVII).

XXVI $\quad Fe_2O_3 + Na_2O \longrightarrow Na_2Fe_2O_4$

XXVII $\quad Cr_2O_3 + Na_2O \longrightarrow Na_2Cr_2O_4$

The reactions are thermodynamically feasible and are likely to continue till entire Na_2O is exhausted. At air/salt interface a_{Na_2O} is considerably low and in consequence, the complex species present in the melt will ultimately reprecipitate as oxides, e.g. Cr_2O_3, FeO or Fe_2O_3 etc.

In $Na_2SO_4 + NiSO_4$ coated steels, NiS is formed at the oxide/salt interface and Ni-NiS eutectic are responsible for aggressiveness of the mixture. In presence of Na_2SO_4-$CoSO_4$, reactions XVIII, XX to XXIII are likely to go along with XV and XVI. The relatively lower weight gains in Na_2SO_4-$CoSO_4$ coated steels are probably due to the reactions XV and XVI which proceed with the evolution and expulsion of SO_2.

Chapter IV deals with the studies on high temperature oxidation behaviour of Ni-base alloys in presence of Na_2SO_4.

The oxidation behaviour of some Ni-base alloys, viz. Inconel 600, Inconel 800, Monel 400, Nimonic 105, B 1900 and Nickel 200 has been studied in presence of Na_2SO_4 at 850 and 1000°C in flowing air. While the chromia former alloys, e.g. Inconel 600, Inconel 800 and Nimonic 105 show relatively small losses at 850 and 1000°C (to the extent of about 3 mg/cm^2 in 10 hrs); B 1900 (alumina former), Nickel 200 and Monel 400 (NiO former) oxidize appreciably following a parabolic and/or linear kinetic. It appears that Na_2SO_4-coated Inconel 600, 800 and Nimonic 105 form chromia film at the very early stage of oxidation. This film reacts with Na_2SO_4 to undergo the following types of reactions at 850 and 1000°C:

XXVIII $$Cr_2O_3 + \tfrac{3}{2}O_2 + 2Na_2SO_4(l) \longrightarrow 2Na_2CrO_4(l) + 2SO_3(g)$$

The evidences for XXVIII are overwhelming such as (i) weight losses during oxidation, (ii) deposition of a yellow product on the walls of the reaction vessel which was identified chemically or by X-ray diffraction analysis as chromates, (iii) detection of SO /SO in the reaction product gases,

(iv) slightly basic nature of the melt. At the end of the induction period when molten Na_2SO_4 comes into contact with the alloy, the following reactions are possible:

XXIX $\quad Ni + SO_4^{2-} \longrightarrow NiS(l) + \frac{3}{2}O_2 + O^{2-}$

XXX $\quad 2Cr + 3SO_4^{2-} \longrightarrow Cr_2O_3 + 3SO_2(g) + 3O^{2-}$

XXXI $\quad 2Cr + 3SO_4^{2-} \longrightarrow Cr_2S_3 + \frac{9}{2}O_2 + 3O^{2-}$

XXXII $\quad 2Al + 3SO_4^{2-} \longrightarrow Al_2O_3 + 3SO_2 + 3O^{2-}$

XXXIII $\quad Fe + SO_4^{2-} \longrightarrow FeS + \frac{3}{2}O_2 + O^{2-}$

Reactions XXIX to XXXI are feasible in Inconel-600, XXIX to XXXI and XXXIII in Inconel-800 and XXIX to XXXII in Nimonic 105. Sulfidation reactions (XXIX, XXXI and XXXIII) are possible when partial pressure of oxygen is substantially lowered and consequently P_{S_2} is increased. This situation can arise at the oxide/salt interface. Isolated pockets of Cr_2S_3 have indeed been found in the oxidised alloys.

The higher oxidation rates of Inconel 800 in presence of Na_2SO_4 in comparison to Inconel 600 have been explained on the basis of high Cr- low Ni contents of Inconel 800 which promotes reaction XXVIII. On the other hand, in Inconel 600 alloy the accumulation of NbC and/or TaC at the grain boundaries restricts the flux of Cr^{3+} ions which

results in the discontinuation of reaction XXVIII. In Inconel 600, FeO will be fluxed according to reaction XXXIV.

XXXIV $\quad FeO + Na_2SO_4 \longrightarrow Na_2FeO_2(l) + SO_2 + \frac{1}{2}O_2$

Reaction XXXIV may continue till all the Na_2SO_4 is exhausted or a decrease in P_{O_2} at the salt/gas interface may result in the precipitation of FeO.

During oxidation of Na_2SO_4-coated Nimonic 105 Cr_2O_3 and Al_2O_3 inner scales are formed with NiS inclusions through reactions XXIX, XXX and XXXII. At the oxide/salt interface the oxygen activity is dropped to such a level that sulfidation reactions commence resulting in the formation of NiS and Cr_2S_3. Due to fragile nature of the sulfidised scales the contact between scale and alloy is lost at some sites and fresh salt directly comes into contact with the alloy surface at these sites. The fragmentation of the alloy surface during hot corrosion supports this view point. Molybdenum is present in appreciable concentrations (about 5.9%) in Nimonic 105 and forms MoO_3 which is present in the inner scales. Although there is evidence of the formation of Na_2MoO_4 (XXXV) in the scales, acidic fluxing reactions XXXVI and XXXVII do not seem to undergo due to high chromium contents of the alloy.

XXXV $MoO_3 + Na_2SO_4 \longrightarrow Na_2MoO_4(l) + SO_3(g)$

XXXVI $Cr_2O_3 + 3MoO_3 \longrightarrow 2Cr^{3+} + 3MoO_4^{2-}$

XXXVII $Al_2O_3 + 3MoO_3 \longrightarrow 2Al^{3+} + 3MoO_4^{2-}$

During corrosion of Nickel-200 in presence of Na_2SO_4, NiO is basically fluxed with Na_2SO_4 and S is released:

XXXVIII $NiO + Na_2SO_4 \longrightarrow Na_2NiO_2 + S + \frac{3}{2}O_2$

The sulfur thus released penetrates through the alloy along the grainboundaries to produce profuse sulfidation. NiS may also form through XXIX and accumulate in the inner layers of the scales. Again with a decrease in Na_2O at the salt/gas interface NiO is precipitated and appears in the form of stratified layers as the outer scales. At the regions where cracking or disruption of scales occurred Ni_3S_2 is oxidised to $NiSO_4$ due to passage of air through cleavages. The Na-Ni-S-O superimposed diagram shows the possibility of $NiSO_4$ existence at the regions of higher oxygen activities.

In presence of Na_2SO_4, B 1900 exhibits a linear kinetic at 850°C and a parabolic kinetic at 1000°C. The coated alloy in the initial stages shows induction periods lasting about 4 hrs and 1 hr at 850 and 1000°C, respectively. The oxidation rates of Na_2SO_4 coated B 1900 are much higher

than the Nimonic and Inconel alloys under corresponding conditions.

At 850°C, during the induction period, Cr_2O_3 formed on the alloy reacts with oxide ion in Na_2SO_4 (XXV) forming soluble chromate and liberating SO_3 (XXVIII). In the later stages of induction period, MoO_3 that has formed under Na_2SO_4 layer by oxidation of surface carbides reacts with the sulfate (XXXV). The occurrence of XXXV is supported by the presence of a soluble molybdate ion in the scale. This reaction proceeds more vigorously at 1000°C. The formation of MoO_4^{2-} and CrO_4^{2-} is resulted by the consumption of oxide ions thus increasing the acidity of Na_2SO_4. The reduction in oxide ion concentration increases the sulfur activity (XXXIX and XL) as a result S is able to diffuse through Al_2O_3 scale into the alloy forming chromium or aluminium sulfides. However, internal sulfides were found to be chromium sulfide because Al_2S_3 formation requires a much lower partial pressure of oxygen. Near the end of induction period, due to breaking of the scales at some localised spots, the underlying nickel will be exposed to Na_2SO_4 and NiS will be formed (XXIX) along with Cr_2O_3 (XXV) and Al_2O_3 (XXXII). This will increase the oxide ion concentration above 10^{-8} atm making Na_2SO_4 melt markedly basic. Consequently, basic fluxing of protective Al_2O_3 occurs (XLI).

XXXIX $SO_4^{2-} \rightleftharpoons O^{2-} + SO_3$

XL $SO_4^{2-} \rightleftharpoons S^{2-} + 2O_2$

XLI $Al_2O_3 + O^{2-} \rightleftharpoons 2AlO_2^-$

The reaction proceeds actively with rapid increase in the rate of oxidation. However, as the oxide ion is used up the attack slows down which is indicated by a parabolic foot in the hot corrosion curve. Since the corrosion studies were restricted to 12 hr the oxidation kinetic curves represent only induction and parabolic regions and there is no evidence for intermediate or linear region.

The Monel 400 is markedly corroded in presence of Na_2SO_4 the intensity of attack increases with increasing temperature.

Initially a NiO film is formed beneath a CuO film. When molten Na_2SO_4 comes into contact with the CuO film the following reaction is feasible:

XLII $CuO + SO_4^{2-} \longrightarrow CuS + O^{2-} + 2O_2$

O^{2-} is consumed by fluxing with NiO present in the inner scales (XXXVIII). $O_2(g)$ penetrates through the scale and preferentially oxidises Ni to NiO. With the depletion of oxygen activity at the oxide/salt interface NiO is sulfidised to NiS due to corresponding increase in S-activity.

The depletion in O^{2-} at the salt/gas interface will result in the precipitation of NiO as a porous scale ahead of CuS scale formed initially (XLII). Again fused Na_2SO_4 will react with NiO to carry out sulfidation reaction forming NiS:

XLIII $\quad NiO + SO_4^{2-} \longrightarrow NiS + O^{2-} + 2O_2$

When XLIII is completed a fall in S-activity will result in the oxidation of underneath copper sulfide layer. In consequence S is released which will penetrate through the alloy to sulfidise Ni. This process of alternate sulfidation and oxidation will continue till all the Na_2SO_4 is consumed. The morphology of the scales consisting of alternate Ni- and Cu enriched layers is in conformity with the above mechanism.

Chapter V deals with the studies on high temperature corrosion behaviour of Ni-base alloys in presence of NaCl.

The high temperature corrosion behaviour of Ni-base alloys in presence of NaCl can be divided into two categories:

(i) Chromia forming alloys, viz. Inconel 600, Inconel 800 and Nimonic 105 which show much higher oxidation rates than those in presence of Na_2SO_4 or air.

(ii) Al_2O_3 formers (B 1900) and NiO formers (Ni-200) which

have much lower oxidation rates than in presence of Na_2SO_4.

Monel 400 which is CuO-NiO former is severely attacked by NaCl.

NaCl breaks down the protective oxide scale by attacking the Cr_2O_3 film formed on the category I alloy producing a volatile product CrO_2Cl_2 (XLIV) which is subsequently converted into Na_2CrO_4 and condensed on the cooler part of the reaction tube in the form of a yellow deposit.

XLIV $\quad 4NaCl + Cr_2O_3 + \frac{3}{2}O_2 \longrightarrow 2CrO_2Cl_2 + 2Na_2O$

The melt adjacent to the alloy consist of NaCl, Na_2CrO_4, CrO_2Cl_2 and Na_2O. NaCl(l) penetrates through the melt and reacts with the alloy components as suggested in the following equations:

XLV* $\quad 2NaCl + 2Ni + O_2 \longrightarrow Na_2NiO_2 + NiCl_2$

XLVI** $\quad 2NaCl + 2Fe + O_2 \longrightarrow Na_2FeO_2 + FeCl_2$

XLVII*** $\quad 2NaCl + Co + \frac{1}{2}O_2 \longrightarrow CoCl_2 + Na_2O$

XLVIII**** $\quad 3NaCl + 4Al + 3O_2 \longrightarrow AlCl_3 + 3NaAlO_2$

* Inconel-600, Inconel-800, Nimonic 105

** Inconel-800

*** Nimonic 105

**** Nimonic 105

The sequence of reactions XLV to XLVIII depends upon the thermodynamic conditions. As metallic chlorides move outward through the melt, oxygen activities are sufficiently high to convert metallic chlorides into metallic oxides:

XLIX $2FeCl_2 + \frac{3}{2}O_2 \longrightarrow Fe_2O_3 + 2Cl_2$

L $3FeCl_2 + 2O_2 \longrightarrow Fe_3O_4 + 3Cl_2$

LI $NiCl_2 + O \longrightarrow NiO + Cl_2$

LII $CoCl_2 + O \longrightarrow CoO + Cl_2$

LIII $2AlCl_3 + \frac{3}{2}O_2 \longrightarrow Al_2O_3 + 3Cl_2$

The chlorine is recycled to react with elements in the alloy.

LIV $xCl_2 + 2M(alloy) \longrightarrow 2MCl_x$

Continuation of this process results in the development of discontinuous, nonprotective and porous oxide scales. Reactions XLV, XLVI and XLVIII indicating the formation of NiO_2^{--}, FeO_2^{--} and AlO_2^{-}, respectively proceed at the backward direction due to the depletion in O^{--} at the melt/salt interface and consequently precipitating corresponding oxides at the salt/gas interface. The conversion of chlorides into oxides (XLIX to LIII) and precipitation of the oxides at the salt/gas interface gives rise to thick porous

scales. Another factor responsible for high oxidation rates in presence of NaCl is the low boiling points of transition metal halides which develop sufficient vapour pressure at the alloy/scale interface to lift up the scales or break down the protective oxide layers.

NaCl-coated B-1900 shows much lower oxidation rates than Na_2SO_4-coated alloy. Little attack was observed with Al_2O_3 in NaCl upto a temperature of 1000°C. Continuous and smooth oxidation curves are obtained and scales seem to be adhered. It appears that the integerity of the Al_2O_3 film is maintained in presence of NaCl.

Nickel-200 seems to be moderately attacked by NaCl in comparison to chromia forming alloys. The corrosion rates of NaCl-coated alloys are much lower than the corresponding Na_2SO_4-coated alloys. Further the oxidation rate at 850°C is much higher than at 1000°C.

When NiO film comes into contact with liquid NaCl, chloridization reaction occurs:

LV $\quad 2NiO + 2NaCl \longrightarrow NiCl_2 + Na_2NiO_2$

Liquid NaCl penetrates through the melt and comes into contact with the metal and reacts according to the reaction:

LVI $\quad 2NaCl + 2Ni + O_2 \longrightarrow NiCl_2 + Na_2NiO_2$

However, LVI may proceed to only a limited extent due to low oxygen potential produced at the alloy/melt interface. In these circumstances the volatile $NiCl_2$ vapours break the oxide scale or pass through the melt and oxidised to NiO at the salt/gas interface (LI). Further, NiO_2^{--} as formed by LV or LVI is dissociated and precipitated as NiO at the salt/gas interface. This results in the formation of porous and copious scales of NiO on the alloy surface. However, the inner layer of the scales seemed to retain some $NiCl_2$.

During corrosion of Nickel-200 in presence of NaCl, two opposing factors affect the corrosion rates; with increasing temperature the increasing amount of liquid tends to accelerate the rate but at the same time the amount of chlorine decreases. The balance between these effects perhaps leads to the occurrence of maximum attack at an intermediate temperature; this is possibly the reason of higher corrosion rates of the alloy at 850°C than at 1000°C.

Monel 400 is severely attacked by NaCl, the intensity of attack increases with increasing temperature. At 1000°C, liquidus NaCl attacks outer scales of CuO to form CuCl (LVII), the liquid further penetrates and reacts with inner NiO film to form $NiCl_2$ and Na_2NiO_2 (LV).

LVII $\quad 2NaCl + 2CuO \longrightarrow 2CuCl + Na_2O + O$

CuCl (LVII) and $NiCl_2$ (LVI) formed in the substrate move outward to oxidise to CuO (LIX) and NiO (LI) at the gas/salt interface:

LVIII $2CuCl + O \longrightarrow Cu_2O + Cl_2$

LIX $Cu_2O + O \longrightarrow 2CuO$

At 1000^oC, LI, LV and LIX continue to provide a thick duplex scale of CuO and NiO. The Cl_2 evolved during the oxidation is available for further corrosion along with NaCl(v) thus increasing the severity of corrosion with time. This is indicated by the onset of a linear kinetic shortly after the culmination of a parabolic kinetic. The scale morphology indicates the presence of a thick duplex scale containing alternate layers of CuO and NiO.

It appears that oxidation and chloridisation reactions (involving O_2 and NaCl) generally follow a parabolic rate law whereas chloridation reactions (involving NaCl and $Cl_2(g)$) producing more severe attack follow a linear rate law.

Chapter VI describes hot corrosion behaviour of some nickel-base alloys in presence of $NaCl-Na_2SO_4$ mixtures.

The high temperature oxidation behaviour of Inconel 600, Inconel 800, Nimonic 105, Nickel 200, B-1900 and

Monel 400 has been studied in presence of mixtures of Na_2SO_4 and NaCl (5:1 and 1:5 molar ratios) at 650 and 1000°C in a current of air.

The weight gain/time curves indicate that chromia forming alloys, e.g. Inconel 600 and 800 and Nimonic 105 show increasing corrosion rates with increasing amount of NaCl in Na_2SO_4 whereas Al_2O_3 former (B-1900) and NiO former (Nickel-200) show decreasing oxidation rates with increasing amount of NaCl in Na_2SO_4 although small amount of NaCl in Na_2SO_4 enhances the oxidation rate initially. Monel 400 (NiO/CuO former) behaves similar to chromia forming alloys.

Oxidation of chromia forming alloys with Na_2SO_4-NaCl mixtures results in the development of degraded microstructure. The degradation is more pronounced in alloys coated with higher amounts of NaCl. Inconel 800 is most severely attacked and Nimonic-105 is least affects.

Inconel 600 coated with 5:1 NaCl:Na_2SO_4 mixture on corrosion shows NiO with Cr_2O_3 inclusions in the outer scales, beneath the oxide scales Cr_2S_3 is present containing some NiS. The same alloy shows less severe attack in presence of 1:5 NaCl:Na_2SO_4 mixture although a sulfide layer is present. Inconel 800 which is more severely attacked shows similar morphology beneath the oxide scales which are comprised of oxides of all elements present in the alloy with

predominant concentration of Ni, Cr and Fe oxides; a sulfide front is present in the form of a zone which extended into the alloy as if internal corrosion product has been formed. The microstructures of Na_2SO_4-NaCl corroded Nimonic 105 show the disruption of otherwise protective scales. The disruption is more distinct in alloy coated with 1:5 Na_2SO_4:NaCl mixture where deep penetration of the salt and fragmentation are observed.

In Na_2SO_4-NaCl coated chromia forming alloys, the chromia scales which were initially protective in presence Na_2SO_4 are attacked by NaCl. The corrosion rates are enhanced by several magnitude due to the formation of volatile CrO_2Cl_2 (XLIV) and subsequent conversion to yellow Na_2CrO_4 which is deposited on the cooler end of the reaction tube. The function of chloride is to remove chromium preferentially thus producing chromium depletion in the alloy. It has two important bearings: NaCl(l) creeps through the melt and attacks the alloy directly, the alloying elements undergo chloridination reactions and form chlorides according to their thermodynamic stabilities. Those chlorides which are volatile move out ward in the form of vapours and get oxidised at the salt/air interface to respective oxides, the chlorine gas given off recycles and induces chlorination reactions. Secondly, due to removal of chromium by chloride the sulfur from Na_2SO_4 begins to sulfidise the alloy much

earlier. The combined effect of two factors results in much higher corrosion rates in Na_2SO_4-NaCl coated alloy than Na_2SO_4-coated alloy. In those cases where the deposits contain mostly NaCl as in 1:5 Na_2SO_4:NaCl mixture the effects due to sulfur will be less pronounced. In this case NaCl will cause rapid depletion of Cr, Ni and other elements in the alloy and in consequence thick and porous scales are developed on the alloy.

The alumina forming B-1900 shows highest corrosion rates in presence of a mixture consisting of Na_2SO_4 and NaCl in the molar ratio of 5:1 and lowest in pure NaCl. Addition of a small amount of NaCl in Na_2SO_4 enhances the oxidation rates of the alloy enormously. It appears that a small amount of NaCl enhances the corrosion rates by decreasing the induction periods (2 hr at 850°C and about 1 hr at 1000°C) and thus on setting of degradation reactions such earlier. This degradation is caused by rapid removal of Al from alloy. With the culmination of reactions LX to LXIV involving oxygen and sulfur removal from the salt deposit, the oxygen and S-activities are consequently reduced at melt/oxide interface and NaCl from the deposit will react with Al_2O_3 and later Al in substrate to form $AlCl_3$ (LXV and LXVI). As $AlCl_3$ moves outward in the pores, higher oxygen activities exist in the liquid because oxygen is

supplied by air. Consequently, $AlCl_3$ is converted into Al_2O_3 and chlorine is free to react again with the alloy (LXII and LXVII). In such a process, a small amount of NaCl can produce a substantial effect because it is recycled.

LX $\quad Cr_2O_3(s) + 2Na_2SO_4(l) + \frac{1}{2}O_2(g) \longrightarrow 2Na_2CrO_4(l) + 2SO_2(g)$

LXI $\quad Ni + SO_4^{2-} \longrightarrow NiS(l) + \frac{3}{2}O_2 + O^{2-}$

LXII $\quad 2Al + 3SO_4^{2-} \longrightarrow Al_2O_3 + 3SO_2(g) + 3O^{2-}$

LXIII $\quad 2Cr + 3SO_4^{2-} \longrightarrow Cr_2O_3 + 3SO_2(g) + 3O^{2-}$

LXIV $\quad Al_2O_3 + O^{2-} \longrightarrow 2AlO_2^-$

LXV $\quad Al_2O_3 + 6NaCl \longrightarrow 2AlCl_3 + 3Na_2O$

LXVI $\quad 2Al + 6NaCl + \frac{3}{2}O_2 \longrightarrow 2AlCl_3 + 3Na_2O$

LXVII $\quad 3Na_2O + 3Cl_2 \longrightarrow 6NaCl + \frac{3}{2}O_2$

Nickel-200 which forms a NiO scale oxidises at a much lower rate in presence of higher concentrations of NaCl in Na_2SO_4 than the salt mixture containing smaller concentrations of NaCl. Alloy coated with NaCl-Na_2SO_4 (1:5) oxidises at a higher rate at 850°C than at 1000°C whereas alloy coated with 5:1 mixture shows higher corrosion rate at 1000°C.

The small amount of NaCl in Na_2SO_4 is perhaps helpful in breaking the protective NiO scales and consequently induction period is greatly reduced. Following sulfidation and basic fluxing reactions in which S and O^{2-} are used up, the chloridination reaction proceeds involving conversion of NiO and Ni metal into $NiCl_2$. $NiCl_2$ decomposes at salt/air interface into NiO, chlorine released is available for recycling. The NiO_2^{2-} formed during fluxing ends up as NiO by precipitation at the salt/gas interface. This provides a porous NiO scale on the alloy. The observed morphology supports this mechanism.

The lower corrosion rates of 1:5 Na_2SO_4 : NaCl coated nickel-200 alloy could perhaps be explained on the basis of reaction of protectiveness by the NiO at 850°C. At 1000°C, a relatively large induction period is observed. By the end of this period sufficient S-activity is developed to sulfidize nickel metal to NiS and sequentially NiO is basically fluxed to NiO_2^{2-}. These reactions perhaps continue till entire Na_2SO_4 is consumed. NaCl(l) creeps inward to carry out the chloridation reactions with NiS and Ni metal (LXVIII to LXXI).

LXVIII $\quad NiS + 2NaCl \longrightarrow NiCl_2 + Na_2S$

LXIX $\quad Ni + 2NaCl + \frac{1}{2}O_2 \longrightarrow NiCl_2 + Na_2O$

LXX $Na_2O + Ni + \frac{1}{2}O_2 \longrightarrow Na_2NiO_2$

LXXI $Na_2S + 2O_2 \longrightarrow Na_2SO_4$

The $NiCl_2$ formed move outward to get oxidise to NiO at the salt/air interface and similarly Na_2NiO_2 is precipitated as NiO. Na_2SO_4 formed by LXXI penetrates into the alloy to carry out internal sulfidation. The amount of Cl_2 available after oxidation of $NiCl_2$ will decline ultimately to nearly zero level at 1000°C and hot corrosion reactions are ceased to proceed further.

Like chromia formers, the corrosion rates of Monel-400 (CuO/NiO former) increase with increasing concentration of NaCl in Na_2SO_4. The effect is more pronounced at 1000°C. NaCl breaks the protective outer scales of CuO and inner scales of NiO. This results in a series of sulfidation fluxing and chloridation reactions which contribute to enhanced corrosion rates. The corrosion rates at 1000°C are much higher than at 850°C; this is presumably due to increase in aggressiveness of the melt inspite of the expected fall in chlorine activity.

Chapter VII describes studies on low temperature hot corrosion in presence of Na_2SO_4-$NiSO_4$ mixture.

The hot corrosion studies have been carried out at

650 and 750°C on Inconel 600, Inconel 800, Nimonic 105, Nickel 200 and Monel 400 in presence of 1:1 molar ratio of $NiSO_4$ and Na_2SO_4. The studies have been carried out under two different conditions. Under one condition the alloys are preoxidised for 20 hours subsequently coated with $NiSO_4$-Na_2SO_4 mixture followed by hot corrosion and under the other condition the alloys are directly coated with the mixture and are then corroded.

In general, the chromia forming alloys (Inconel 600 and 800 and Nimonic 105) show weight losses in presence of salt mixture at 650 and 750°C. In contrary, NiO forming alloys (Nickel 200 and Monel 400) after initial weight losses show weight gains and oxidised by a parabolic rate law. With a few exceptions, the preoxidised alloys have higher corrosion rates than unoxidised alloys. The preoxidised alloys when corroded in presence of Na_2SO_4-$NiSO_4$ mixture show morphologies in which scales are greatly disrupted and the substrate is relatively less affected. On the other hand, alloys which were directly corroded in presence of salt mixture show a morphology in which substrate is deleteriously attacked.

During hot corrosion of preoxidised Inconel 600 and 800 and Nimonic 105 in presence of $NiSO_4$-Na_2SO_4 mixture, the outer scales are expected to get thickened due to the

presence of NiO of the decomposed $NiSO_4$ (XII) plus NiO produced by nickel migration from the metal zone.

The liquid salt mixture will penetrate through NiO scale and will attack inner Cr_2O_3 scales and reactions XV, XVI and LXXII are expected at the salt/oxide interface.

LXXII $\quad 2Cr_2O_3 + 3NiSO_4 + 2Na_2SO_4 \longrightarrow$

$$Cr_2S_3 + Ni_3S_2 + 2Na_2CrO_4 + 9\,O_2$$

Reactions XII, XV and XVI will result in the expulsion of sulfurous gases and subsequently loss in weight. The release of oxygen by LXXII will result in rapid oxidation of the alloy by Cr/Ni diffusion and thickening the oxide scales. CrO_4^{2-} and FeO_2^{2-} formed moved outward to the salt interface and precipitate as Cr_2O_3 and FeO (or Fe_2O_3) at some distance from the gas/salt interface and beneath NiO scale due to fall off in Na_2O. Reactions XV, XVI and LXXII will terminate when the salt is consumed.

In NiO forming Nickel-200 and Monel-400 alloys under preoxidized conditions, reactions XV, XVI and LXXII are not possible but in Monel 400, the liquid salt extrudes through outer CuO and attacks NiO scales (LXXIII and LXXIV).

LXXIII $\quad NiO + 2NiSO_4 \longrightarrow Ni_3S_2 + \frac{9}{2}O_2$

LXXIV $\quad 5NiO + 2Na_2SO_4 \longrightarrow 2Na_2NiO_2 + Ni_3S_2 + \frac{9}{2}O_2$

The oxygen released during LXXIII and LXXIV will react with diffusing Ni and Cu (from the metal) to form copious oxide scales. Some Ni_3S_2 formed may also get oxidised and consequently sulfur released produces internal sulfidation by forming Ni_3S_2 and Cu_2S in the matrix. In Nickel-200 similar reactions are expected; NiO_2^{--} formed in LXXIV moves outward and precipitated as NiO at the gas/salt interface. During hot corrosion of unoxidised NiO forming alloys, the liquid salt penetrates the thin oxide film and directly attacks the underlying metal:

LXXV $\quad 9Ni + 2NiSO_4 \rightleftharpoons 6\ NiO + Ni_3S_2 \quad (\Delta G^\circ = -77\ Kcal)$

The $Ni-Ni_3S_2$ eutectic which forms below the surface oxide seems primarily responsible for the hot corrosion attack.

During corrosion of unoxidized Na_2SO_4-$NiSO_4$ coated chromia forming alloys initially a chromia film is formed on the alloy. Reactions XV and LXXII are expected to proceed only to a limited extent. The oxidation kinetic curves show that preoxidized alloys have usually shorter induction periods whereas unoxidized alloys show relatively longer induction periods. This is perhaps one of the important reasons that preoxidised alloys have comparatively higher oxidation rates. The induction periods are relatively longer in chromia former than NiO former.

C O N C L U S I O N S

The following conclusions may be drawn from the hot corrosion studies:

Chapter II

(i) At 800°C, Na_2SO_4 coated sensitized (AISI 321) and unsensitized (AISI 303) steels show highest oxidation rates at a certain concentration which is 4.0 and 9.0 mg/cm^2, respectively followed by a gradual decrease in oxidation rate with increasing salt concentration.

(ii) At 1000°C, a linear relationship exists between amount of salt deposition and oxidation rate.

(iii) At 1000°C, with relatively large amount of Na_2SO_4, sensitized 321 steel oxidizes at a much faster rate than the unsensitized 303 steel. During corrosion a Cr-depleted zone is established in the matrix and TiC which is present on the grainboundaries is now subjected to be attacked by Na_2SO_4

$$TiC + Na_2SO_4 \longrightarrow TiO_2 + Na_2O + CO + S$$

Release of S and Na_2O enhances the degradation of the alloy.

Chapter III

(i) At 800°C, 303 and 321 steels coated either with tran-

sition metal salt or its mixture with Na_2SO_4 show relatively heavy weight losses and the weight loss increases with increasing salt deposition. This can be attributed to the fact that inner chromium oxide scales initially formed on the alloy remain intact and perhaps do not interact with decomposition products of metallic sulfates, e.g. oxides, SO_2 and O_2. The gaseous product escape resulting in weight losses.

(ii) At 800°C, the Na_2SO_4-$CoSO_4$ and Na_2SO_4-$NiSO_4$ coated steels show much severe corrosion due to the formation of low temperature eutectics (Na_2SO_4-$CoSO_4$: 575°C and Na_2SO_4-$NiSO_4$: 671°C). The liquidus phase breaks the protective oxide film and the alloy oxidizes at a much faster rate.

(iii) At 1000°C, both steels show increasing oxidation rates with increasing salt/mixture deposition till a maxima is reached, this is followed by weight losses on further increase in salt deposition.

(iv) Higher corrosion rates of $NiSO_4$ coated steels at 1000°C are attributed to the formation of NiS which accumulates beneath the Cr_2O_3 scales and undergo the following or similar type of reaction:

$$3NiS + Cr_2O_3 \longrightarrow 3NiO + Cr_2S_3$$

NiS also penetrates through the oxide scales and interact with nickel in the substrate to form low melting Ni-NiS eutectic.

(v) The Na_2SO_4 and transition metal sulfate coated steels undergo severe corrosion at 1000°C due to sequential progress of sulfidation and fluxing reactions.

Chapter IV

(i) Chromia forming Inconel 600, Inconel 800 and Nimonic 105 oxidise slowly in presence of Na_2SO_4 whereas alumina former B-1900 and NiO former Nickel-200 oxidise at a faster rates following a parabolic and/or linear kinetic.

(ii) In presence of Na_2SO_4, the chromia forming alloys show well defined induction periods indicated by weight losses.

(iii) The aggressive action of Na_2SO_4 on B-1900 is due to the presence of MoO_3 in the alloy which is formed under Na_2SO_4 layer and undergo following or similar types of acid fluxing reactions:

$$MoO_3 + Na_2SO_4 \longrightarrow Na_2MoO_4(l) + SO_3(g)$$

$$Cr_2O_3 + 3MoO_3 \longrightarrow 2Cr^{3+} + 3MoO^{2-}$$

$$Al_2O_3 + 3MoO_3 \longrightarrow 2Al^{3+} + 3MoO_4^{2-}$$

The reduction in oxide ion concentration increases the acidity of the melt and as a result sulfur is able to diffuse through Al_2O_3 scale into the alloy forming internal sulfides.

(iv) Monel-400 is appreciably corroded in presence of Na_2SO_4 and a mechanism involving alternate sulfidation and oxidation reactions seems responsible for development of a scale morphology consisting of alternate Ni and Cu enriched layers.

Chapter V

(i) Chromia forming nickel-base alloys show much higher oxidation rates in presence of NaCl than in presence of Na_2SO_4 or air.

(ii) Al_2O_3 or NiO forming alloys show much lower oxidation rates than in presence of Na_2SO_4.

(iii) Molten NaCl attacks the protective chromia scales forming volatile product CrO_2Cl_2 which is subsequently converted to Na_2CrO_4. NaCl then penetrates through the chromate melt and reacts with alloy components to form respective chlorides. As metallic chlorides move outward through the melt, oxygen activity is sufficiently high to convert metallic chlorides into metallic oxides. The chlorine is recycled to react with elements in the alloy.

(iv) Integrity of Al_2O_3 is maintained in B-1900 in presence of NaCl at 850 and 1000°C.

(v) During corrosion of Nickel-200 formation of volatile $NiCl_2$ and Na_2NiO_2 at the alloy/melt interface and subsequent dissociation and precipitation into NiO, respectively result in the formation of porous and copious scales on the alloy.

(vi) In Monel-400, oxidation and chloridisation reactions (involving O_2 and NaCl) generally follow a parabolic rate law whereas chloridation and chlorination reactions (involving NaCl and Cl_2) producing more serious attack follow a linear rate law.

Chapter VI

(i) Chromia forming Inconel 600 and 800 and Nimonic 105 show increasing corrosion rates with increasing amount of NaCl in Na_2SO_4.

(ii) Al_2O_3 former (B-1900) and NiO former (Nickel-200) show decreasing oxidation rates with increasing amount of NaCl in Na_2SO_4 although a small amount of NaCl in Na_2SO_4 enhances the oxidation rate initially.

(iii) During corrosion of chromia forming alloys in presence of Na_2SO_4 and NaCl mixture, NaCl creeps through the melt and duplicates the reactions which occur in presence of NaCl

alone. Due to the removal of chromium by NaCl the sulfur from Na_2SO_4 begins to sulfidise the alloy much earlier. The combined effect of two factors results in much higher corrosion rates in Na_2SO_4-NaCl coated alloy than Na_2SO_4-coated alloy.

(iv) Al_2O_3 former (B-1900) shows highest corrosion rates in presence of a mixture consisting Na_2SO_4:NaCl in the molar ratio of 5:1 and lowest in the pure NaCl. Addition of a small amount of NaCl in Na_2SO_4 enhances the corrosion attack enormously. This is perhaps due to a reduction in induction period and an early on set of degradation reactions. The degradation is caused by rapid removal of Al from the alloy.

(v) The corrosion rate of Monel-400 increases with increasing NaCl concentration in Na_2SO_4. A sequel of sulfidation, fluxing and chloridation reactions are responsible for high corrosion rates.

Chapter VII

(i) At 650 and 750°C, the preoxidized and Na_2SO_4-$NiSO_4$ coated Ni-base alloys have higher oxidation rates than the corresponding unoxidized Na_2SO_4-$NiSO_4$ coated alloys.

(ii) The preoxidized alloys when corroded in presence of Na_2SO_4-$NiSO_4$ mixture show morphologies in which scales are

greatly disrupted and are relatively less affected. On the other hand, alloys which were directly corroded in presence of a salt mixture show a morphology in which substrate is deleteriously attacked.

(iii) Preoxidized alloys have usually shorter induction periods whereas unoxidized alloys show relatively longer induction periods. This is perhaps on account of the important reasons that preoxidized alloys have comparatively higher oxidation rates. The induction periods are relatively longer in chromia former than NiO former.

(iv) In NiO former, the Ni-Ni_3S eutectic which forms below the surface oxide seems primarily responsible for the hot corrosion attack.

In Cr_2O_3 formers, the sulfidation involving formation of Cr_2S_3 and Ni_3S_2 and fluxing reactions are responsible for high corrosion rates.

HOT CORROSION OF SOME INDUSTRIALLY IMPORTANT STEELS AND SUPERALLOYS

A THESIS SUBMITTED FOR THE DEGREE OF

Doctor of Philosophy

IN

CHEMISTRY

BY

NAUSHA ASRAR

M. Sc., M. Phil (Alig)

DEPARTMENT OF CHEMISTRY

ALIGARH MUSLIM UNIVERSITY

ALIGARH

NOV. 1983

A. U. Malik
M.Sc., Ph.D. (Alig.)
Ph.D. (Liverpool), D.Sc. (Alig)
Reader in Materials Science

CHEMISTRY SECTION
Zakir Husain College of
Engg. & Technology
Aligarh Muslim University
ALIGARH-202001 INDIA
Dated 14. 11. 1983

This is to certify that the Ph.D. thesis entitled, "Hot Corrosion of Some Industrially Important Steels and Superalloys", which has been submitted by Mr. Nausha Asrar contains an original piece of research. The entire work has been carried out under my supervision and it has not been submitted elsewhere for the award of a degree or a diploma.

A. U. Malik

(A. U. MALIK)

DEDICATED
TO
MY PARENTS

A C K N O W L E D G E M E N T S

It gives me immense pleasure to acknowledge my great sense of indebtness to my reverend teacher and considerate guide Dr. Anees U. Malik, Ph.D. (Alig.), Ph.D. (Liverpool), D.Sc. (Alig.), Reader in Materials Science, Z. H. College of Engg. and Technology, Aligarh Muslim University, Aligarh. It was only his learned guidance and supervision that made this work possible.

Sincere thanks are also due to Prof. Mohsin Qureshi, Chairman, Chemistry Section, Z. H. College of Engineering & Technology, A.M.U., Aligarh for providing research facilities during the entire course of this work.

Obligation and affection can never be repaid — I can only extend my profound regards and sense of gratitude for Dr. Naseer Ahmed, a great scholar of chemistry, for his yeoman's service and jacking me up during the entire course of my study at A.M.U., Aligarh.

I can never forget the affection and sympathetic attitude of Dr. Fasih A. Siddiqi, Dr. Mohammad Hamiuddin and Dr. (Mrs.) Zohra Malik. My most sincere gratitude is for these esteemed personalities who have always been constant source of inspirations and encouragement for me.

I am thankful to my friends for their cooperation and whose company never made me feel away from home. As a matter of fact I always found my young friend Suhail Sabir side by side in every odds and evens. His constant amicable coordination is highly acknowledged.

Last but not the least, my thanks are also due to my laboratory colleagues for rendering help and providing congenial atmosphere to work.

The financial assistance from CSIR, New Delhi is gratefully acknowledged.

(NAUSHA ASRAR)

C O N T E N T S

CHAPTER I

GENERAL INTRODUCTION : Part I

HOT CORROSION BEHAVIOUR OF METALS AND ALLOYS

1.1.1 Introduction

In most of the environments in which engineering alloys are used oxygen is very often present. Other reactants in addition to oxygen, however, can be present and corrosion of alloys concomitantly by a number of reactants (mixed gas attack) is an important form of high temperature degradation. Deposits formed on alloys during use at high temperature significantly affect the gas-induced corrosion process. Deposit modified high temperature corrosion is called "hot corrosion" and is an important means of alloy degradation. In the broadest sense hot corrosion refers to the accelerated oxidation of metals or alloys induced by the presence of surface deposits of thin salt films.

Historically, hot corrosion was initially encountered in industrial gas turbines in the late 40's. The use of low grade of fuel, crude and residual oils, led to severe effects caused by metallic constituents, primarily vanadium (referred to as vanadium hot corrosion).

Hot corrosion is associated with the formation of corrosive, molten, electrolytic deposit on the surface of the hot component. These deposits are mainly composed of Na_2SO_4 and NaCl and other salts which lower the liquidus

temperature. Na_2SO_4 may, in some cases, be formed from a reaction between NaCl from ingested sea water aerosols in the air and sulfur dioxide or trioxide of the reaction product gases by the following reaction[1]

$$2NaCl \begin{Bmatrix} SO_3 \\ SO_2 \end{Bmatrix} + \begin{Bmatrix} \frac{1}{2}O_2 \\ O_2 \end{Bmatrix} = Na_2SO_4 + Cl_2$$

The severity of hot corrosion reaction will depend upon several factors, namely, the composition of the combustion gases, impurities in the gases, rate of flow of gases, composition and nature of the deposit etc.

1.1.2 Systems experiencing hot corrosion problems

A survey carried out by Rapp, Devan, Douglass, Nordine, Pettit and Whittle[2], illustrates that most of the high temperature energy system experience hot corrosion problem.

(a) High temperature secondary batteries:

Several high temperature batteries involve fused or solid alkali halide electrolytes for the reaction of an alkali metal (Na or Li) with either sulfur (Argon battery, 450°C) or iodine (Mallory battery, Los Alamos thermocells, 325°C). For the fused alkali chloride (450°C) battery leakage and evaporation - condensation of the salt can lead to a hot corrosion problem aggravated by the presence of sulfur.

(b) Coal conversion and combustion system:

In combustion systems, much of the sodium and potassium is volatilised from the mineral matter in the flame to form Na_2O and K_2O vapours. Sulfur released from coal forms SO_2 and some SO_3 and react with volatilised alkalis to form sodium sulfate vapour, which then condenses together with flyash on the pendant superheater and reheater tubes in the boiler. These are the major areas where critical high temperature fire-side corrosion problems have occurred.

Coal gasification systems operate at a temperature of upto $930^{o}C$ and the product coal generated gas in addition to hydrogen and carbon-containing gaseous species may contain many undesirable species including sulfides, sulfites, sulfates, ammonia, cyanides, volatilised oils, phenols and aggressive trace elements such as K, Na, V and Pb. The overall gaseous environment creates a severe hot corrosion problem.

(c) Refuse incineration and pyrolysis:

There are a number of hot corrosion problems which limit the lives of metallic components in incinerators and pyrolysis equipments.

During combustion or pyrolysis processes, some times thin fused layer containing alkali sulfates, chlorides, and oxides as well as some other phases (e.g. V_2O_5, PbO) are

formed which causes corrosion of alloys.

Particulate matter (e.g. non-combustibles, carbon particles, spalled corrosion products)often hits the surface of the alloy during the corrosion processes, so the protective scale is subjected to erosive conditions which greatly accelerates the corrosion process.

(d) Solar energy and energy storage:

Special problems in high temperature solar energy systems arise from the daily temperature variations (low cycle) and abrupt temperatures transients (high cycle) resulting from cloud cover etc.

(e) Nuclear energy systems:

Fast breeder reactor used for conversion of potential binding energies of atomic nuclei into useful work experiences two types of corrosion problems: (i) interaction between the fuel and fuel cladding, (ii) interaction between the reactor ecolant (He or Na) and structural metals. Corrosion of fuel cladding is associated with the migration and condensation of the more volatile fission products (e.g. Cs_2O) to the lower temperature regions which corrode the cladding by uniform oxidation, or by hot corrosion. Reactor cooled by liquid sodium, are subjected to temperature gradient mass transfer of selected elements comprising the fuel cladding, reactor piping and heat exchanger surfaces.

(f) Gas turbines:

Gas turbines have a wide range of applications extending from propulsion of aircraft and marine vehicles to use in power generation from coal gasification systems. In gas turbine usage as a whole hot corrosion problem arises by the mixed oxidants like oxygen, nitrogen, SO_2, SO_3, CO, CO_2 and H_2O and deposits predominently of Na_2SO_4. The hot corrosion problem is most severe at temperatures between about 600 and 900°C, and even in aircraft engines operating at higher temperatures some hot corrosion attack takes place on the cooler surfaces of blades and vanes.

(g) Gas oil recovery and magma energy:

In the case of tertiary oil recovery (fire flooding and steam injection), shale oil recovery and magma energy (geothermal systems involving the highest temperatures) severe corrosion problem arises due to the presence of sulfur. The actual environments and temperatures may be vastly different from one system to another, but there is a common dominator in all these systems, namely, sulfidising environment.

1.1.3 Factors affecting the hot corrosion phenomenon

1.1.3.1 Composition of alloys:

Numerous example can be cited to illustrate the influence of alloy composition on the hot corrosion phenomenon.

There is a general agreement that chromium content is the most important factor in contributing protection against corrosion. It has been found that by increasing the Cr content of a Ni-8Cr-6Al alloy to 15%, the initiation stage for hot corrosion induced by a large amount of Na_2SO_4 in air, is substantially increased[3]. Generally for a Ni-base alloy to form a chromia scale it must contain 15% Cr or more and less than 5% Al. An alloy with over 5 wt.% Al and more than 5 wt.% Cr will generally form an alumina scale.

Some elements can produce beneficial effects over others. It has been observed that the degradation of a Ni-30Cr-6Al alloy is less than that for a Ni-30Cr alloy after about 80 hours, but substantially more than 100 hours. This occurs because, in Ni-base alloys which are not Al_2O_3 formers, aluminum causes the sulfidation propagation mode to be especially pronounced. In such alloys sulfur is very rapidly removed from the Na_2SO_4 due to the formation of numerous sulfide particles in the alloys. The Ni-30Cr-6Al alloy is not attacked severely as long as it can maintain a continuous external scale of Al_2O_3 on its surface. As other oxide becomes stable, however, very severe degradation ensues. Hence, aluminum in alloys can produce both beneficial and deleterious effects on their hot corrosion resistance.

Kaufman[4] concluded on the basis of his small burner rig that for Ni-15Cr-base alloys, aluminum increased the corrosion resistance greatly, Co and Ti increased it slightly, Ta had no effect and W decreased it slightly. Bergman et al[5] also using small burner rig reported similar results for Ni-base alloys.

Small addition of rare earths seem to be beneficial in increasing the corrosion resistance of Ni and Co-base alloys. Vishwanathan[6] reported a significant improvement in the corrosion resistance of U-700 by the addition of 0.1-0.3% lanthanum and yttrium. Seybolt[7] found 0.5% cerium suitable for improving the corrosion resistance of U-500.

According to Stringer[8], there is a critical amount of Mo above which it can induce severe corrosion in aggressive circumstances, the critical amount probably increases with increasing Cr content, at least for chromia forming alloys, the value is probably 4-5% for 15% Cr alloys, rising to perhaps 10% Mo for 25% Cr alloys, although this has yet to be established.

Co-base alloys are generally regarded as having better corrosion resistance than those based on Ni, but this may be due to higher Cr contents of most cobalt base alloys.

Nagarajan and Stringer[9], using Dean rig found that

Mo was harmful for Co-25Cr alloys. In the test they observed clear evidence of a breakaway reaction.

A fairly large number of references are available regarding the influence of alloying elements on the hot corrosion behaviour of iron base alloys. It has been found that the additions of Cr, Al, Si, Ti, Nb and Ta are beneficial to the oxidation resistance of iron whereas V, Mo and W have adverse effect and Ni has no effect until and unless it is present in very high concentrations. Small additions of rare earths Y, Ce, La etc. seem to enhance the mechanical adhesion of scale on the alloy and therefore, indirectly decrease the oxidation rate of the alloy.

1.1.3.2 Composition of gases:

The composition of the gas phase can produce very substantial effects on the initiation and degradation rate of hot corrosion attack. On carrying out the oxidation of Na_2SO_4 coated CoCrAlY alloy in oxygen and oxygen containing SO_3 at 10^{-4} atm, it was found that there is an increase in weight in oxygen containing SO_3, but after 2.9 hours no attack was observed in pure oxygen. When CoCrAlY is oxidised at 700°C in SO_3, a liquid solution of Na_2SO_4-$CoSO_4$ is formed due to which hot corrosion attack is more easily induced[3]. Sulfur trioxide, however, also influences the rate at which the hot corrosion attack is propagated. For

example, the attack in oxygen is not as severe as in oxygen with SO_3 even when a deposit of Na_2SO_4-$MgSO_4$ is used which is liquid at 700°C in oxygen.

1.1.3.3 Salt composition:

Many of the earlier investigators reported that pure Na_2SO_4 is not very corrosive provided it is not contaminated with certain impurities. There is a substantial amount of data available[10] which show that extremely small concentrations of NaCl (3-5 ppm) in deposits on surface of alloys or in the gas phase cause the oxide scales to spall more profusely and accelerates the rate of oxidation.

Bornstein et al[11] have examined the effect of other additives to the salt on the corrosion of a number of alloys. The addition of 5.5 wt.% V_2O_5 to the Na_2SO_4 resulted in an oxidation rate of Ni-1%V alloy at 900°C which was virtually the same as the uncoated alloy. The accelerating effect of the sulfate coating was also greatly reduced by the addition of 5.5% MoO_3. A coating of 1 mg/cm^2 of Na_2SO_4 produced a considerable enhancement in the rate of oxidation of B-1900, but the enhancement was virtually eliminated by the addition of 1 mg/cm^2 Cr_2O_3 to the coating. Conversely, the addition of 1 mg/cm^2 MoO_3 increased the attack still further. Bornstein and DeCrescente[12] showed that B-1900 also suffered accelerated oxidation when coated with $NaNO_3$, although of

course the alloy did not contain any sulfates.

Hendry and Lees[13] studied the corrosion behaviour of austenitic stainless steel in molten sulfate deposits consisting of Na_2SO_4-K_2SO_4 mixtures under a simulated flue gas (N_2 + 15 v/o CO_2 + 1 v/o O_2 + 0.3 v/o SO_2). Addition of 5.3 m/o $Fe_2(SO_4)_3$ to Na_2SO_4-K_2SO_4 mixtures reduce the melting point from 820°C to below 550°C. Alkali-iron trisulfates are formed which resolidify on heating above 720°C by decomposition of $Fe_2(SO_4)_3$ at low thermodynamic activity.

Recently, Luthra[14,18] has reported the hot corrosion behaviour of Co-base alloys at lower temperatures (650-750°C). This sort of corrosion has also been reported by Jones[15]. This low temperature hot corrosion behaviour has been attributed to the formation of a low-melting Na_2SO_4-$CoSO_4$ eutectic (m.p. 565°C). Jones and Godowski[16] have also found that when $NiSO_4$ is mixed with Na_2SO_4 in 50% molar ratio, a liquid phase begins to form (by NiO + Na_2SO_4 at 750°C) at 500 ppm (5×10^{-4} atm) and causes hot corrosion.

1.1.3.4 Temperature:

Hot corrosion processes are dependent upon temperature. In many cases the time to initiate hot corrosion attack decreases as temperature is increased.

Lewis and Smith[17] found in a crucible test that

Nimonic 80A shows a maximum attack of Na_2SO_4 + 25% NaCl mixture at 900°C, decreasing markedly upto 1000°C. Luthra and Shores[18] studied Na_2SO_4 induced hot corrosion of Co-30Cr and Ni-30Cr as a function of temperature (600-900°C). Alloys rapidly attacked between 650-750°C when liquid sulfate phase was obtained from initially pure solid Na_2SO_4 deposit.

Page and Taylor[19] remarked that 870°C seems to be close to the peak"sulfidation" temperature for most metals, but that Nimonic-105 has a peak temperature lower than this. However, plot of the temperature dependence of penetration are shown for the temperature range 870-1050°C and these show a monotonic increase for X-40,little change for IN-738 and Nimonic 105, and a marked minima at 950°C or so far IN-100, Udimet-700 and M-432. This is because another high temperature process becomes important at around 1000°C.

When chloride are present in the vapour phase only, the extent of corrosion is found to increase with increasing temperature. However, under deposition conditions, attack occurs at lower temperatures, and, although fluxing mechanism suggests that the rate of attack should increase with increasing temperature, several authors have shown that the rate of attack exhibits maximum value at intermediate temperatures. This is because of the fact that the amount of Cl_2,

which accelerates the corrosion by disrupting the oxide scale, decreases with increasing temperature and the balance occurs at some intermediate temperature. For this there are other factors also, for example, integrity of the oxide scale[10]. Bruce and Hancock showed that the plasticity of oxide scales on ferrous alloys increases with temperature.

1.1.4 Chemistry of hot corrosion

Hot corrosion is a two stage process, namely, the initiation stage and the propagation stage[3].

In initiation stage, the reaction product formed at the surface of the alloy is predominantly composed of the most protective phase; this is followed by a propagation stage in which there is a rapid degradation and the reaction product consists of less protective phases.

1.1.4.1 Initiation stage:

During the initiation stage of hot corrosion of an alloy coated with salt deposit, elements in the alloy are oxidised and the electrons can be considered to be transferred from metallic atoms to reducible substances in the deposit. When the reducible substances are the same as those which would have reacted with the alloy in the absence of the deposit, the reaction product barrier forms beneath the salt on the alloy surface, and exhibits mostly features

arising from the gas-alloy reaction. As the hot corrosion process is continued, however, features begin to become apparent which indicates that the salt is affecting the corrosion process and gradually the selective oxidation process is rendered ineffective. The increasing amount of sulfide particles in the scale is an example of this condition. The time for which the most effective reaction product barrier is stable beneath the salt layer is influenced by a number of factors listed in figure 1.1.1.

1.1.4.2 Propagation stage:

The propagation stage which is followed by initiation stage involves salt induced alloy degradation reactions resulting in the formation of less protective or nonprotective scales. The propagation stage for degradation of alloys with salt deposits has been classified into three general categories.

In the first category the salt is innocuous and degradation in the propagation stage proceeds by the mechanism determined by the alloy and the gas. Such a situation is likely to occur with porous, solid deposits through which gas can easily penetrate. The other two categories involve degradation mechanisms which are different from that which occur in absence of salt deposits. One category requires the salt, or the product of the salt-alloy-gas reaction, to

be liquid. Reaction between element in the alloy and component from the gas in the presence of liquid results in the formation of nonprotective reaction products. The nature of the reaction that take place under such conditions are similar to those where surfaces are cleaned by using salt baths for descaling or fluxes[20,21]. Hence this category of propagation stages has been labelled as salt fluxing reaction.

The final category involves propagation reactions in which a component from the salt is added to the alloy, or reaction with the alloy or its corrosion products, such that nonprotective reaction barriers are developed. This category of the propagation stages can be called salt component induced hot corrosion, or degradation resulting from salt component-alloy reactions. Figure 1.1.2 shows a schematic diagram to illustrate the three general categories of propagation stages involving breakdown of protective scales during hot corrosion.

1.1.4.3 Salt fluxing reactions:

The results from fireside corrosion in boilers first conceived the idea that protective oxide scales could be removed by molten salt deposits[22]. In these investigations corrosion observed in certain temperature regions was associated with certain types of deposits, in particular, alkali metal pyrosulfates (e.g., $Na_2S_2O_7$) at temperatures between

480-730°C, and alkali sulfates at temperatures above 750°C.

Bornstein and DeCrescente[12] were among the firsts to propose that the hot corrosion of alloys involved a basic fluxing process. It was proposed that protective oxide scales were destroyed as a result of reaction with oxide in the salt where the oxide ions were produced by removal of S from Na_2SO_4:

$$SO_4^{2-} \text{ (sulfate deposit)} \longrightarrow \tfrac{1}{2}S_2 \text{ (for reaction with alloy)} + O^{2-} \text{ (for reaction with AO)} + \tfrac{3}{2}O_2 \text{ (for reaction with alloy)}$$

AO is reaction product on alloy A formed during initiation reaction.

Goebel et al[23] extended high temperature fluxing reactions to acidic processes, where the component to make the salt acidic was proposed to be certain oxides of elements in the alloys (e.g. MoO_3, WO_3), and suggested that porous oxide scales may be formed during either basic or acidic fluxing by precipitation from the molten salts into which these oxide scales had initially dissolved. The dissolution and reprecipitation processes were controlled by the oxide ion activity of the melt which in turn was regulated by the removal of sulfur from the salt (Na_2SO_4),

or by the addition of oxides of certain metals to the salt (e.g. MoO_3, WO_3).

1.1.4.4 Basic fluxing:

There are at least two processes by which Na_2SO_4 becomes more basic (i.e. production of oxide ions). One involves the removal of sulfur from Na_2SO_4 by the alloy whereby

$$SO_4^{2-} \longrightarrow S(\text{alloy}) + \tfrac{3}{2}O_2 + O^{2-}$$

and oxide ions are produced.

The other process arises because the oxide product formed on the surface of alloy may donate oxide ions to the salt as proposed by Rapp and Goto[24]. While the oxide that is attempting to be formed at the alloy surface may donate oxide ions to the salt, it could also react with existing oxide ions by reactions such as:

$$MO + O^{2-} \longrightarrow MO_2^{2-}$$

The latter reaction is a means by which the salt can become more acidic.

Na_2SO_4 induced hot corrosion of nickel in presence of air is a typical example of basic fluxing. At the beginning of attack NiO is formed and an oxygen gradient is developed across the Na_2SO_4. As a result of this gradient

in oxygen pressure, the sulfur activity is increased and NiS is formed on the alloy surface. The oxide ion concentration in Na_2SO_4, which has been increased due to NiS formation, reaches value at which NiO forms nickelate ion at the oxide/salt interface:

$$NiO + O^{2-} \longrightarrow NiO_2^{2-}$$

As NiO_2^{2-} is soluble in fused salt difuses to the salt/gas interface, where the activity of oxide ion is quite low, owing due to high P_{O_2}.

$$SO_2 + \tfrac{1}{2}O_2 + O^{2-} \rightleftharpoons SO_4^{2-}$$

Therefore nickelate ion is reprecipitated at the salt/gas interface as NiO. Thus the protective NiO layer is fluxed from the metal surface and is formed at the salt/gas interface, figure 1.1.3.

In the case of alumina forming alloys, alumina is also precipitated at the salt/gas interface, but formation of aluminate ion by the dissolution of Al_2O_3 at the oxide/salt interface does not take place, because the activity of oxide ion at the oxide/salt interface under 1 atm of oxygen is not sufficient to derive the following reaction to the right side:

$$Al_2O_3 + O^{2-} \longrightarrow 2AlO_2^-$$

At the alloy/salt interface, however, aluminum in the alloy reacts with the salt to raise the oxygen ion activity and to form Al_2S_3 by the following reaction:

$$\frac{2}{3}Al + SO_4^{2-} \rightleftharpoons O^{2-} + \frac{1}{3}Al_2S_3 + \frac{3}{2}O_2$$

Consequently, a gradient of oxygen ion is developed as a result of which aluminate ion formation occurs. Thus alumina is dissolved at the oxide/salt interface, and is precipitated near the salt/gas interface to form a porous layer of Al_2O_3.

In the case of the chromia forming alloys the oxide ion activity is sufficient to form chromate ion at the salt/oxide interface according to the following reaction:

$$Cr_2O_3 + \frac{3}{2}O_2 + O^{2-} \rightleftharpoons 2CrO_4^{2-}$$

Thus, Cr_2O_3 is dissolved in the molten salt and is reprecipitated at the salt/air interface.

This type of fluxing of nickelate ion, aluminate ion and chromate ion is called the "basic fluxing". Basic fluxing is not self-sustaining, because decomposition of Na_2SO_4 is here necessary, and the amount of Na_2SO_4 is limited.

1.1.4.5 Acidic fluxing:

A feature of acidic fluxing that differs from basic

fluxing is that acidic-induced attack is usually self sustaining. Hence small amounts of deposits produce much more attack for acidic fluxing compared to basic fluxing. Two types of acidic fluxing are known, alloy-induced acidity and gas-induced acidity. In the former, oxides are formed on the surface of alloys which have greater affinity for oxide ions (e.g. MoO_3, WO_3, Cr_2O_3) and in the latter most common gas components such as SO_3 and V_2O_5 which are often introduced to the gas via combustion of fuels containing sulfur and vanadium make the deposit acidic (Fig. 1.1.4).

1.1.4.5.1 Alloy-induced acidic fluxing:

The Na_2SO_4-induced hot corrosion of Ni-8Cr-6Al-8Mo alloy has been studied in some details.[3] This alloy eventually exhibits alloy/induced hot corrosion. At the scale/alloy interface, a thin zone of sulfide particles is evident in the alloy and the scale immediately adjacent to the alloy, contains Na, S, O, Mo, Ni, Cr and Al. It appears that this zone may be a solution of Na_2SO_4 and Na_2MoO_4 into which Al_2O_3, Cr_2O_3 and NiO are dissolved.

Ni-25Al-12W and Ni-8Cr-6Al-8Mo alloys undergo alloy-induced acidic hot corrosion which involves following important steps:

(a) Oxides of W and Mo dissolves into the Na_2SO_4 and some SO_3 is displaced from the Na_2SO_4.

(b) The Na_2SO_4 solutions gradually become enriched in the oxides of these metals since such solutions probably have a higher solubility for the oxides[25].

(c) It appears though Al_2O_3, Cr_2O_3 and CoO can dissolve into these refractory metal oxide enriched metals by donating oxide ions to the melts. The reactions that may take place are:

$$2Al + 3W + 6O_2 \longrightarrow Al_2O_3 + 3WO_3 = 2Al^{3+} + 3WO_4^{2-}$$

$$2Cr + 3W + 6O_2 \longrightarrow Cr_2O_3 + 3WO_3 = 2Cr^{3+} + 3WO_4^{2-}$$

$$Co + W + 2O_2 \longrightarrow CoO + WO_3 = Co^{2+} + WO_4^{2-}$$

These ions diffuse through the solution (i.e. the zone enriched in refractory metal) to the outer zone of the melt where reaction listed above proceed in the reverse direction due to the lower activity of the refractory metal oxides in this region as a result of the loss of the refractory metal oxides to the gaseous phase. Hence, oxides of Al_2O_3, Cr_2O_3 and CoO are dissolved at one side of the melt, (alloy/melt interface) and reprecipitated as a nonprotective scale at the other side (metal/porous oxide interface).

The most important feature of alloy-induced acidic fluxing is that a zone of liquid is formed immediately above the alloy due to accumulation of certain refractory metal

oxides (MoO_3, WO_3, V_2O_5) in the Na_2SO_4, and the oxides normally relied upon for protection against attack (e.g. Al_2O_3, Cr_2O_3, CoO, NiO etc.) become nonprotective due to a solution precipitation process. This attack is self-sustaining because a small amount of salt appears adequate to cause the development of refractory oxide zone.

1.1.4.5.2 Gas-induced acidic fluxing:

Taking CoCrAlY as an example of this type of fluxing, substantial attack on this alloy is observed at rather low temperatures (700°C), but the rate of attack is decreased abruptly when SO_3 is removed from the gas. After thousands of hours, this alloy is not noticeably attacked using Na_2SO_4 in air, but substantial attack is observed within hours when SO_3 is added to the gas. The attack of this alloy requires a Na_2SO_4 deposit since exposure to gases containing SO_3 and O_2 without Na_2SO_4 does not produce significant degradation[3].

A schematic model to describe the gas-induced acidic fluxing of a Co-Cr-Al-Y alloy is presented in figure 1.1.5. At low temperatures the salt becomes molten as $CoSO_4$ dissolves into it. Beneath this liquid layer the alloy begins to react with components in the liquid. The principal reaction is one of oxygen removal from the melt since the most favourable reactions for elements in the alloy are those involving oxide formation. It has been determined

that SO_3 is much more mobile in Na_2SO_4 than oxygen[26]. Consequently, it is reasonable to propose that gradients in both oxygen and SO_3 are developed across the liquid layer with SO_3 also supplying oxygen to react with the elements in the alloy. The processes by which the SO_3 and oxygen diffuse through the liquid layer is not known, but it would seem reasonable that the SO_3 combines with SO_4^{2-} ions and diffuses as pyrosulfate ions ($S_2O_7^{2-}$) where oxygen may be dissolved in the liquid as atoms.

The preferential removal of Al from the alloy and its subsequent precipitation as Al_2O_3 is believed to occur because of sulfite formation at the liquid/alloy interface where the oxygen pressure is low and then conversion of the sulfite to oxide in the liquid which has higher oxygen pressure. At low oxygen pressure the oxidation of Al is proposed to be accompanied by reduction of SO_3 rather than by reduction of oxygen. The existance of SO_3^{2-} ions seems plausible since, at low oxygen pressure, with a supply of SO_3 from the gas, the SO_2 pressure should be relatively high.

As the temperature is increased the liklihood of acidic fluxing reactions involving sulfite becomes less likely. Since higher SO_3 pressure are required to form sulfites and sulfates as the temperature is increased and

lower SO_3 pressures exist in gas due to the presence of a larger proportion of SO_2. Hence, as the temperature is increased the gas induced acidic component of the degradation becomes less, and the sulfide phases are formed with increased frequency in the alloy. Eventually, oxidation of these sulfides is the primary means of hot corrosion degradation.

1.1.4.6 Rapp and Goto criterion for hot corrosion:

According to this model, the continued hot corrosion of a metal, which is signified by dissolution and precipitation processes, may occur whenever a negative gradient exists in the solubility of the protective oxides (as acid or basic species) at the oxide/salt interface.

$$\left(\frac{d(\text{oxide solubility})}{dx}\right)_x = 0 < 0$$

By this criterion (illustrated schematically in figure 1.1.6) the continuous reprecipitation of the oxide in the salt film away from the oxide/salt interface is expected to permit local equilibrium between the oxide and the salt throughout the film.

Because a reprecipitation oxide cannot form as a continuous protective layer, a voluminous, porous oxide product interspersed with salt is expected, this morphology is indeed representative of hot corrosion products.

1.1.4.7 Salt component-induced hot corrosion:

As a result of salt deposition, elements from the salt can be introduced into the corrosion product or the surface regions of alloys and eventually affect the oxidation behaviour. A great variety of elements could produce such an effect depending upon the deposit composition. In the case of Na_2SO_4 and NaCl, the significant elements are S and Cl. Another element that can be important is C. This is because of the fact that the environment causing hot corrosion attack usually results from the combustion of some type of fuel.

1.1.4.7.1 Sulfur-induced hot corrosion:

The oxygen pressure in Na_2SO_4 at alloy/Na_2SO_4 or oxide/Na_2SO_4 interfaces can be very low. Under such conditions the sulfur pressure is usually high enough to form sulfides of Cr and Al and in some cases sulfides of Co, Ni and Fe unless the SO_3 pressure is very low. The accumulation of these sulfides in the alloy can result in substantial degradation during subsequent oxidation. Weight gain/time data obtained for Na_2SO_4-coated Ni-25Cr-6Al specimens are comparable to those of a presulfidized specimens, containing equivalent amounts of S. The degradation of presulfidized specimen is about the same as that for the Na_2SO_4 coated and both are degraded substantially more than the specimen with neither sulfidizing treatment nor Na_2SO_4

application. This shows that the primary mode of hot corrosion degradation for Na_2SO_4-coated specimens of Ni-25Cr-6Al exposed at 1000°C in air is sulfur-induced degradation.

Sulfur-induced hot corrosion causes accelerated oxidation as a result of the formation of less protective oxide scales. Such scales are formed due to the presence of sulfides in the alloys. S-induced accelerated oxidation is also observed during the oxidation of alloys in SO_2-O_2 or H_2S-H_2O-H_2 gas mixtures, where the sulfide formation occurs due to S in the gas rather than from the S in the Na_2SO_4. Sulfide formation in alloys, as a result of S in the gas or deposits on the surface of the alloys, can cause the formation of nonprotective oxide barriers on alloys by at least three different mechanisms. In one mechanism the oxidation of Al and Cr dissolved in Ni or Cr sulfide results in the formation of discontinuous particles of Al_2O_3 or Cr_2O_3 rather than continuous protective layers. Another mechanism involves the formation of nonprotective oxides during the conversion of certain sulfides to oxides. The smaller volume of oxide compared to the sulfide may cause the oxide to be subjected to tensile stresses. The third mechanism by which nonprotective oxides are formed involves effects produced by internal sulfides on the selective oxidation process. When S diffuses into the surface of the alloys, it usually reacts with the same elements that are diffusing to

the surfaces of the alloy to combine with oxygen to form continuous oxide barriers. The formation of such sulfides appears to cause the flux of the elements being selectively oxidized to be decreased. This condition develops even though the sulfide particles usually dissolve and release the metal to react with oxygen. The metal in solution in the alloy is apparently more suitable for selective oxidation than the dispersion of metal sulfides in the alloy. At any rate, the decrease in the flux of such elements to the surfaces of the alloy can result in the formation of oxide scales which are less protective than those that would have formed in the absence of sulfide precipitates.

1.1.4.7.2 Chloride-induced hot corrosion:

According to Spahn[27] approximately one third of all failures in chemical plants are caused by stress corrosion and petting corrosion. These two types of corrosive attack are strongly associated with the chloride content of the aggressive medium.

When chlorides are present then oxidation occurs in such a way that instead of formation of a continuous protective oxide layer, oxides are formed as discontinuous particles.

Alloy with Cr and Al as alloying elements show less corrosion resistance in presence of NaCl when there is a

coating of Na_2SO_4 + NaCl. The reason attributed for this is that due to greater stabilities of oxides and sulfides the mixture of the salt becomes deficient of oxygen and sulfur and as a result P_{NaCl} increases and following reactions may be expected[3]:

$$\text{I} \quad (Na_2SO_4\text{-}NaCl)_{liq} + (Al, Cr)_{alloy} \xrightarrow{P_{O_2},\ P_{S_2},\ P_{NaCl}} \xrightarrow{P'_{O_2},\ P'_{S_2},\ P'_{NaCl}} Al_2O_3 + Cr_2O_3 + CrS + (Na_2SO_4\text{-}NaCl)_{liq}$$

where $P'_{O_2} < P_{O_2}$; $P'_{S_2} < P_{S_2}$; $P'_{NaCl} > P_{NaCl}$

$$\text{II} \quad NaCl + 2Al(alloy) + O_2 \longrightarrow NaAlO_2 + AlCl$$

$$\text{III} \quad 2AlCl + \tfrac{3}{2}O_2 \longrightarrow Al_2O_3 + Cl_2$$

$$\text{IV} \quad Cl_2 + 2Al(alloy) \longrightarrow 2AlCl$$

Figure 1.1.7 shows a schematic diagram to illustrate the hot corrosion attack of alloys induced by Na_2SO_4-NaCl mixtures.

Equation (I) and figure 1.1.7(a) indicate that the melt adjacent to the alloy can become enriched in NaCl due to oxide and sulfide formation. In localized areas, the NaCl component of the Na_2SO_4-NaCl melt may then begin to react with certain components in the alloy as proposed by

equation (II). This reaction takes place first with elements for which the thermodynamic conditions are most favourable. For example, reaction with Al is observed before Cr but Cr does react when Al concentration has reduced. As the metallic chloride is converted to metallic oxide (Eqn. III) and (Fig. 1.1.7(b)), and chloride is recycled to react with elements in the alloy (Eqn. IV), development of pores that are coated with discontinuous, nonprotective oxide particles takes place (Fig. 1.1.7(c)). As the process of pore development continues chloride is gradually lost to the gas phase. The time at which the chloride concentration becomes insufficient to react with the alloy depends upon temperature, salt composition, gas composition and alloy composition. When such a condition is reached the innermost portions of the pores begin to react with sulfur and the degradation process proceeds via Na_2SO_4-induced hot corrosion.

After exposure to gaseous NaCl, an alloy surface is generally covered with blistered and cracked layers. Davin et al[28] attributes this blistering to the formation of volatile metallic chlorides, like $NiCl_2$, in locally reducing conditions. When these chlorides are exposed to oxidising conditions, they transform to oxides, releasing Cl_2 or HCl gases, as shown schematically in figure 1.1.8. Jones[29] gave the same mechanism.

Iron-base alloys are very much affected by NaCl during hot corrosion according to the following reactions:

V $\quad Fe + HCl \longrightarrow FeCl_2 + H_2$

VI $\quad$ or $HCl + \frac{1}{2}O_2 \longrightarrow H_2O + Cl_2$

VII $\quad$ then $Fe + Cl_2 \longrightarrow FeCl_2$

Except this the oxidation of chromia formers is accelerated, either when a gaseous environment or a salt coat contains some amount of NaCl[28-30]. A series of simple chemical tests involving a range of oxides and metals with deposits of both Na_2SO_4 and NaCl in atmosphere of Argon and air have been performed. These results showed that little attack was observed with Al_2O_3 in either Na_2SO_4 or NaCl at temperatures upto 1000°C, but Cr_2O_3 was found to react with NaCl in air to produce a volatile product[30]. At 650°C slight reaction takes place, at 700°C, 32% and at 750°C, 60% of the Cr_2O_3 was converted after exposure times of 22 hours. These observations led to suggest that an intermediate volatile compound CrO_2Cl_2 was formed, which may cause scale lifting and cracking. Once the protective oxide film is broken, fresh salt with high oxygen potential and high NaCl concentration can make direct contact with the metal surface as schematically shown in figure 1.1.9. The intermediate volatile compound CrO_2Cl_2 subsequently converted to Na_2CrO_4,

which condensed at some distance away from the specimen. Fryburg et al[31] opposed this model, as they did not find chromium chloride or oxychloride in the vapour phase during their examination of volatile products in the hot corrosion of superalloys exposed to oxygen containing NaCl gas by high pressure mass spectrometry.

1.1.4.8 Interaction between the various hot corrosion propagation modes:

A hot corrosion attack may not necessarily follow a single mechanistic path. There are definite instances of Na_2SO_4-induced hot corrosion propagation modes consisting of basic and acidic fluxings and sulfidation degradation modes.

Basic fluxing and sulfur-induced degradation are two propagation modes that are often followed in sequence with the basic fluxing mode preceding the sulfidation mode. Such a situation arises since the basic fluxing mode requires oxide ions and sulfur formation in the metal or alloy is a means of producing oxide ions. Eventually, the accumulation of sulfides in the alloy can result in degradation via oxidation of these sulfides.

Ni- and Co- base alloys containing more than 20% Cr and no Al are not substantially degraded by basic fluxing and significant propagation mode for alloys with no ref-

ractory metals is sulfidation. On the other hand, the Na_2SO_4-induced hot corrosion of Ni- and Co- via basic fluxing is significant in comparison to the oxidation of sulfides formed in these metals.

Gas-induced acidic fluxing and sulfidation degradation are propagation modes whose dominance can change with temperature. At low temperatures (600-700°C), the gas-induced acidic fluxing process can be extremely rapid and sulfide formation in the alloy is therefore, often negligibly small. The amount of sulfide formation progressively increases with temperature, however, since the thermodynamic conditions become less favourable for the SO_3-induced fluxing process and sulfur diffusion into the alloy becomes more pronounced. At temperatures above 1000°C, excessive amounts of sulfur can be formed and their subsequent oxidation result in severe degradation.

Alloy-induced acidic fluxing is usually preceded by some other propagation modes since Mo or W from the alloy must be oxidized and added as oxides to the salt deposit. The most common propagation modes to precede alloy-induced acidic fluxing are basic fluxing and sulfidation. Since these two modes are favourable at high temperatures, alloy-induced acidic fluxing is often observed at temperatures above 900°C.

Chloride-induced degradation can precede any of the propagation modes described. Chloride-induced attack will normally be observed with alloys that are resistant to degradation and the chloride-induced attack will produce depletion of elements to levels at which the other propagation modes can become dominant.

REFERENCES

1. M. A. DeCrescente and N. S. Bornstein, Corrosion, 24, 127 (1968).
2. R. A. Rapp, J. H. Devan, D. L. Douglass, P. C. Nordine, F. S. Pettit and D. P. Whittle, Rev. "High Temperature Corrosion in Energy Systems", Mat. Sc. & Engg., 50, 1-17 (1981).
3. C. S. Giggins and F. S. Pettit, "Hot Corrosion of Metals and Alloys — A Unified Theory", Final Scientific Report (June 1979); Pratt and Whitney Aircraft Group, Report No. FR-11545.
4. M. Kaufman, Trans. ASM, 62, 590 (1969).
5. P. A. Bergman, C. T. Sims and A. N. Beltran, "Hot Corrosion Problems Associated with Gas Turbines", ASTM Special Technical Publication STP, 421, 38 (1967).
6. R. Vishwanathan, Corrosion, 24, 359 (1968).
7. A. U. Seybolt, Trans. AIME, 242, 1955 (1968).
8. J. Stringer, Ann. Rev. Mat. Sci., 7, 477 (1977).
9. V. Nagrajan and J. Stringer, Annual Report of Ministry of Defence Contract AT/2067/028 AML (Jan. 1975).
10. P. Hancock, "The Role of Halides in High Temperature Gas Corrosion", Proceeding on High Temperature Metal Halide Chemistry, D. L. Hildebrand and D. D. Cubicciotti, eds., The Electrochemical Soc., Inc., Princeton, N.J., 645-69 (1978).

11. N. S. Bornstein, M. A. DeCrescente and H. A. Roth, 'Deposition and Corrosion in Gas Turbines', A. B. Hart and A. J. B. Cutler (eds.). (Applied Science Publishers, London, 1975) 70.

12. N. S. Bornstein and M. A. DeCrescente, Trans. AIME, 245, 1947 (1969); Met. Trans., 2, 1991 (1971).

13. A. Hendry, D. J. Lees, Corros. Sci., 20, 383-404 (1980).

14. K. L. Luthra, Technical Information Series, General Electrical Company, Report No. 81CRD150 (1981).

15. R. L. Jones, Presented in Int. Conf. on High Temperature Corrosion, SanDiego, Calf. U. (1981).

16. R. L. Jones, S. T. Godomski, J. Electrochem. Soc., 129, 7 (July 1982).

17. H. Lewis and R. A. Smith, Proc. First Int. Congr. Met. Corros., 202 (1965).

18. K. L. Luthra and D. A. Shores, J. Electrochem. Soc., 127, 2202-10 (1980).

19. K. Page and R. J. Taylor, 'Deposition and Corrosion in Gas Turbines', A. B. Hart and A. J. B. Cutler (eds.), (Applied Science Publishers, London, 1975) 350.

20. Metals Hand Book, 5th ed., 2, "Heat Treating, Cleaning and Finishing", 356-63, American Society for Metals, Metals Park, Ohio (1964).

21. G. Charlot and B. Tremellon, Chemical Reactions in Solvents and Metals, Chapter-15, Pergamon Press, New York (1969).

22. W. T. Reid, External Corrosion and Deposit, Elsevier Press, New York (1971).

23. J. A. Goebel, F. S. Pettit and G. W. Goward, Met. Trans., 4, 261 (1973).

24. R. A. Rapp and K. S. Goto, Proc. 2nd Int'l Symp. Molten Salts, J. Braunstein (ed.), Electrochem. Soc., Princeton (1979).

25. E. M. Levin, C. R. Robbins and H. F. McMurdie, Phase Diagrams for Ceramists, The American Ceramic Society, Columbus, Ohio, p. 95 (1964).

26. A. J. B. Cutler, J. Appl. Electrochem., 1, 19 (1971).

27. H. Spahn, VDI-Berichte Nr. 235, p. 103 (1975).

28. A. Davin, D. Coutsouradis and L. Habraken, "Metal-Slag-Gas Reactions and Processes", Symposium, Z. A. Foroulis and W.W. Smeltzer eds., The Electrochem. Soc., 678 (1975).

29. R. L. Jones, ibid., 762 (1975).

30. R. C. Hurst, J. B. Johnson, M. Davies and P. Hancock, "Deposition and Corrosion in Gas Turbines", A. B. Hart and A. J. B. Cutler eds., 143, John Wiley and Sons Inc. New York (1973).

31. G. C. Fryburg, R. A. Miller, F. J. Kohl and C. A. Stearns, J. Electrochem. Soc., 124, 1738 (1977).

Table 1.1.1: Possible salt fluxing reactions for Na_2SO_4 deposits on alloys.

BASIC PROCESSES

A. Dissolution of Reaction Product, (i.e. AO) Due to Removal of Sulfur and Oxygen from the Na_2SO_4 by the Metal or Alloy:

SO_4^{2-} (sulfate deposit) $\longrightarrow$ $\frac{y}{2}SO_4$ (for reaction with alloy) + $\frac{x}{2}O_2$ (for reaction with alloy) + O^{2-} (for reaction with AO).

Reaction between AO and oxide ions can follow 2 courses:

(1) Continuous dissolution of AO

$$A \text{ (alloy)} + \tfrac{1}{2}O_2 + O^{2-} \longrightarrow AO_2^{2-}$$

Na_2SO_4 is converted to Na_2AO_2 and attack is dependent on amount of Na_2SO_4 initially present.

continued ..

Table 1.1.1: continued ..

(2) Solution and reprecipitation

$$A\ (alloy) + \tfrac{1}{2}O_2 + O^{2-} \longrightarrow AO_2^{2-}\ (solution) \longrightarrow AO\ (precipitate) + O^{2-}$$

A supply of SO_3 is required in order for attack to proceed indefinitely, otherwise attack will stop when melt becomes sufficiently basic at precipitation site.

B. Solution and Precipitation of AO as a Result of a Negative Gradient in Solubility of AO in Na_2SO_4.

ACIDIC PROCESSES

Gas Phase Induced:

C. Formation of ASO_4 in Na_2SO_4

$$A\ (alloy) + SO_3 + \tfrac{1}{2}O_2 \longrightarrow A^{2+} + SO_4^{2-}$$

Continuous solution of ASO_4 in Na_2SO_4 requires continuous supply of SO_3 and O_2 from gas.

continued ..

Table 1.1.1: continued ..

D. Solution and Precipitation of AO in Na_2SO_4 Due to Reduction of SO_3

$$A\ (\text{alloy}) + SO_3\ (\text{from gas}) \longrightarrow A^{2+} + SO_3^{2-}\ (\text{in melt})$$

$$A^{2+} + SO_3^{2-} + \tfrac{1}{2}O_2\ (\text{from gas}) \longrightarrow AO\ (\text{precipitate}) + SO_3$$

E. Solution and Precipitation of AO as a result of a Negative Gradient in Solubility of AO in Na_2SO_4 as in B.

<u>Alloy Phase Induced:</u>

F. Solution of AO in Na_2SO_4 Modified by Second Oxide from Alloy (i.e. BO_3)
- Modification of Na_2SO_4 by BO_3

$$B\ (\text{alloy}) + \tfrac{3}{2}O_2 + SO_4^{2-} \longrightarrow BO_4^{2-} + SO_3$$

continued ..

Table 1.1.1: continued ..

- Solution reaction for AO, Na_2SO_4 becomes enriched in ABO_4

  $$A\ (alloy) + B\ (alloy) + 2O_2 \longrightarrow A^{2+} + BO_4^{2-}$$

- Solution - Precipitation

  $$A\ (alloy) + B\ (alloy) + 2O_2 \longrightarrow A^{2+} + BO_4^{2-} \longrightarrow AO + BO_3$$

  Precipitation of AO in Na_2SO_4 as a result of loss of BO_3 from Na_2SO_4 permits substantial attack with small amounts of Na_2SO_4

Table 1.1.2: Alloy systems which are susceptible to attack via the principal hot corrosion propagation modes and procedures to inhibit such degradation.

O_2-Na_2SO_4 ENVIRONMENT			O_2-SO_3-Na_2SO_4
BASIC FLUXING	**SULFUR-INDUCED DEGRADATION**	**ALLOY-INDUCED ACIDIC DEGRADATION**	**GAS-PHASE-INDUCED ACIDIC FLUXING**
SUSCEPTIBLE SYSTEMS	SUSCEPTIBLE SYSTEMS	SUSCEPTIBLE SYSTEMS	SUSCEPTIBLE SYSTEMS
Ni, Co, Ni-Al alloys, Co-Al alloys, Ni-Cr-Al alloys with Cr and Al contents below that required to form external scales of Cr_2O_3 or Al_2O_3. Ex. Ni-8Cr-6Al	Nickel-base alloys containing about 1.6% Al. Ex. IN 792, U-700	Alloys containing Mo, W or V. Ex. B-1900, IN 100, Mar-M 200, Wl-52, HX-188	Virtually all alloys depending on SO_3 pressure or amount of V_2O_5 deposited.
MORE RESISTANT SYSTEMS	MORE RESISTANT SYSTEMS	MORE RESISTANT SYSTEMS	MORE RESISTANT SYSTEMS
Ni-Cr, Co-Cr, Fe-Cr alloys, Co-Cr-Al, Fe-Cr-Al alloys, Ni-Cr-Al alloys with Al concentrations of 10-12%. Ex. Co-20Cr-12Al-0.5Y	Ni-Cr, Co-Cr, Fe-Cr alloys, Co-Cr-Al, Fe-Cr-Al, Ni-Cr-Al alloys with Al concentrations of 10-12%. Ex. TD NiC, X-40, HA-188, HAST-X, 304 SS, CoCrAlY coatings.	IN 738, HA-188, HAST X	High chromium alloys, Silica formers (Hot pressed Si_3N_4).
PROCEDURE FOR INHIBITING ATTACK	PROCEDURE FOR INHIBITING ATTACK	PROCEDURE FOR INHIBITING ATTACK	CONTRIBUTORY FACTORS
o High Cr, High Cr and Al o No Al in nickel-base systems or well above 10% o If low concentrations of Al are required, replace Ni with Co.	o High Cr o Use Co in place of Ni in alloys with Al concentrations between 1.6% o In Ni-base alloys containing Al, Keep the Al concentrations above 10%.	o High chromium o Lower refractory metal content.	Chloride-induced alloy depletion. Carbon-induced oxygen depletion.
CONTRIBUTORY FACTORS	CONTRIBUTORY FACTORS	CONTRIBUTORY FACTORS	
Chloride-induced alloy depletion. Carbon-induced oxygen depletion.	Chloride-induced alloy depletion (Especially effective for high Cr and Al alloys). Carbon-induced oxygen depletion.	Chloride-induced alloy depletion (HA-188, HAST X extremely susceptible) Carbon-induced oxygen depletion.	

CAPTIONS

Fig. 1.1.1 Schematic diagram to illustrate the conditions that developed during the initiation and propagation of hot corrosion attack and to identify the factors that determine the time at which the transition from the initiation stage to the propagation stage occurs.

Fig. 1.1.2 Schematic diagram to illustrate the three general categories of protective scale breakdown to a lesser protective reaction product when a salt deposit is present during the corrosion process.

Fig. 1.1.3 Schematic diagram for basic fluxing model for hot corrosion of pure nickel.

Fig. 1.1.4 Schematic diagram for Acidic fluxing model for alloy containing Mo, W and/or V.

Fig. 1.1.5 Schematic diagrams to illustrate the hot corrosion attack of a CoCrAlY alloy when SO_3 is present in the gas. At low temperatures solid Na_2SO_4 can be converted to a liquid Na_2SO_4-$CoSO_4$ solution due to the formation of small amounts of CoO.

HOT CORROSION CHRONOLOGY

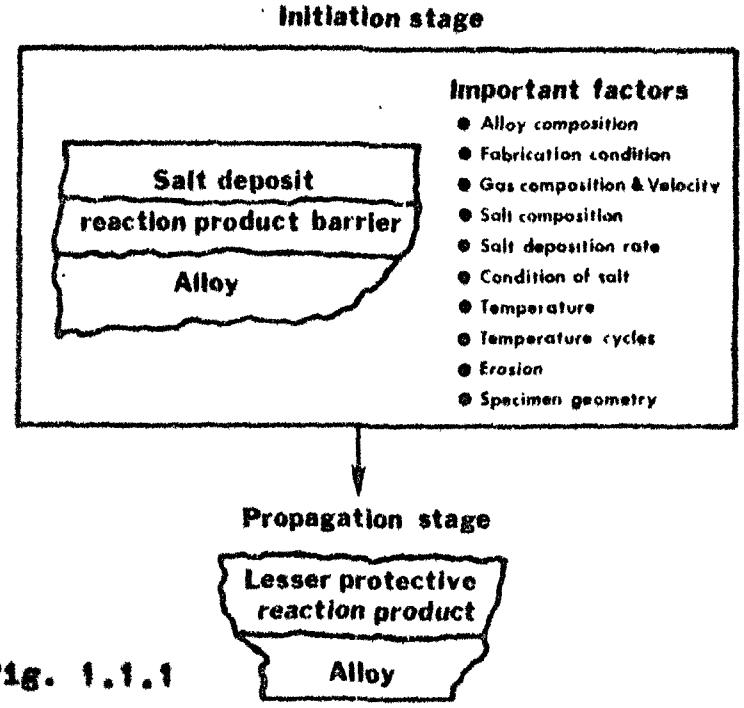

Fig. 1.1.1

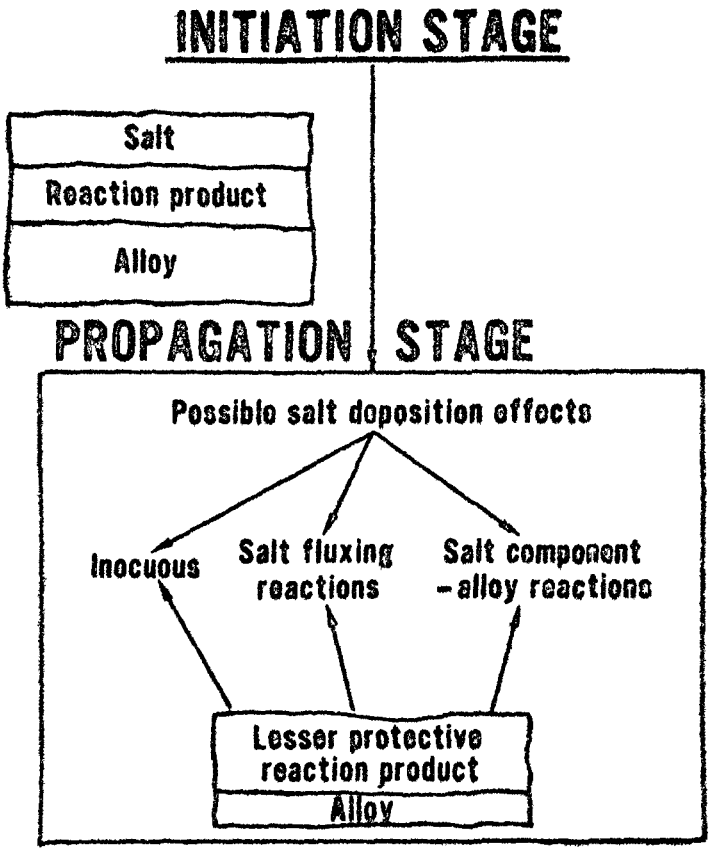
INITIATION STAGE
Salt
Reaction product
Alloy
PROPAGATION STAGE
Possible salt deposition effects
Inocuous
Salt fluxing reactions
Salt component - alloy reactions
Lesser protective reaction product
Alloy

Fig. 1.1.2

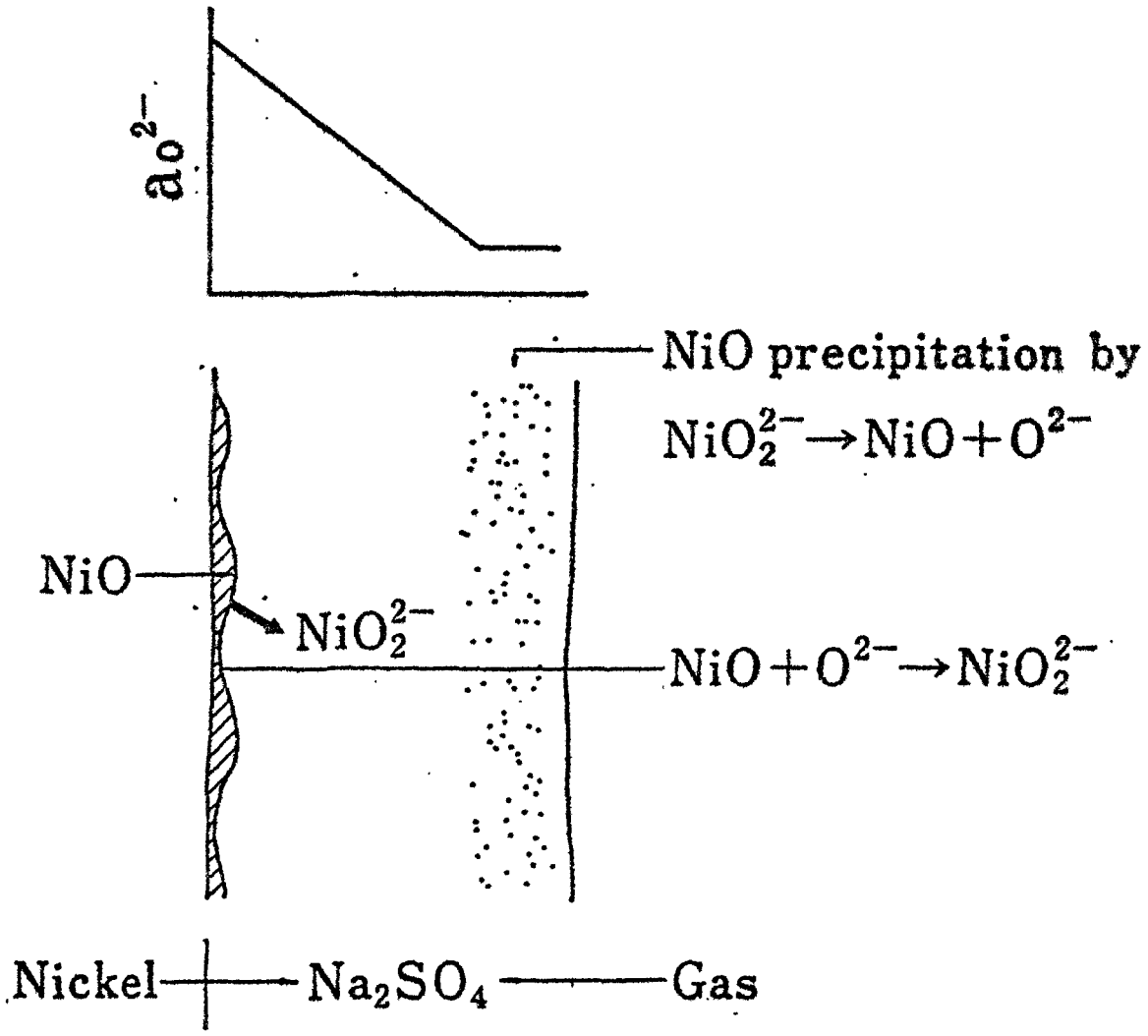
$a_{O^{2-}}$
NiO precipitation by
$NiO_2^{2-} \rightarrow NiO + O^{2-}$
NiO
NiO_2^{2-}
$NiO + O^{2-} \rightarrow NiO_2^{2-}$
Nickel
Na_2SO_4
Gas

Fig. 1.1.3

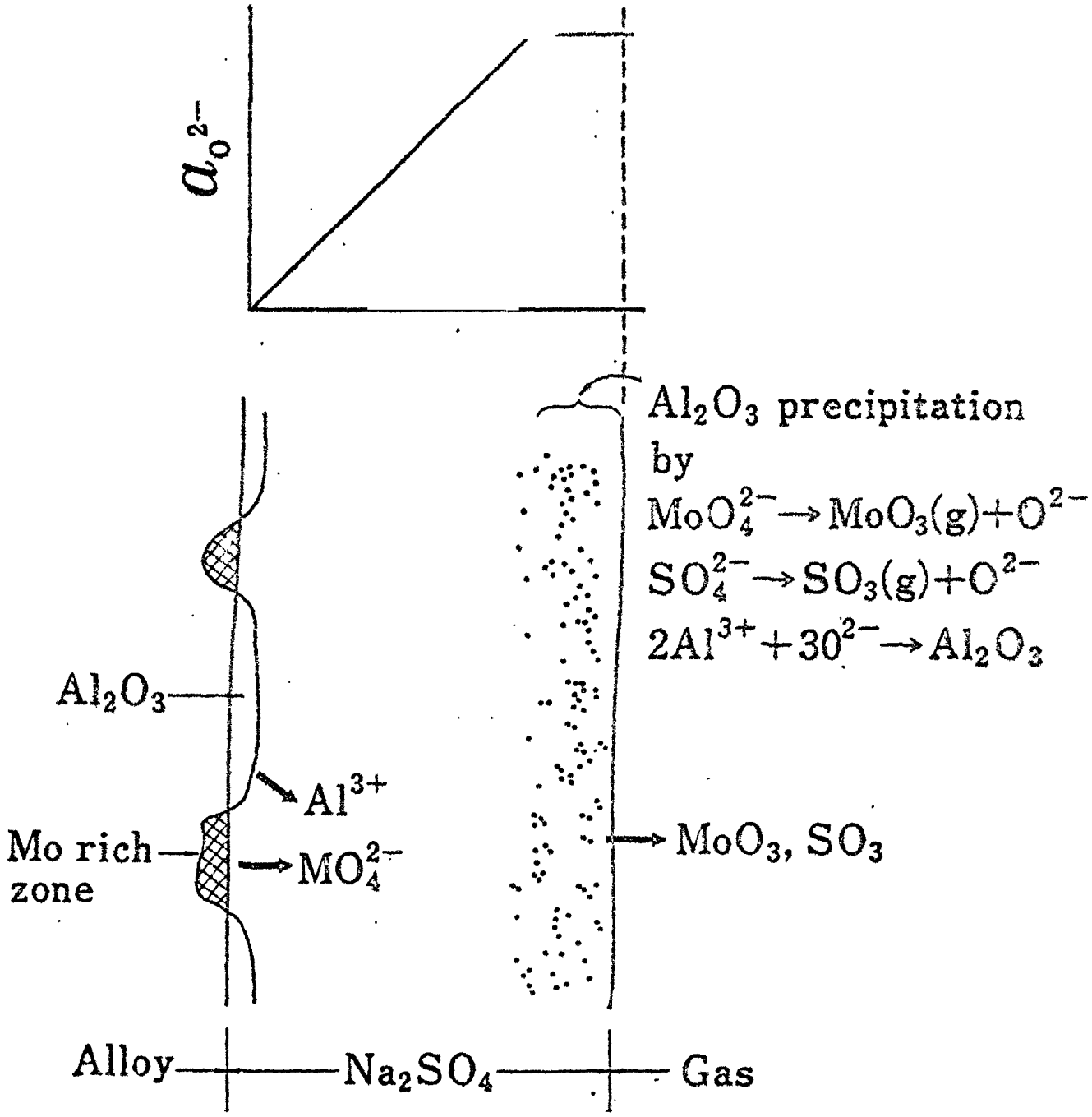
a_{O}^{2-}
Al_2O_3 precipitation by
$MoO_4^{2-} \rightarrow MoO_3(g)+O^{2-}$
$SO_4^{2-} \rightarrow SO_3(g)+O^{2-}$
$2Al^{3+}+3O^{2-} \rightarrow Al_2O_3$
Al_2O_3
Al^{3+}
Mo rich zone
MO_4^{2-}
MoO_3, SO_3
Alloy
Na_2SO_4
Gas

Fig. 1.1.4

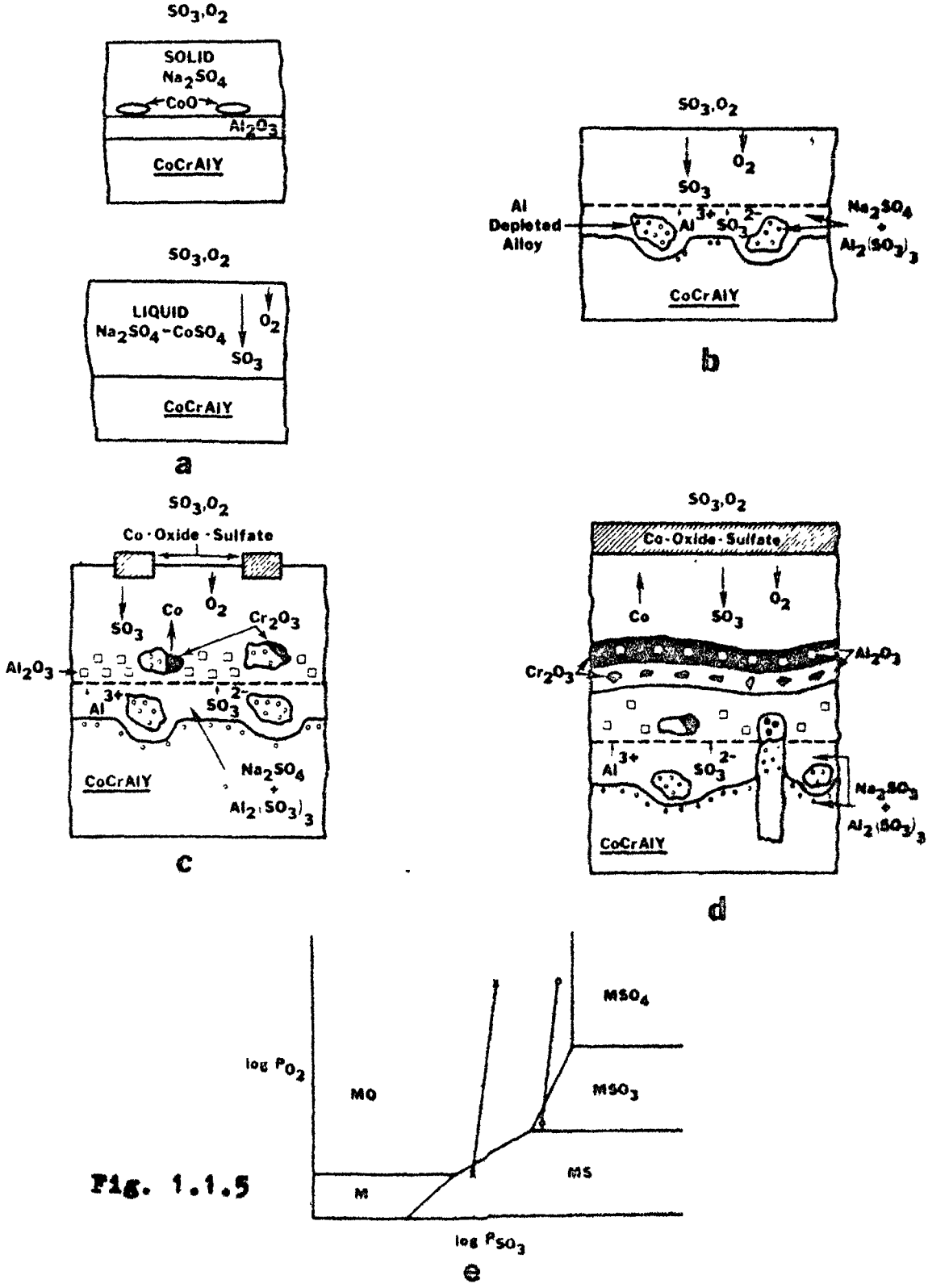
SO_3, O_2
SOLID
Na_2SO_4
CoO
Al_2O_3
CoCrAlY
SO_3, O_2
LIQUID
Na_2SO_4-$CoSO_4$
O_2
SO_3
CoCrAlY
a
SO_3, O_2
Al
Depleted
Alloy
SO_3
O_2
Al^{3+}
SO_3^{2-}
Na_2SO_4
+
$Al_2(SO_3)_3$
CoCrAlY
b
SO_3, O_2
Co · Oxide · Sulfate
SO_3
Co
O_2
Cr_2O_3
Al_2O_3
Al^{3+}
SO_3^{2-}
CoCrAlY
Na_2SO_4
+
$Al_2(SO_3)_3$
c
SO_3, O_2
Co · Oxide · Sulfate
Co
SO_3
O_2
Al_2O_3
Cr_2O_3
Al^{3+}
SO_3^{2-}
Na_2SO_4
+
$Al_2(SO_3)_3$
CoCrAlY
d
MSO_4
MSO_3
MS
MO
M
$\log P_{O_2}$
$\log P_{SO_3}$
e

Fig. 1.1.5

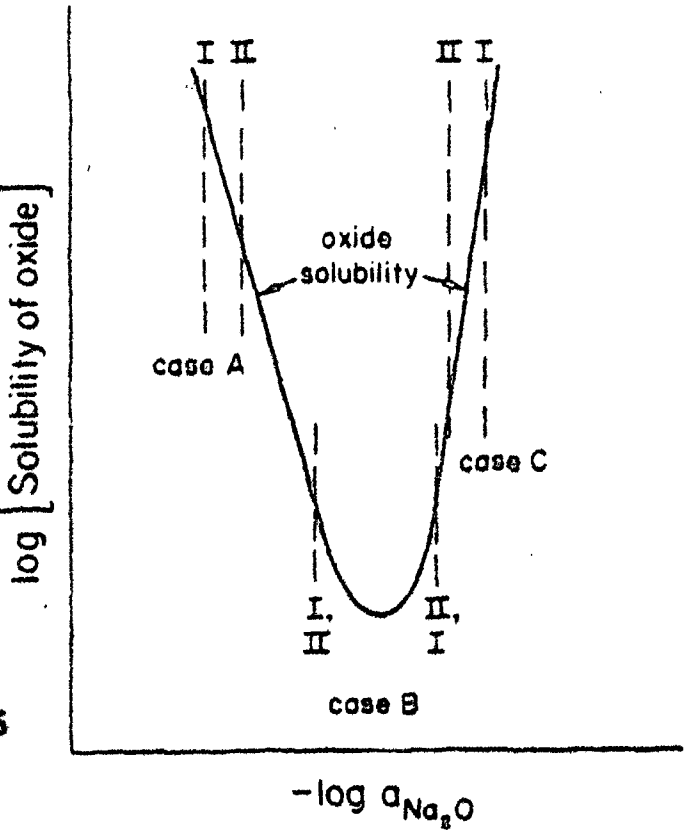
log [Solubility of oxide]
I II
II I
oxide
solubility
case A
case C
I,
II
II,
I
case B
-log a_{Na_2O}

Fig. 1.1.6

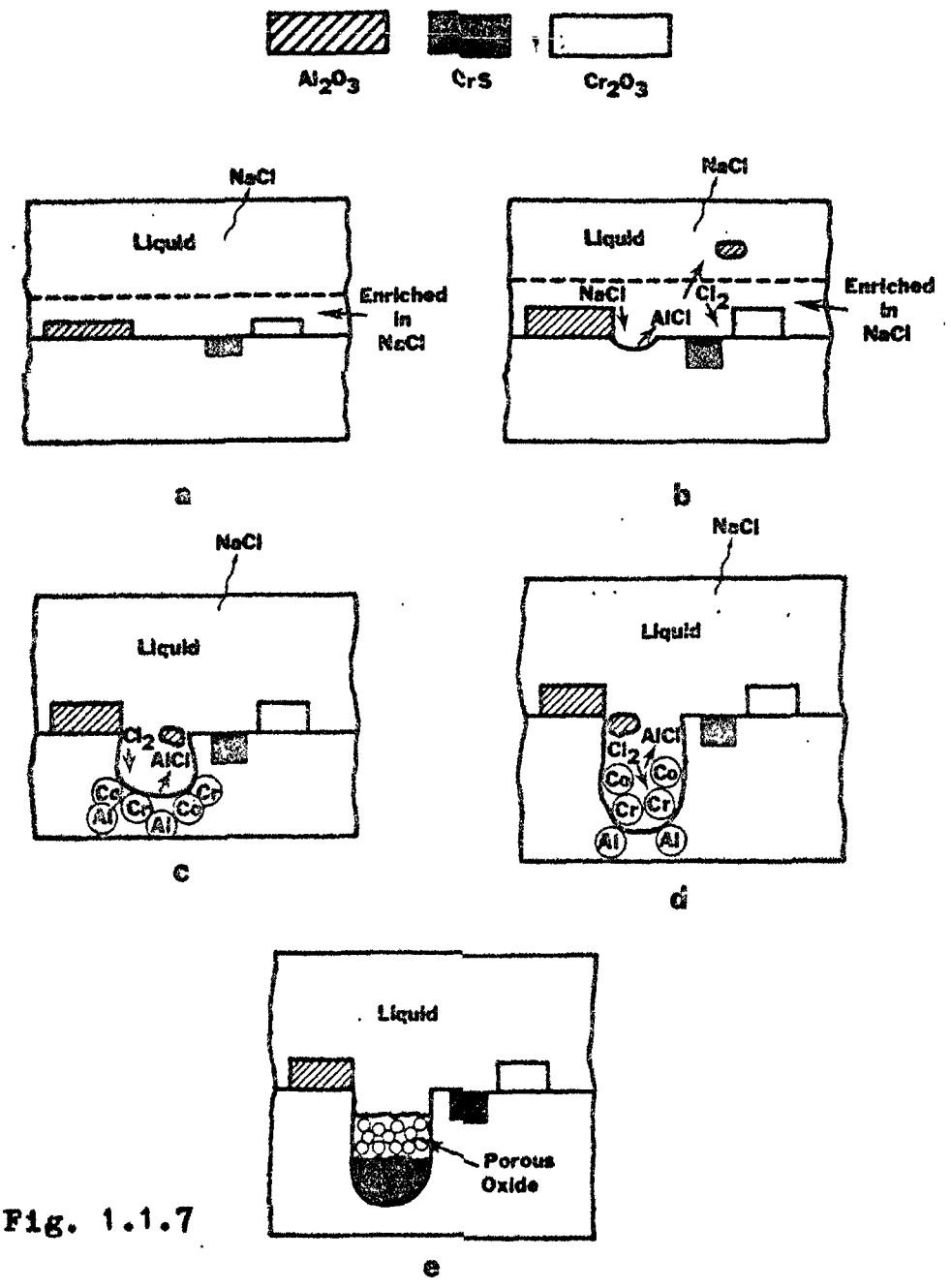
Al_2O_3
CrS
Cr_2O_3
NaCl
Liquid
Enriched in NaCl
a
NaCl
Liquid
NaCl
Cl_2
AlCl
Enriched in NaCl
b
NaCl
Liquid
Cl_2
AlCl
Co
Cr
Al
c
NaCl
Liquid
AlCl
Cl_2
Co
Cr
Al
d
Liquid
Porous Oxide
e

Fig. 1.1.7

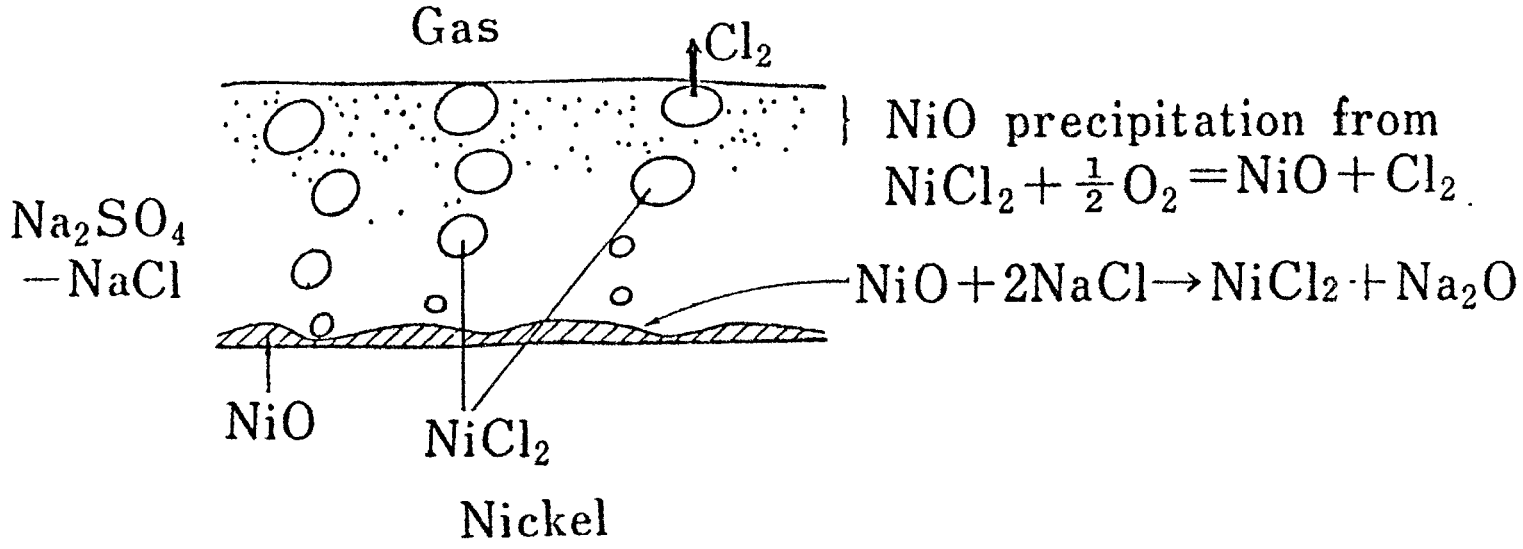
Gas
Cl_2
Na_2SO_4
$-NaCl$
NiO
$NiCl_2$
Nickel
NiO precipitation from
$NiCl_2+\frac{1}{2}O_2=NiO+Cl_2$
$NiO+2NaCl\rightarrow NiCl_2+Na_2O$

Fig. 1.1.8

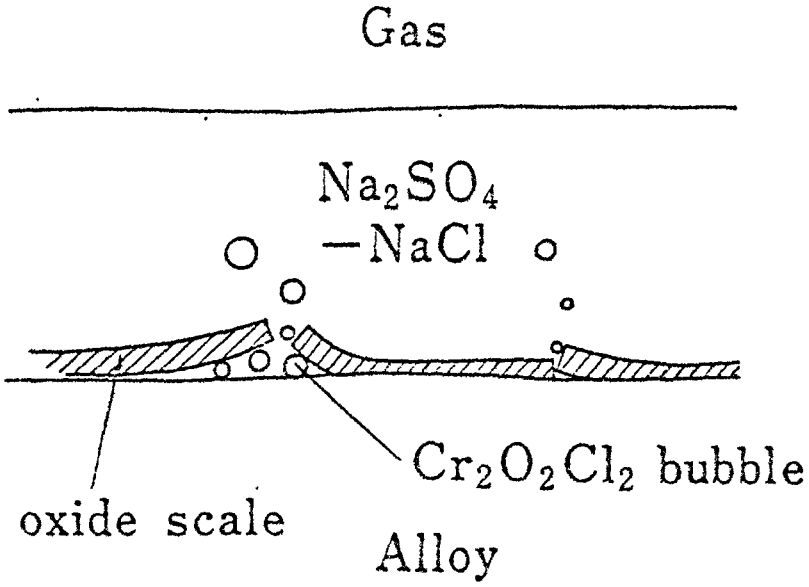

Fig. 1.1.9

CHAPTER I

GENERAL INTRODUCTION: Part II

SOME ASPECTS OF THE OXIDATION BEHAVIOUR OF IRON-BASE ALLOYS

1.2.1 Oxides of iron

Iron is unique amongst the metals to form multioxides scale when subjected to oxidation at high temperatures.

As shown by the Hansen[1] iron-oxygen phase diagram (Fig. 1.2.1), in oxydizing atmosphere and temperature above 560°C iron forms three oxides. The lowest valency oxide, FeO, also called wustite has a NaCl type cubic lattice and is metal deficient having 5-12% iron valencies. Being cation conducting it grows entirely by the diffusion of iron and forms innermost scale layer. Fe_3O_4, magnetite, has a spinel type structure and is an excess oxygen compound and grows largely by oxide ion diffusion with an appreciable contribution from iron ion diffusion (12%). Fe_2O_3, hematite, the highest valency oxide is in contact with atmosphere and has a rhombohedral crystal structure. It is slightly oxygen deficient, metal excess, and largely grows by oxide ion diffusion.

The relative percentage of FeO, Fe_3O_4 and Fe_2O_3 in the scales varies with temperature, duration of oxidation and the nature of the oxidizing gas. However, above 600°C FeO is the predominant species. Due to the formation of the

multilayered scales containing different oxides, the mechanism of oxidation is not simple and requires several mechanistic approaches at various stages of oxidation.

1.2.2 Parabolic scale growth

In the oxidation of pure metals at high temperatures to form a single-product oxide phase, the rate of growth is controlled by ionic diffusion over defect sites in the scale if the following conditions are satisfied:

(i) the scale is microscopically dense;

(ii) the scale exhibits predominant electronic conduction, and

(iii) the scale adheres uniformly to the metal.

If these conditions are met, the rate of oxidation of a pure metal should be parabolic with respect to time, and the oxidation rate should fit each of several differential and integration equations commonly given in the literature. The diffusional growth of this type of scale can be further analysed using the most practical form of Wagner's theoretical parabolic rate constant.

$$I \qquad K_p = \gamma 2 \int_{P_{O_2}(m)}^{P_{O_2}(g)} \left(\frac{Z_a}{Z_a} D_c^* + D_a^*\right) d\,(\ln P_{O_2})$$

where Z_c and Z_a are the valencies of the cation and anion

in the scale, respectively. D_c^* and D_a^* are their selfdiffusion coefficients and $P_{O_2}(g)$ and $P_{O_2}(m)$ are oxygen activities at the gas/scale and metal/scale interfaces, respectively. For FeO and to some extent Fe_3O_4, $D_a^* \ll D_c^*$ and for Fe_2O_3, $D_a^* \gg D_c^*$. The measured and calculated values of the parabolic rate constant for the oxidation of iron to wustite were found to be in good agreement as shown in the table 1.2.1[2].

A diffusional model for the mechanism of multilayered growth of scale involving outward migration of iron through cation vacancies in wustite and magnetite layers and inward migration of oxygen through the anion vacancies in the external layer was proposed by Hauffe[3] (Fig. 1.2.2).

1.2.3 Diffusional scale growth

Diffusion in the superficial scale and metal substrate often determines the reaction rate controlling processes during oxidation of an alloy at elevated temperature. In 1969, Wagner[4] derived equations for metal diffusion through oxide or sulfide scales which described the parabolic oxidation rate, the composition and activity profiles in the solid phases as depicted in the model shown in fig. 1.2.3. He expressed the flux of metal A and B by ambipolar diffusion relative to the oxide sublattice. Upon expressing the metal activities in terms of the oxide acti-

vities, a_{AO} and a_{BO}', and the oxygen activity a_O' the metal flux is related to the scale growth by

$$\text{II} \quad D_A(1-\varepsilon)\left(\frac{-\partial \ln a_{AO}}{d}\frac{d\varepsilon}{dy} + \frac{Z_A}{Z_O}\frac{Z_A\, d\ln a_O}{dy}\right) +$$

$$D_B\left(\frac{-\partial \ln a_{BO}}{d\varepsilon}\frac{d\varepsilon}{dy} + \frac{Z_B}{Z_O}\frac{d\ln a_O}{dy}\right) = K$$

Here, the symbols D, a, ε, Z refer to an appropriate metal self diffusion coefficient, activity, composition and valency respectively, where $y = X/X_s$ is the fractional distance within the scale and K is parabolic rate constant. If the continuity condition is applied to Eq. II, the second order differential equation

$$\text{III} \quad yK\frac{d}{dy} = \frac{d}{dy}\; D_B\left(\frac{\ln\; BO}{d}\frac{d}{dy} - \frac{Z_B}{Z_O}\frac{d\ln\; O}{dy}\right)$$

is obtained to describe the metal distribution in the scale. Several auxiliary equations can be used in the numerical analysis. Values for $(d\varepsilon/dy)_y = 1$ are estimated from a mass balance at the scale/gas interface and the ratio of metal fluxes in the scale at $y = 0$ equals the metal atom ratio in the alloy when diffusion in the alloy is the slowest process.

This phenomenological diffusion model describes growth of the turnary oxide solution scale on a binary alloy

if the cation diffusivities in the oxide, D_A and D_B, are known as functions of composition, and oxygen activity, a_O. The parabolic oxidation rate constant K, ξ and a_O as a function of the scale dimensionless parameter, y, and N_B, as a function of the metal distance parameter, λ, can be calculated from Eq. II and III.

1.2.4 Effect of scale cracking

Burce and Hancock[5-7] demonstrated occurrence of cracking during oxidation. It was found that while the oxide layer on iron cracks continually, the scale on nickel remains intact. The observed deviation from parabolic rate law during the oxidation of iron has been attributed to the loss of contact between the metal and oxide layers since this always disturbs the $FeO:Fe_3O_4:Fe_2O_3$ ratio of the scale and can be recognised by an increase in Fe_3O_4 and Fe_2O_3 contents. The separation of the oxide layer from the metal core is also influenced by the structural state of the iron.

Rahmel[8] suggested a modification in the oxidation mechanism proposed by Hauffe[3] since all the oxidation mechanism proposed by Hauffe could not be explained by diffusion through lattice defects. He proposed that besides migration of oxygen via oxygen ion vacancies and migration of iron ions via interestitial sites there is a possibility of oxygen via dislocation pipes or cracks. The scheme is

schematically represented in figure 1.2.4.

Several other mechanisms relating to the removal of contact between the metal and the scale have been suggested[5,6,9].

1.2.5 Oxidation of iron base alloys

It has already been mentioned that wustite appears as thermodynamically stable phase at temperatures above 560°C. Due to highly defective structure of wustite it grows very rapidly on iron surface via outward diffusion of iron ions. The appearance of wustite phase in the scale gives rise to a marked deterioration in the protective properties of scales on iron. It follows that one of the first measures to improve scaling resistant properties of iron base alloys is the creation of conditions restricting the growth of wustite phase. Therefore, practical applications of iron at temperatures above 500°C, demands the presence of an alloying element which has a higher oxygen affinity than iron and where oxide grows at a slow rate. Generally, Cr or in some cases Al or Si serve this purpose, and when present in sufficient concentrations, protective scales of Cr_2O_3, Al_2O_3 or SiO_2 are formed exclusively.

Studies relating to enhancement of the oxidation resistance of steels by the addition of more than 5 wt.% Al and more than 12 wt.% Cr has been carried out[10-12].

Recently, it has been shown that small amounts of Al and Cr in low alloy steels could enhance the oxidation resistance of oil refinery materials. Huang and Zhu[13] have carried out some kinetic experiments on oxidation of low alloy steels containing Al and Cr additions in the temperature range of 700-850°C. These investigators found a shift in the temperature of wustite function to the higher side as a result of alloying element additions accompanied by an enrichment of the elements on the surface of the steels. This probably is the main reason in the improvement of oxidation resistance of steels.

1.2.6 Internal oxidation

The classical description of internal oxidation defines general precipitation of the oxide of the selectively oxidised alloy elements as small polyhedral or acicular particles at a volume fraction small enough not to interfere with diffusion. The kinetics for inward migration of the reaction front are parabolic and the theoretical treatment of Wagner[14] is commonly invoked wherein the parabolic rate constant is expressed in terms of the oxygen and metal diffusivities and boundary value compositions. However, sometimes several other types of precipitation modes operate which supresses the general precipitation.

One mode of internal oxidation encompasses cellular

and discontinuous precipitation whereby the oxygen saturated parent alloy phase (α) decomposes to the solute-depleted but structurally identical phase (α') and an oxide precipitate phase (β). That is, $\alpha \longrightarrow \alpha' + \beta$ by growth of parallel $\alpha' + \beta$ lamellae into α. In discontinuous precipitation, lateral segregation of the alloying element occurs by diffusion along a boundary separating α' from α. Another mode involves eutectic or eutectoid decomposition whereby the oxygen supersaturated liquid or solid parent phase (γ) transforms into two new phases ($\alpha + \beta$). Thus, $\gamma \longrightarrow \alpha + \beta$ by growth of parallel lamellae of two oxides into the γ phase.

A criterion to define the limiting alloy composition for prevention of depletion of the alloying element by internal oxidation is of significant importance when considering oxidation of heat-resistant alloys. Wagner[15] has placed forward the following criterion: internal oxidation occurs if diffusion causes the product of the metal and oxygen concentrations to exceed the solubility product of the oxide at a distance in the alloy behind the scale/alloy interface.

Analysis of the internal oxidation problem by concepts of ternary diffusion is of recent origin and it is thus only now being applied. Lesychyn[16] has investigated

the transition from internal to external oxidation for Ag-Zn alloys.

1.2.7 Effect of sensitisation on the corrosion of steels

Some austenitic stainless steels (e.g. AISI-321, 347, 348 etc.) are stabilised with Ti, Nb or Ta. By doing so various phases of austenitic stainless steels such as carbides or intermetallic compounds precipitate when the alloys are held at temperatures between 400°C and 1000°C. Such heat treatments are commonly referred to as aging or sensitization treatments because the precipitates so formed affect the alloys in some of their most valuable properties, e.g. low temperature toughness, stability of the austenitic matrix, intergranular corrosion resistance etc.

Austenitic stainless steels of the 18/8 Cr-Ni type may transform partially to a ferromagnetic phase on cooling to room or lower temperatures after prolonged sensitisation treatments[17-19] or cold working at low temperatures[20]. This ferromagnetic phase when present in large quantities has been shown to have a cubic martensitic crystal structure[21]. This partial martensitic transformation in sensitised austenitic steels has been linked to a depletion in Cr and C of the matrix adjacent to the precipitated Cr-rich carbide particles[17,18]. It is shown in the Schaeffler diagram[22] that a decrease in the Cr and C content in the

Fe-Cr-Ni alloys causes an instability of the austenite with martensite as the transformation product. However, Buehl et al[23] suggested that the martensite transformation in less stable austenitic structures is strain induced and is caused by the stresses set up by a difference in thermal expansion between the carbide and matrix on cooling from the heat treatment temperature. Albritton[24] has shown that the ferromagnetic phase is caused by stresses resulting from carbide precipitation.

Sensitisation of austenitic stainless steels also results in a susceptibility of the alloys to the intergranular attack by certain corrosive media[25-27]. Such a susceptibility is generally explained by a depletion of the matrix in Cr close to the carbide particles. This Cr depleted layer will be rapidly dissolved by corrosive liquids.

Other hypotheses to explain the susceptibility to intergranular attack have been suggested, e.g. that the preferential attack is caused by the local strain fields around the precipitate[28], or is due to an electrochemical reaction between precipitate and matrix and governed by the distribution[29,30] and morphology[31,32] of the carbides. Precipitation of intermetallic phases, however, does not appear to affect intergranular corrosion resistance[33]. Improvements in the intergranular corrosion resistance of

austenitic stainless steels were claimed to have been achieved by thermomechanical pretreatments resulting in uniformly dispersed particles of sigma-phase[34].

Recently, a detailed study[35] has been carried out on the effect of sensitisation on the Na_2SO_4-induced hot corrosion of stainless steels in the temperature range 600-900°C. Below 750°C, formation of $NaCrO_2$(s) in the scales is presumably the most important factor responsible for enhanced oxidation rates of 18-8 Cr-Ni austenitic steel and 303 unsensitised steel. These steels provide unrestricted supply of Cr^{3+} ions till all the Na_2O is consumed whereas in sensitised steels due to lower flux of Cr^{3+} ions, formation of $NaCrO_2$(s) is restricted. At higher temperatures (above 750°C), when Na_2SO_4 is molten, increased S-activity results in the formation of alloy component sulfides beneath the oxide layer in the order of decreasing priority: Cr_2S_3 > CrS > FeS > Ni_3S_2 > NiS, this permits increased salt basicity to allow dissolution of protective oxide near the oxide/salt interface to form $NaCrO_2$, Na_2CrO_4, $NaFeO_2$ etc, the latter precipitate into respective oxides at the low basicity region of salt/gas interface to form nonprotective scales. After the salt is exhausted, it is the sulfide and cationic species that diffuse out and get oxidised. In sensitised steels subsequent internal sulfidation is restricted. The above mechanism was found in

confirmity with the thermodynamic predictions.

1.2.8 Hot corrosion of iron-base alloys

Inspite of extensive use of iron-base alloys in power generating units and petroleum refinary plants and possible applications in coal gassifiers or liquifiers only a limited references are available on the studies relating to their hot corrosion behaviour[36-39]. For example, the alloy components of the power generating units come into contact with gaseous species such as O_2, CO, CO_2, SO_2 etc. and/or fluel contaminants in ash slags or other deposits which might collect on the hot metal surface producing accelerated corrosion. Detailed mechanistic studies have been reported on Ni- and Co-base alloys under above mentioned corrosive environments but such studies are lacking in iron-base alloys[40]. Addition of Cr or Al does improve the high temperature corrosion resistance of steels, however, presently the iron-base alloys found suitable only at the lower end of supper alloy applications due to rapid decline in strength above 650°C.

Hot corrosion of iron-base alloys occurs under Na_2SO_4 alone and the addition of NaCl to sulfate deposits has been shown to produce increased corrosive attack. Trafford and Whittle[41] studied Na_2SO_4-induced hot corrosion of Fe-Cr alloys at 900°C. In dilute alloy (5% Cr), after initial

enhanced oxidation, the oxidation rate becomes similar to that of uncoated alloy when limited supply of salt was exhausted. In high Cr-alloys (13 and 18% Cr), Na_2SO_4 coatings markedly enhances the oxidation rates and result in the formation of thick, compact and stratified scales. Formation of sulfides in the alloy substrate and mechanical failure of scales are responsible for enhanced oxidation. Irrespective of chromium contents, the formation of Na_2CrO_4 which is a feature of hot corrosion of Ni- and Co-base superalloys is not found in equivalent iron-base alloys but instead sodium-iron oxide formation (Na_2FeO_2 or $Na_2Fe_2O_4$) occurs invariably in these alloys and is capable of assisting in the corrosion reactions. Effect of Ni and Al additions on Na_2SO_4-NaCl induced hot corrosion of Fe-19Cr and Fe-31Cr was reported by Okanda et al[42]. Fe-19Cr-11Ni and Fe-31Cr-4Ni are violently corroded at 1000°C by forming porous oxide scales of spinel type whereas Fe-31Cr-4Al shows corrosion resistance and form protective oxide film of α Al_2O_3. Ishaq et al[43] studied Na_2SO_4-NaCl induced hot corrosion of Fe-5M-C (M is 5 wt% of Cr, W, V, Nb, Ta, Ni or Si and C is 0, 0.1, 0.4, 0.8 and 1.2 weight%) at 800 and 1000°C. The alloys are severely corroded in presence of the salt mixture albeit Ni and Si containing alloys which are more resistant and show much lower oxidation rates than the corresponding Cr-containing alloys.

Hendry and Lees[44] studied the corrosion behaviour of austenitic stainless steel in molten sulfate deposits consisting of Na_2SO_4-K_2SO_4 mixtures under a simulated fuel gas (N_2 + 15 v/o O_2 + 0.3 v/o SO_2). The deposits were typically those found on superheater tubes in coal-fired power station boilers. Addition of 5-30 m/o $Fe_2(SO_4)_3$ to Na_2SO_4-K_2SO_4 mixtures reduce the melting point from 820°C to below 550°C. Alkali-iron trisulfates are formed which resolidify on heating above 720°C by decomposition of $Fe_2(SO_4)_3$ at low thermodynamic activity. It is suggested that the effect of heat flux and SO_3 potential gradient on the melting behaviour of a superheater deposit could account for the observed "bell shaped" temperature dependence of corrosion rate in the range of 550-750°C. A model is proposed for corrosion by an acid fluxing involving refractory metal alloy elements in the steels. The model offers a quantitative basis for production of fire side corrosion resistance in coal fired boilers.

Presence of V_2O_5 deposits on alloys leads to catastrophic failure due to formation of low melting complex vanadates[45-49]. Recently, Nowak et al[50] reported the effect of V_2O_5 deposits on high temperature oxidation behaviour of various commercial steels which include plain carbon steel, Cr-Mo steels and Cr-Ni austenitic steel at 750°C. Plain carbon steel (ASTM 1030) follows a parabolic rate whereas

the other steels show two distinct kinetic regions. In the first region, the specific weight increases during the first 2.5 hours and then it decreases to a minimum at approximately 7.5 hours. In the second 7.5-50 hours a parabolic law is followed. For the plain carbon steels Fe_3O_4 was initially formed at the V_2O_5/metal interface and coarse $FeVO_4$ particles were gradually precipitated in the molten V_2O_5 and for larger stages of oxidation and external Fe_2O_3 layers was observed. For Cr-Mo ferritic steels, a different oxide scale morphology was observed, α Fe_2O_3 particles were distributed in the outer part of a polycrystalline $FeVO_4$ matrix. For the austenitic stainless steels which oxidise by a very slow rate, a very fine compact inner layer of Cr_2O_3 was observed.

REFERENCES

1. M. Hansen, "Constitution of Binary Alloys", McGraw-Hill, Inc., New York (1958).
2. L. Himmel, R. F. Mehl and C. E. Birchenall, Trans. AIME, 197, 827 (1953).
3. K. Hauffe, Oxidation of Metals, Plenum Press, New York (1965).
4. C. Wagner, Corr. Sci., 9, 91 (1969).
5. D. Bruce and P. Hancock, J. Inst. Met., 97, 140 (1969).
6. D. Bruce and P. Hancock, J.I.S.I., 208, 1021 (1970).
7. P. Hancock, Werkstoffe Korr., 21, 1002 (1970).
8. A. Rahmel, "Fundamental Processes of Metal Oxidation at High Temperatures and their Significance in the Oxidation of Iron, Iron Alloys, Steels, Proc. Inst. Symp. Met. Chem. (1971), Published by I.S.I. (London), pp. 395-401 (1973).
9. B. Chattopadhyay and J. C. Measor, Brit. Corr. J., 4, 216 (1969).
10. S. Mrowec, T. Walec and T. Werber, Oxid. Met., 1, 93 (1969).
11. T. Narita and K. Nishida, Oxid. Met., 6, 157 (1973).
12. W. E. Boggs, Oxid. Met., 10, 227 (1976).
13. Z. L. Huang and R. Z. Zhu, Proc. JIMIS-3, "High Temperature Corrosion of Metals and Alloys", Mt. Fuji (1982), Published by Japan Institute of Metals, 24, 231 (1983).

14. C. Wagner, Z. Elektrochem., 63, 772 (1959).

15. C. Wagner, Corr. Sci., 8, 889 (1968).

16. M. N. Lesychyn, M. Engg. Thesis, McMaster University Hamilton, Ontario, Canada (1980).

17. F. C. Hull and J. Eichelman, Trans. ASM, 45, 77-104 (1953).

18. B. Cina, J. Iron and Steel Inst., 179, 230-239 (1955).

19. E. Dullis and G. Smith, Trans. ASM, 44, 621-642 (1952).

20. P. L. Magonon and G. Thomas, U.C.R.L. 18869, "Structure and Properties of Thermal-Mechanically Treated 304 S.S."

21. P. L. Magonon and G. Thomas, U.C.R.L. 18868, "The Martensite Phases in 304 S.S."

22. A. Schaeffler, Met. Progr., 56, 680 (1949).

23. R. Buehl, H. Hollomon and J. Wulff, Trans. ASME, 140, 368-386 (1940).

24. O. W. Albritton, Corrosion NACE, 24, 389-392 (1961).

25. B. Strauss, H. Schottky and J. Hinnueber, Z. Anorg. Allgem. Chemie, 188, 390-424 (1930).

26. E. Bain, R. Aborn and J. Rutherford, Trans. ASM, 21, 481-509 (1933).

27. C. Stawstorm and M. Hillert, J. Iron and Steel Inst., 193, 77 (1969).

28. A. Kinzel, Trans. ASME, 194, 469-488 (1952).

29. N. Stefanides, Trans. ASM, 19, 742-746 (1931).

30. P. Payson, Symp. "Evaluation Tests for Stainless Steels", ASTM-STP, 93, 175-177 (1950).

31. R. Stickler and A. Vinckier, Trans. ASM, 54, 362-380 (1961).

32. K. T. Aust, Trans. AIME, 245, 2117-2126 (1969).

33. E. O. Hall and S. H. Algie, Met. Rev., 11, 61 (1966).

34. U.S. Patent 3473-973/1969.

35. M. Ishaq, S. Ahmed and A. U. Malik, Proc. JIMIS-3 on "High Temperature Corrosion of Metals and Alloys", Mt. Fuji, Japan (1982), Published by Japan Institute of Metals, 24, 327-335 (1983).

36. W. T. Reid, "External Corrosion of Deposits in Boilers and Gas Turbines", Elsvier, New York (1971).

37. W. T. Reid, "The Mechanism of Corrosion by Fuel Impurities, H. R. Johnson and D. J. Littler (eds.), Butter Worths, London (1963).

38. J. Stringer and D. P. Whittle in "High Temperature Materials and Gas Turbines", P. R. Sahm and M. D. Spiedel (eds.), Elsvier, New York, 283 (1974).

39. J. Stringer, "High Temperature Alloys", Z. A. Forroulis and F. S. Pettit (eds.), The Electrochem. Soc., New Jersey, 513 (1976).

40. J. Stringer, Ann. Rev. Mater. Sci., 7, 477-509 (1977).

41. D. N. H. Trafford and D. P. Whittle, Corr. Sci., 20, 497-530 (1980).

42. Y. Okanda, M. Fukusumi and S. Nenno, Proc. JIMIS-3 on "High Temperature Corrosion of Metals and Alloys", Mt. Fuji (1982), Published by Japan Institutes of Metals, 327-335 (1983).

43. M. Ishaq, "Influence of Carbon on the High Temperature Oxidation and Hot Corrosion Behaviour of Iron-base Alloys", Ph.D. Thesis, A.M.U., Aligarh, March (1982).

44. A. Hendry and D. J. Lees, Corr. Sci., 20, 383 (1980).

45. R. C. Kerby and J. R. Wilson, J. Eng. Power, Trans. ASME, 95, 36 (1973).

46. R. B. Dooley and J. R. Wilson, Trans. ASME, 422 (July 1975).

47. H. D. Philips and C. L. Waggoner, Corrosion, 17, 396 (1961).

48. D. M. Ward and G. L. Swales, "Fuel Ash Corrosion of IN 657 and Heat Resisting Steels in Oil Fired Refinery Furnaces and Boilers", INC Technical Publication, P-BL-377 (1979).

49. G. L. Swales, "High Temperature Corrosion Problems in the Petroleum Refining and Petrochemical Industries", Paper presented at International Conference on High Temperature Alloys in Aggressive Environment Patten (NH) — The Netherlands, Oct. (1979).

50. J. F. Nowak, G. D. Guistina and J. R. Sanoja, Proc. JIMIS-3 " High Temperature Corrosion of Metals and Alloys", Mt. Fuji (1982), Published by Japan Institutes of Metals, 24, 269-278 (1983).

Table 1.2.1: Measured and calculated parabolic rate constants for the oxidation of iron to wustite at 1 atm.

Temperature °C	K_p, $g^2\ cm^{-4}\ sec^{-1}$	
	Experimental, 10^{-8}	Calculated, 10^{-8}
800	5.3	5.3
897	25.0	23.0
983	67.0	59.3

CAPTIONS

Fig. 1.2.1 FeO-Phase diagram.

Fig. 1.2.2 Scheme of the diffusion on processes and phase boundary reactions during the oxidation of iron in oxygen.

Fig. 1.2.3 Temary diffusion model for growth of an oxide scale on a binary alloy[4].

Fig. 1.2.4 Corrected scheme of the diffusion processes and phase boundary reactions during the oxidation of iron in oxygen.

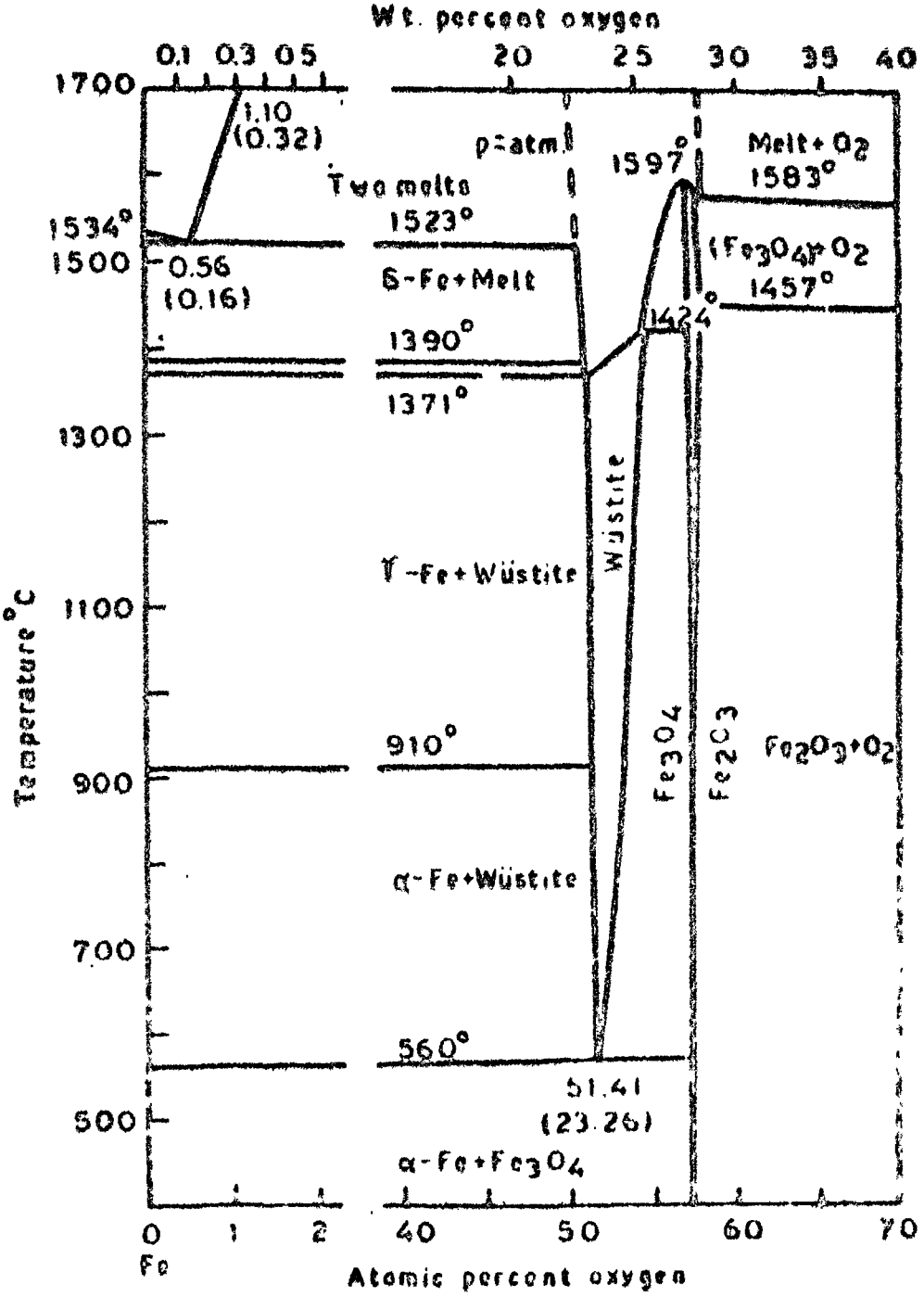
Wt. percent oxygen
0.1 0.3 0.5
20 25 30 35 40
1700
1500
1300
1100
900
700
500
Temperature °C
1.10
(0.32)
p=atm
Two melts
1523°
1534°
0.56
(0.16)
δ-Fe+Melt
1390°
1371°
γ-Fe+Wüstite
910°
α-Fe+Wüstite
560°
51.41
(23.26)
α-Fe+Fe3O4
1597°
Melt+O2
1583°
(Fe3O4)+O2
1457°
1424°
Wüstite
Fe3O4
Fe2O3
Fe2O3+O2
0 1 2
40 50 60 70
Fe
Atomic percent oxygen

Fig. 1.2.1

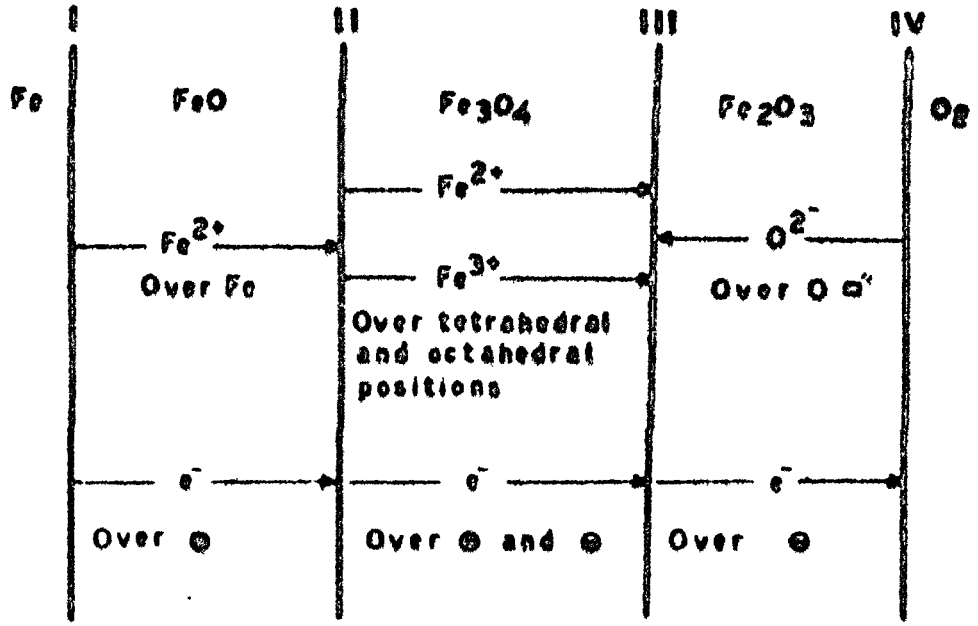
I
II
III
IV
Fe
FeO
Fe_3O_4
Fe_2O_3
O
Fe^{2+}
Fe^{2+}
O^{2-}
Fe^{3+}
Over Fe
Over O a^{2-}
Over tetrahedral and octahedral positions
e^-
e^-
e^-
Over ⊕
Over ⊕ and ⊕
Over ⊕

FIG. 1.2.2

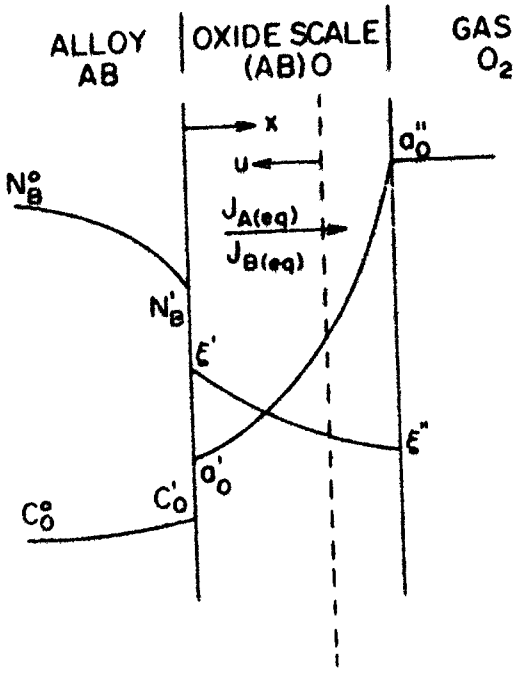
ALLOY
AB
OXIDE SCALE
(AB)O
GAS
O_2
x
u
a_O''
N_B°
$J_{A(eq)}$
$J_{B(eq)}$
N_B'
ξ'
ξ''
a_O'
C_O'
C_O°

Fig. 1.2.3.

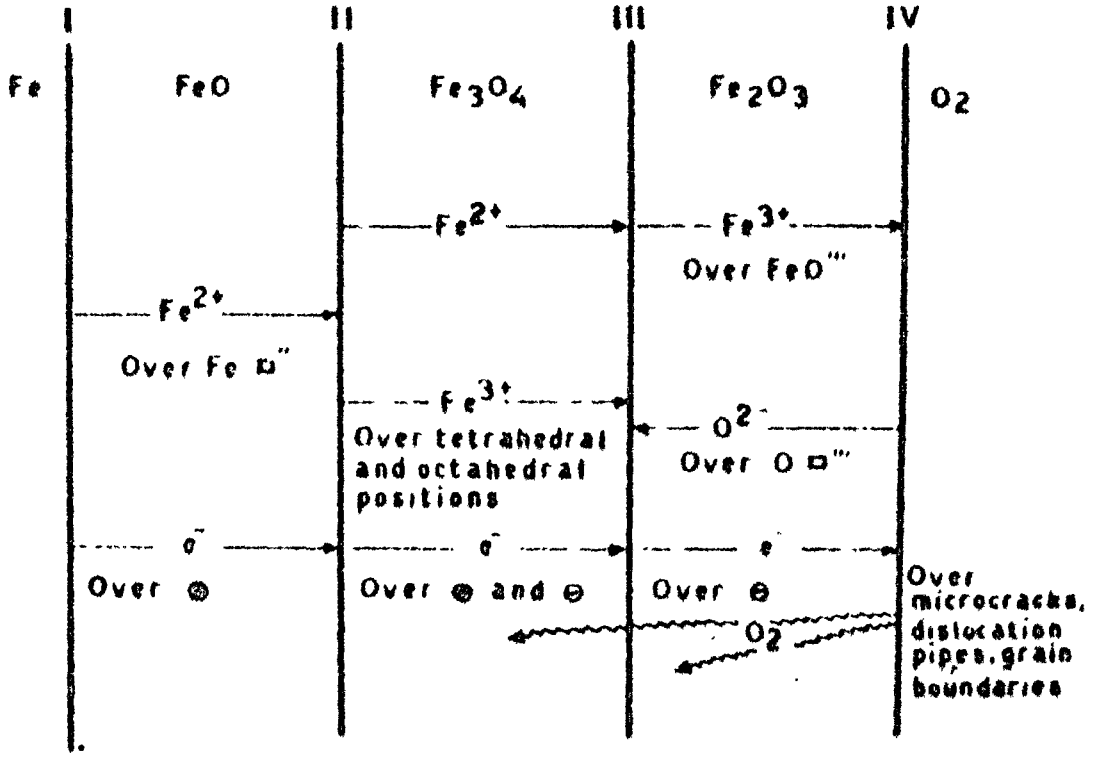
I
II
III
IV
Fe
FeO
Fe_3O_4
Fe_2O_3
O_2
Fe^{2+}
Fe^{3+}
Over $FeO^{'''}$
Fe^{2+}
Over $Fe\,\square''$
Fe^{3+}
O^{2-}
Over tetrahedral and octahedral positions
Over $O\,\square'''$
e^-
e^-
e^-
Over ⊙
Over ⊙ and ⊖
Over ⊖
Over microcracks, dislocation pipes, grain boundaries
O_2

FIG. 1.2.4

CHAPTER - II

HOT CORROSION BEHAVIOUR OF SENSITIZED AND UNSENSITIZED STEELS IN PRESENCE OF SODIUM SULFATE

EXPERIMENTAL

2.1.1 Selection of alloys

High Cr-Ni-steels, viz. AISI-303 (unsensitised) and AISI-321 (sensitised) were chosen for the hot corrosion studies in the presence of Na_2SO_4. Their nominal compositions are given in the table 2.1.

2.1.2 Preparation of the specimens

Specimens of 1.5 cm x 0.5 cm x 0.1 cm size were cut from the sheets of the steels. These specimens were sealed in vacuo in quartz tubes and were annealed at 900°C for 4 hours. The annealed specimens were then abraded sequentially with 180, 320 and 600 grade SiC papers. The polished specimens were washed with water and alcohol and degreased with CCl_4.

2.1.3 Coating of specimens with Na_2SO_4

The alloy specimens were uniformly coated with varying amounts of Na_2SO_4 (1.0 to 15.0 mg/cm^2) by spraying a nearly saturated solution of Na_2SO_4 on specimens previously heated to about 200°C. This provides salt thickness in the range of 5 um to 80 um.

2.1.4 Hot corrosion studies

The hot corrosion studies were carried out in pre-

sence of Na_2SO_4 at 800 and 1000°C, in flowing air. The oxidation runs were usually of 6 hours duration.

The coated alloys were kept in silica boats and weighed, the weighed boats were then transfered to a nichrome wire wound tubular furnace maintained at the desired temperature. The coated specimens were oxidised in a current of air for 6 hours. At the end of the run, the boats were taken out slowly from the furnace, cooled in a desiccator and weighed.

2.1.5 Morphological studies

2.1.5.1 Metallography:

The corroded specimens with adherent scales, were mounted using Araldite as cold setting resin. The mounted specimens were abraded with 180, 320 and 600 grade SiC papers, respectively, using Kerosene oil as the lapping liquid to avoid dissolution of soluble inorganic compounds in the scales. The mounted specimens were then polished on a motor driven disc polisher using sequentially different grades of diamond paste (e.g. 30 μ, 6 μ and 1 μ). The polished specimens were washed with alcohol and finally degreased with CCl_4. The polished specimens were etched in a solution of H_2O_2, HNO_3, HCl and Glycerol, mixed in the ratio of 1:1:2:2, respectively, and examined under a Leitz

Photographic Metallurgical Microscope. The portions of microstructure giving relevent details were photographed.

2.1.5.2 Scanning Electron Microscopy (SEM):

The surface morphology (topography) of the scales and the matrix was studied by using a Scanning Electron Microscope (Model S4-10). The specimens were coated with colloidal emulsion of gold before taking scanning micrograph.

2.1.6 X-ray diffraction analysis

The X-ray diffraction patterns of the scales on the corroded alloys were obtained using a diffractometer assembly. Table 2.2 lists the different constituents identified in the scales of corroded alloys by X-ray diffraction analysis.

RESULTS

The oxidation behaviour of AISI-303 (unsensitised) and 321 (sensitized) steels coated with varying amounts of Na_2SO_4 has been studied at 800 and 1000°C. The studies have been carried out in a current of air for 6 hours.

2.2.1 Hot corrosion studies

At 800°C, there is an increase in weight gain values with increasing amounts of Na_2SO_4 deposited till a maxima is reached, after which there is a decrease in weight gain values with further increase in salt deposition. The sensitized steel, AISI-321 attains maximum weight gain in presence of 4.0 mg/cm^2 Na_2SO_4, on further addition in the amount of Na_2SO_4 deposited there is a sharp decrease in weight gain values, the corresponding value for the unsensitised steel, AISI-303 is 9.5 mg/cm^2 Na_2SO_4. On further increasing the amount of Na_2SO_4 it shows slight decrease in weight gain. Total weight gain observed in the case of 303 is higher than that found in the case of 321 (Figure 2.1).

At 1000°C, unsensitised steel-303 shows higher weight gain than sensitised steel-321 upto 3.5 mg/cm^2 Na_2SO_4, on exceeding this amount of the salt, the sensitised steel-321 shows higher weight gains. Unlike the behaviour shown at 800°C, these steels show continuous increase in weight gain

with the amount of Na_2SO_4 deposited. It appears that amount of salt deposited and weight gain (or oxidation rate) has a linear relationship at 1000°C in both cases (Figure 2.2).

2.2.2 Morphological studies

AISI-303:

Figure 2.3 shows the optical micrograph of a Na_2SO_4-coated steel-303, oxidized at 800°C in air for 6 hours. The inner scales are richer in chromium sulfide with iron sulfide inclusions, and the outer scales contain chromium, iron and nickel oxides, e.g. Cr_2O_3, Fe_2O_3 and NiO. There is evidence of internal sulfidation and chromium seems to preferentially sulfidized. Due to extensive sulfidation the matrix appears to be the part of the scales.

Figure 2.4 shows the micrograph of a cross section of Na_2SO_4 coated steel oxidized at 1000°C in air for 6 hours. Porous sulfide layers of $(Fe,Cr)S_x$ with inclusions of NiS (white) form inner scales, whereas the outermost scales contain Fe_2O_3. There is a depletion of chromium along the grainboundaries and the penetration of the molten salt is quite evident. Figures 2.5a & b show morphological details of the scales and the substrate of steel-303, corroded in presence of Na_2SO_4 at 1000°C. Presence of sulfides in the inner scales and porous thick oxides as outer scales is

indicated along with penetration of the salt along the grainboundaries.

AISI-321:

Figure 2.6 shows optical micrograph of a cross section of 321 steel coated with Na_2SO_4 and oxidised at 1000°C for 6 hours in air. The scales are porous, inner scales perhaps contain sulfospinel $(Fe,Cr)_2S_x$, outer scales comprise of oxides of Fe, Cr and Ni with Fe_2O_3 present in the outermost region. At the alloy/scale interface the alloy is fragmented due to the penetration of the molten salt along the grainboundaries. The micrograph shows the presence of internal sulfide particles in the matrix.

The SEM picture of cross section of steel-321 coated with Na_2SO_4 and oxidised at 1000°C for 6 hours. Figure 2.7a shows the details of the structure of scales at lower magnification, while the figure 2.7b shows the details of the outer region of the scale at higher magnification. The information delivered from SEM studies regarding the morphology of the scales is consistent with that arrived from optical metallography.

Figures 2.8a and 2.8b show clearly the cracking of the scales and profuse internal sulfidation in the matrix of the oxidised alloys.

DISCUSSION

The high temperature oxidation studies carried out on high Cr-Ni- austenitic steels (AISI 303 and 321) shows extensive attack in presence of Na_2SO_4 during a course of a relatively short run of 6 hours. At 800°C, both 303 and 321 steels show increasing weight gains with increasing salt concentration till a maxima is reached in the oxidation curves. This is followed by decreasing weight gain with increasing salt deposition. The oxidation rates of 303 are higher than those of 321 steel.

At 800°C, Na_2SO_4 reacts with the Cr_2O_3 film formed on steels and undergo following types of reactions.

Initially a sulfidation reactions is favoured.

$$\text{I} \qquad Cr_2O_3 + 3Na_2SO_4 \longrightarrow Cr_2S_3 + 3Na_2O + 6O_2$$

With the consumption of sulfur, the oxygen activity increases and Cr_2O_3 is converted into chromate,

$$\text{II} \qquad Cr_2O_3 + 2Na_2O + 3O \longrightarrow 2Na_2CrO_4$$

the II is thermodynamically favoured and Cr_2O_3 is unlikely to be present as a free species in these circumstances.

Na_2CrO_4 dissolves in the melt and due to low activity of O^{2-} at melt/salt interface, is reprecipitated as Cr_2O_3 at the salt/gas interface.

FeO and NiO formed during the oxidation may also undergo following types of reactions:

III $FeO + Na_2SO_4 \longrightarrow FeS + Na_2O + 2O_2$

IV $Na_2O + FeO \longrightarrow Na_2FeO_2$

V $NiO + Na_2SO_4 \longrightarrow NiS + Na_2O + 2O_2$

VI $Na_2O + NiO \longrightarrow Na_2NiO_2$

VII $2FeO + \frac{1}{2}O_2 \longrightarrow Fe_2O_3$

At lower temperature (800°C) the reactions I to VII proceed only to a limited extent and once a compact oxide layer is formed beneath the Na_2SO_4 coating, the oxidation rates fall gradually and Na_2SO_4 acts only as a protective barrier.

At higher temperatures (1000°C) the same mechanism will be followed but aggressiveness of the melt increases with increasing salt deposition. In these circumstances there is continuing increase in corrosion rate with increasing amounts of salt deposition. In addition, the following reactions may also undergo involving direct contact of the alloy with liquidus salt:

VIII $4Cr + 3Na_2SO_4(l) \longrightarrow Cr_2O_3 + 3Na_2O + Cr_2S_3 + 3O_2$

IX $Cr + Na_2O + 3O \longrightarrow Na_2CrO_4$

X $4Fe + Na_2SO_4 \longrightarrow FeS + 2FeO + Na_2FeO_2$

The above reactions are thermodynamically feasible. NiO_2^{2-}, CrO_4^{2-} and FeO_2^{2-} are ultimately reprecipitated as NiO, Cr_2O_3 and FeO (or Fe_2O_3) at the salt/air interface.

Sensitised AISI-321 steel oxidizes at much faster rate than AISI-303 at 1000°C in presence of relatively large amount of Na_2SO_4 deposition. Due to rapid oxidation at this temperature a chromium depleted zone is established in the matrix and TiC is now subjected to be attacked by molten Na_2SO_4

XI $TiC + Na_2SO_4 \longrightarrow TiO_2 + Na_2O + S + CO$

TiO_2 presumably concentrated at the alloy/oxide interface or in the matrix as oxide dispersion. Release of S, CO and Na_2O will result in still further enhancement of corrosion rates.

The Fe-Cr-Ni-O-S superimposed diagrams at 1000 and 1200K (Fig. 4.20 and 4.21) indicate the presence of the species which have been stipulated on the basis of corrosion experiments, optical metallography and X-ray diffraction

analysis. Figure 2.9 shows a schematic representation of the oxidation of austenitic steels in presence of Na_2SO_4.

The hot corrosion of iron-base alloys induced by Na_2SO_4 has been the subject of several investigators[1-4]. The presence of Na_2SO_4 markedly enhances the oxidation rates of iron-based alloys, these results are not different from those obtained in the present studies. Trafford and Whittle[5] studied the oxidation behaviour of chromia forming iron-based alloys at 900°C and attributed the formation of sulfides in the alloy substrate and mechanical failure of scales to the enhanced oxidation. Instead of Na_2CrO_4 (which is a common product during hot corrosion of Na_2SO_4-coated chromia forming Ni- and Co-based alloys), salt/scale reactions proceed with the formation of sodium-iron oxides. In another study[6], the formation of $NaCrO_2$(s) at temperatures below 750°C was found responsible for the enhanced oxidation rates of 18Cr-8Ni unsensitized steels whereas at higher temperatures (above 750°C), the formation of $NaFeO_2$ along with $NaCrO_2$ and Na_2CrO_4 enhances oxidation rates of the alloys. The sensitized steels have comparatively lower oxidation rates.

REFERENCES

1. W. T. Reid, 'External Corrosion in Boilers and Gas Turbines', Elsvier, New York (1971).

2. A. U. Seybolt, Oxidation of Metals, 2, 161 (1970).

3. A. Hendry and D. J. Lees, Corrosion Sci., 20, 383 (1980).

4. Y. Okanda, M. Fukusumi and S. Nenno, Proc. on 'High Temperature Corrosion of Metals and Alloys', (JIMIS-3), Mt. Fuji Japan, p. 327 (Nov. 1982).

5. D. N. H. Trafford and D. P. Whittle, Corrosion Sci., 20, 509 (1980).

6. M. Ishaq, S. Ahmed and A. U. Malik, Proc. on 'High Temperature Corrosion of Metals and Alloys', (JIMIS-3) Mt. Fuji Japan, p. 343 (Nov. 1982).

Table 2.1: Nominal composition of austenitic stainless steels.

AISI Designation	Nominal chemical composition%							
	C	Mn	Si	S	P	Cr	Ni	Other elements
303	0.1	1.5	0.5	0.3	0.15	18.0	8.5	
321	0.08	1.5	0.5	0.025	0.03	18.0	10.0	Ti = 0.5

Table 2.2: Hot corrosion products of steels in presence of Na_2SO_4 at 800 and 1000°C.

Steels	Temperature °C	Hot corrosion products
AISI-303	1000	Fe_2O_3; $FeS.Cr_2S_3$; Cr_2O_3
	800	Fe_2O_3; Fe_3O_4; Cr_2O_3
AISI-321	1000	Fe_2O_3; NiO; $(Fe.Ni)S_2$; Cr_2O_3
	800	Fe_2O_3; NiO; Cr_2O_3

CAPTIONS OF THE PLOTS OF OXIDATION STUDIES

Fig. 2.1 Plots of weight gain versus amount of Na_2SO_4 deposited steel AISI-303 and 321, oxidized at 800°C for 6 hours.

Fig. 2.2 Plots of weight gain versus amount of Na_2SO_4 deposited steel AISI-303 and 321, oxidized at 1000°C for 6 hours.

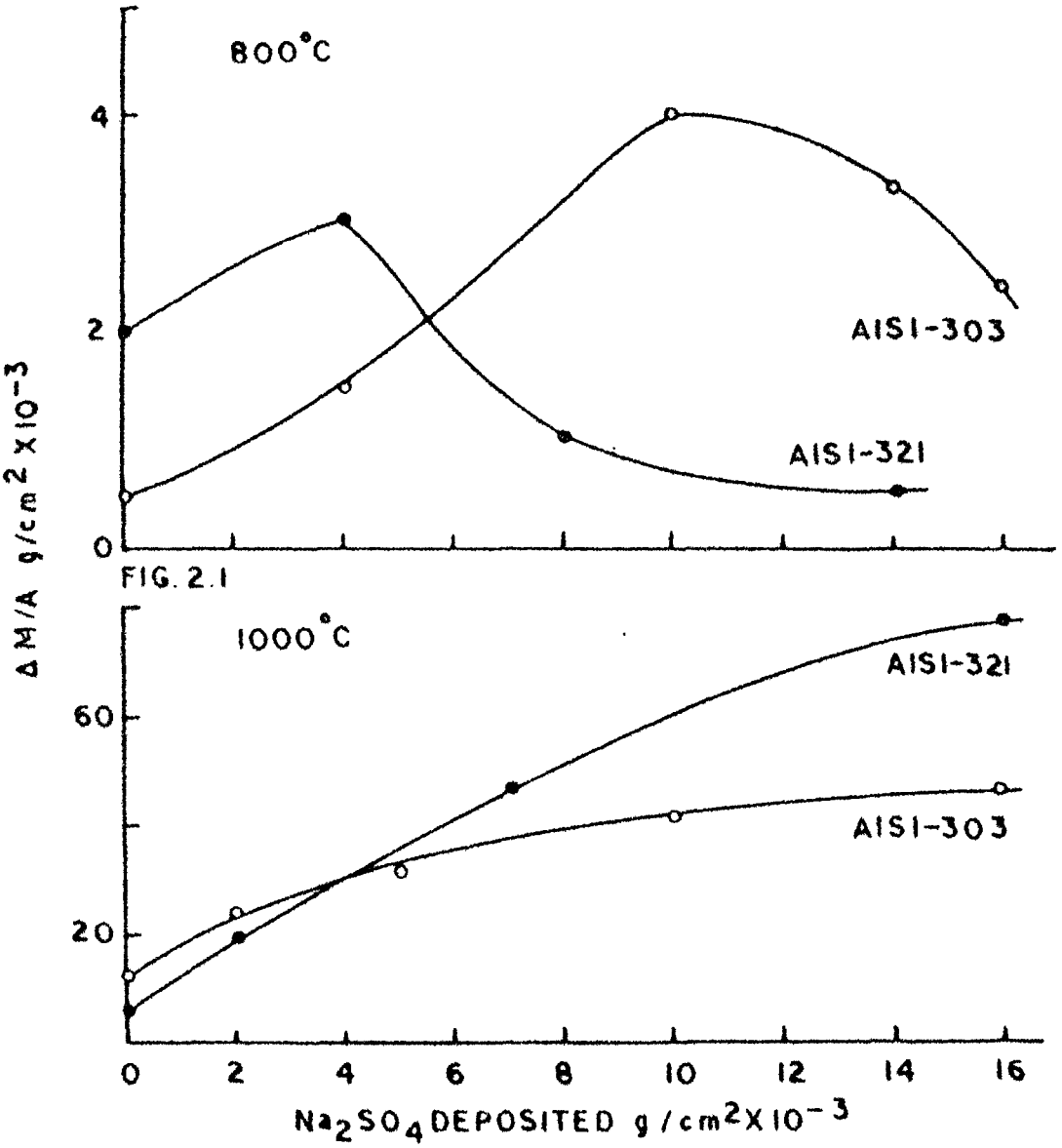
800°C
4
2
0
AISI-303
AISI-321
ΔM/A g/cm² X10⁻³
1000°C
60
20
AISI-321
AISI-303
0
2
4
6
8
10
12
14
16
Na₂SO₄ DEPOSITED g/cm² X10⁻³

FIG. 2.1

FIG 2.2

CAPTIONS OF METALLOGRAPHS

Fig. 2.3 Photomicrographs of AISI-303 steel coated with Na_2SO_4 and oxidized at 800°C for 6 hours.

(400x)

Fig. 2.4 Photomicrographs of AISI-303 steel coated with Na_2SO_4 and oxidized at 1000°C for 6 hours.

(400x)

Fig. 2.5(a & b) Scanning electron micrograph of AISI-303 steel coated with Na_2SO_4 and oxidized at 1000°C for 6 hours.

(a. 150x b. 1000x)

Fig. 2.6 Photomicrograph of AISI-321 steel coated with Na_2SO_4 and oxidized at 1000°C for 6 hours.

(400x)

Fig. 2.7(a & b) Scanning electron micrograph of AISI-321 steel coated with Na_2SO_4 and oxidized at 1000°C for 6 hours.

(a. 55x b. 550x)

Fig. 2.8(a & b) Scanning electron micrograph of AISI-321 steel coated with Na_2SO_4 and oxidized at 1000°C for 6 hours.

(a. 100x b. 520x)

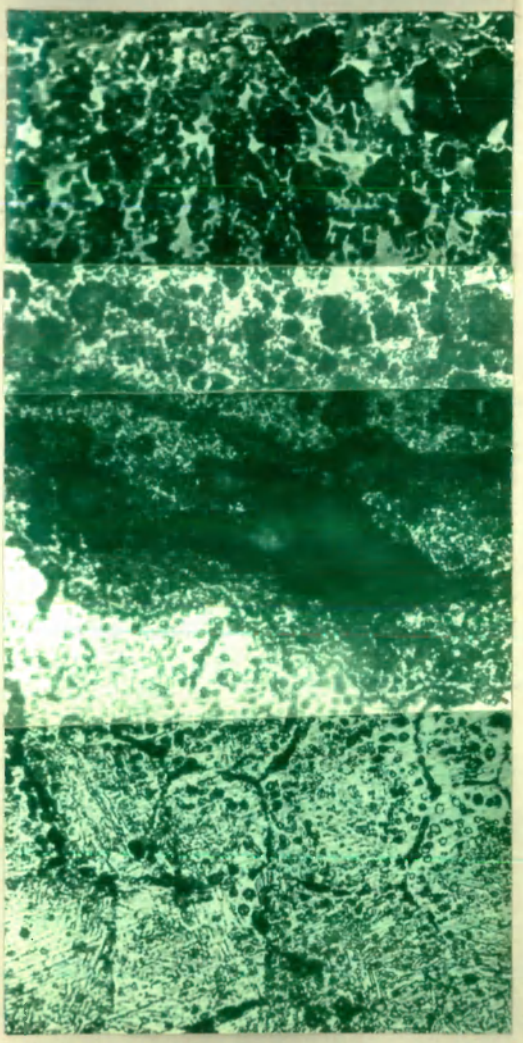

2.3

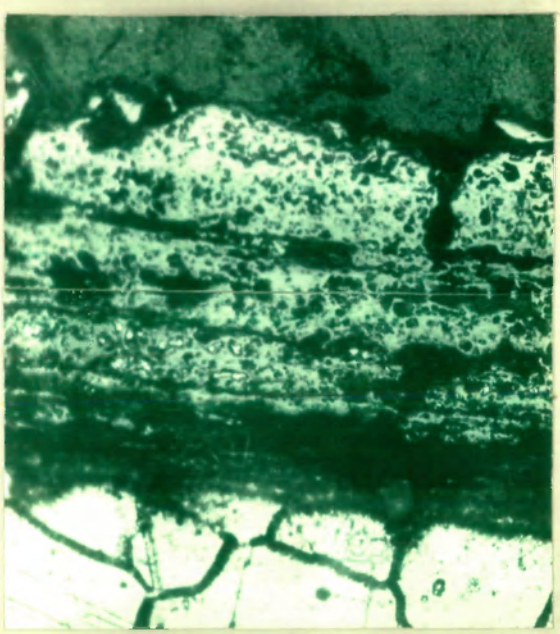

2.4

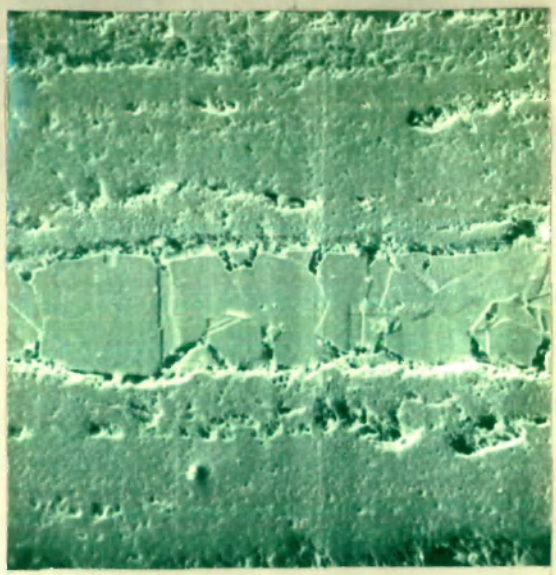

(a)

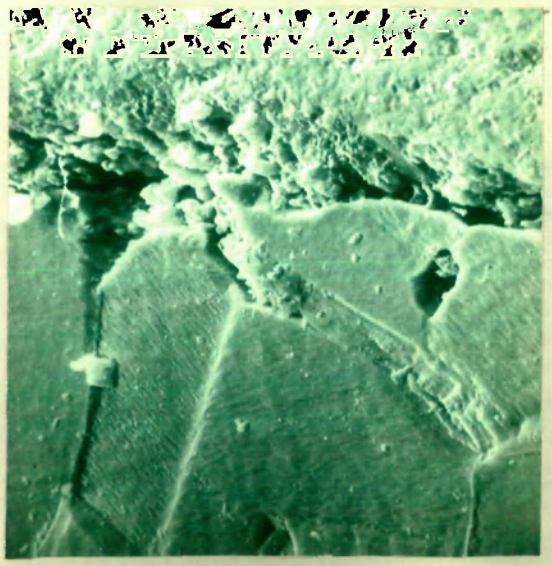

(b)

2.5

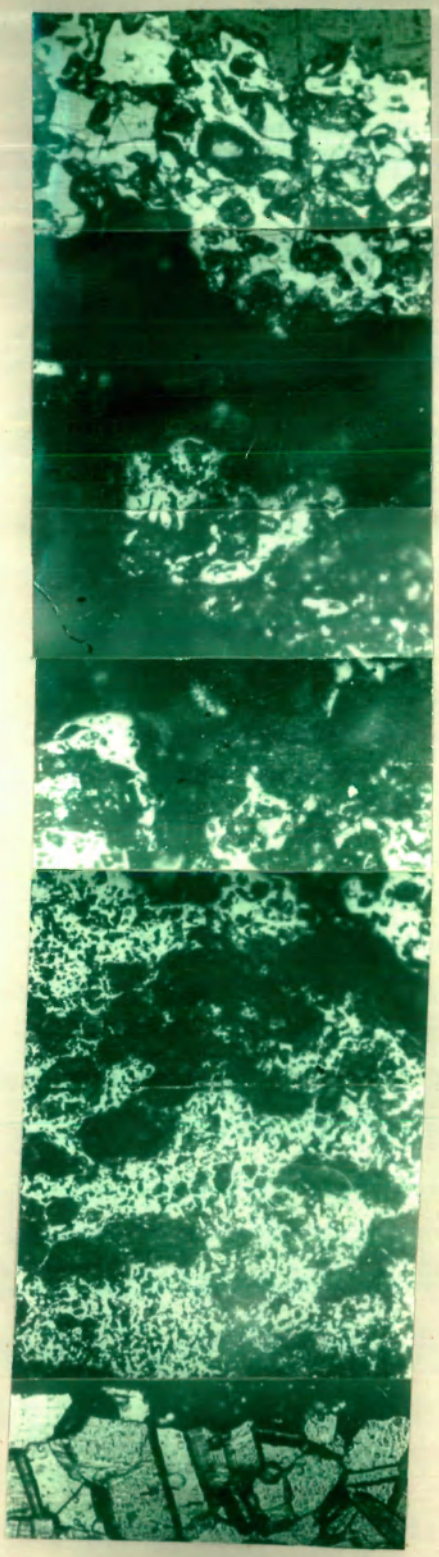

2.6

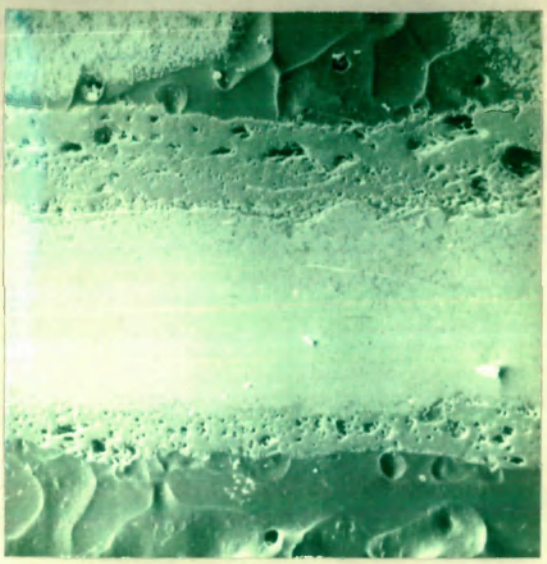

(a)

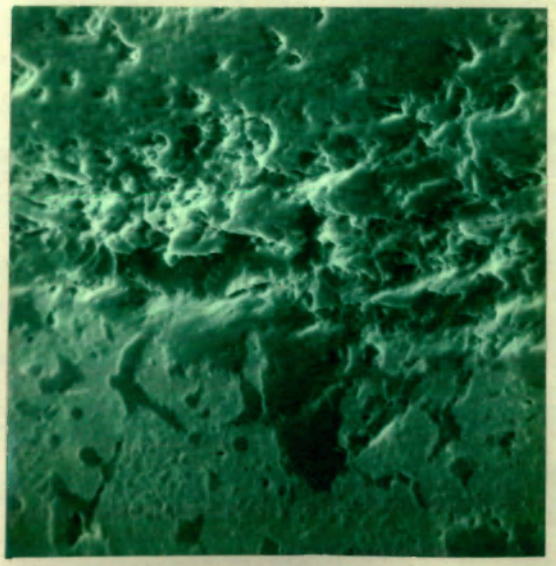

(b)

2.7

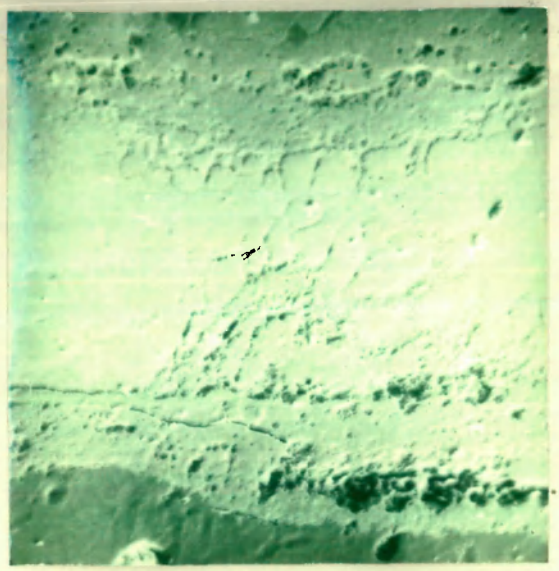

(a)

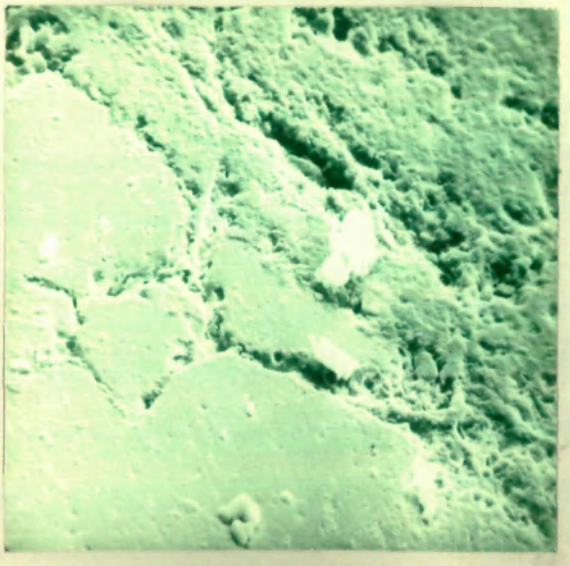

(b)

2.8

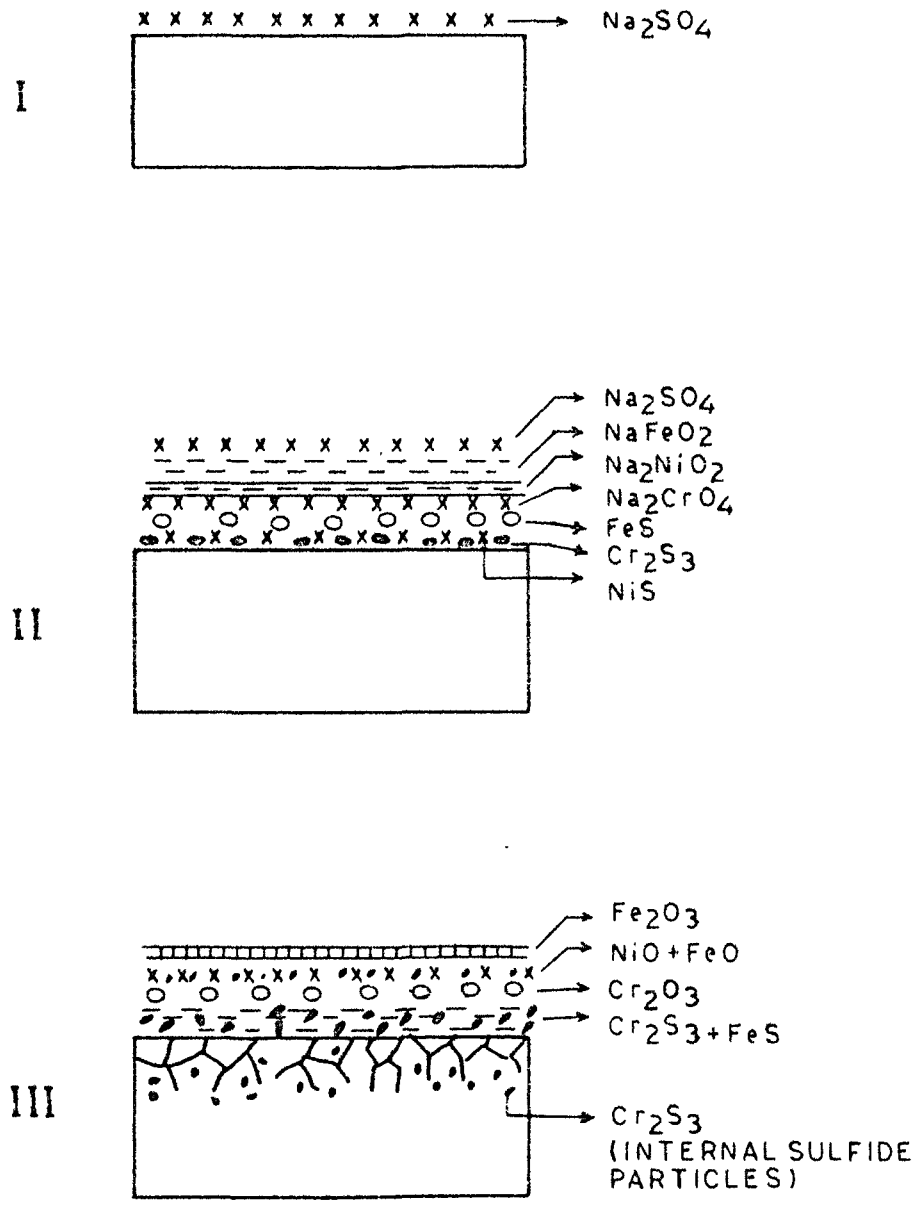

FIG. 2.9 Na_2SO_4-INDUCED HOT CORROSION OF STEEL AISI-303 AND AISI-321 AT 1000°C

CHAPTER III

HOT CORROSION BEHAVIOUR OF AUSTENITIC STEELS IN PRESENCE OF Na_2SO_4 AND TRANSITION METAL SALTS

EXPERIMENTAL

3.1.1 Selection of the alloys

AISI 303 and 321 were chosen for the hot corrosion studies in presence of some transition metal salts or their mixtures with Na_2SO_4. The nominal compositions of the steels are given in the table 2.1.

3.1.2 Preparation of the specimens

Specimens of 1.5 cm x 0.5 cm x 0.1 cm size were cut from the sheets of the steels and annealed at 900°C for 4 hours. Annealed specimens were then abraded sequentially with 180, 320 and 600 grade SiC papers. The specimens were washed with water and alcohol and then degreased with CCl_4.

3.1.3 Coating of specimens with salts and mixtures

Saturated solutions of $NiSO_4$, $CoSO_4$ and $Cr_2(SO_4)_3$ were prepared and polished specimens were uniformly coated with varying thickness of these salts by spraying technique. Other polished specimens were similarly coated with varying thickness of Na_2SO_4 + $NiSO_4$, Na_2SO_4 + $CoSO_4$ or Na_2SO_4 + $Cr_2(SO_4)_3$ mixtures containing 1:2 molar ratio of the salts.

3.1.4 Hot corrosion studies

Hot corrosion studies were carried out at 800 and 1000°C in a current of air. The oxidation runs were usually of 6 hours duration.

The coated specimens were kept in silica boats and weighed. Then these boats were transferred to a tubular furnace maintained at the desired temperature and oxidized in a current of air for 6 hours. At the end of the run, the boats were taken out, cooled in the desiccator and weighed.

3.1.5 X-ray diffraction analysis

The X-ray diffraction patterns were obtained using a diffractometer assembly. Table 3.1 lists the different constituents identified in the scales of the corroded alloys by X-ray diffraction analysis.

3.1.6 Morphological studies

3.1.6.1 Optical metallography:

Corroded specimens were mounted using Araldite as a cold setting resin. The mounted specimens were abraded with 180, 320 and 600 grade SIC papers, respectively, using Kerosene oil as a lapping liquid to avoid dissolution of soluble inorganic compounds present in the scale. The mounted specimens were then polished on a motor driven disc polisher using sequentially different grades of diamond paste (30 u, 6 u and 1 u). The polished specimens were washed with alcohol and dried in hot air blower, and finally degreased with CCl_4. These specimens were then etched and examined under a Leitz Photometallurgical Microscope. Part of microstruc-

tures giving relevent details was photographed.

3.1.6.2 Scanning Electron Microscopy (SEM):

The surface morphology of the scales and the matrix was studied by using a Scanning Electron Microscope (Model S4-10). The specimens were coated with colloidal silver emulsion before taking scanning electron micrographs.

3.1.6.3 Energy Dispersion X-ray Analysis (EDAX):

Elemental distribution within the scale and matrix was determined from EDAX by obtaining Kα concentration profiles using a S4-10 Electron microscope.

RESULTS

3.2.1 Hot corrosion studies

High temperature oxidation behaviour of high Cr-Ni- steels, viz. AISI 321 and 303 were studied in the presence of some transition metal salts, e.g. $NiSO_4$, $CoSO_4$ or $Cr_2(SO_4)_3$ and their mixtures with Na_2SO_4, at 800 and 1000°C for 6 hours.

$NiSO_4$ (Figures 3.1-3.4):

At 800°C $NiSO_4$ coated samples show increase in weight loss on increasing the amount of salt coating. The rate of weight loss is higher in the case of steel 321 than 303. In presence of salt mixtures of Na_2SO_4 and $NiSO_4$, steel 303 and 321 show a steep increase in weight losses upto 3.0 and 7.5 mg/cm^2 of the mixture, respectively. This is followed by a decrease in weight loss values on further increase in the salt deposition. At a salt deposition of about 10.5 mg/cm^2 both the steels show minimum weight losses.

At 1000°C, there is a rapid increase in weight gain with increasing salt/mixture concentration when the salt/mixture deposited is in the range of 6-10 mg/cm^2. On further increasing the amount of salt/mixture the weight gain decreases. Weight gain shown by the sensitized steel-321 is higher than the unsensitized steel-303.

$Cr_2(SO_4)_3$ (Figures 3.5-3.8):

At 800°C both the steels show increase in weight loss with increasing the amount of salt/mixture deposited. Weight loss is higher in the presence of mixture than in the presence of $Cr_2(SO_4)_3$ alone.

At 1000°C in the presence of small amount of mixture (upto 6 mg/cm^2) both the steels show a steep increase in the weight gain. On further increasing the amount of mixture a sharp decrease in weight gain has been observed. But in the presence of $Cr_2(SO_4)_3$ alone these steels show quite opposite behaviour. Upto 6.0 mg/cm^2 of coating a decrease in weight gain has been found, while on further increasing the amount of salt, weight gain increases. In the presence of salt as well as mixture, sensitized steel 321 show higher weight gain than the unsensitised steel 303.

$CoSO_4$ (Figures 3.9-3.12):

At 800°C both the steels show increase in the weight loss with increasing the amount of salt/mixture deposited. At 1000°C oxidation behaviour shown by both the steels is similar to that found in the presence of $NiSO_4$ and $Cr_2(SO_4)_3$ salt and their mixtures with Na_2SO_4, i.e. in the presence of small amount of salt/mixture (5-6 mg/cm^2) there is a steep increase in weight gain, while on further increasing the amount of salt/mixture weight gain decreases.

These results of oxidation studies of steel-321 and 303 in the presence of $NiSO_4$, $CoSO_4$ and $Cr_2(SO_4)_3$ and their mixtures with Na_2SO_4 can be generalised as follows:

(i) At 800°C, both the steels show weight loss which increases with increasing the amount of salt or mixture deposited.

(ii) At 1000°C, in the presence of small amount of salt or mixture (upto 5-6 mg/cm^2) steels show rapid increase in weight gain. On further increasing the concentration of salt or mixture a sharp decrease in weight gain has been observed.

(iii) At 1000°C sensitised steel show higher weight gain than the unsensitised steel.

3.2.2 X-ray analysis

Table 3.1 lists the constituents identified in the scales of 303 and 321 steels oxidised in presence of $Cr_2(SO_4)_3$ $NiSO_4$, $CoSO_4$ or their mixtures with Na_2SO_4 at 800 and 1000°C for 6 hours.

3.2.3 Morphological studies

Figure 3.13 shows an optical micrograph of cross section of the steel-321 coated with a mixture of Na_2SO_4 and $NiSO_4$ and oxidised at 1000°C for 6 hours. The inner layer

which is relatively compact contains the mixture of Cr_2S_3 and FeS with inclusions of some NiS or $NiCr_2S_4$ (white) particles. The middle layer which is porous constitutes a duplex scale of FeO and NiO. Above the porous scale there is a formation of Fe_2O_3 as the outermost scale with the inclusions of NiO (white) and Cr_2O_3 (grey). Along the grainboundaries the molten salt has penetrated causing fragmentation of the matrix.

Figure 3.14 shows a photomicrograph of a cross section of steel-303, coated with $NiSO_4$ and oxidised at 1000°C for 6 hours. The scale comprises three distinct layers: the innermost layer which is compact, contains $FeO.Cr_2O_3$ (spinel), the middle layer which is porous, constitutes FeO and NiO. The outermost layer which is separated from the inner and middle layers, contains Fe_2O_3 with inclusions of NiO (white).

Figures 3.15 and 3.16 show the SEM micrographs of Na_2SO_4-$NiSO_4$ mixture coated steels 303 and 321, respectively. These steels have been oxidised at 1000°C for 6 hours. Figure 3.17 shows the SEM picture of cross section of steel 321 coated with only $NiSO_4$ and oxidised at 1000°C. These pictures show the details of the oxide layers and are in good agreement with the optical micrographs.

Figure 3.18 shows the SEM micrograph of a cross sec-

tion of steel 321, coated with a mixture of Na_2SO_4 + $NiSO_4$ and oxidised at 800°C for 6 hours. There is a formation of a thin scale layer mainly comprised of Cr_2O_3 and NiO. Severe penetration of the molten salt through the grain-boundaries are evident from the picture, which might be due to eutectic formation.

Figure 3.19 shows the photomicrograph of a cross section of steel 321, coated with Na_2SO_4-$CoSO_4$ mixture and oxidised at 800°C for 6 hours. The inner oxide layer contains CoO admixed with Cr_2O_3, and the outer scales are relatively massive and contain Fe_2O_3. SEM picture of the scales has been shown in the figure 3.20.

Figure 3.21 shows the photomicrograph of cross section of steel 321, coated with $CoSO_4$ and oxidised at 1000°C for 6 hours. The inner uneven scales comprise of CoO followed by stratified layers of FeO and Cr_2O_3. The outer layer is predominantly enriched in Fe_2O_3. Figure 3.22 shows the details of the scales.

Figure 3.23 shows a cross section of the steel 321, coated with a mixture of Na_2SO_4-$CoSO_4$ and oxidised at 1000°C for 6 hours. The inner layer of the multilayered scale constitutes Cr_2S_3, middle layer contains a mixture of FeO and CoO and the outer layer contains Fe_2O_3 with grey inclusions of Cr_2O_3. The depletion of chromium from the matrix

results in the dispersion of precipitated cementite, Fe_3C from $(Fe,Cr)_7C_3$.

Figure 3.24 shows a photomicrograph of cross section of steel 303 coated with Na_2SO_4-$CoSO_4$ mixture, and oxidised at 1000°C for 6 hours. The inner layer of the multilayered scales contain Cr_2S_3 followed by thick layer of $CoO.Cr_2O_3$ and FeO.CoO. The outer layers contain Fe_2O_3 with Cr_2O_3 forming the outermost fringe of the scale.

Figure 3.25 represents the photomicrograph of steel-303 coated with $Cr_2(SO_4)_3$ and oxidised at 1000°C for 6 hours. The inner scales contain Cr_2S_3 which is present at the alloy/scale interface. The outer scales seem to contain Fe_2O_3 with Cr_2O_3 inclusions. The alloy is fragmented and presumably some of the sulfur released from the dissociation of $Cr_2(SO_4)_3$ has reacted with nickel to form liquid NiS which is penetrated inside the alloy matrix. Solidified NiS can be observed at a few sites in the matrix. Figure 3.26 shows the SEM micrograph of the scales.

Figure 3.27 represents the photomicrograph and figure 3.28 shows the SEM picture of the cross section of the steel 321, coated with $Cr_2(SO_4)_3$ and heated at 1000°C for 6 hours. The inner scales comprise $Cr_2S_3/FeCr_2S_4$ followed by thicker layers of a mixture of iron and chromium oxides and the outer layers of Fe_2O_3.

Figure 3.29 shows heavy corrosion of the steel 303 coated with a mixture of Na_2SO_4 + $Cr_2(SO_4)_3$ at 1000°C for 6 hours. With deep penetration of salt along the grain-boundaries, the inner stratified scales contain Cr_2S_3 (grey) with FeS/$FeCr_2S_4$ inclusions. The outermost porous layer presumably contain Fe_2O_3. SEM micrograph also shows the penetration of the molten salt causing dissolution of the matrix along the grainboundaries in the steel 303, coated with Na_2SO_4-$Cr_2(SO_4)_3$ mixture and oxidised at 1000°C for 6 hours (figure 3.30).

3.2.4 Energy Dispersion X-ray Analysis

Figure 3.31(a, b, c and d) shows respectively electron image, FeKα , CrKα and NiKα X-ray concentration pictures of steel 321 coated with $Cr_2(SO_4)_3$ and oxidised at 1000°C for 6 hours. The inner scales are relatively thicker and enriched in Cr with considerable inclusions of Fe and Ni. The outer scales are rich in Fe with minor inclusions of Cr.

Figure 3.32 shows the X-ray profiles of Ni, Cr and Fe of Na_2SO_4-$CoSO_4$ mixture coated steel 321, oxidised at 1000°C for 6 hours. The inner scales seem to contain a Cr-rich layer, this is followed by Fe enriched thick scales with inclusions of Cr.

Figure 3.33 shows the X-ray profiles of Ni, Cr and Fe of $Cr_2(SO_4)_3$ coated steel 303, oxidised at 1000°C for

6 hours. The inner scales seem to comprise of Cr with inclusions of Fe, this is followed by Fe enriched outer scales with minor inclusions of Cr.

DISCUSSION

Certain generalisation emerge from the oxidation studies carried out on steels in presence of varying concentrations of transition metal salts, Na_2SO_4 or their mixtures:

(i) At 800°C, 303 and 321 steels show increase in weight gain with increasing Na_2SO_4 concentration till a maxima is reached followed by decreasing weight gain with increasing salt concentration. At 1000°C, however, the oxidation rates continuously increase with increasing Na_2SO_4 deposition (Chapter II).

(ii) At 800°C, steels coated with transition metal salt or its mixture with Na_2SO_4 show relatively heavy weight losses with increasing salt deposition. The weight losses are usually higher in steels coated with salt mixtures than coated with single salt.

(iii) At 1000°C, both steels show increasing oxidation rate with increasing salt (transition metal salt or the mixture) deposition till a maxima is reached, this is followed by weight losses on further increase in salt deposition.

At 800°C, the continued loss in weight with increasing transition metal salt, viz. $Cr_2(SO_4)_3$, $NiSO_4$ and $CoSO_4$

deposition on the steel can be attributed to the fact that inner chromium oxide scales initially formed on the alloy remain intact and probably do not react with the degradation products of the metallic sulfates, and SO_2 and O_2 evolved are given off resulting in weight losses. The mode of decomposition of the salts at the salt/gas interface can be described as follows:

(a) $NiSO_4$ (m.p. 760°C and decomp. 848°C)

(I) $NiSO_4 \longrightarrow NiO + SO_2 + O$

(b) $CoSO_4$ (m.p. 635°C with decomposition)

(II) $CoSO_4 \longrightarrow CoO + SO_2 + \frac{1}{2}O_2$

(c) $Cr_2(SO_4)_3$ (Probably stable at 800°C)

(III) $Cr_2(SO_4)_3 \longrightarrow Cr_2O_3 + 3SO_2 + \frac{3}{2}O_2$

Considering the oxidation of steels at 800°C in presence of transition metal salt and Na_2SO_4 mixtures. Initially the steel has a thin film of Cr_2O_3 and may be but not necessarily an external oxide layer of Fe_2O_3 formed if during coating of the salt sufficient oxygen activity is present at the oxide/salt interface. The Na-Fe-Cr-Ni-S thermal stability diagram at 1000°K shows that $Cr_2O_3(s)$ overlaps Na_2O stability region at all values of P_{S_2} and therefore, most easily fluxible. On the other hand, $Fe_2O_3(s)$

overlaps at the lower P_S values (or higher a_{Na_2O}) and therefore, can only be fluxed in a highly basic melt (corresponding to $P_S \sim 35$ atm). The weight losses in Na_2SO_4-$Cr_2(SO_4)_3$ coated steel may be attributed to the following reactions:

IV $\quad 2Cr_2O_3(s) + Na_2SO_4(l) + \frac{1}{2}O_2(g) \longrightarrow Na_2CrO_4(l) + SO_2(g)$

V $\quad FeO + Na_2SO_4 \longrightarrow Na_2FeO_2(l) + SO_2(g) + \frac{1}{2}O_2(g)$

At 800°C, the Na_2SO_4-$CoSO_4$ coated steels show higher corrosion rates than the corresponding Na_2SO_4-$Cr_2(SO_4)_3$ coated steels due to the formation of a low temperature eutectic (m.p. 565°C) (Na_2SO_4-$CoSO_4$ equilibrium diagram, fig. 3.34). The liquidus eutectic breaks the protective chromia oxide film and the alloy oxidizes at a much higher oxidation rates. Similarly, enhanced oxidation rates of Na_2SO_4-$NiSO_4$ coated steels at 800°C are the result of formation of low temperature eutectic which is responsible for the disruption of otherwise protective chromia scales.

At 1000°C, steels coated with $Cr_2(SO_4)_3$ have the lowest oxidation rates in comparison to other salts or salt mixtures. At air/salt interface the decomposition of $Cr_2(SO_4)_3$ will be followed by III and at the oxide/salt interface decomposition will be followed by VI.

VI $Cr_2(SO_4)_3 \longrightarrow Cr_2S_3 + 6O_2$

Conversion of $Cr_2(SO_4)_3$ into Cr_2S_3 will increase the activity of oxygen at the oxide/salt interface resulting in the conversion of Cr_2S_3 into Cr_2O_3 and Fe into FeO, the release of sulfur may contribute towards further sulfidation making Cr_2O_3 scales more protective. However, reaction II seems to proceed only to a limited extent and reaction III is likely to be predominant throughout the oxidation. This is shown by relatively lower oxidation rates and the presence of relatively compact and adhered chromia scales.

At 1000°C, the Na_2SO_4-$Cr_2(SO_4)_3$ coated steels have much higher oxidation rates than either $Cr_2(SO_4)_3$-coated or Na_2SO_4-coated steel. Initially reaction III and VII will proceed at the air/salt interface.

VII $Na_2SO_4 \rightleftharpoons Na_2O + S + \frac{3}{2}O_2$

and reaction VI at the salt/oxide interface. In the propagation stage, there will be a sufficient activity of sulfur to form FeS and Cr_2S_3. The formation of sulfides will result in a decrease in sulfur activity and consequently an increase in oxygen activity. The increasing oxygen activity at the oxide/salt interface results in the oxidation of some of the sulfides and sulfur thus released is available for internal sulfidation. FeO/Cr_2O_3 formed as a result of

oxidation of sulfide should flux with Na_2O melt to form Na_2FeO_2 and $Na_2CrO_4/Na_2Cr_2O_4$.

VIII $Cr_2O_3 + Na_2O + \frac{3}{2}O_2 \longrightarrow 2Na_2CrO_4$

IX $Cr_2O_3 + Na_2O \longrightarrow Na_2Cr_2O_4$

X $FeO + Na_2O \longrightarrow Na_2FeO_2$

XI $Fe_2O_3 + Na_2O \longrightarrow Na_2Fe_2O_4$

The reactions are thermodynamically feasible and likely to continue till the entire Na_2O is exhausted. At salt/air interface a_{Na2O} is very low and in consequence, Na_2CrO_2 and Na_2CrO_4 would dissociate to reprecipitate as Cr_2O_3 and Na_2FeO_2 and $Na_2Fe_2O_4$ as FeO or Fe_2O_3.

At 1000°C, $CoSO_4$-coated steels show much higher oxidation rates than Na_2SO_4-coated steels. $CoSO_4$ seems to decompose in the following manner at the oxide/salt interface.

XII $CoSO_4 \longrightarrow CoS + 2O_2$

CoS formed at the oxide/salt interface may undergo following reactions which are thermodynamically feasible:

XIII $CoS + Cr_2O_3 \longrightarrow 3CoO + Cr_2S_3$

XIV $CoS + FeO \longrightarrow CoO + FeS$

} oxide/salt interface

XV $FeS.Cr_2S_3 \longrightarrow FeS + Cr_2S_3$)oxide/salt interface

XVI $CoS + 2O_2 \longrightarrow CoSO_4$)gas/salt interface

No CoS has been detected in the scales and the observed morphology is consistent with the above reactions.

In presence of a mixture of Na_2SO_4-$CoSO_4$ at 1000°C, the reactions XII to XVI are likely to go along with IV, V and VIII to XI and the eutectic ($CoSO_4$-Na_2SO_4) does not seem to play any important role. The relatively lower weight gains in Na_2SO_4-$CoSO_4$ coated alloys are probably the effect of reactions IV and V which proceed with the evolution of SO_2 gas.

The corrosion behaviour of $NiSO_4$-coated steels is similar to that of $CoSO_4$-coated steels at 1000°C. At the oxide/salt interface $NiSO_4$ decomposes as,

XVII $NiSO_4 \longrightarrow NiS + 2O_2$

NiS formed in XVII accumulates beneath the Cr_2O_3 scale and may undergo following reaction:

XVIII $3NiS + Cr_2O_3 \longrightarrow 3NiO + Cr_2S_3$

There is also a possibility of penetration of NiS through oxide scale and interacting with Ni in the substrate to form low melting Ni-NiS eutectic. When the S-activity at

the salt/oxide interface is sufficiently lowered due to the formation of sulfides, the sulfides get oxidised to NiO and Cr_2O_3 and sulfur thus released produces internal sulfidation. Cr_2S_3 as internal sulfide particles along with NiS are found in the matrix. The $NiSO_4 + Na_2SO_4$ coated steels also show enhanced corrosion rates while comparing with the corresponding Na_2SO_4-coated steel. The formation of NiS at the oxide/salt interface and Ni-NiS eutectic is again responsible for aggressiveness of the mixture. The slightly lower oxidation rates of the Na_2SO_4-$NiSO_4$ coated steels are perhaps due to the expulsion of SO_2 during the fluxing of Cr_2O_3 and FeO (reactions IV and V).

Only a limited number of references[4-7] are available on the influence of transition metal salts on the Na_2SO_4-induced hot corrosion of iron-base alloys. A few studies[1-3] have been undertaken to investigate alkali sulfate - $Fe_2(SO_4)_3$ induced hot corrosion of iron-base alloys.

The present studies indicate that transition metal salt does not significantly influence the corrosion rates of iron-base alloys at temperatures upto 800°C, this is because the transition metal salt coating decomposes into respective oxide(s) without disturbing the original morphology of the oxide scales. In presence of Na_2SO_4-transition metal sulfate mixture at 800°C, the higher corrosion rates

of $NiSO_4$ and $CoSO_4$ are attributed to the formation of low melting eutectics with Na_2SO_4 which break the otherwise protective oxide scales. $Cr_2(SO_4)_3$-Na_2SO_4 does not exhibit any aggressive action at this temperature.

At 1000°C, the transition metal salts or their mixtures with Na_2SO_4 produce substantial hot corrosion attack. Sulfidation and the basic fluxing are the main features of hot corrosion. The slightly lower corrosion rates in case of mixtures have been attributed to the expulsion of SO_2/O_2 during formation of CrO_4^{2-} and FeO_2^{2-}.

Figures 3.35 (a, b) and 3.36 (a, b) show schematic diagrams indicating the oxidation of iron-base alloys in presence of transition metal sulfates and their mixtures with Na_2SO_4 at 800 and 1000°C, respectively.

REFERENCES

1. K. A. Bol'shkov, P. I. Federov and N. I. Il'ina, Russ. J. Inorg. Chem. (Eng. Trans.), 1351 (1965).
2. A. Rahmel and W. Jaeger, Z. anorg. Chem., 303, 90 (1960).
3. C. Cain and W. Nelson, Am. Soc. Mech. Engrs Paper, 60 - WA - 180 (1961).
4. A. U. Malik, N. Asrar and M. Ishaq, 'High Temp. Behaviour of some commercial steels in presence of ionic salts', Korrosion (in press).
5. A. U. Malik, M. M. Amin and S. Ahmed, 'Hot corrosion of 18Cr-8Ni austenitic steel in presence of Na_2SO_4 and transition metal salts', Japan Inst. of Metals (under publication).
6. A. U. Malik, M. M. Amin and S. Ahmed, 'Hot corrosion of austenitic steel in presence of $NiSO_4$ and Na_2SO_4', J. Metallography (in press).
7. A. U. Malik and Sultan Ahmed, 'Hot corrosion of Ni-base alloys in presence of transition metal salts', Z. Metallkunde (in press).

Table 5.1: Different constituents identified in scales of the corroded sample by X-ray diffraction analysis.

Duration of run = 6 hrs.

Steel	Salt/Mixture	Temp. °C	Constituents identified
AISI-303	$NiSO_4$	800	Cr_2O_3, FeO, NiO
	Na_2SO_4-$NiSO_4$	800	Cr_2O_3, Fe_2O_3
	$NiSO_4$	1000	Cr_2O_3, Fe_2O_3, NiO, NiS
AISI-321	Na_2SO_4-$NiSO_4$	1000	Cr_2O_3, Fe_2O_3, NiO, Cr_2S_3, NiS
	Na_2SO_4-$Cr_2(SO_4)_3$	800	Cr_2O_3, Fe_2O_3
	Cr_2SO_4	1000	Cr_2O_3, Cr_2S_3, FeO
	Na_2SO_4-$Cr_2(SO_4)_3$	1000	Cr_2O_3, FeS.Cr_2S_3, Fe_2O_3, NiO
AISI-303	$CoSO_4$	800	Cr_2O_3, CoO, FeO
	Na_2SO_4-$CoSO_4$	800	Cr_2O_3, FeO
AISI-321	$CoSO_4$	1000	Cr_2O_3, Fe_2O_3, CoO
	Na_2SO_4-$CoSO_4$	1000	Cr_2O_3, Fe_2O_3, CoO, Cr_2S_3, NiO

CAPTIONS OF THE PLOTS OF OXIDATION STUDIES

Fig. 3.1 Plots of weight change versus amount of Na_2SO_4/$NiSO_4$/Na_2SO_4-$NiSO_4$ mixture deposited AISI-303 steel, oxidized at 800°C for 6 hours.

Fig. 3.2 Plots of weight gain versus amount of Na_2SO_4/$NiSO_4$/Na_2SO_4-$NiSO_4$ mixture deposited AISI-303 steel, oxidized at 1000°C for 6 hours.

Fig. 3.3 Plots of weight change versus amount of Na_2SO_4/$NiSO_4$/Na_2SO_4-$NiSO_4$ mixture deposited AISI-321 steel, oxidized at 800°C for 6 hours.

Fig. 3.4 Plots of weight gain versus amount of Na_2SO_4/$NiSO_4$/Na_2SO_4-$NiSO_4$ mixture deposited AISI-321 steel, oxidized at 1000°C for 6 hours.

Fig. 3.5 Plots of weight change versus amount of Na_2SO_4/$Cr_2(SO_4)_3$/Na_2SO_4-$Cr_2(SO_4)_3$ mixture deposited AISI-303 steel, oxidized at 800°C for 6 hours.

Fig. 3.6 Plots of weight gain versus amount of Na_2SO_4/$Cr_2(SO_4)_3$/Na_2SO_4-$Cr_2(SO_4)_3$ mixture deposited AISI-303 steel, oxidized at 1000°C for 6 hours.

Fig. 3.7 Plots of weight change versus amount of Na_2SO_4/$Cr_2(SO_4)_3$/Na_2SO_4-$Cr_2(SO_4)_3$ mixture deposited AISI-321 steel, oxidized at 800°C for 6 hours.

Fig. 3.8 Plots of weight gain versus amount of Na_2SO_4/$Cr_2(SO_4)_3$/Na_2SO_4-$Cr_2(SO_4)_3$ mixture deposited AISI-321 steel, oxidised at 1000°C for 6 hours.

Fig. 3.9 Plots of weight change versus amount of Na_2SO_4/$CoSO_4$/Na_2SO_4-$CoSO_4$ mixture deposited AISI-303 steel, oxidised at 800°C for 6 hours.

Fig. 3.10 Plots of weight gain versus amount of Na_2SO_4/$CoSO_4$/Na_2SO_4-$CoSO_4$ mixture deposited AISI-303 steel, oxidised at 1000°C for 6 hours.

Fig. 3.11 Plots of weight change versus amount of Na_2SO_4/$CoSO_4$/Na_2SO_4-$CoSO_4$ mixture deposited AISI-321 steel, oxidised at 800°C for 6 hours.

Fig. 3.12 Plots of weight gain versus amount of Na_2SO_4/$CoSO_4$/Na_2SO_4-$CoSO_4$ mixture deposited AISI-321 steel, oxidised at 1000°C for 6 hours.

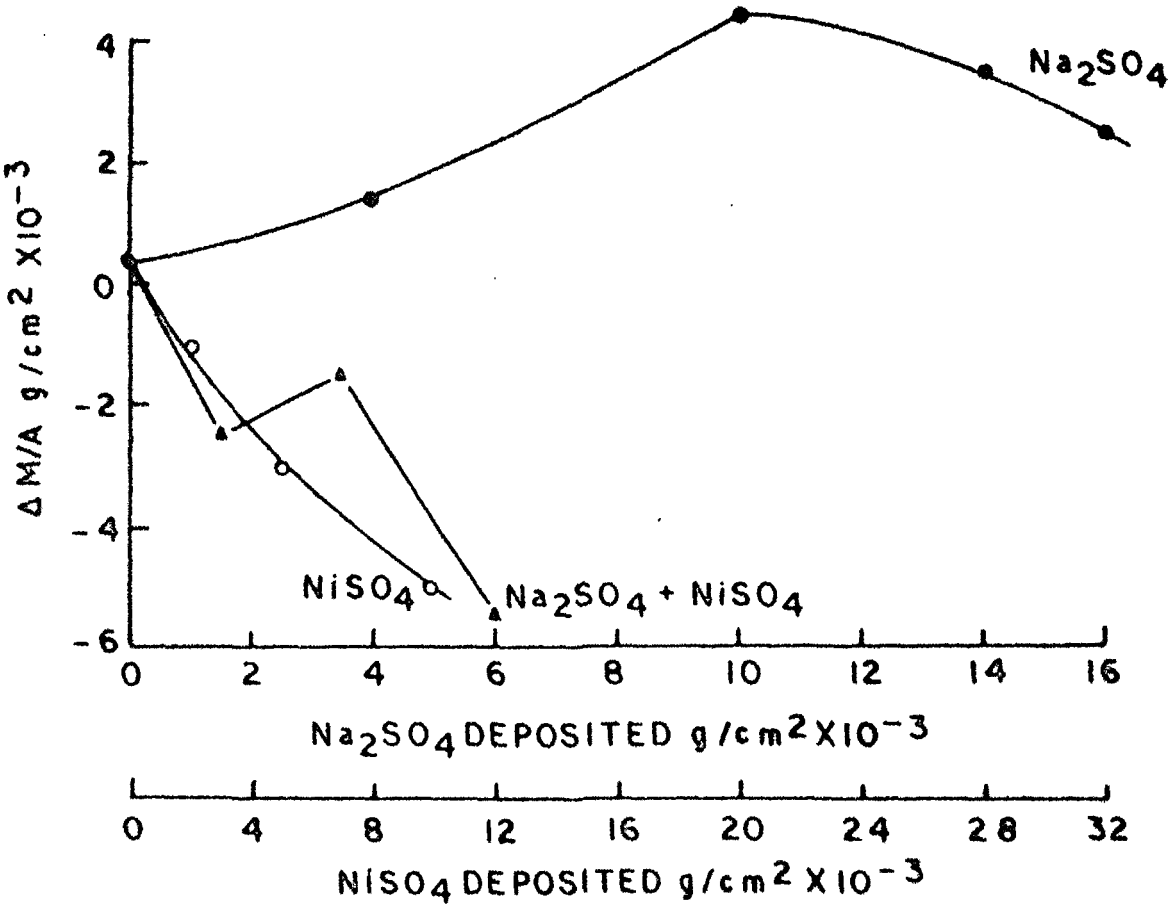
4
2
0
-2
-4
-6
ΔM/A g/cm² X10⁻³
Na₂SO₄
NiSO₄
Na₂SO₄ + NiSO₄
0
2
4
6
8
10
12
14
16
Na₂SO₄ DEPOSITED g/cm² X10⁻³
0
4
8
12
16
20
24
28
32
NiSO₄ DEPOSITED g/cm² X10⁻³

FIG. 3.1

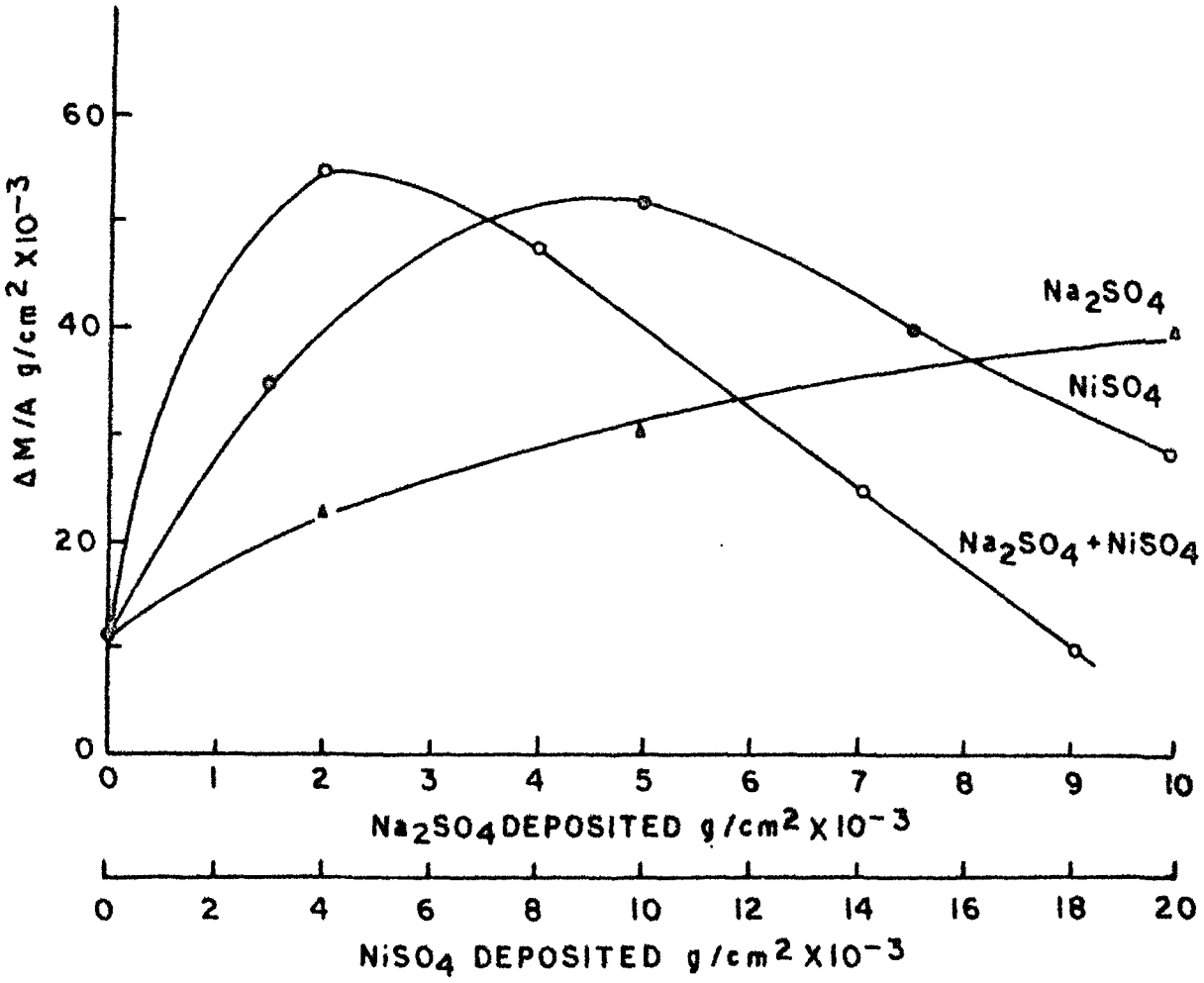
60
40
20
0
ΔM/A g/cm² X10⁻³
Na2SO4
NiSO4
Na2SO4 + NiSO4
0 1 2 3 4 5 6 7 8 9 10
Na2SO4 DEPOSITED g/cm² X10⁻³
0 2 4 6 8 10 12 14 16 18 20
NiSO4 DEPOSITED g/cm² X10⁻³

FIG. 3.2

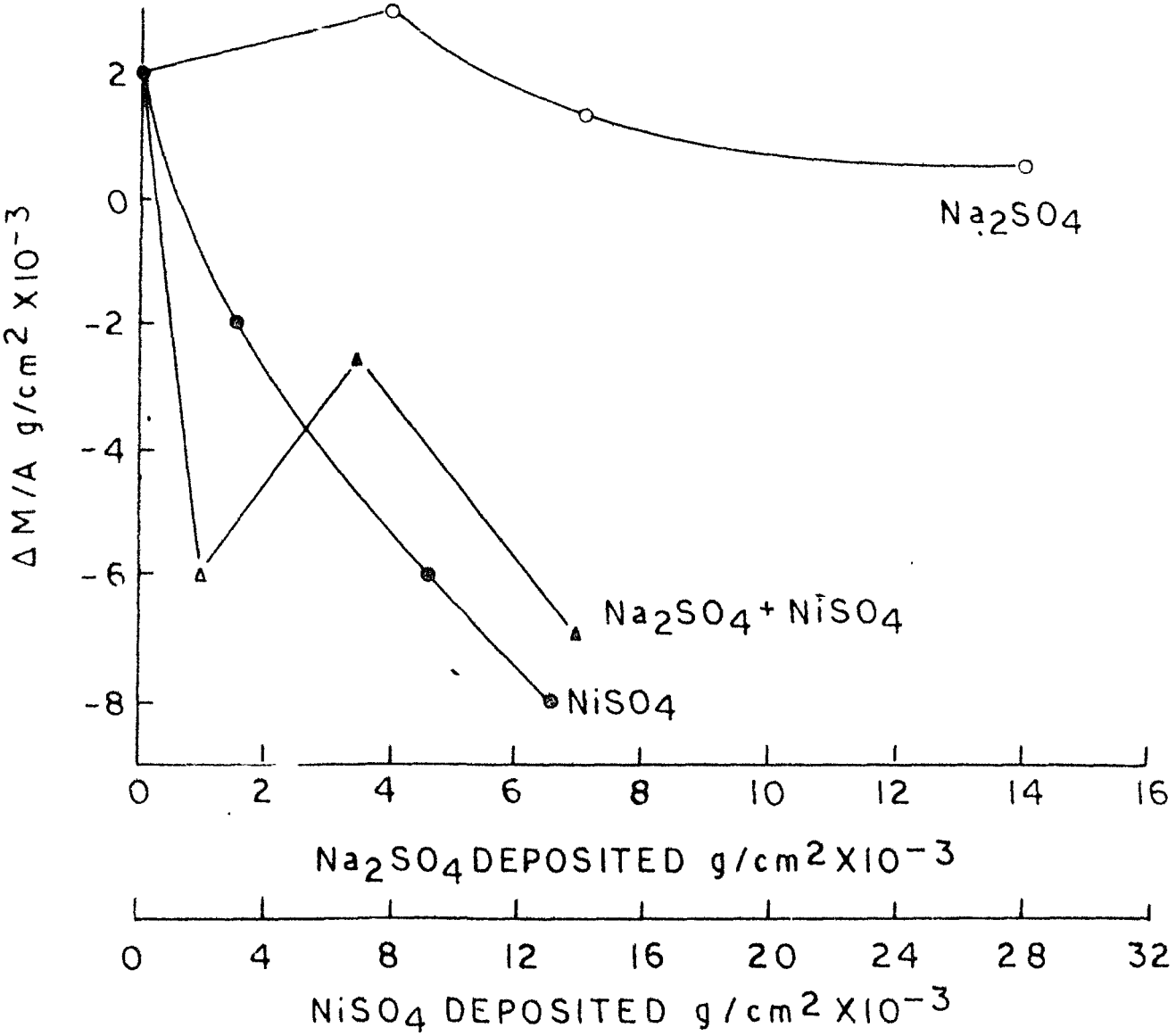
2
0
-2
-4
-6
-8
ΔM/A g/cm² X10⁻³
Na2SO4
Na2SO4 + NiSO4
NiSO4
0
2
4
6
8
10
12
14
16
Na2SO4 DEPOSITED g/cm² X10⁻³
0
4
8
12
16
20
24
28
32
NiSO4 DEPOSITED g/cm² X10⁻³

FIG. 3.3

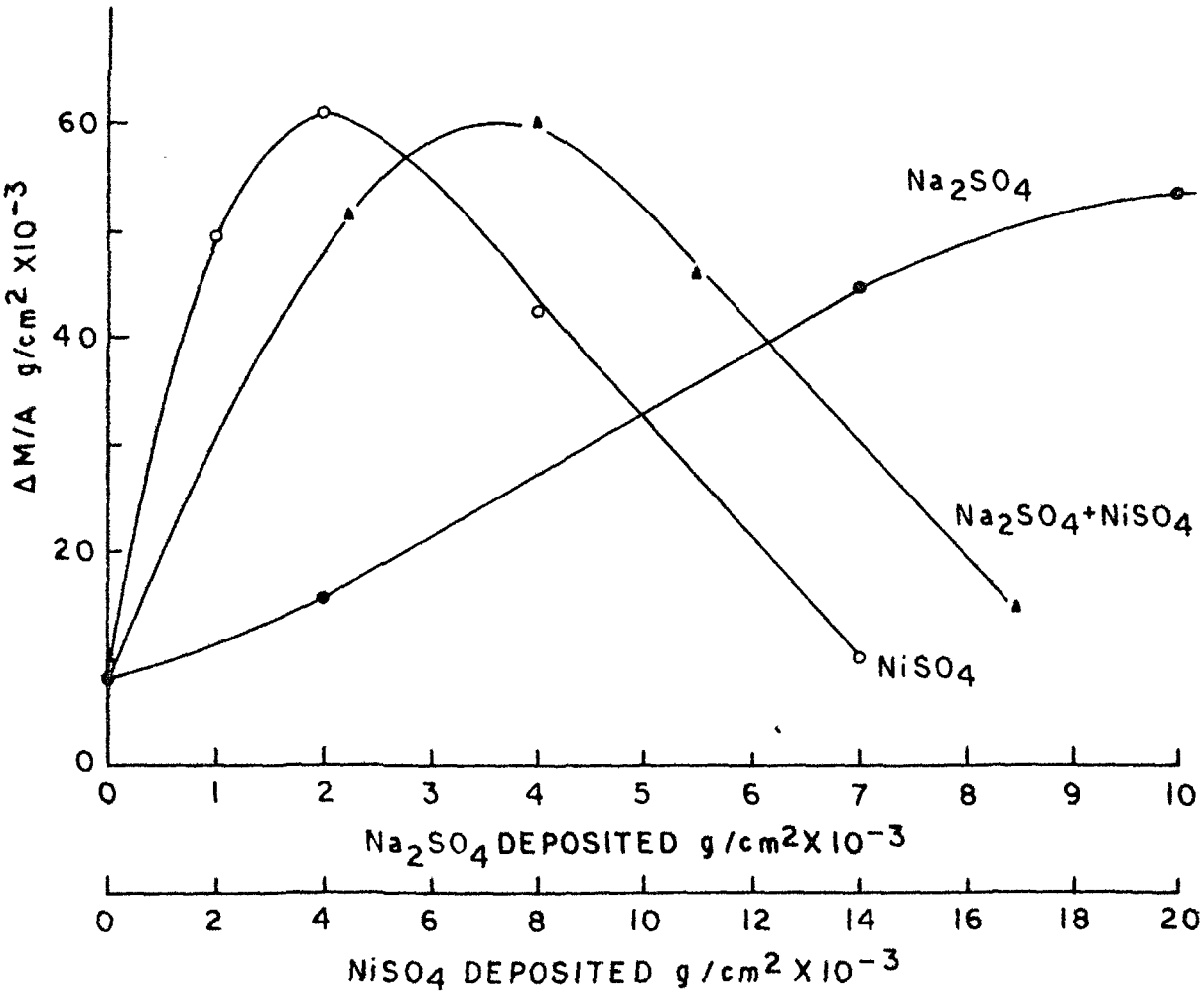
60
40
20
0
ΔM/A g/cm² X10⁻³
Na2SO4
Na2SO4+NiSO4
NiSO4
0 1 2 3 4 5 6 7 8 9 10
Na2SO4 DEPOSITED g/cm² X10⁻³
0 2 4 6 8 10 12 14 16 18 20
NiSO4 DEPOSITED g/cm² X10⁻³

FIG. 3.4

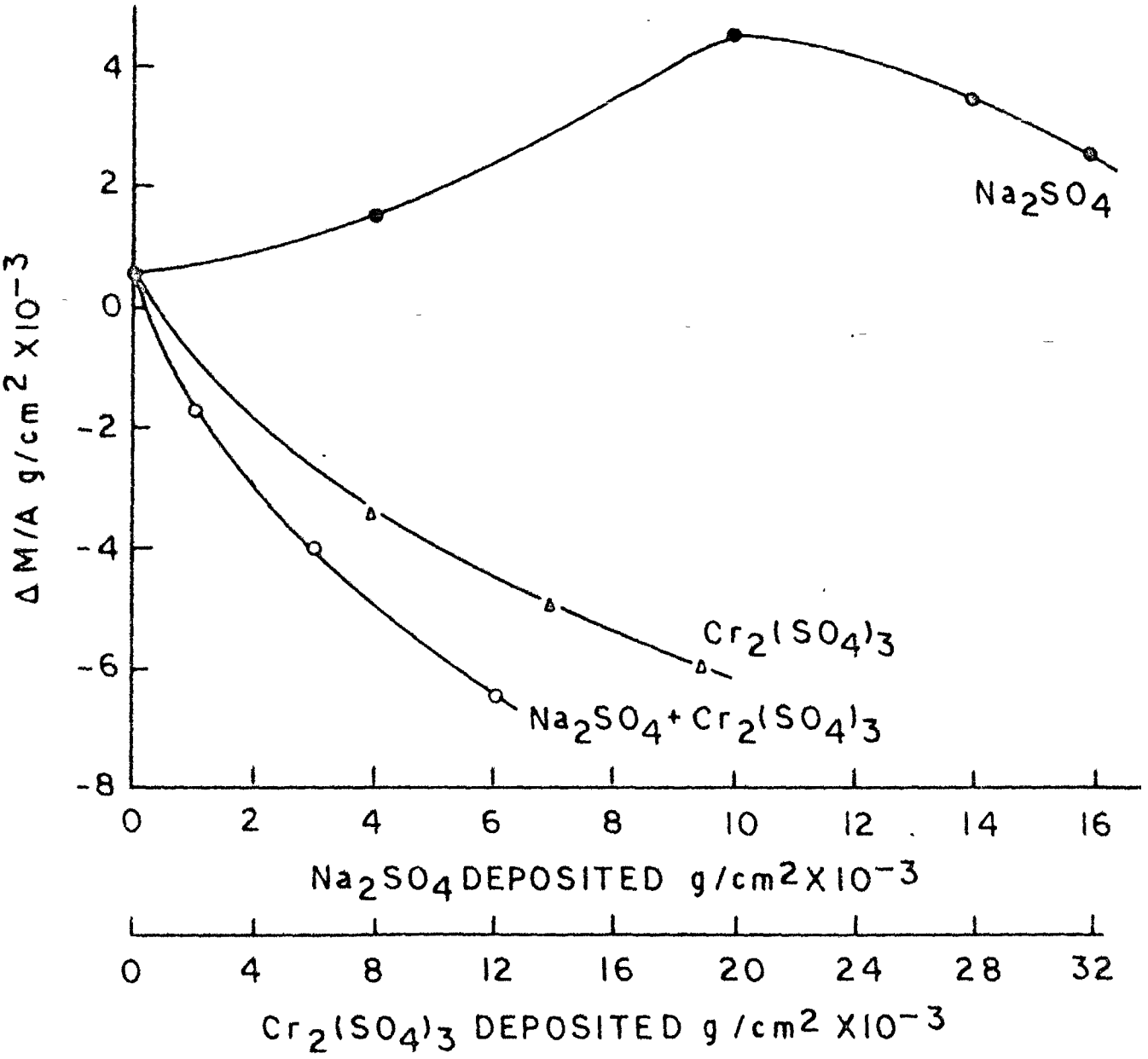
4
2
0
-2
-4
-6
-8
ΔM/A g/cm² X10⁻³
Na2SO4
Cr2(SO4)3
Na2SO4 + Cr2(SO4)3
0
2
4
6
8
10
12
14
16
Na2SO4 DEPOSITED g/cm² X10⁻³
0
4
8
12
16
20
24
28
32
Cr2(SO4)3 DEPOSITED g/cm² X10⁻³

FIG. 3.5

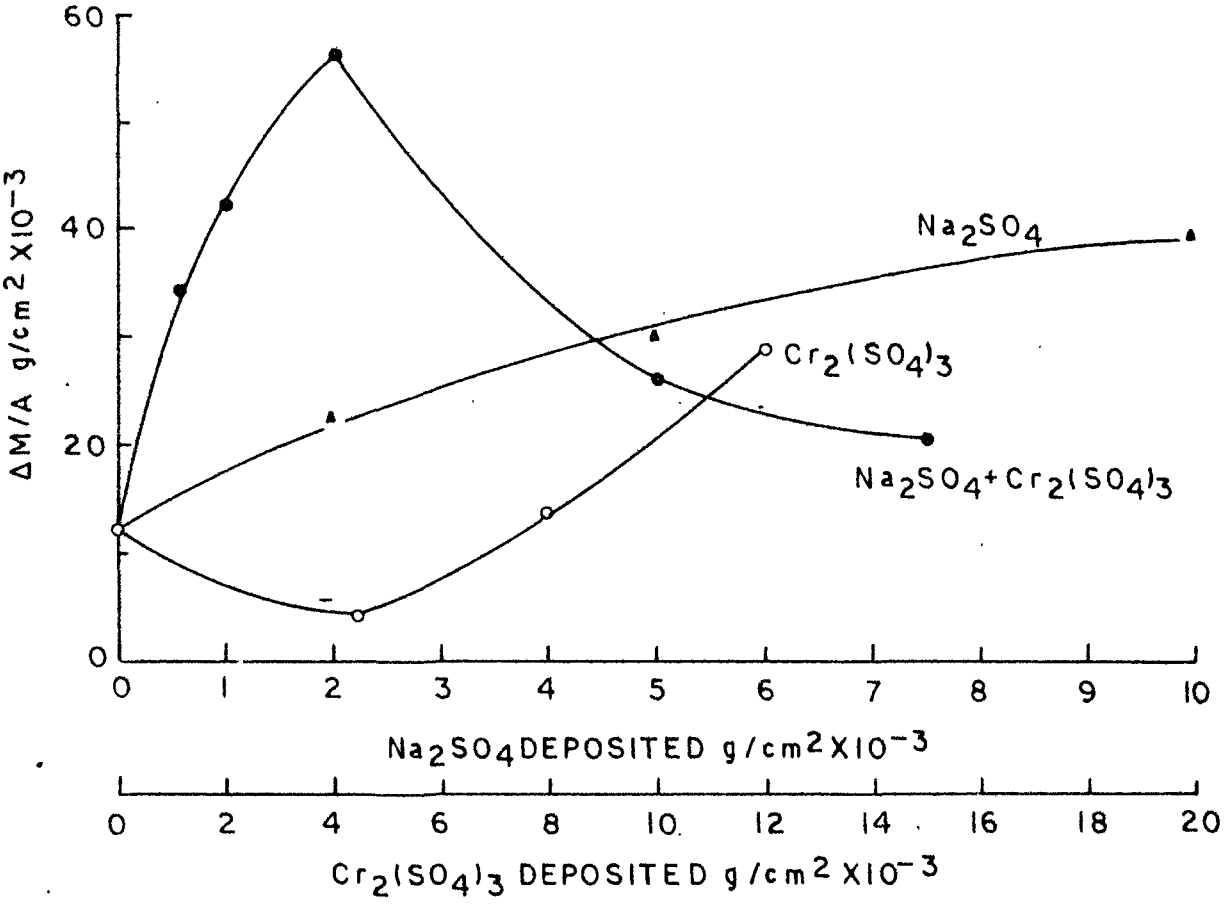
60
40
20
0
ΔM/A g/cm² X10⁻³
Na₂SO₄
Cr₂(SO₄)₃
Na₂SO₄+Cr₂(SO₄)₃
0 1 2 3 4 5 6 7 8 9 10
Na₂SO₄DEPOSITED g/cm² X10⁻³
0 2 4 6 8 10 12 14 16 18 20
Cr₂(SO₄)₃ DEPOSITED g/cm² X10⁻³

FIG. 3 6

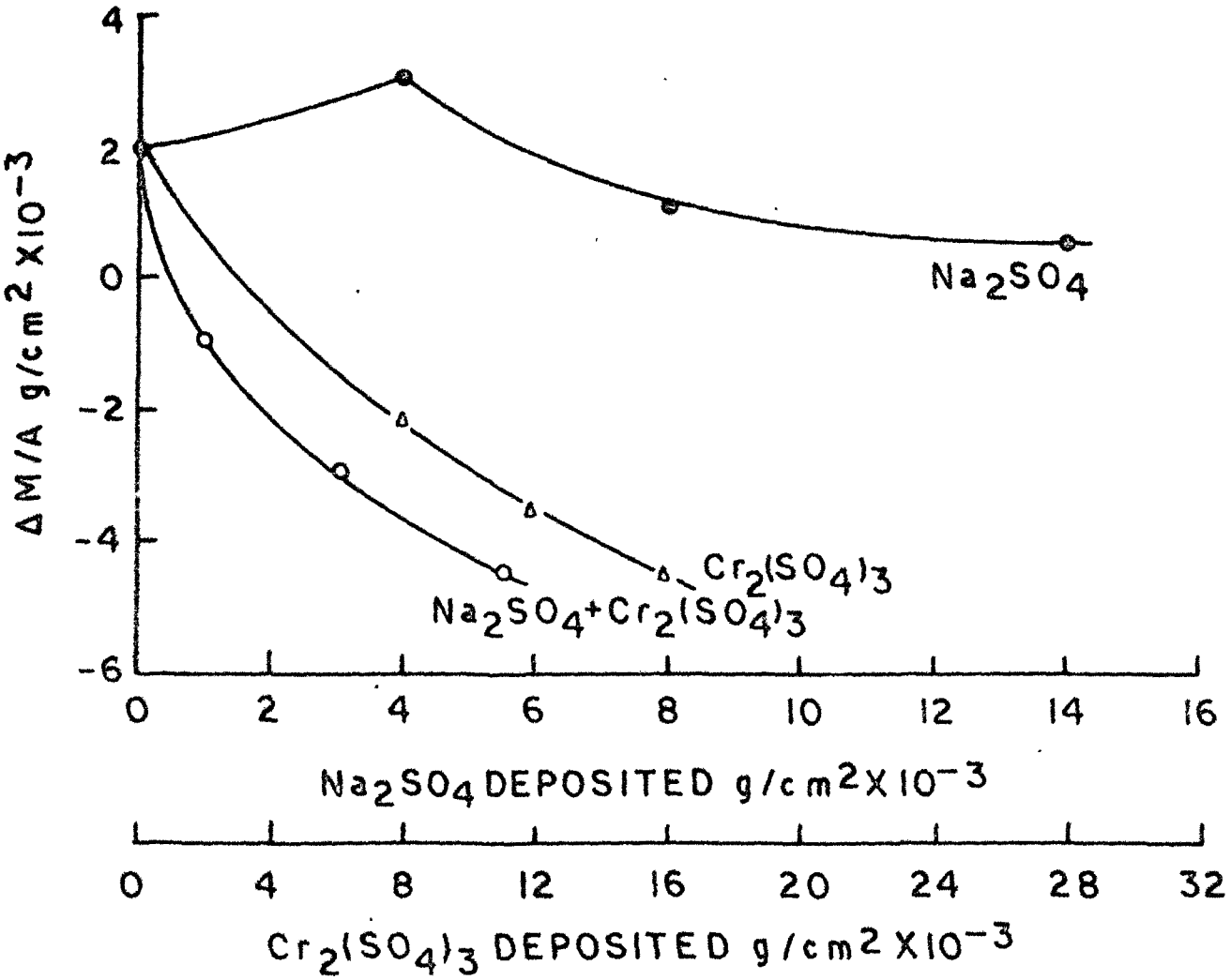
4
2
0
-2
-4
-6
ΔM/A g/cm2 X10-3
Na2SO4
Cr2(SO4)3
Na2SO4+Cr2(SO4)3
0
2
4
6
8
10
12
14
16
Na2SO4 DEPOSITED g/cm2X10-3
0
4
8
12
16
20
24
28
32
Cr2(SO4)3 DEPOSITED g/cm2 X10-3

FIG. 3.7

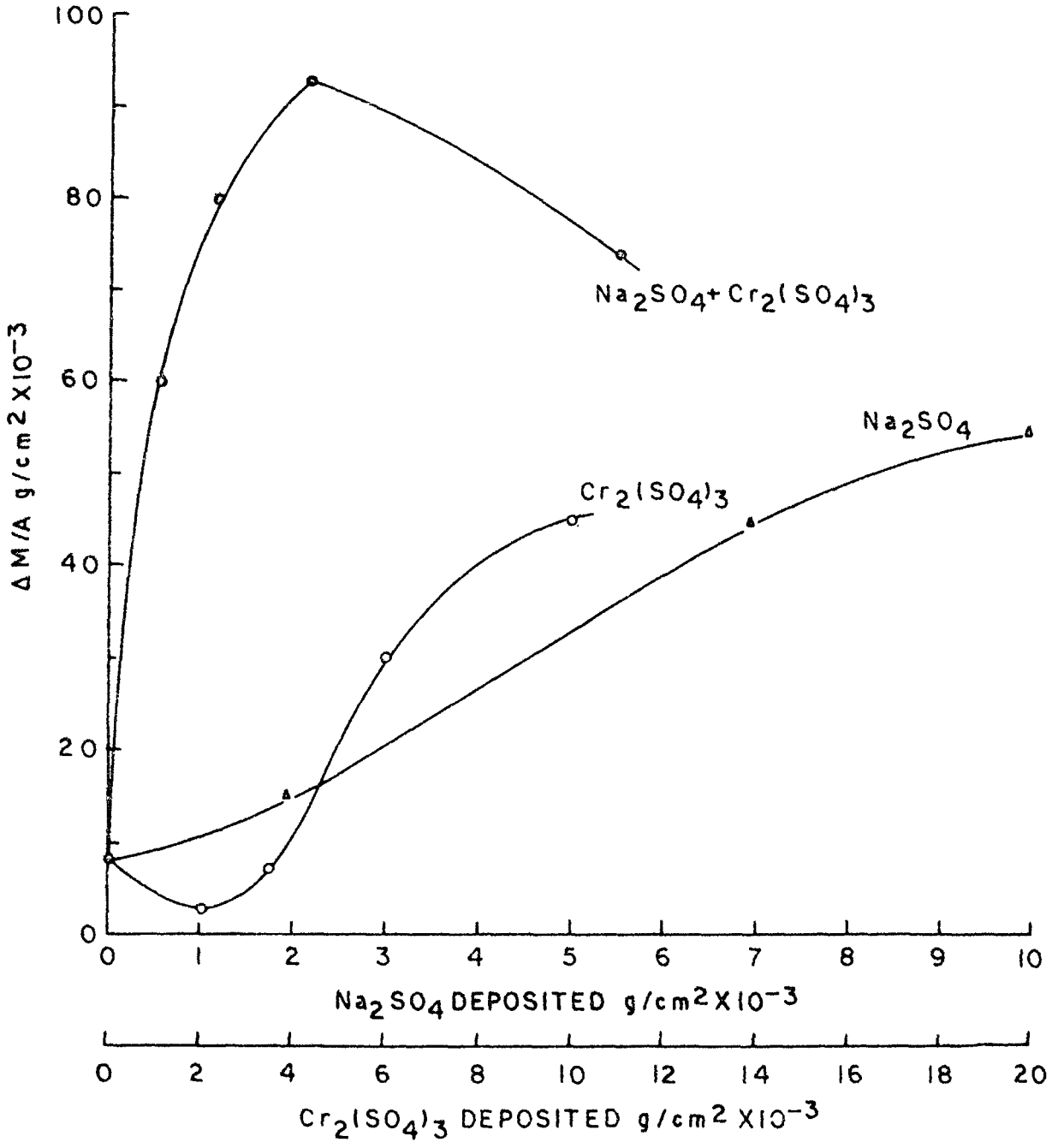
100
80
60
40
20
0
ΔM/A g/cm² X10⁻³
Na2SO4+Cr2(SO4)3
Na2SO4
Cr2(SO4)3
0 1 2 3 4 5 6 7 8 9 10
Na2SO4 DEPOSITED g/cm² X10⁻³
0 2 4 6 8 10 12 14 16 18 20
Cr2(SO4)3 DEPOSITED g/cm² X10⁻³

FIG. 3.8

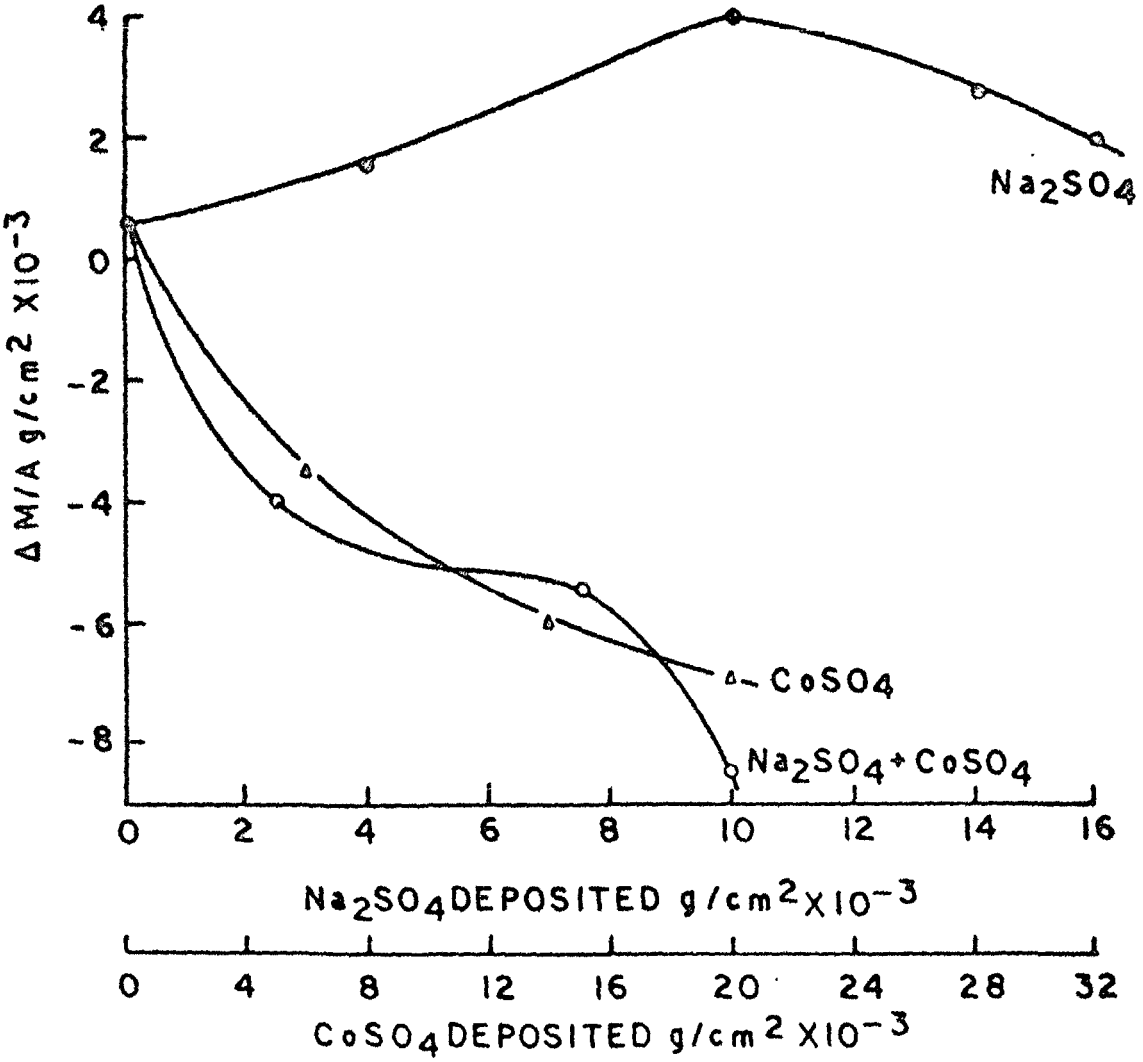
4
2
0
-2
-4
-6
-8
ΔM/A g/cm² X10⁻³
Na2SO4
CoSO4
Na2SO4+CoSO4
0
2
4
6
8
10
12
14
16
Na2SO4 DEPOSITED g/cm² X10⁻³
0
4
8
12
16
20
24
28
32
CoSO4 DEPOSITED g/cm² X10⁻³

FIG. 3.9

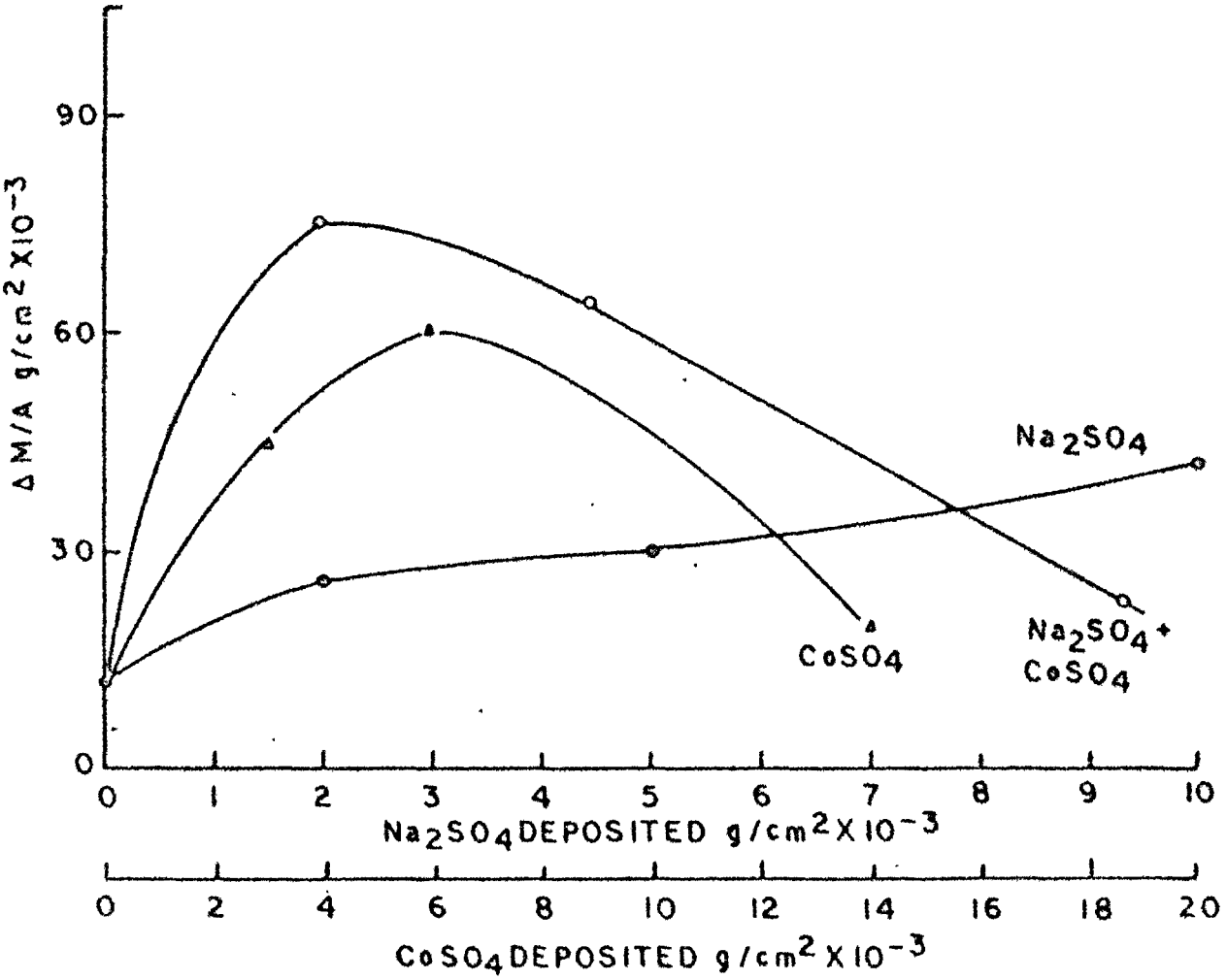
ΔM/A g/cm² X10⁻³
90
60
30
0
Na2SO4
CoSO4
Na2SO4 + CoSO4
0 1 2 3 4 5 6 7 8 9 10
Na2SO4 DEPOSITED g/cm² X10⁻³
0 2 4 6 8 10 12 14 16 18 20
CoSO4 DEPOSITED g/cm² X10⁻³

FIG. 3.10

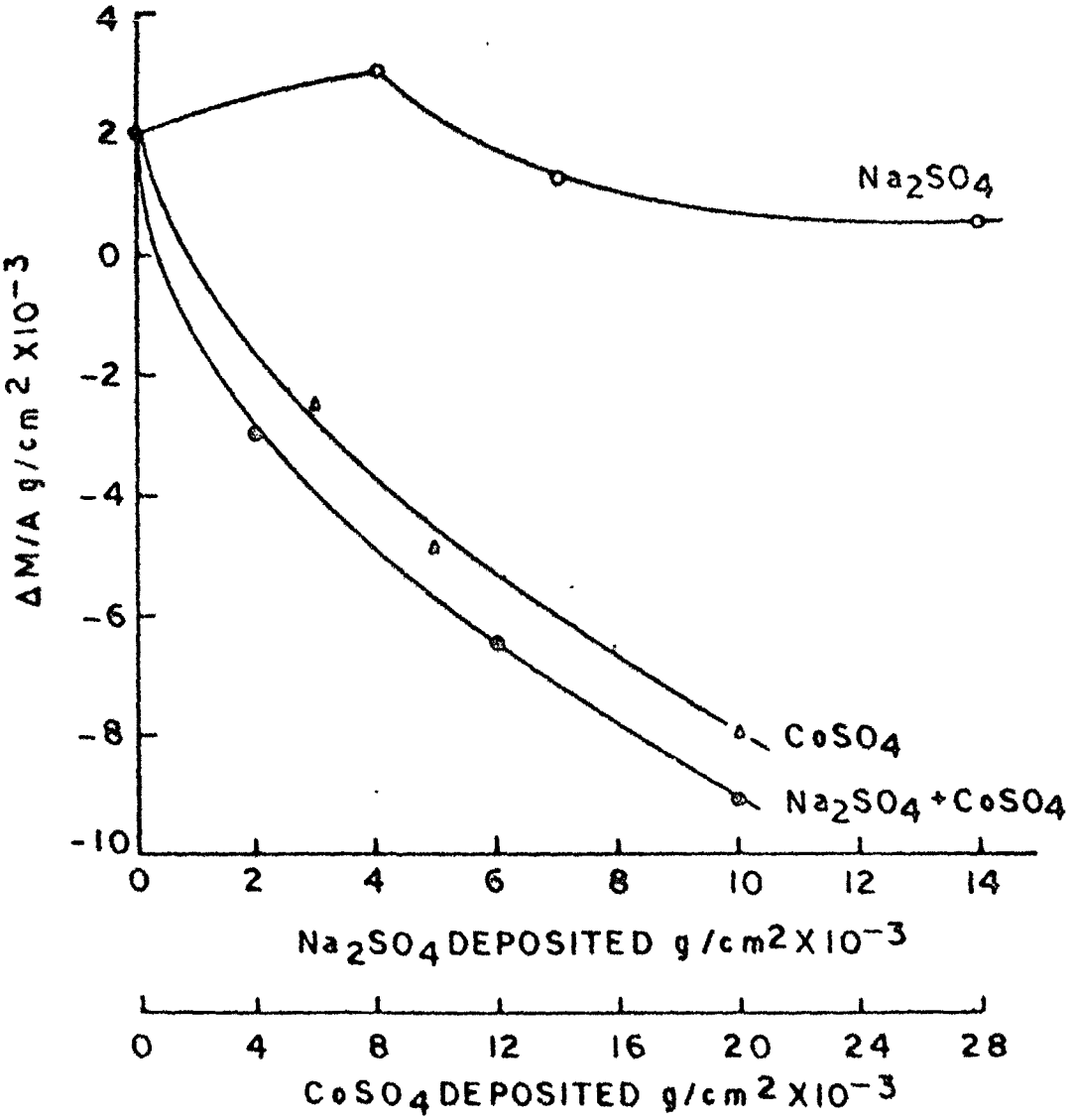
4
2
0
-2
-4
-6
-8
-10
ΔM/A g/cm² X10⁻³
Na2SO4
CoSO4
Na2SO4 + CoSO4
0
2
4
6
8
10
12
14
Na2SO4 DEPOSITED g/cm² X10⁻³
0
4
8
12
16
20
24
28
CoSO4 DEPOSITED g/cm² X10⁻³

FIG. 3.11

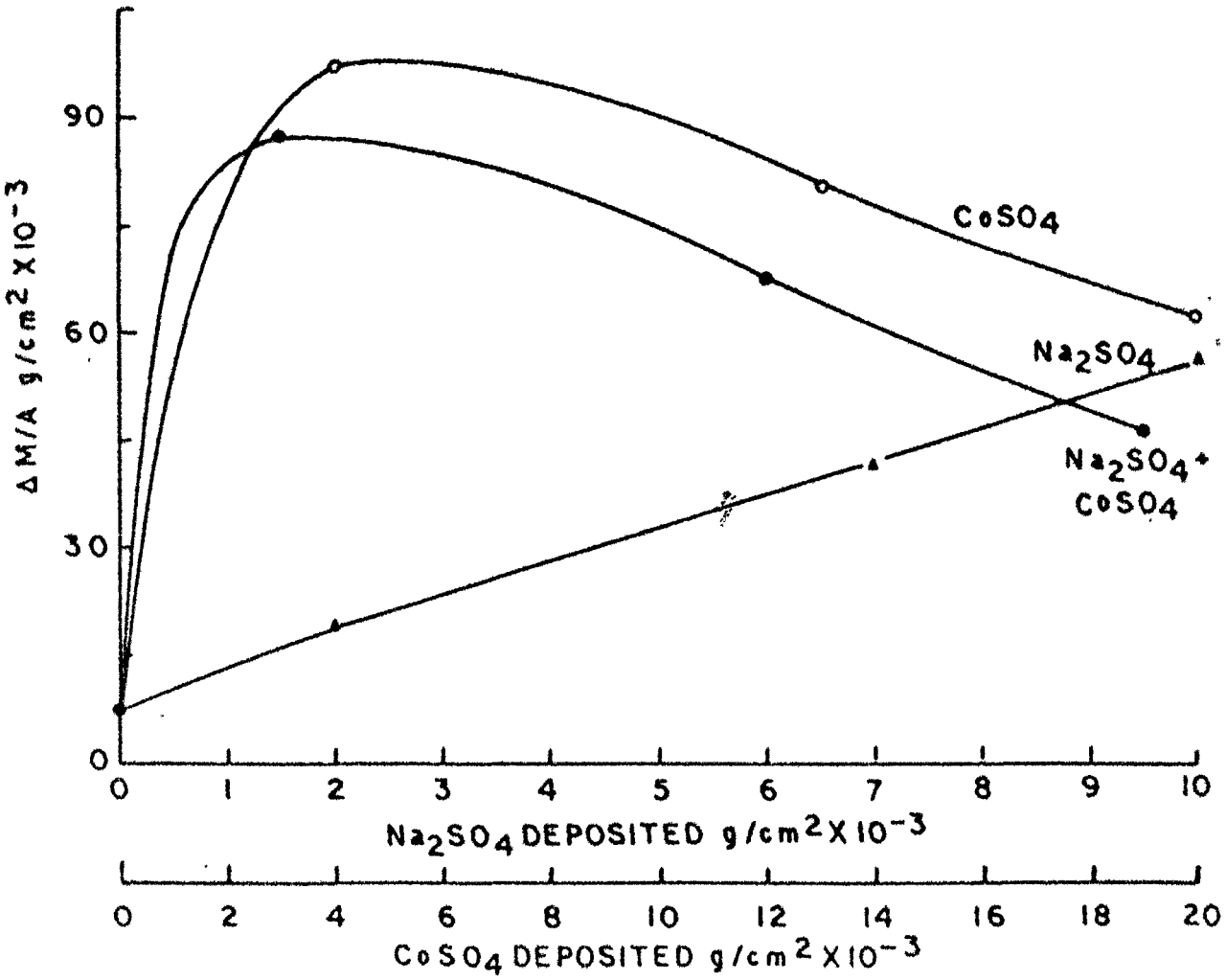
ΔM/A g/cm² X10⁻³
90
60
30
0
CoSO4
Na2SO4
Na2SO4 + CoSO4
0 1 2 3 4 5 6 7 8 9 10
Na2SO4 DEPOSITED g/cm² X10⁻³
0 2 4 6 8 10 12 14 16 18 20
CoSO4 DEPOSITED g/cm² X10⁻³

FIG. 3.12

CAPTIONS OF METALLOGRAPHS

Fig. 3.13 Photomicrograph of AISI-321 steel coated with Na_2SO_4-$NiSO_4$ mixture and oxidised at 1000°C for 6 hours.
(400x)

Fig. 3.14 Photomicrograph of AISI-303 steel coated with $NiSO_4$ and oxidised at 1000°C for 6 hours.
(400x)

Fig. 3.15(a & b) Scanning electron micrograph of AISI-321 steel coated with Na_2SO_4-$NiSO_4$ mixture and oxidized at 1000°C for 6 hours.
(a. 47x b. 430x)

Fig. 3.16(a & b) Scanning electron micrograph of AISI-303 steel coated with Na_2SO_4-$NiSO_4$ mixture and oxidised at 1000°C for 6 hours.
(a. 90x b. 1800x)

Fig. 3.17(a & b) Scanning electron micrograph of AISI-321 steel coated with $NiSO_4$ and oxidised at 1000°C for 6 hours.
(a. 50x b. 1000x)

Fig. 3.18(a & b) Scanning electron micrograph of AISI-321 steel coated with Na_2SO_4-$NiSO_4$ mixture and oxidised at 800°C for 6 hours.
(a. 85x b. 850x)

Fig. 3.19 Photomicrograph of AISI-321 steel coated with Na_2SO_4-$CoSO_4$ mixture and oxidised at 800°C for 6 hours.

(400x)

Fig. 3.20(a & b) Scanning electron micrograph of AISI-321 steel coated with Na_2SO_4-$CoSO_4$ mixture and oxidised at 800°C for 6 hours.

(a. 120x b. 820x)

Fig. 3.21 Photomicrograph of AISI-321 steel coated with $CoSO_4$ and oxidised at 1000°C for 6 hours.

(400x)

Fig. 3.22(a & b) Scanning electron micrograph of AISI-321 steel coated with $CoSO_4$ and oxidised at 1000°C for 6 hours.

(a. 50x b. 1000x)

Fig. 3.23 Photomicrograph of AISI-321 steel coated with Na_2SO_4-$CoSO_4$ mixture and oxidised at 1000°C for 6 hours.

(400x)

Fig. 3.24 Photomicrograph of AISI-303 steel coated with Na_2SO_4-$CoSO_4$ mixture and oxidised at 1000°C for 6 hours.

(400x)

Fig. 3.25 Photomicrograph of AISI-303 steel coated with $Cr_2(SO_4)_3$ and oxidised at 1000°C for 6 hours.

(400x)

Fig. 3.26(a & b) Scanning electron micrograph of AISI-303 steel coated with $Cr_2(SO_4)_3$ and oxidised at 1000°C for 6 hours.

(a. 48x b. 800x)

Fig. 3.27 Photomicrograph of AISI-321 steel coated with $Cr_2(SO_4)_3$ and oxidised at 1000°C for 6 hours.

(400x)

Fig. 3.28(a & b) Scanning electron micrograph of AISI-321 steel coated with $Cr_2(SO_4)_3$ and oxidised at 1000°C for 6 hours.

(a. 120x b. 2000x)

Fig. 3.29 Photomicrograph of AISI-303 steel coated with Na_2SO_4-$Cr_2(SO_4)_3$ mixture and oxidised at 1000°C for 6 hours.

(400x)

Fig. 3.30(a & b) Scanning electron micrograph of AISI-303 steel coated with Na_2SO_4-$Cr_2(SO_4)_3$ mixture and oxidized at 1000°C for 6 hours.

(a. 120x b. 500x)

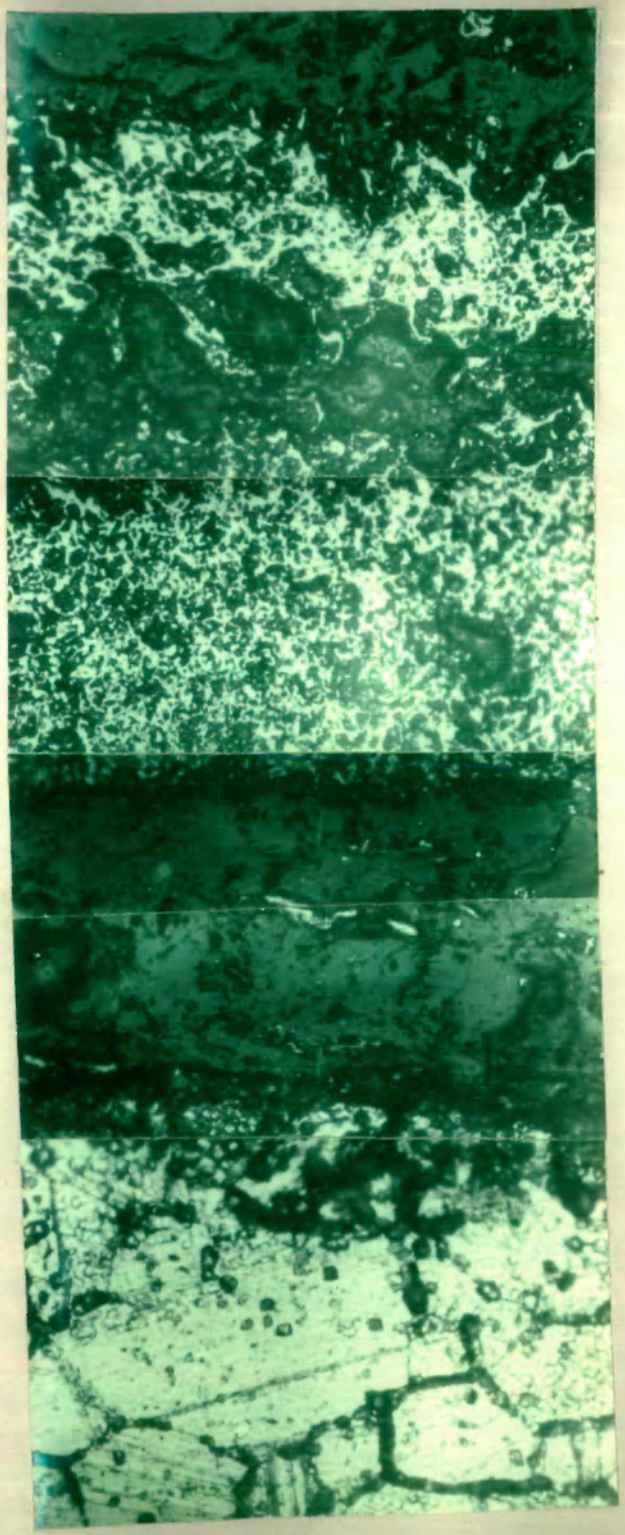

3.13

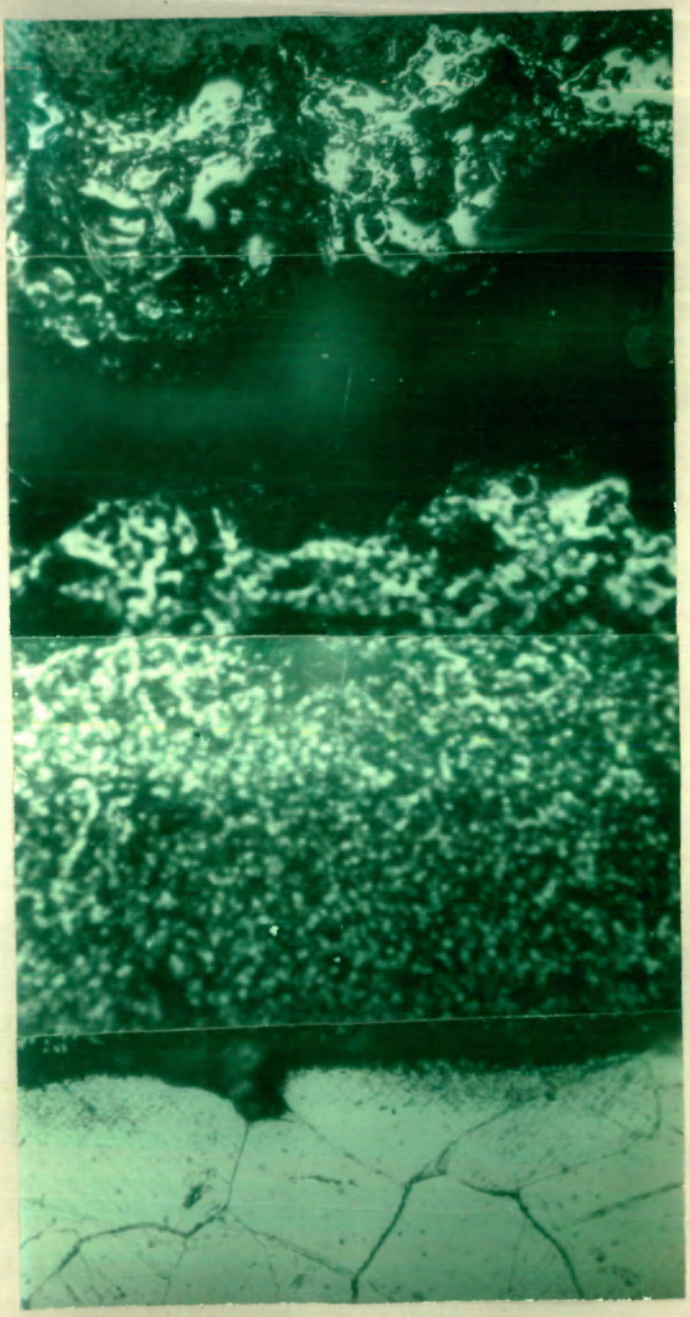

3.14

(a)

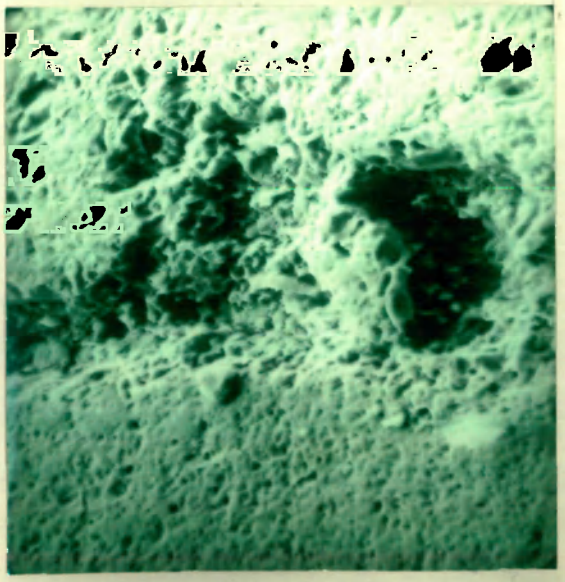

(b)

3.15

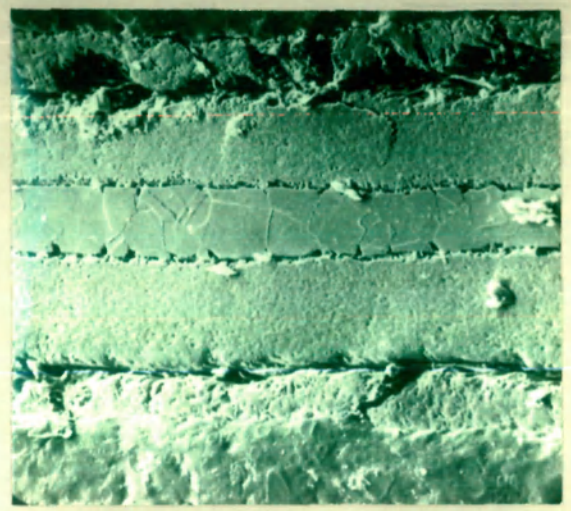

(a)

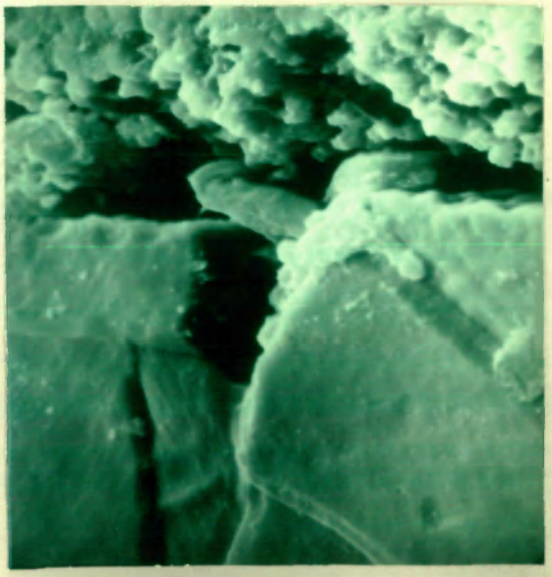

(b)

3.16

(a)

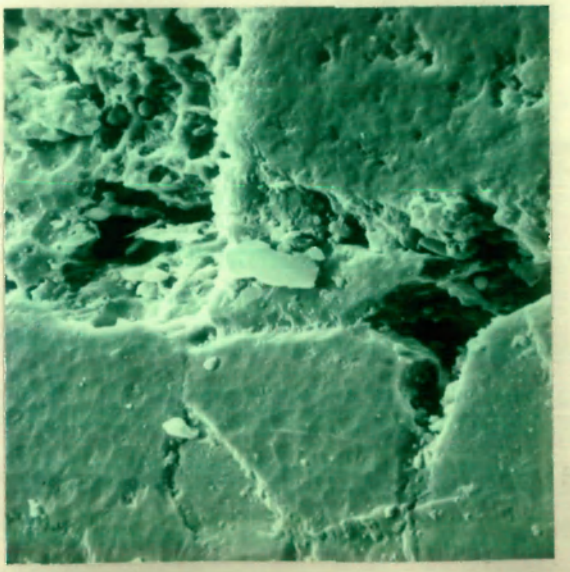

(b)

3.17

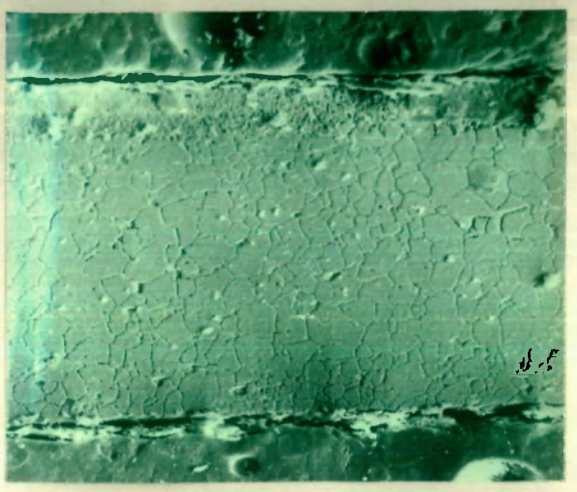

(a)

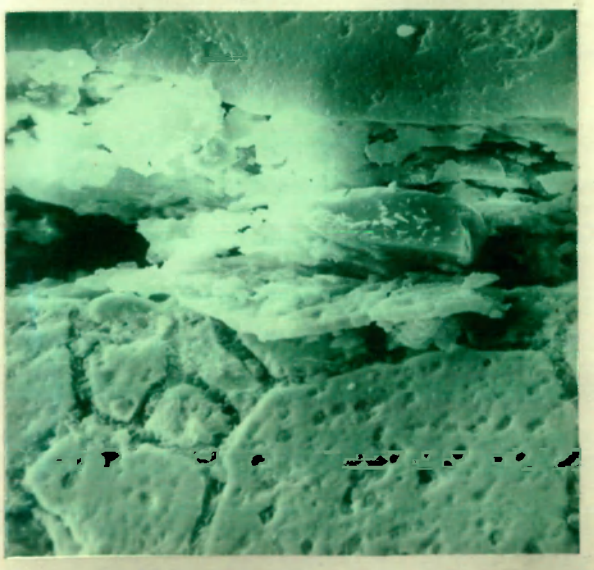

(b)

3.18

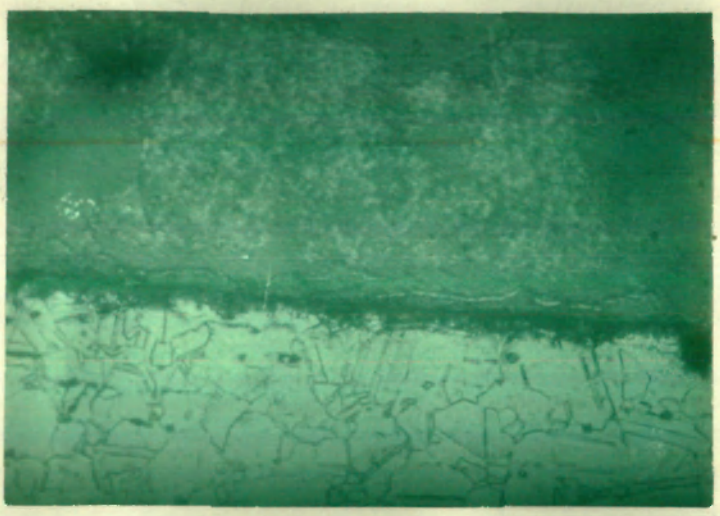

3.19

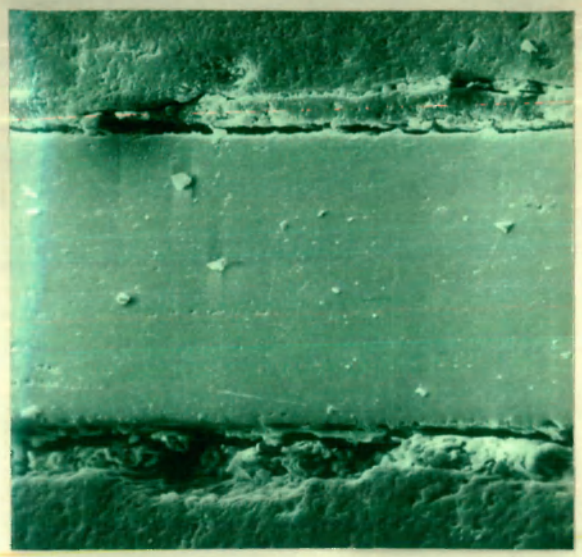

(a)

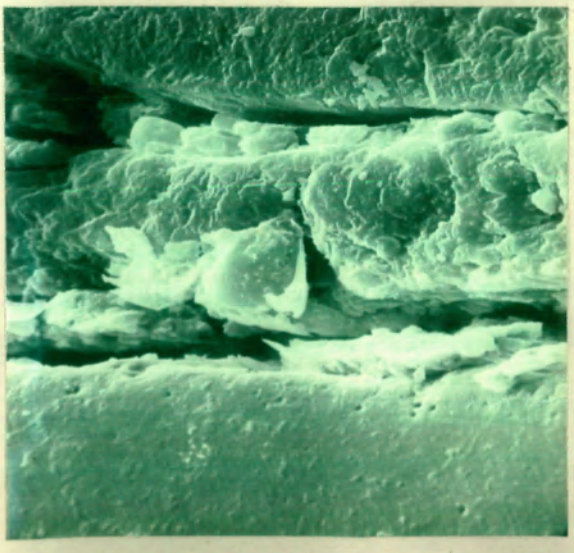

(b)

3.20

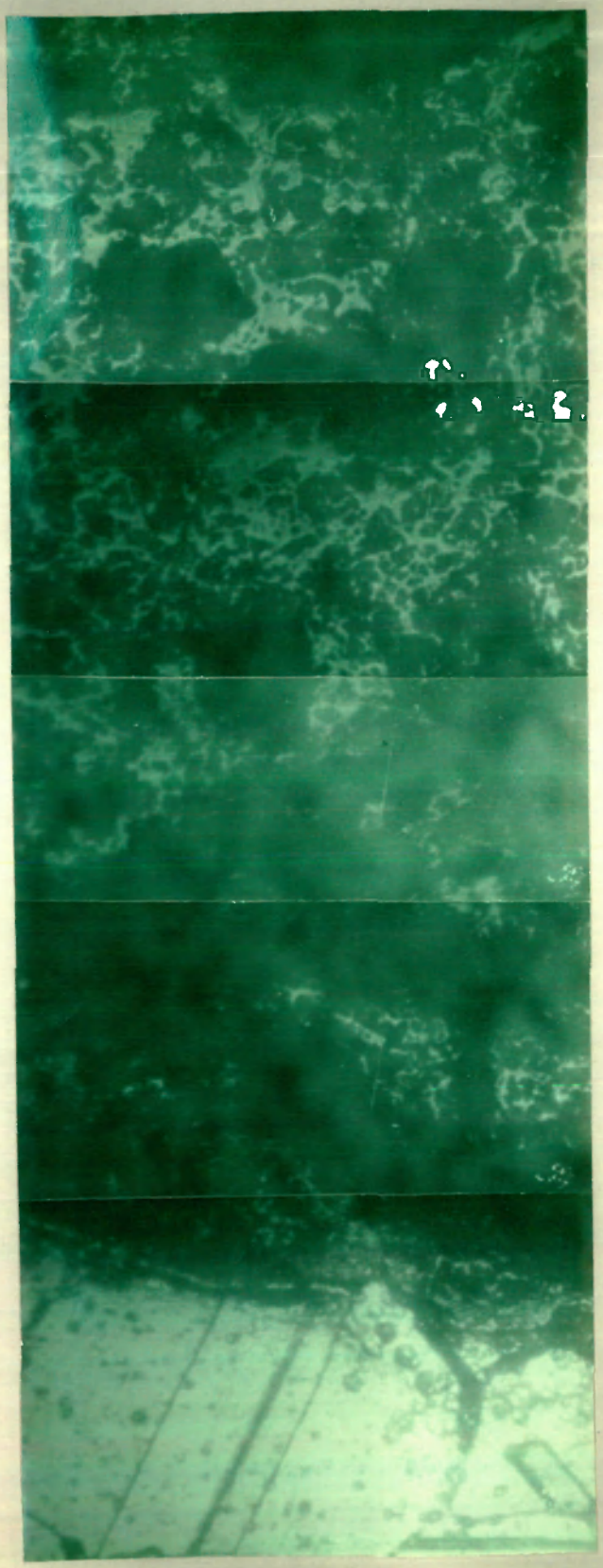

3.21

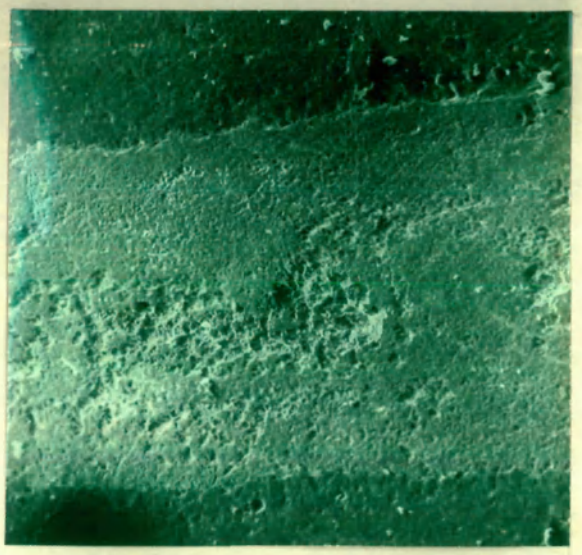

(a)

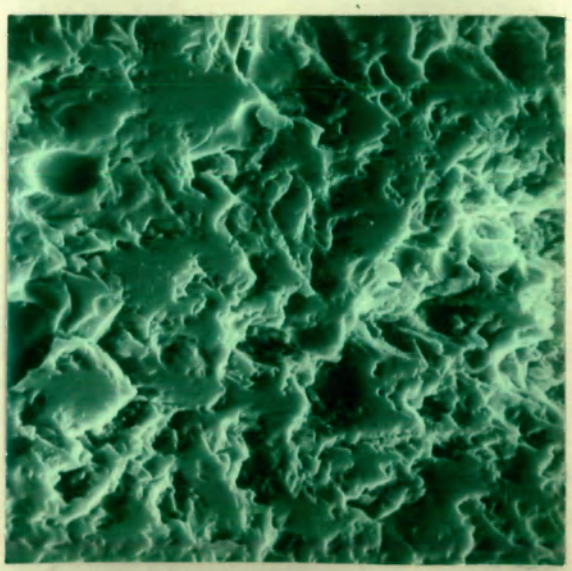

(b)

3.22

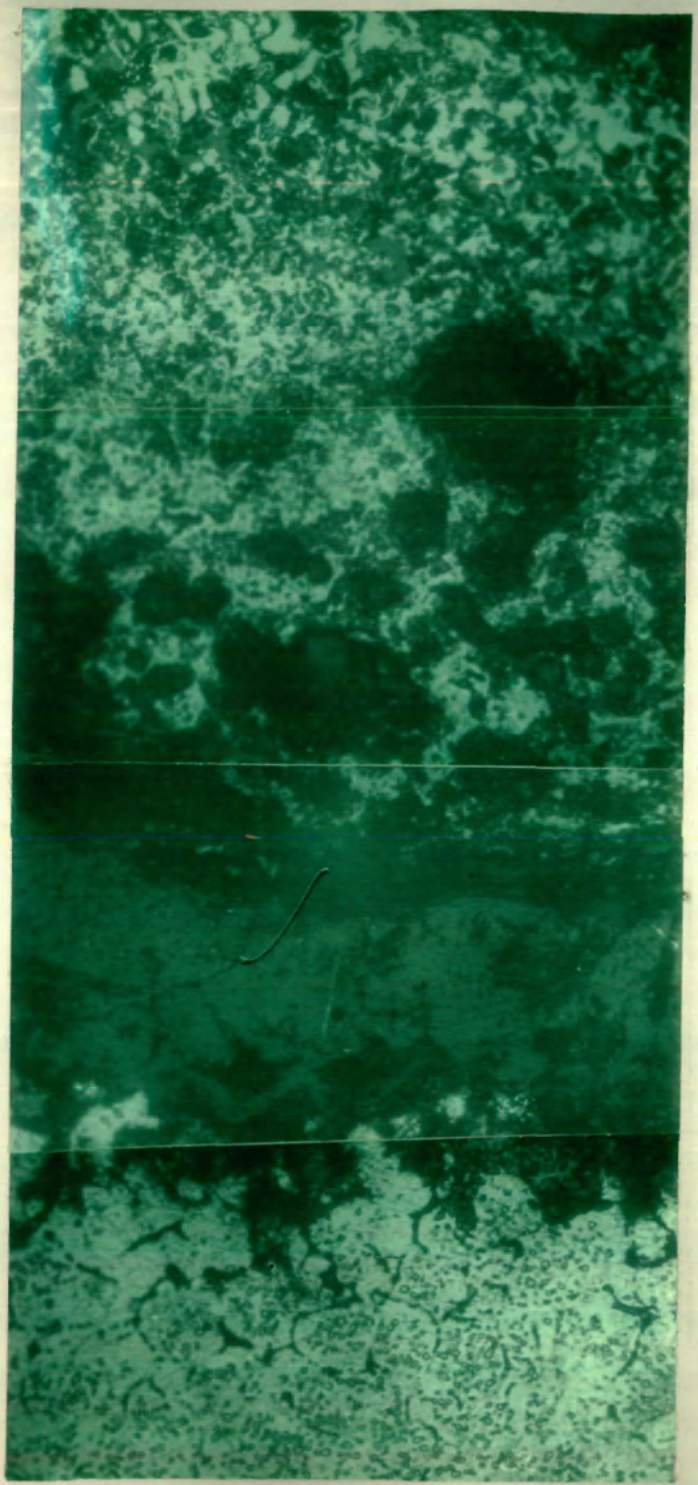

3.23

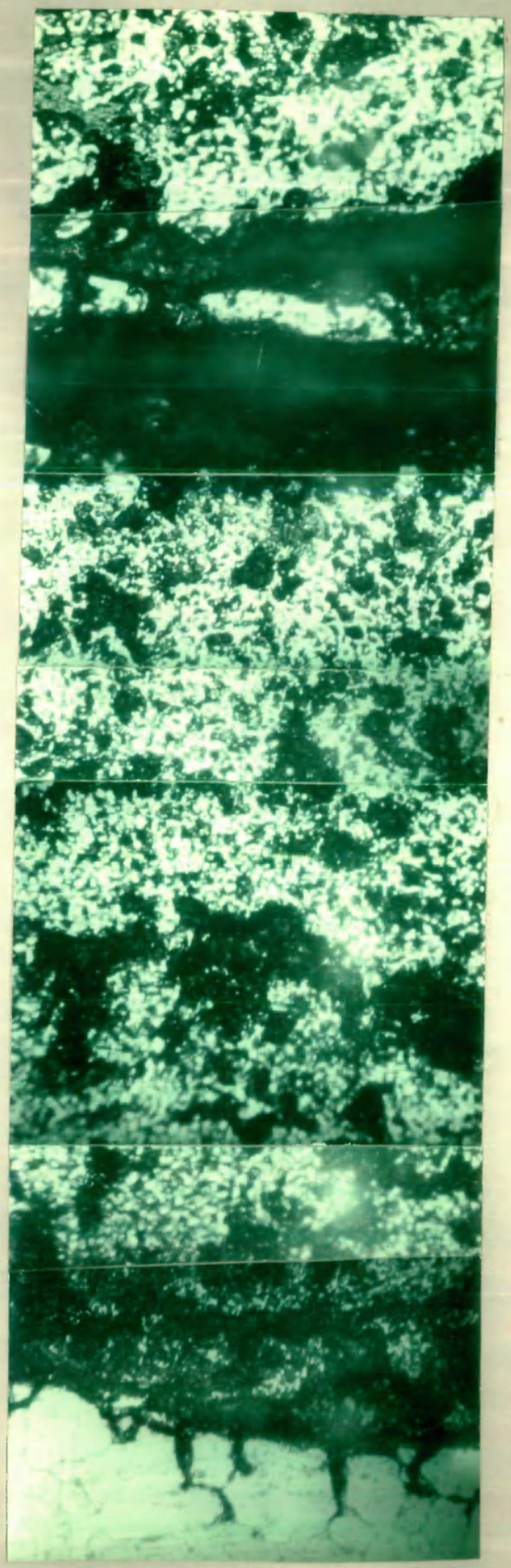

3.24

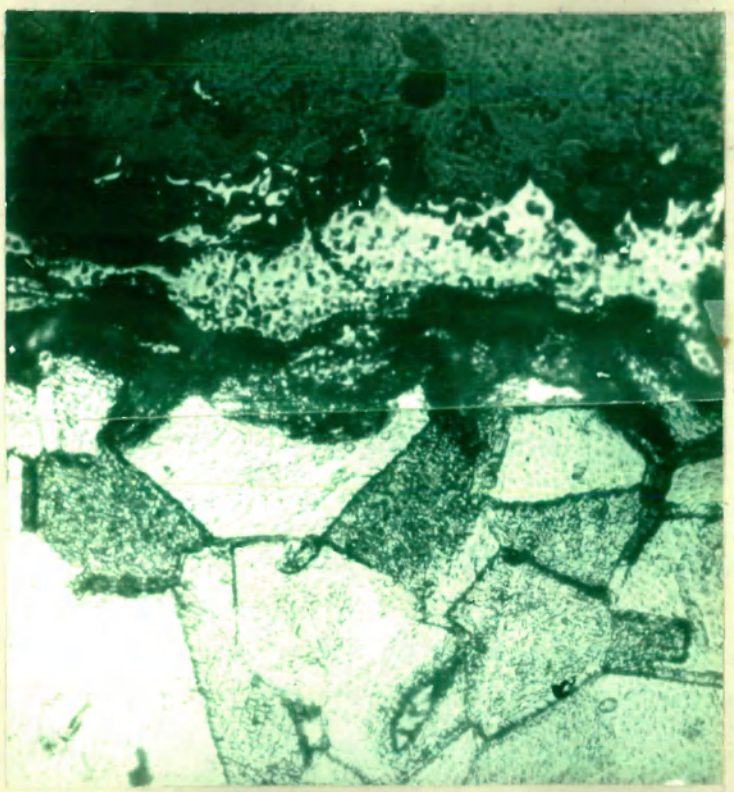

3.25

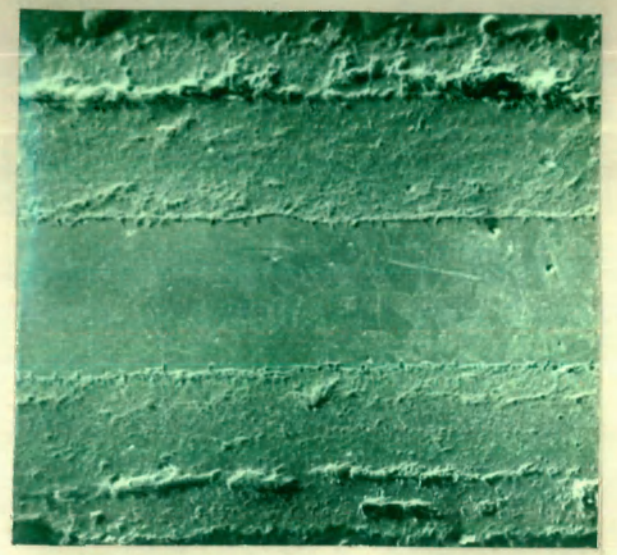

(a)

(b)

3.26

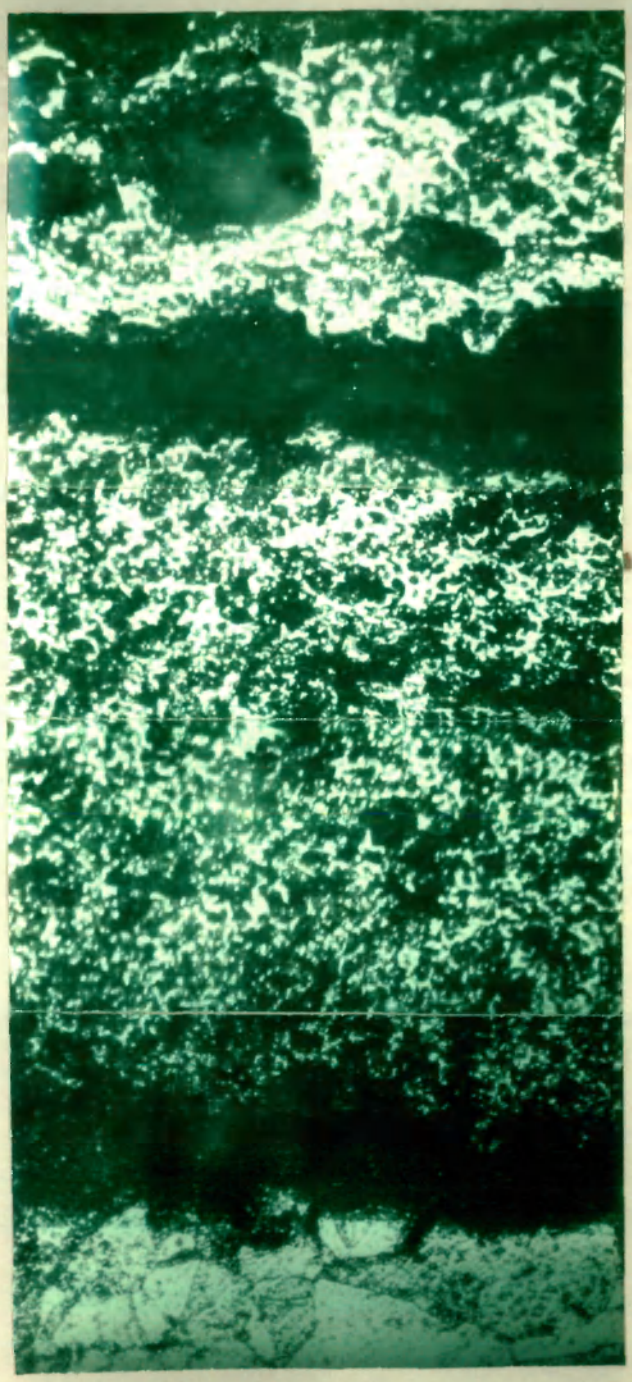

3.27

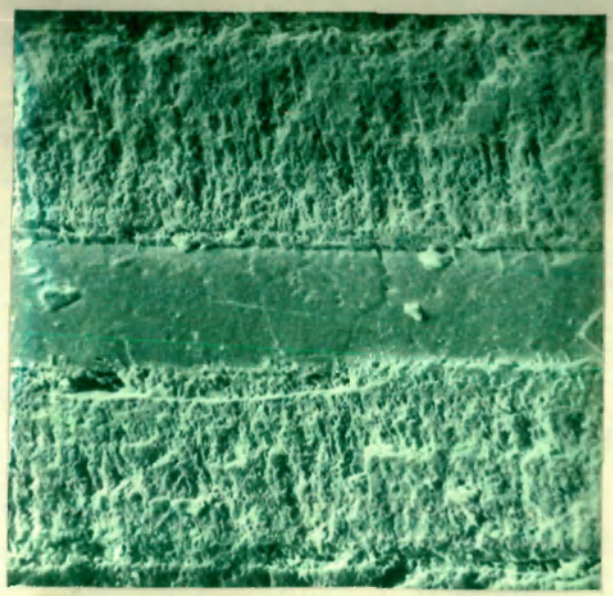

(a)

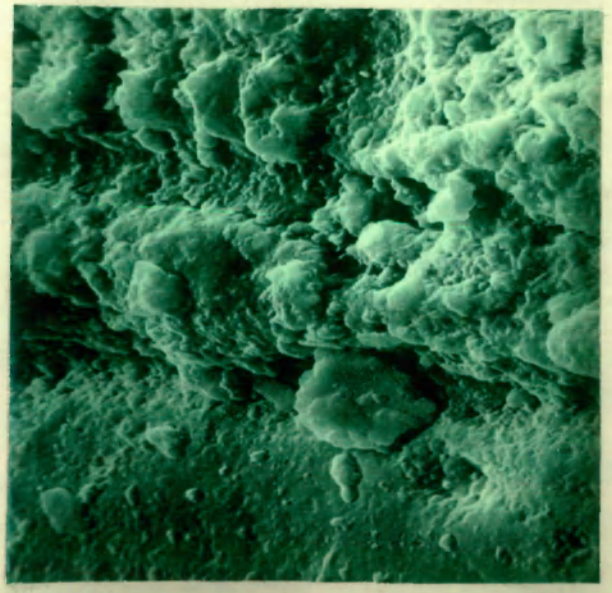

(b)

3.28

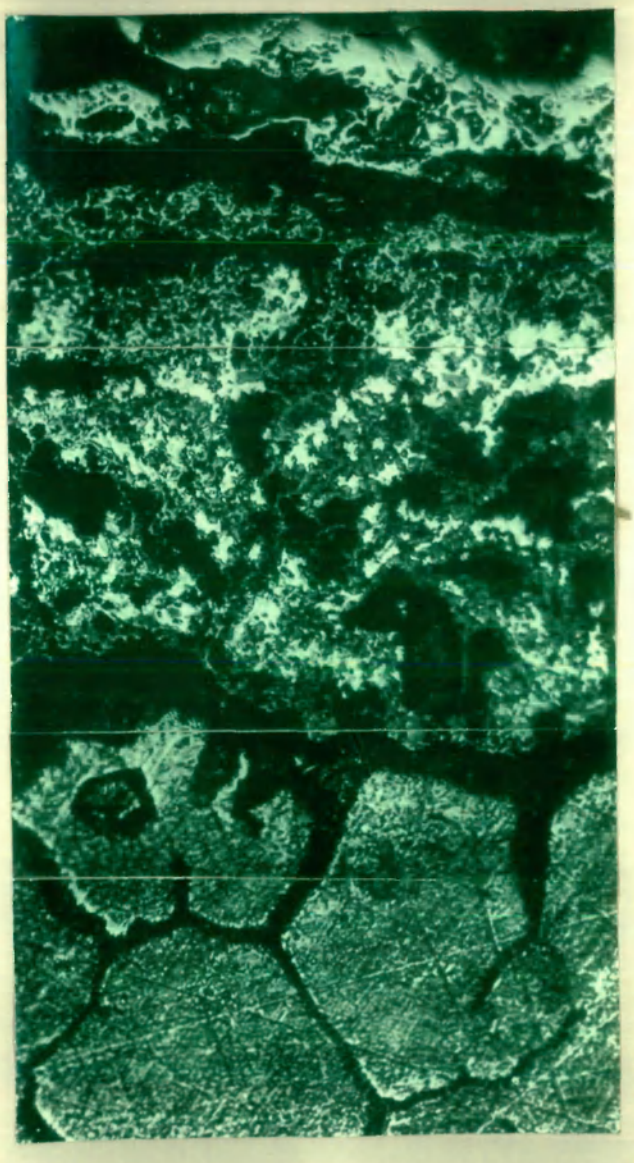

3.29

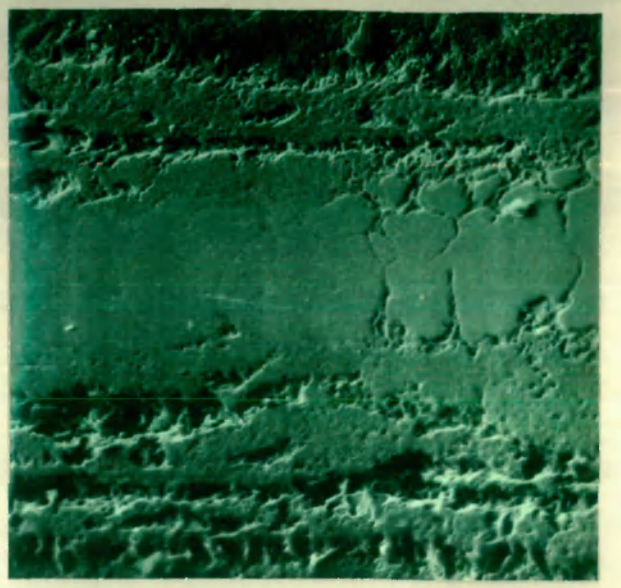

(a)

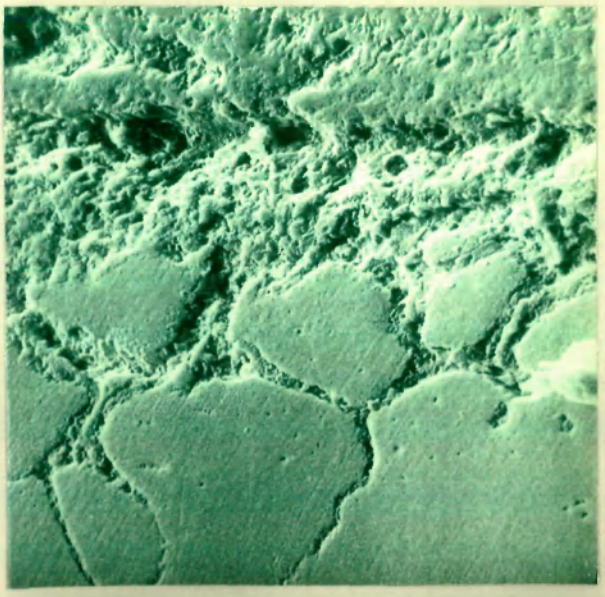

(b)

3.30

CAPTIONS OF EDAX

Fig. 3.31 EDAX of the scale formed on AISI-321 steel coated with $Cr_2(SO_4)_3$ and heated at 1000°C for 6 hours.
(a) Electron image, (b) FeK , (c) CrK ,
(d) NiK

Fig. 3.32 EDAX concentration profiles of AISI-321 coated with Na_2SO_4 + $CoSO_4$ mixture and oxidised at 1000°C for 6 hours.

Fig. 3.33 EDAX concentration profiles of AISI-303 steel coated with $Cr_2(SO_4)_3$ and heated at 1000°C for 6 hours.

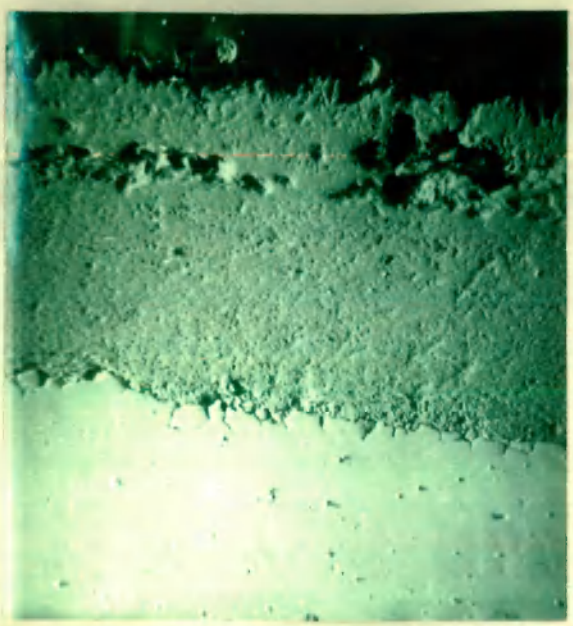

(a)

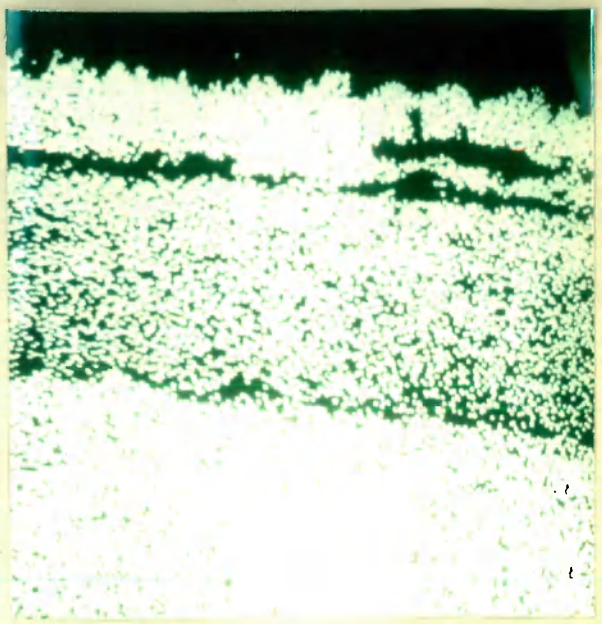

(b)

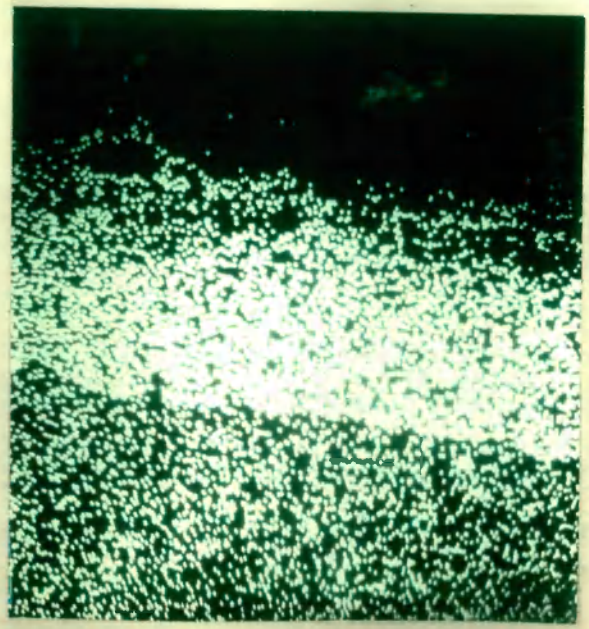

(c)

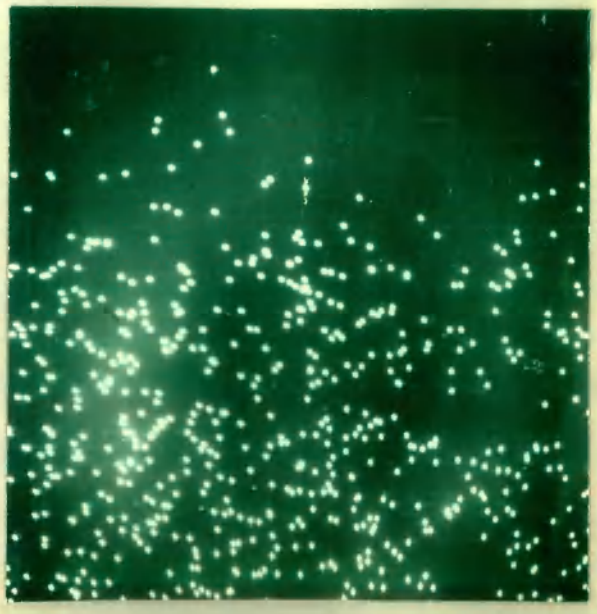

(d)

3.31

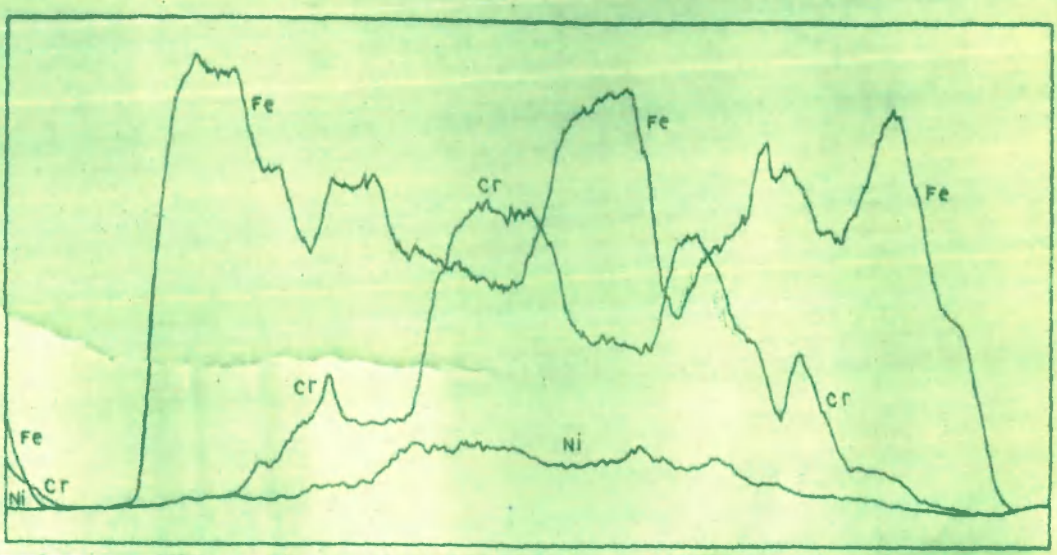

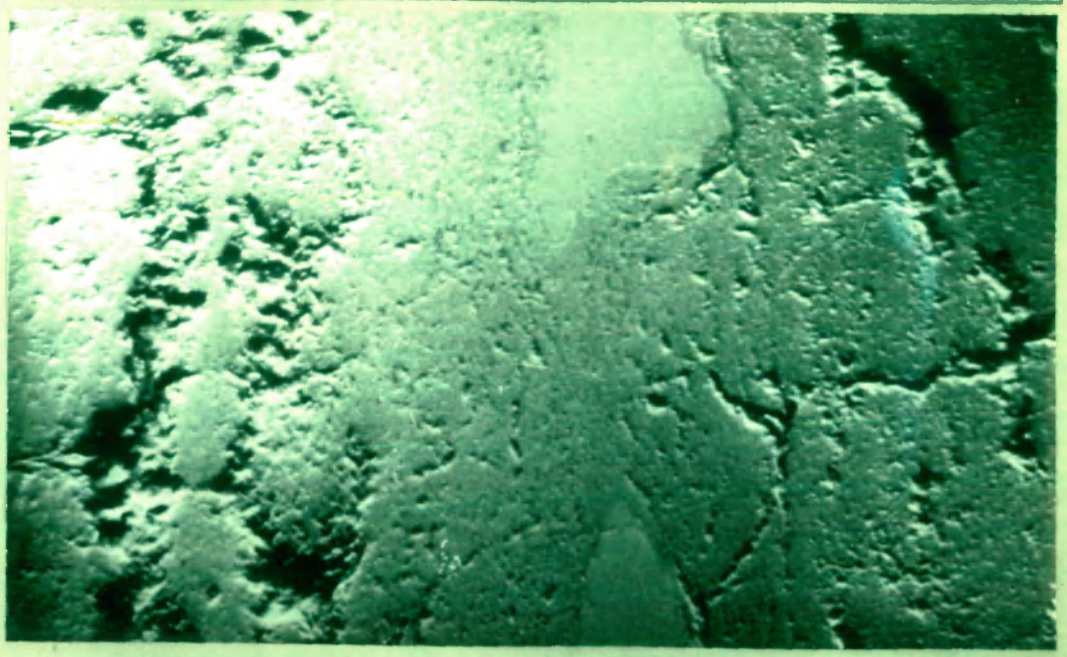

3.32

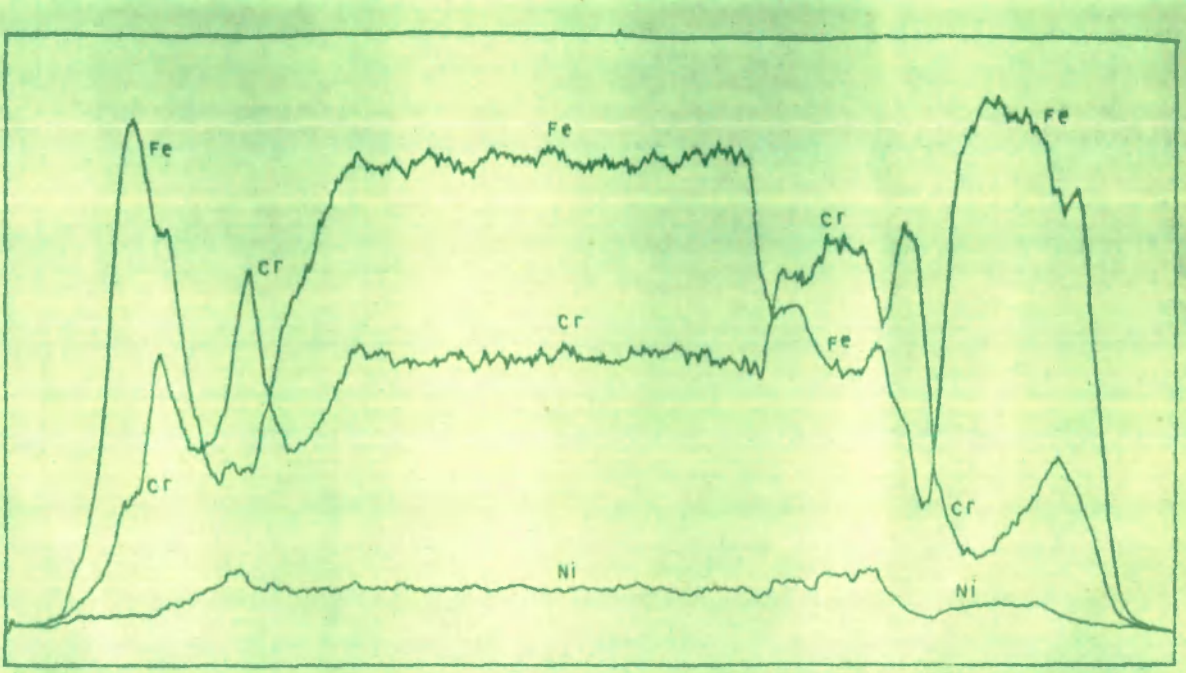

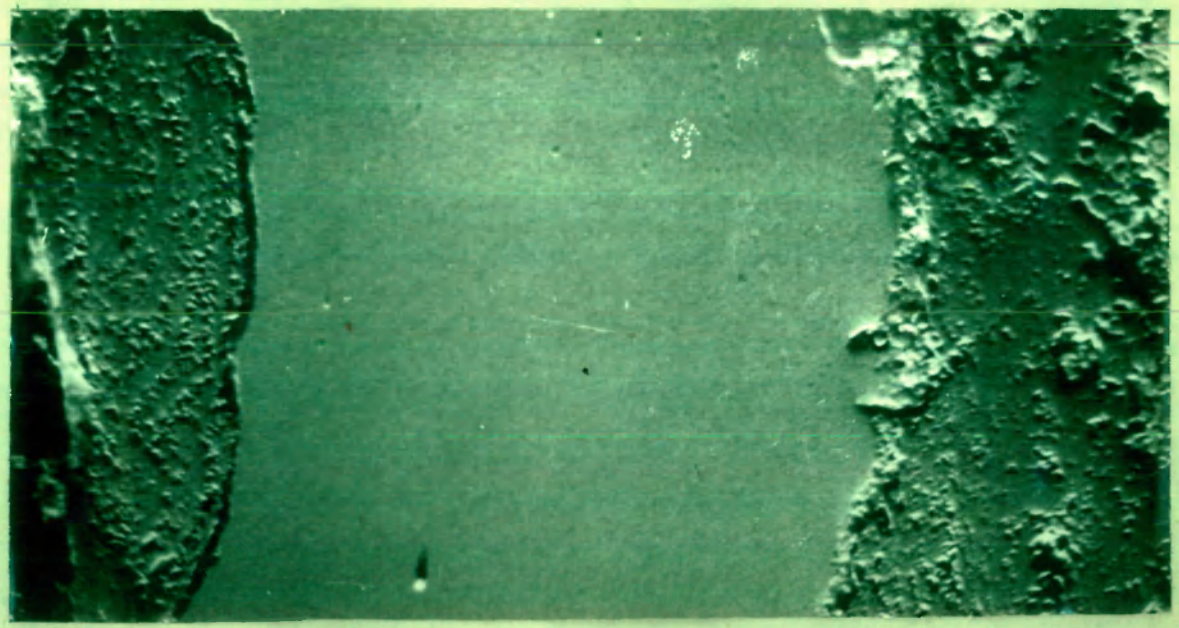

3.33

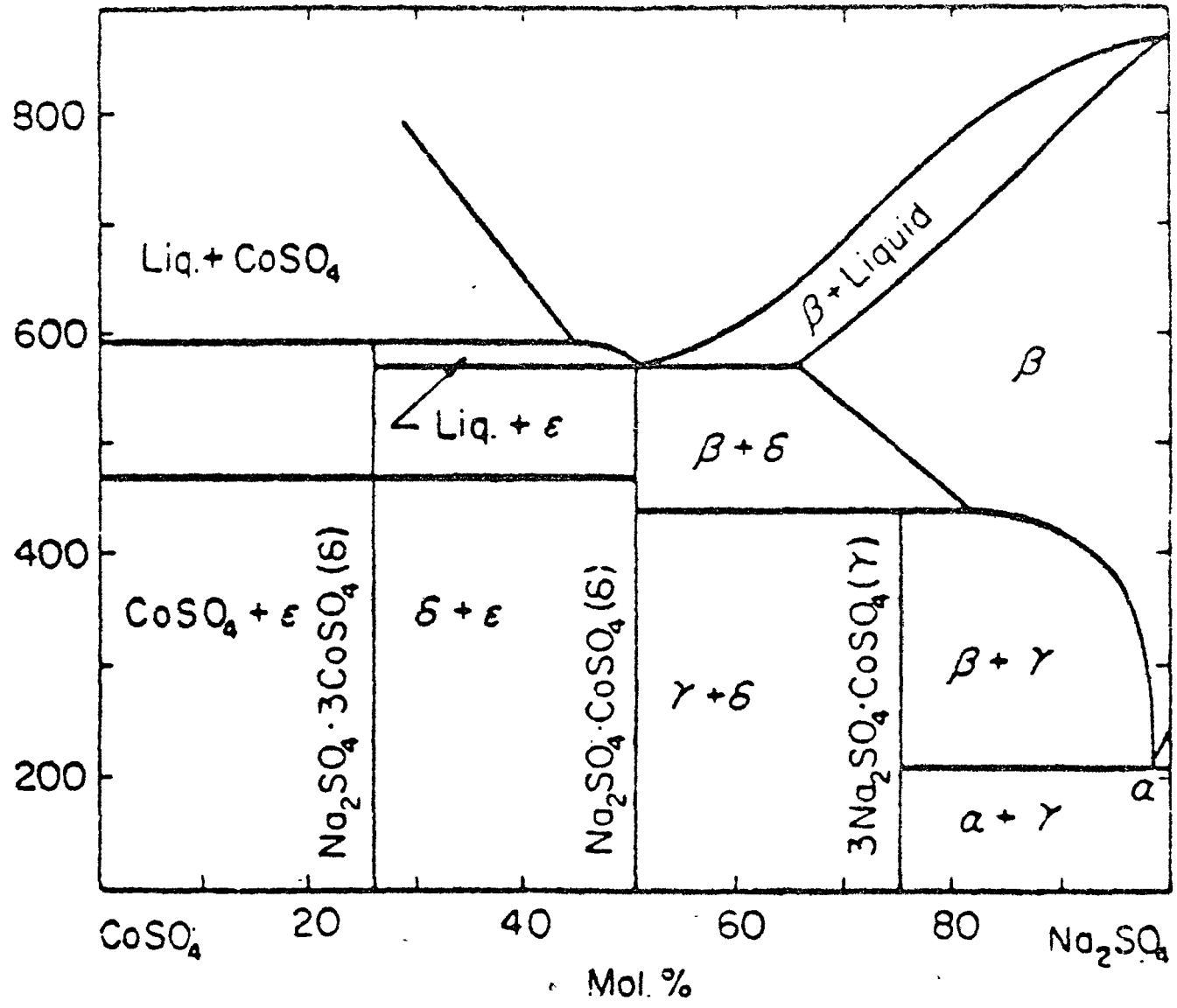

FIG. 3.34. $CoSO_4$-Na_2SO_4 PHASE DIAGRAM

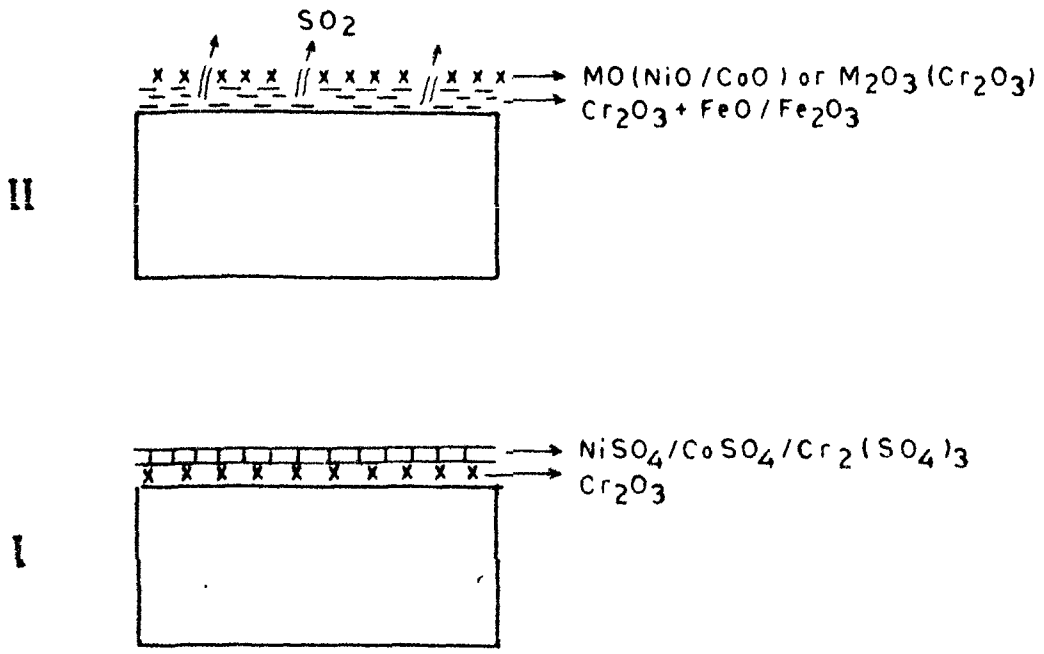

FIG. 3.35(a)

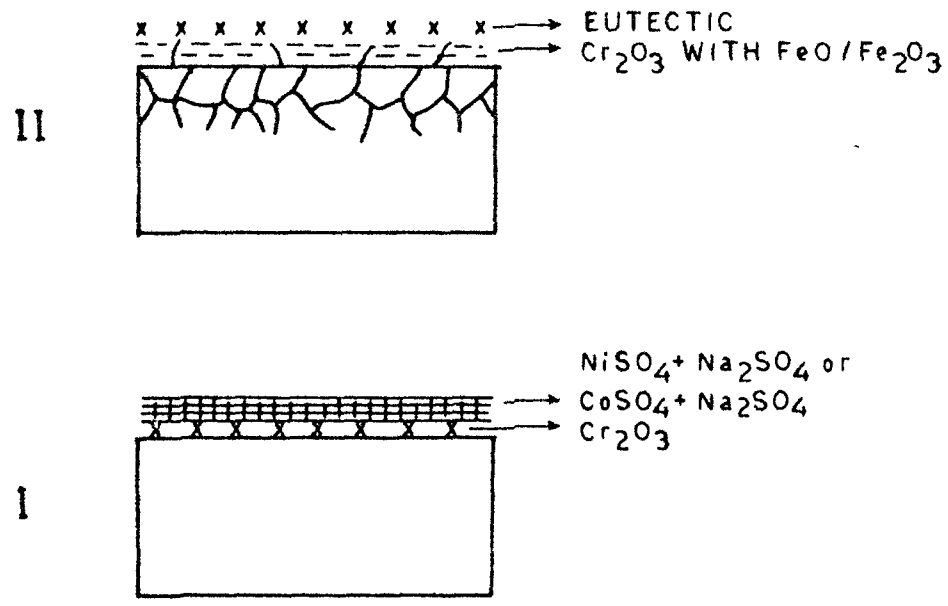

FIG. 3.35(b) HOT CORROSION OF STEEL AISI-303 or 321 COATED WITH (a) TRANSITION METAL SULFATES (b) $CoSO_4 + Na_2SO_4$ or $NiSO_4 + Na_2SO_4$, AT 800°C

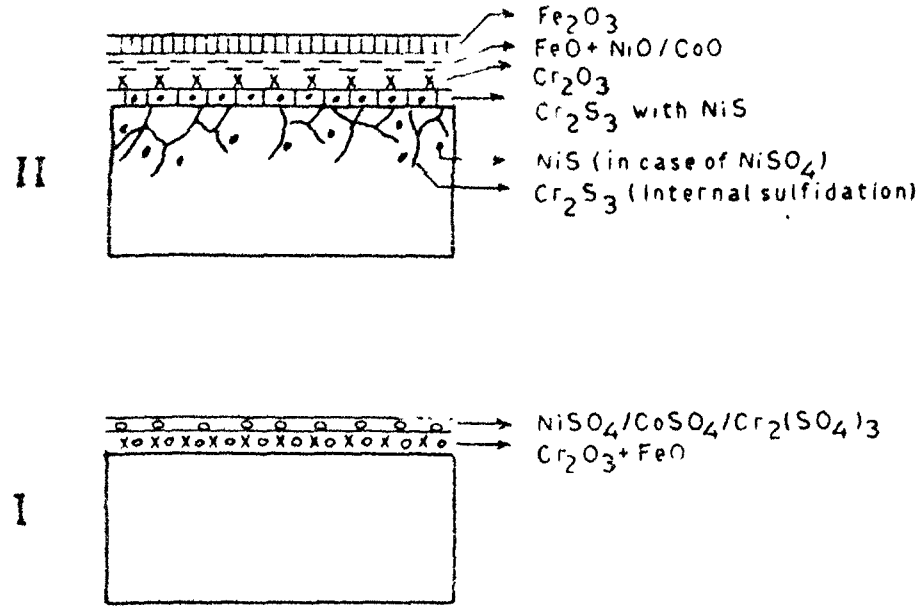

FIG. 3.36 (a) HOT CORROSION OF STEEL AISI 303 AND AISI 321 IN PRESENCE OF TRANSITION METAL SULFATES AT 1000°C

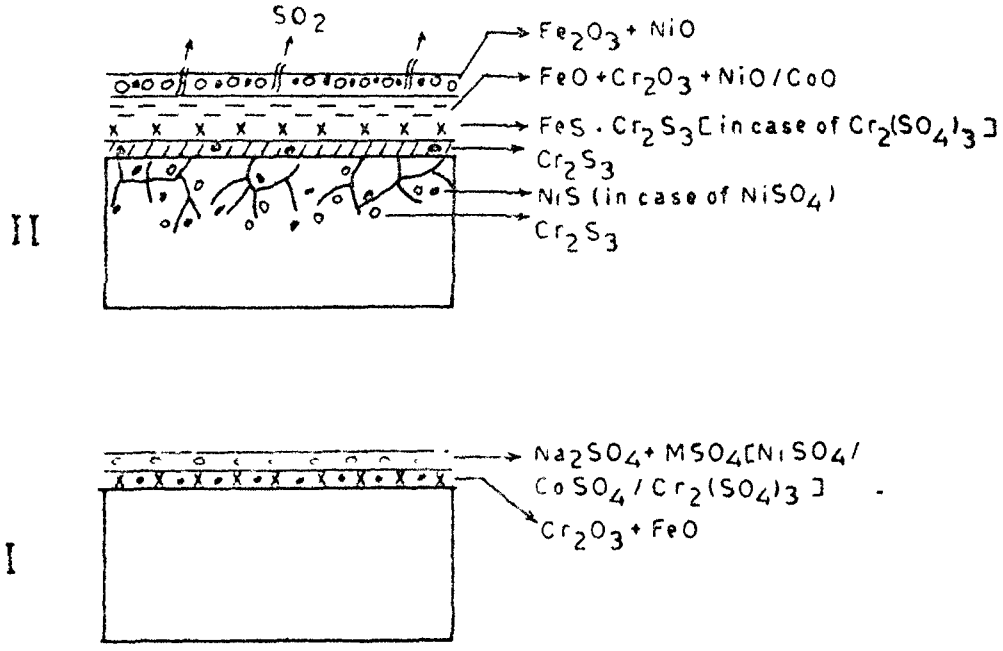

FIG 3 36 (b) HOT CORROSION OF STEEL AISI 303 AND AISI 321 IN PRESENCE OF TRANSITION METAL SULFATES AND SODIUM SULFATE AT 1000°C

CHAPTER - IV

HIGH TEMPERATURE OXIDATION BEHAVIOUR OF NICKEL-BASE ALLOYS IN PRESENCE OF Na_2SO_4

EXPERIMENTAL

4.1.1 Selection of the alloys

Six commercial Ni-base alloys, viz., Inconel-600, Inconel-800, Monel-400, B-1900, Nimonic-105 and Nickel-200, were used for the hot corrosion studies in presence of Na_2SO_4. The nominal composition of the alloys is given in Table 4.1.

4.1.2 Preparation of the specimens

Rectangular specimens of 1.5 cm x 0.5 cm x 0.1 cm size from sheets or round specimens of about 1.3 cm diameter x 0.2 cm thickness size from rods of the alloys were cut. These specimens were abraded sequentially with 180, 320 and 600 grade SiC papers, washed with alcohol and were degreased with CCl_4.

4.1.3 Coating of the specimens

The alloy coupons were uniformly coated with a thin film of Na_2SO_4 ($\sim$ 5 μm thick) containing about 1.0 mg/cm^2 of the salt. The coating was carried out by spraying a nearly saturated solution of Na_2SO_4 on a hot specimen ($\sim$ 300°C). The operation was continued till a nearly uniform coating of the salt covering all the faces is obtained. Coated specimens were dried overnight in an air oven maintained at 150°C, cooled in a desiccator and weighed. The

coated specimens were subsequently employed for hot corrosion studies.

4.1.4 Hot corrosion studies

Hot corrosion studies were carried out under atmospheric pressure, in presence of Na_2SO_4 at 800 and 1000°C. The corrosion runs were usually of 12 hrs durations.

The coated specimens were transfered to a quarts bucket and suspended in a nichrome wound tubular furnace of laboratory fabricated helical thermal balance with an accuracy of ± 0.1 mg/cm^2 and maintained at the desired temperature. Variation in weight of the sample were recorded on an interval of one hour.

Uncoated samples were also oxidized under conditions similar to those maintained during the oxidation of coated alloys.

For a particular oxidation experiments, three coated/uncoated specimens were oxidized under nearly identical conditions. Out of the three corroded samples, the first was used for chemical identifications of the scale, soluble and insoluble species, and pH of the soluble species. The second sample was used for X-ray diffraction analysis and last of the samples was mounted in a cylindrical shaped paper mould, using a cold setting resin such as Araldite.

The mounted specimens were then prepared for metallographic studies followed by SEM and EDAX studies.

4.1.5 X-ray diffraction analysis

The presence of different constituents in the scales of the corroded alloys was identified by conventional X-ray diffraction analysis.

The X-ray diffractograms were obtained by a X-ray diffractometer assembly, using $CuK\alpha/CoK\alpha/FeK\alpha$ radiations with an appropriate filter.

4.1.6 Morphological studies

4.1.6.1 Optical metallography

The mounted specimens were abraded with 180, 320 and 600 grade SiC papers, respectively. The abraded specimens were then polished on a motor driven disc polisher using alumina powder of 1 μ grade. In order to avoid dissolution of water soluble inorganic compounds present in the scales, Kerosene oil were used as a lapping liquid during the entire polishing operation. Polished specimens were washed with alcohol and degreased with CCl_4. Samples were examined under a Leitz photometallurgical microscope. The polished samples were either etched chemically with 1% acidic $FeCl_3$ solution or etched electrolytically in a 2% HNO_3 for 2-3 minutes. In most cases repeated alternate operations of

polishing and etching gave satisfactory results.

The polished and etched specimens were examined under a Leitz photometallurgical microscope attached with a 35 mm camera. The regions of the microstructure giving relevent details were photographed.

4.1.6.2 Scanning Electron Microscopy (SEM)

Polished specimens were coated with silver or gold emulsion and were examined under a Cambridge Scanning Electron Microscope Model S4-10 and desired regions of the scale were photographed at an appropriate magnification.

4.1.7 Energy Dispersion X-ray Analysis (EDAX)

Elemental distributions within the scale and the matrix were obtained by EDAX from corresponding Kα concentration profiles of the relevent elements. A Cambridge Scanning electron microscope (model S4-10) attached with EDAX arrangement was used for this purpose.

RESULTS

The oxidation behaviour of some commercial Ni-base alloys, viz., IN-600, IN-800, Monel-400, Nimonic-105, B-1900 and Nickel-200, has been studied in presence of Na_2SO_4 at 850 and 1000°C in flowing air. Parallel oxidation studies were also carried out with the same alloys without salt coatings.

The following sections describe the oxidation kinetic behaviour of the alloys in the presence and absence of Na_2SO_4. This is followed by the results of morphological studies conducted on oxidised and corroded alloys.

4.2 Kinetic Studies

4.2.1 Oxidation kinetics of uncoated alloys

Inconel-600:

The alloy oxidises with a loss in weight though the weight loss are relatively small (Fig. 4.1 & 4.2). Weight losses of 0.5 mg/cm^2 and 1.7 mg/cm^2 are observed at 850 and 1000°C, respectively after 12 hours oxidation run. Initially there is relatively rapid loss in weight followed by a period of constant weight upto the end of the run. The period upto which there is rapid loss in weight varies according to the temperature: 6 and 10 hours at 850 and 1000°C, respectively.

Inconel-600:

The alloy shows continuous weight loss at 850°C sustaining a total weight loss of about 1 mg after 12 hours oxidation run (Fig. 4.1). At 1000°C, Inconel-600 shows virtually no change in weight upto the end of run (Fig. 4.2).

Monel-400:

At 850°C, after initial weight losses (extending upto a period of about 4 hours) the alloy oxidizes linearly with relatively large weight gains with a total weight gain of 5 mg/cm^2 after 12 hours oxidation run (Fig. 4.1). At 1000°C, the alloy oxidises by a parabolic rate with a total weight gain of about 90 mg/cm^2 at the end of the 12 hours oxidation run (Fig. 4.2).

Nimonic-105:

The alloy shows small weight losses during oxidation at 850 and 1000°C, the weight losses are comparatively smaller at the higher temperature (Fig. 4.1 and 4.2).

Nickel-200:

The metal oxidises by a parabolic rate law at 850 and 1000°C. At 1000°C, however, there is a sudden increase in weight gain after 8 hour oxidation run.

B-1900:

Upon oxidation, the alloy shows small weight losses

at 850°C. Total weight loss of about 1.25 mg/cm^2 is observed at the end of 12 hour oxidation run. At 1000°C, B-1900 exidises by a parabolic rate law with an oxidation rate much lower than Monel-400 and slightly higher than Nickel-200 (Fig. 4.2).

4.2.2 Oxidation kinetics of Na_2SO_4 coated alloys

Inconel-600:

The alloy shows weight losses at both the temperatures and, as expected, the losses are higher at 1000°C. At both the temperatures the curves show continuous weight losses upto 6 hours and after that no further weight loss has been observed (Fig. 4.3 and 4.4). The total weight loss at the end of the 12 hour run is 2 mg/cm^2 at 1000°C corresponding to 0.5 mg/cm^2 at 850°C.

Inconel-800:

The alloy shows similar behaviour as that observed in case of Inconel-600 though the rate of weight loss is higher in Inconel-800 at both the temperatures (850 and 1000°C) (Fig. 4.3 & 4.4).

Nimonic-105:

The Na_2SO_4 coated alloy shows weight losses at 850 and 1000°C. The nature of the curves is similar to those of Inconel-600 and Inconel-800. At 850°C there is a weight

loss of 1.5 mg/cm^2 at the end of the 12 hour oxidation run corresponding to a total weight loss of 2.8 mg/cm^2 at 1000°C.

B-1900:

At 850°C, the Na_2SO_4 coated B-1900 after relatively slow oxidation upto a period of 4 hours, oxidizes at a much faster rate following a linear rate law with a total weight gain of about 10.5 mg/cm^2 at the end of 12 hour oxidation run. However, the coated alloy shows an approximately parabolic behaviour at 1000°C and the weight gain is about 16.5 mg/cm^2.

Nickel-200:

At 850°C, the coated alloy shows a higher weight gain (10 mg/cm^2) than at 1000°C (4.5 mg/cm^2).

Monel-400:

The weight gain/time curve for the Na_2SO_4 coated Monel-400, at 850°C, shows alternate regions of rapid weight gain and constant weight. The curve may be considered of consisting two parabolic curves.

At 1000°C, the coated alloy oxidizes linearly with much faster rate than at 850°C. Comparing the oxidation behaviour of Monel-400 under Na_2SO_4 coated and uncoated conditions, it appears that the presence of Na_2SO_4 suppresses the oxidation of the alloy.

4.3 Metallographic Studies

Inconel-600:

Figure 4.5 shows the optical micrograph of a cross section of IN-600 alloy, oxidised at 850°C in the presence of 1 mg/cm^2 Na_2SO_4 for 12 hours, in flowing air. Presence of Cr_2S_3 at the grainboundaries indicates the internal sulfidation. The outer scale is mainly composed of Cr_2O_3 with inclusions of NiO.

The SEM picture of the same alloy provides more information regarding the composition of the scales (Fig. 4.6). The inner layers mainly contain Cr_2O_3 followed by layers rich in NiO and Fe_2O_3. Presence of internal Cr_2S_3 can also be seen in the micrograph.

Inconel-800:

Figure 4.7 presents Scanning Electron Micrograph of a cross section of the Na_2SO_4 coated IN-800 alloy corroded at 850°C for 12 hours in flowing air.

The inner most scale in the form of a relatively thin layer, contains Cr_2S_3 (dark), this is followed by a fragile but thicker layer of $(Fe,Cr)_2O_3$. This layer is broken due to tensile stresses developed during polishing. The outer scales which are present in the form of a very thick layer contains NiO in predominent concentration.

Monel-400:

The optical metallograph of the cross section of M-400 alloy, coated with Na_2SO_4 and corroded at 850°C has been shown in figure 4.8. The scale consists of three distinct layers. The innermost layer consists of (Cu,Ni)S_x with some inclusions of NiO. The middle layer contains CuO with NiO inclusions and the outermost thick layer which is porous has NiO in predominent concentration.

Nimonic-105:

Figure 4.9 represents an optical micrograph of a cross section of Nim-105 alloy specimen coated with Na_2SO_4 and oxidized at 1000°C for 12 hours in flowing air. The outer surface is fragmented and in between the fragments and at the peripheries Cr_2S_3 is present, apparently there is no evidence of Al_2O_3, this is followed by an external scale which is perhaps separated from the inner scale due to polishing artifacts. The external scale consists of two layers, a mixed oxide layer which is relatively thick and discontinuous, and a porous layer of NiO. The presence of chromium rich NiS particles can be seen in the innermost scales. Figure 4.10.a and 4.10.b show SEM pictures of the same alloy at lower and higher magnifications. The inner scales are quite compact and contain a 2-phase material, Cr_2O_3 and probably Al_2O_3. The outer layer of the scale contains NiO.

Nickel-200:

Figures 4.11 and 4.12 show the micrographs of the cross sections of Ni-200 specimens coated with Na_2SO_4 and corroded at 850 and 1000°C, respectively.

The alloy corroded at 850°C shows stratified layers of NiO with Na_2SO_4 inclusions. The molten salt is penetrated along grainboundaries and fragmented the outer fringes of the alloy surface. Along the grainboundaries, concentration of Ni_3S_2 and (Ni + Ni_3S_2) can be clearly seen, the latter appears to be present in the form of cooled liquid.

Figure 4.13 shows the SEM picture of the coated alloy at 850°C. There Ni_3S_2 constitutes the inner scale. The outer scales are richer in NiO admixed with $NiSO_4$. There is a high concentration of $NiSO_4$ in the regions where cracking has occurred in the scale. This may be due to conversion of Ni_3S_2 into $NiSO_4$ due to access of air through the cleavages. Figure 4.14 shows the presence of NiO in the outer scales in the form of stratified layers. The inner scales which are relatively thin and discontinuous contain Ni_3S_2 with inclusions of NiO.

Figure 4.12 shows a photomicrograph of the Na_2SO_4 coated alloy at 1000°C. Here only the structural details of the matrix are revealed. There is profuse internal sulfidation in the grain and along the grainboundaries. Two types of phases can be distinguished: NiS (light grey) and Ni +

$NiSO_4$ (dark). Some of the NiS is perhaps oxidised to $NiSO_4$ in the vicinity of alloy/scale interface.

4.4 X-ray Diffraction Analysis:

Table 4.2 lists the constituents which are identified in the scales of Na_2SO_4 coated and uncoated oxidised alloys.

4.5 Energy Dispersion X-ray Analysis (EDAX)

Oxidised Inconel-600:

Figure 4.15 shows NiKα , CrKα , and FeKα X-ray concentration profiles of Inconel-600 oxidised at 1000°C for 12 hours. The inner scales which are relatively thicker, are enriched in chromium with considerable inclusion of iron. The innermost layer of the scale seem to contain only chromium. The outer scales are rich in iron with Ni and Cr with minor inclusions.

Na_2SO_4 coated Inconel-600:

Figure 4.16 represents X-ray concentration profiles of Ni, Cr and Fe of Na_2SO_4 coated Inconel-600 oxidised at 850°C. The inner scales seem to contain a Cr-rich layer, this is followed by Ni-enriched thick scales with Cr inclusions.

Na_2SO_4 coated Inconel-800:

Figure 4.17 shows EDAX concentration profiles of Inconel-800 oxidised at 1000°C in presence of Na_2SO_4. The inner scales mainly contain chromium and the outer scales are though rich in chromium but contain iron in appreciable con-

centration. There is no evidence of presence of Ni in the scales.

Na_2SO_4 coated Monel-400:

Figure 4.18 represents X-ray Kα concentration profiles of Fe, Cu and Ni in the Na_2SO_4-coated Monel-400 alloy sample oxidised at 850°C. The innermost scale seems to contain alternate layers of Cu and Ni (probably in the form of a duplex scale of CuS and NiS). The outer scales are rich in nickel with copper in appreciable concentrations perhaps in the form of (Cu,Ni)O. There is evidence of the presence of Fe in very low concentrations in the outer scales.

Na_2SO_4 coated Monel-400 oxidised at 1000°C:

The X-ray concentration profile (Figure 4.19) of the Na_2SO_4 coated oxidised alloy indicates the presence of a scale containing mixed nickel and copper oxides with isolated pockets of CuS and NiS. The profile of the substrate indicates a gradual increase in nickel concentrations and a similar decrease in copper concentrations. This is an indication of internal sulfidation of nickel particles present in the matrix. The concentration of these particles is high in the vicinity of alloy/scale interface.

DISCUSSION

The high temperature oxidation studies carried out on some Ni-base alloys, e.g. Inconel-600, Inconel-800, Nickel-200, Monel-400, Nimonic-105 and B-1900 show relatively little or no weight change during 12 hr exposure to air at 850 and 1000°C, with an exception of Monel-400. Monel-400 which is primarily a Ni-Cu alloy oxidises fairly rapidly at 850°C and still faster at 1000°C. The chromia film which is formed initially on the majority of the alloys seem to provide reasonable protection against oxidation upto 1000°C. The CuO film which is formed on the alloy surface does not seem to be protective and is partially broken down at 850°C and thus facilitates further oxidation. The film is completely disrupted at 1000°C when the alloy oxidizes at a much faster rate.

In presence of Na_2SO_4, while the chromia former alloys, e.g. Inconel-600, Inconel-800 and Nimonic-105 show small weight losses at 850 and 1000°C (to the extent of about 5 mg/cm^2 in 10 hr), the B-1900 (alumina former) and Nickel-200 and Monel-400 (NiO former) oxidise appreciably following a linear or a parabolic kinetic.

In typical isothermal hot corrosion tests, the initial period during which little or no weight gain or slight weight loss is observed is usually referred to as induction (incuba-

tion) period. This can be defined as the time at which abrupt change in slope occurs in the corrosion curves.

Induced hot corrosion of superalloys displays two types of behaviour: "catastrophic" - in which the attack (as manifested by weight change) proceeds at an approximately linear rate until the sample is largely consumed or "accelerated" - in which the attack is largely enhanced over that normally encountered in plain oxidation but finally the rate decreases at longer times[1]. This type of behaviour exhibited depends upon alloy composition, temperature and the amount of the salt applied[2]. Smaller amounts of salt usually favour accelerated oxidation whereas large concentration of the deposited salt and/or volatile phase (oxide, sulphide or a salt) result in catastrophic oxidation. It will be seen in the following sections that both types of situations are encountered in the alloy systems under study.

It appears that Na_2SO_4-coated Inconel-600, 800 and Nimonic-105 form chromia film at the very early stage of oxidation. This film reacts with Na_2SO_4 to undergo the following types of reactions at 850 and 1000°C.

$$\text{I} \qquad Cr_2O_3 + \tfrac{3}{2}O_2 + 2Na_2SO_4\ (l) \longrightarrow 2Na_2CrO_4\ (l) + 2SO_3\ (g)$$

The evolution of SO_3 will result in the weight loss and a net

weight loss may ultimately be observed if the oxidation of Cr to Cr_2O_3 or sulfidation to Cr_2S_3 is a much slower process. The evidence for reaction I is overwhelming such as (i) weight loss during oxidation, (ii) presence of a yellow product on the wall of the reaction vessel in the form of a condensed deposit; the yellow compound was identified chemically or by X-ray diffraction analysis as chromate, (iii) detection of SO_2/SO_3 in the reaction product gases, (iv) slightly basic nature of the melt. At the end of the induction period when molten Na_2SO_4 comes into contact with the alloy, the following reactions are possible:

$$\text{II} \qquad Ni + SO_4^{2-} \longrightarrow NiS(l) + \tfrac{3}{2}O_2 + O^{2-}$$

$$\text{III} \qquad 2Cr + 3SO_4^{2-} \longrightarrow Cr_2O_3 + 3SO_2(g) + 3O^{2-}$$

$$\text{IV} \qquad 2Cr + 3SO_4^{2-} \longrightarrow Cr_2S_3 + \tfrac{9}{2}O_2 + 3O^{2-}$$

$$\text{V} \qquad 2Al + 3SO_4^{2-} \longrightarrow Al_2O_3 + 3SO_2 + 3O^{2-}$$

$$\text{VI} \qquad Fe + SO_4^{2-} \longrightarrow FeS + \tfrac{3}{2}O_2 + O^{2-}$$

Reactions II to IV are feasible in Inconel-600, II, III, IV and VI in Inconel-800 and II to V in Nimonic-105. Sulfidation reactions (II, IV and VI) are possible when partial pressure of oxygen is substantially lowered and consequently P_{S_2} is increased (see thermodynamic phase stability diagrams at 1000 and 1200 K where Cr-, Al-, Fe- and Ni-O-S diagrams

are superimposed on Na-O-S diagram, Figs. 4.20 and 4.21). This situation can arise at the oxide/salt interface. Isolated pockets of Cr_2S_3 have indeed been found in the oxidised alloys.

The higher oxidation rates of Inconel-800 alloy in presence of Na_2SO_4 in comparison to Inconel-600 have been explained on the basis of high Cr- low Ni contents of Inconel-800 which promotes I. On the other hand, in Inconel-600 alloy the accumulation of NbC and/or TaC at the grainboundaries restricts the flux of Cr^{3+} ions which results in the discontinuation of reaction I. In Inconel-800, FeO will be fluxed according to the reaction:

VII $$FeO + Na_2SO_4 \longrightarrow Na_2FeO_2(l) + SO_2 + \tfrac{1}{2}O_2$$

Reaction VII may continue till all the Na_2SO_4 is exhausted or a decrease in P_{O_2} at the salt/melt interface may result in the precipitation of FeO. The relatively low magnitude of oxidation rates of Inconel-800 favours the discontinuation of VII.

During oxidation of Na_2SO_4-coated Nimonic-105 reactions III and V seem to proceed in the early stages followed by reactions II and V as is evident by the presence of NiS inclusions in the inner scales containing Cr_2O_3 and Al_2O_3. At the oxide/salt interface the oxygen activity is dropped to such an extent that sulfidation reactions commence result-

ing in the formation of NiS and Cr_2S_3. Due to fragile nature of the sulfidised scales the contact between scale and the alloy is lost at some sites and fresh salt comes into contact with the alloy surface at these sites. The fragmentation of the alloy surface during hot corrosion supports this view point. Mo is present in appreciable concentrations (about 5.5%) in the alloy and forms MoO_3 which is present in the inner scales. The following reactions are feasible involving formation of molybdate:

VIII $\quad MoO_3 + Na_2SO_4 \longrightarrow Na_2MoO_4(l) + SO_3(g)$

IX $\quad Cr_2O_3 + 3MoO_3 \longrightarrow 2Cr^{3+} + 3MoO_4^{2-}$

X $\quad Al_2O_3 + 3MoO_3 \longrightarrow 2Al^{3+} + 3MoO_4^{2-}$

Although there is evidence of the formation of Na_2MoO_4 in the scales, acidic fluxing reactions IX and X do not seem to undergo due to high Cr contents of the alloy. NiO which is present in the outer layers of the scales is basically fluxed as

XI $\quad NiO + O^{2-} \longrightarrow NiO_2^{2-}$

at the oxide/salt interface. NiO is precipitated at salt/air interface as porous oxide due to lowering in a_{Na_2O}.

During corrosion of Ni-200 in presence of Na_2SO_4, NiO is basically fluxed with Na_2SO_4 and the sulfur is released:

XII $NiO + Na_2SO_4 \longrightarrow Na_2NiO_2 + S + \frac{3}{2}O_2$

The sulfur thus released penetrates through the alloy along the grainboundaries to produce profuse sulfidation. NiS may also be formed through II and accumulates in the inner layers of the scales. Again with decrease in a_{Na_2O} at the salt/gas interface NiO is precipitated and appears in the form of stratified layers as the outer scale. At the regions where cracking or disruption of the scales occurred Ni_3S_2 is oxidized to $NiSO_4$ due to passage of air through cleavages. The Na-Ni-S-O diagram (fig. 4.20) shows the possibility of the formation of $NiSO_4$ at the regions of higher oxygen activities.

In presence of Na_2SO_4, B-1900 exhibits a linear kinetic at 850°C and a parabolic kinetic at 1000°C. The oxidation rates are much higher than Nimonic and Inconel alloys.

Na_2SO_4-coated B-1900 in the initial stages show induction periodslasting about 4 hr at 850°C and 1 hr at 1000°C. Fryburg et al[3] studied the chemical reactions occurred during the initiation of hot corrosion of B-1900 in presence of Na_2SO_4 at 900°C. The present study which is carried out with thinner salt films (about 5 μm) and at two temperatures indicate the plausibility of similar reactions though the corrosion attack seems to be less severe.

At 850°C, during the induction period of about 4 hr, Cr_2O_3 formed on the alloy reacts with oxide ion in Na_2SO_4 forming soluble chromate and liberating SO_3 as given in I. The behaviour is predicted by the Na-Cr-O-S stability diagram. The Cr_2O_3 is not stable in Na_2SO_4 above 10^{-4} atm and Na_2CrO_4 is the stable phase. In the later stages of induction period, MoO_3 that has formed under Na_2SO_4 liquid layer by oxidation of surface carbides reacts with the sulfate (Reaction VIII). The occurrence of VIII is supported by the presence of soluble molybdate ion in the scale. Further, this reaction proceeds to a larger extent at 1000°C. It has been suggested that major portion of Na_2MoO_4 formed during post induction period probably results from reaction of MoO_3 with other sodium coating salts with thermodynamic stabilities lower than Na_2MoO_4.

XIII $\quad MoO_3(l) + O^{2-} \longrightarrow MoO_4^{2-}$

XIV $\quad MoO_3(l) + 2NaAlO_2 \longrightarrow Al_2O_3 + Na_2MoO_4(l)$

XV $\quad 2MoO_3(l) + 2Na_2CrO_4 \longrightarrow Cr_2O_3 + 2Na_2MoO_4 + \frac{3}{2}O_2$

The formation of MoO_4^{2-} and CrO_4^{2-} is resulted by the consumption of oxide ion thus increasing the acidity of Na_2SO_4. The reduction in oxide ion concentration increases the sulfur activity because of the following or similar types of reactions:

XVI $SO_4^{2-} \rightleftharpoons O^{2-} + SO_3$

XVII $SO_4^{2-} \rightleftharpoons S^{2-} + 2O_2$

As a result sulfur is able to diffuse through the Al_2O_3 scale into the alloy. The sulfur activity is increased to an extent or P_{O_2} is low enough to allow formation of chromia and/or aluminum sulfide. However, internal sulfides were found to be chromium sulfides probably because aluminum sulfide formation requires a lower partial pressure of oxygen.

Near the end of the induction period, due to breaching of the scales at some localized spots, the underlying nickel will be exposed to Na_2SO_4 and reaction II may proceed involving the formation of NiS. Similarly reactions III and V may also occur. All these reactions increase the oxide ion concentration above 10^{-8} making the Na_2SO_4 melt markedly basic. Consequently, basic fluxing of the protective Al_2O_3 occurs.

XVIII $Al_2O_3 + O^{2-} \longrightarrow 2AlO_2^-$

The reaction proceeds actively with rapid increase in the rate of oxidation. However, as the oxide ion is used up the attack slows down which is indicated by a parabolic foot in the hot corrosion curve.

In the present hot corrosion studies the 12 hour exposure time given to the alloy specimens represent only induction and parabolic region and there is no evidence for intermediate or linear region, perhaps a longer run would have provided these regions characterised by reactions IX, X, XIII, XIV and XV.

Irrespective of acid fluxing of Al_2O_3 by $MoO_3/NaMoO_4$, there is disruption of the scale by the molten molybdenum compounds which allows oxygen penetration of the scale and results in the oxidation of the NiS that was formed at the end of induction period.

XIX $\quad NiS(l) + \frac{3}{2}O_2(g) \longrightarrow NiO + SO_2(g)$

If hot corrosion is induced with smaller amounts of Na_2SO_4 accelerated oxidation results instead of catastrophic oxidation. The decelaration of the linear rate is affected by conversion of liquid MoO_3 to solid $NiMoO_4$.

XX $\quad MoO_3(l) + NiO \longrightarrow NiMoO_4$

In fact in the present investigation presence of $NiMoO_4$ is indicated in the scales by X-ray diffraction analysis. Apart Fryberg et al, similar behaviour was reported by Bourhis et al[4] for IN713LC and IN-100 alloys - two nickel-base alloys containing molybdenum. The catastrophic oxidation encountered with large amounts of Na_2SO_4 probably

results because Na_2MoO_4 forms a larger fraction of the molten phase and removal of $MoO_3(l)$ by reaction XX was not as critical as with smaller amounts of Na_2SO_4.

In the present studies the presence of Mo has been found to be deleterious with respect to hot corrosion, affecting the catastrophic behaviour observed with this alloy. This is in agreement with the previous work carried out on catastrophic hot corrosion behaviour of Mo-containing alloys[5,6,7].

The scale morphology of the oxidized Na_2SO_4-coated Monel-400 alloy shows the presence of NiO at the alloy/scale interface at 850°C. The outer scales are comprised of CuO. At 1000°C, CuS is present in the form of localized pockets in the inner scale.

Initially NiO film seems to form beneath a CuO film. When molten Na_2SO_4 comes into contact with the CuO film the following reactions may occur:

XXI $$CuO + SO_4^{2-} \longrightarrow CuS + O^{2-} + 2O_2$$

O^{2-} is consumed by fluxing with NiO present in the inner scales(XI). Oxygen gas penetrates through the scale and preferentially oxidises NiO. With the depletion of oxygen activity at the oxide/salt interface NiO is sulfidized to NiS due to corresponding increase in sulfur activity. The

depletion in O^{2-} at the gas/salt interface also results in the precipitation of NiO as a porous scale ahead of CuS scale formed in the initial stages. Again fused Na_2SO_4 will react with NiO to carry out sulfidisation reaction forming NiS.

XXII $\quad NiO + SO_4^{2-} \longrightarrow NiS + O^{2-} + 2O_2$

and fall in S-activity will result in the oxidation of underneath copper sulfide layer. The sulfur so released will penetrate through the alloy to sulfidise Ni. These processes of alternate sulfidation and oxidation will continue till all the Na_2SO_4 is consumed. The morphology of the corroded alloy consisting of alternate Ni and Cu rich layers is in conformity with the above mechanism.

REFERENCES

1. J. A. Goebel, F. S. Pettit and G. W. Goward, Met. Trans, 4, 261 (1975).
2. C. A. Stearns, F. J. Kohl and G. C. Fryburg, NASA TM D-8461 (1977).
3. G. C. Fryburg, F. J. Kohl, C. A. Stearns and W. L. Felder, J. Electrochem. Soc., 129, 571 (1982).
4. Y. Bourhis and C St. John, Oxd. Met., 9, 507 (1975).
5. C. A. Stearns, F. J. Kohl and G. C. Fryburg, J. Electrochem. Soc., 121, 945 (1974).
6. K. R. Peters, D. P. Whittle and J. Stringer, Corros. Sci., 16, 791 (1976).
7. J. Stringer, Ann. Rev. Materials Sci., 7, 477 (1977).

Table 4.1: Chemical composition of alloys.

(Weight in %)

Alloys	Ni	C	Mn	Fe	S	Si	Cu	Cr	Al	Co	Mo	Other elements
Nickel-200	99.5	0.06	0.26	0.05	0.005	0.04	0.01	-	-	-	-	-
Inconel-600	76.9	0.06	0.20	6.66	0.007	0.38	0.16	15.58	-	-	-	Cb+Ta = 0.91
Inconel-800	31.9	0.09	0.81	45.10	0.007	0.67	0.29	20.99	-	-	-	-
Monel-400	64.7	0.17	1.02	1.29	0.005	0.24	32.57	-	-	-	-	-
Nimonic-105	45.9	0.20	1.00	2.00	-	1.00	0.20	15.8	4.9	22.0	5.5	Ti = 1.5
B-1900	64.7	-	-	-	-	-	-	8.0	6.0	10.0	6.0	Ti = 1.0

Table 4.2: Constituents identified in scales of Na_2SO_4-coated and uncoated alloys by X-ray diffraction technique.

Alloy	Salt	Temperature °C	Constituents
IN-600	Na_2SO_4	1000	FeO, Cr_2O_3, Cr_2S_3, NiO
IN-800	Na_2SO_4	850	Fe_2O_3, Cr_2O_3, NiO
M-400	Na_2SO_4	1000	CuO, NiO
Nim-105	Na_2SO_4	1000	NiO, Cr_2O_3, Al_2O_3
B-1900	Na_2SO_4	850	CoO, Al_2O_3, NiO, $NiMoO_4$
Ni-200	Na_2SO_4	850	NiO, Ni_3S_2
IN-600	Uncoated	1000	Fe_3O_4, NiO, Cr_2O_3
IN-800	Uncoated	1000	Fe_2O_3, Cr_2O_3, NiO
M-400	Uncoated	850	CuO, Cr_2O_3
Nim-105	Uncoated	1000	Cr_2O_3, NiO
B-1900	Uncoated	1000	NiO, Al_2O_3

(IN = Inconel; M = Monel; Nim = Nimonic; Ni = Nickel)

Table 4.3: Visual observations of the Na_2SO_4 -coated alloys after high temperature oxidation.

Alloys	Temperature (in degree Centigrade)	
	850	1000
Inconel-600	(i) Formation of a black coloured scale. (ii) Yellowish compound deposition on the wall of the bucket.	(i) Formation of black coloured scale. (ii) Needle like, green shining crystals deposited on the wall of the bucket.
Inconel-800	(i) and (ii) same as found in the case of Inconel-600.	(i) and (ii) same as found in the case of Inconel-600.
Monel-400	(i) Grey coloured thin scale formation. (ii) Greyish compound deposition on the wall of the bucket.	(i) Grey adherent scale. (ii) Cracks in the scale at the rim of the sample.
Nickel-200	Grey coloured thin scale.	(i) Outer layer of the scale is thick and of dark green colour. (ii) Inner layer is of grey colour.

continued ...

Table 4.5: continued ...

Alloys	Temperature (in degree Centigrade)	
	850	1000
Nimonic-105	Thin bluish green scale.	Scale formed on the sample oxidised for 4 hrs is of dark green colour, while scale formed on a sample heated for 12 hrs is of light green colour.
B-1900	(i) Outer layer thin and of grey colour. (ii) An inner thick layer of green colour. (iii) Scales are poorly adherent.	(i) Formation of a thick poorly adherent scale comprised of three distinct layers: (a) Outer layer - grey; (b) Middle layer - bluish green; (c) Inner layer - green powder like.

CAPTIONS OF KINETIC STUDIES

Fig. 4.1 Weight change versus time plots of uncoated alloys oxidised at 800°C.

Fig. 4.2 Weight change versus time plots of uncoated alloys oxidised at 1000°C.

Fig. 4.3 Weight change versus time plots of Na_2SO_4 coated alloys oxidised at 800°C.

Fig. 4.4 Weight change versus time plots of Na_2SO_4 coated alloys oxidised at 1000°C.

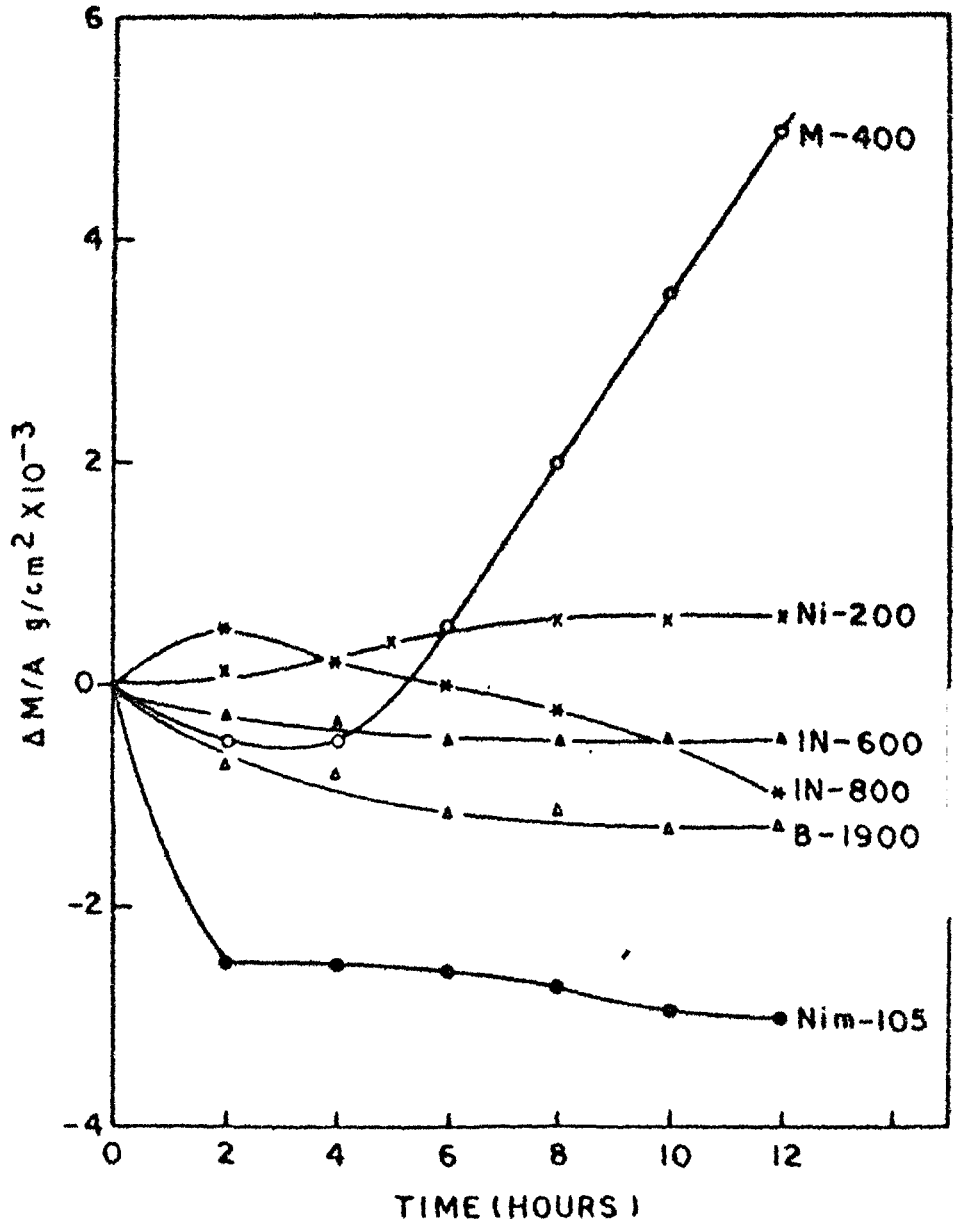
6
4
2
0
-2
-4
0
2
4
6
8
10
12
ΔM/A g/cm² X10⁻³
TIME (HOURS)
M-400
Ni-200
IN-600
IN-800
B-1900
Nim-105

FIG. 4.1

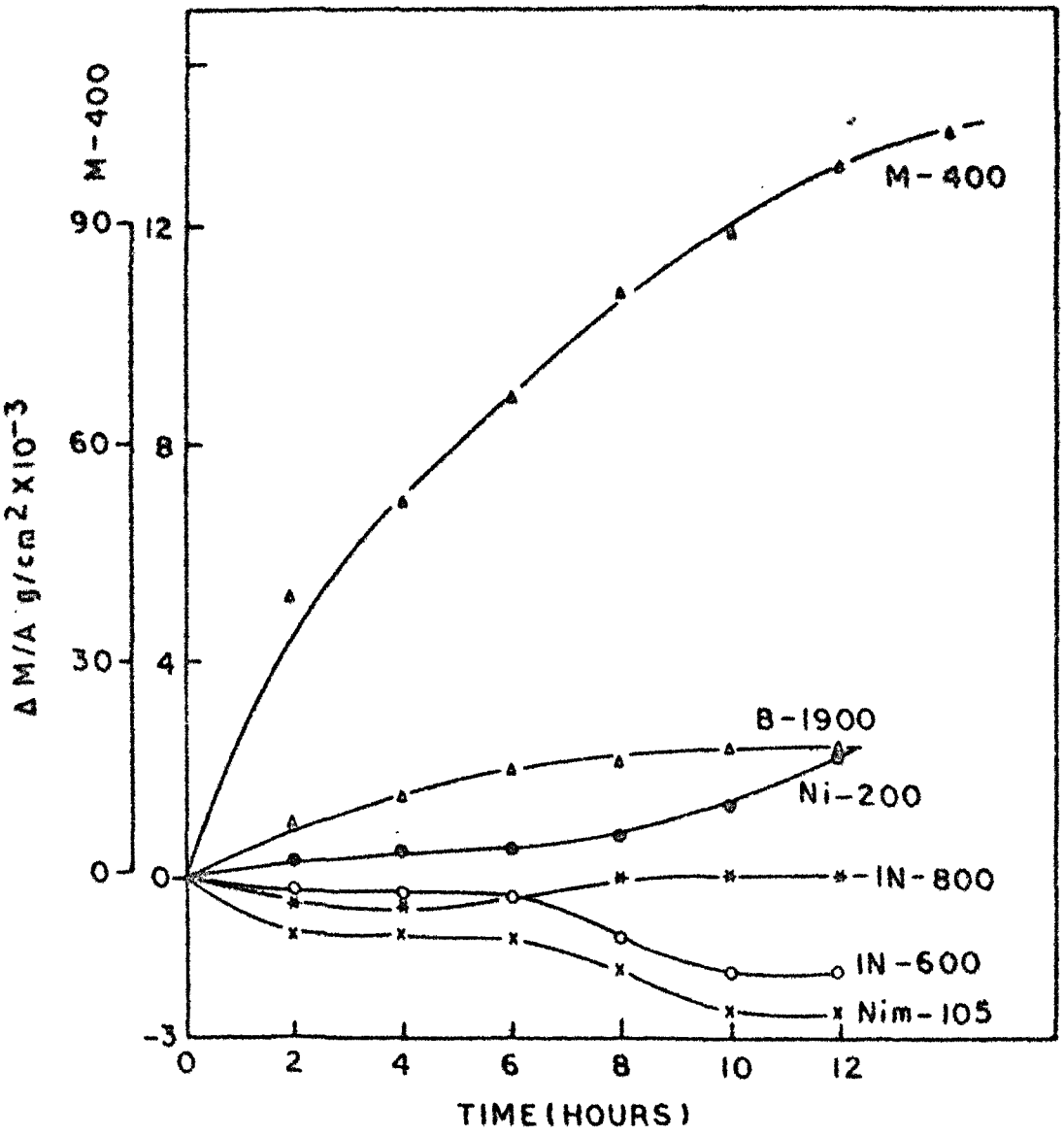
M-400
90
60
30
0
12
8
4
0
-3
ΔM/A g/cm² X10⁻³
M-400
B-1900
Ni-200
IN-800
IN-600
Nim-105
0
2
4
6
8
10
12
TIME (HOURS)

FIG. 4.2

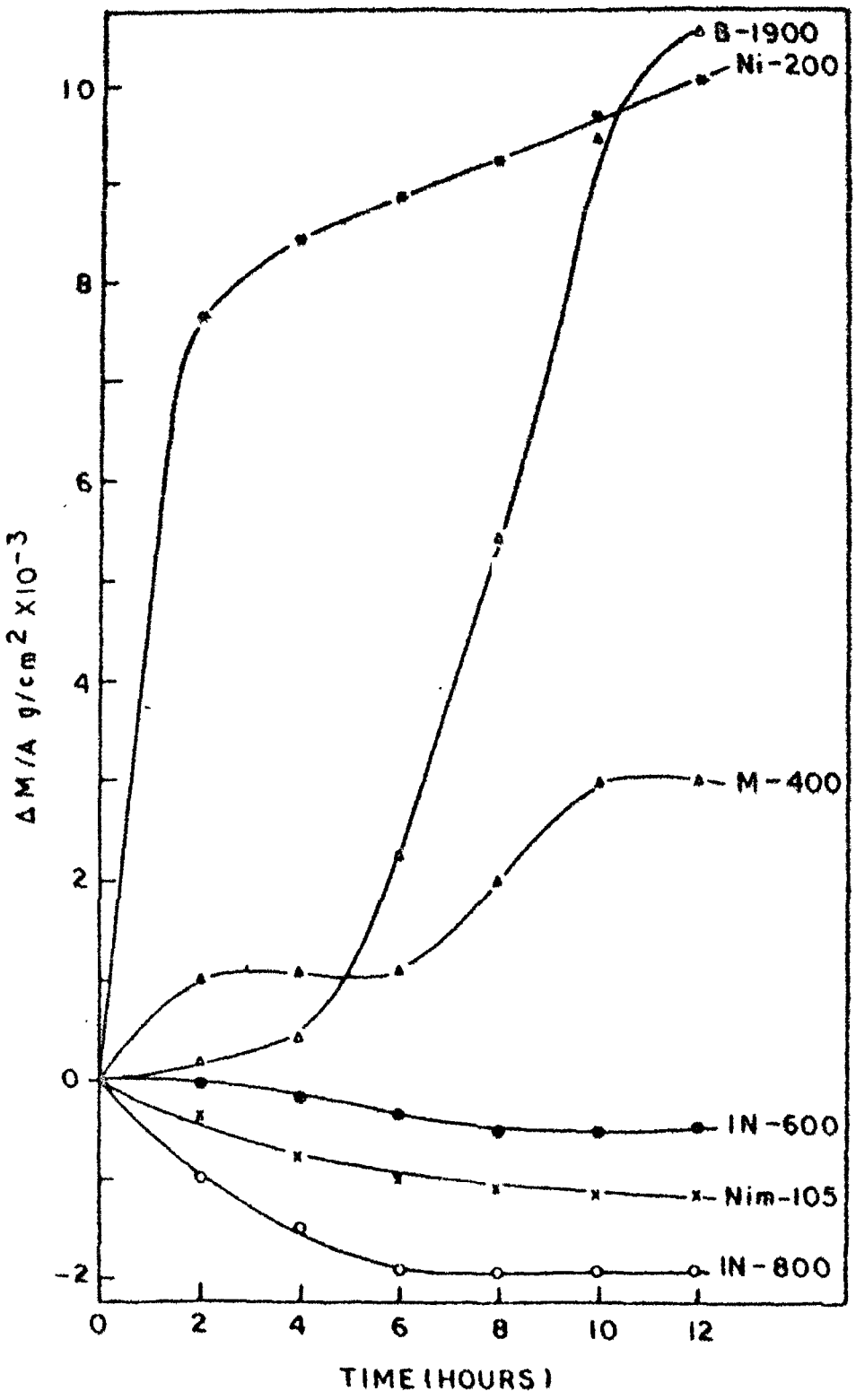
B-1900
Ni-200
M-400
IN-600
Nim-105
IN-800
10
8
6
4
2
0
-2
0
2
4
6
8
10
12
ΔM/A g/cm² X10⁻³
TIME (HOURS)

FIG 4 3

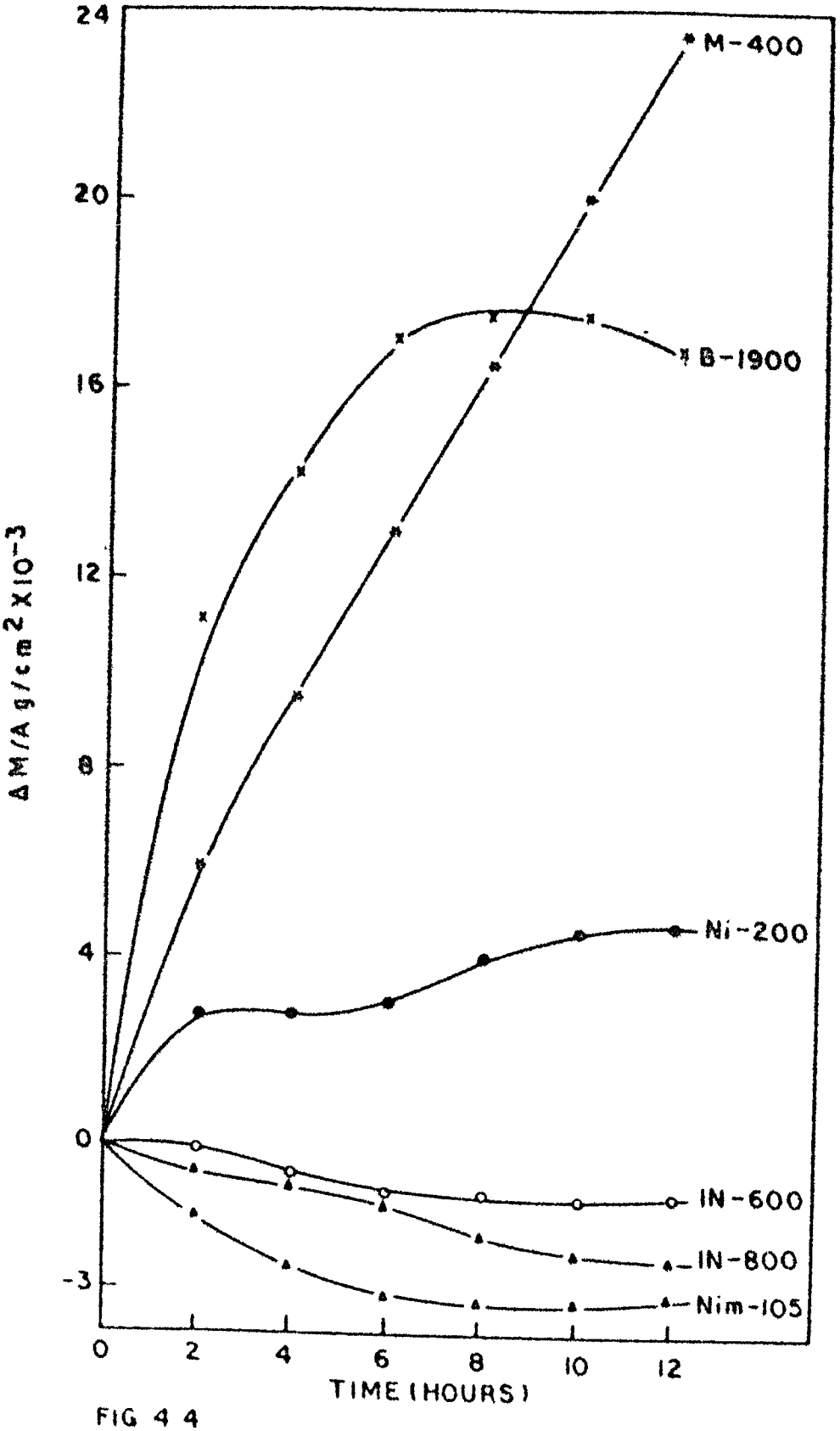
24
20
16
12
8
4
0
-3
ΔM/A g/cm² X10⁻³
M-400
B-1900
Ni-200
IN-600
IN-800
Nim-105
0
2
4
6
8
10
12
TIME (HOURS)

FIG 4 4

CAPTIONS OF METALLOGRAPHS

Fig. 4.5 Photomicrograph of Inconel-600 coated with Na_2SO_4 and oxidised at 850°C for 12 hours. (400x)

Fig. 4.6 Scanning electron micrograph of Inconel-600 coated with Na_2SO_4 and oxidised at 1000°C for 12 hours. (1050x)

Fig. 4.7(a & b) Scanning electron micrograph of Inconel-800 coated with Na_2SO_4 and oxidised at 850°C for 12 hours. (a. 500X b. 5000x)

Fig. 4.8 Photomicrograph of Monel-400 coated with Na_2SO_4 and oxidised at 850°C for 12 hours. (400x)

Fig. 4.9 Photomicrograph of Nimonic-105 coated with Na_2SO_4 and oxidised at 1000°C for 12 hours. (400x)

Fig. 4.10(a & b) Scanning electron micrograph of Nimonic-105 coated with Na_2SO_4 and oxidised at 1000°C for 12 hours. (a. 430x b. 1700x)

Fig. 4.11 Photomicrograph of Nickel-200 coated with Na_2SO_4 and oxidised at 850°C for 12 hours. (400x)

Fig. 4.12 Photomicrograph of Nickel-200 coated with Na_2SO_4 and oxidised at 1000°C for 12 hours. (400x)

Fig. 4.13 Scanning electron micrograph of Nickel-200 coated with Na_2SO_4 and oxidised at 850°C for 12 hours. (1000x)

Fig. 4.14 Scanning electron micrograph of Nickel-200 coated with Na_2SO_4 and oxidised at 1000°C for 12 hours. (600x)

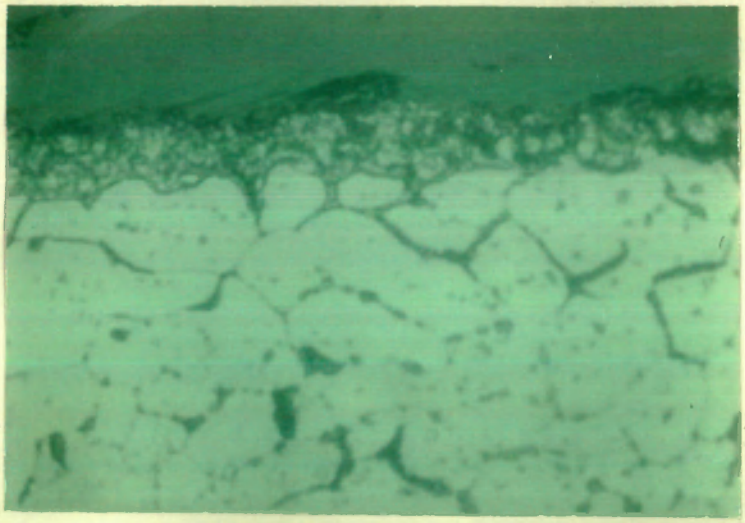

4.5

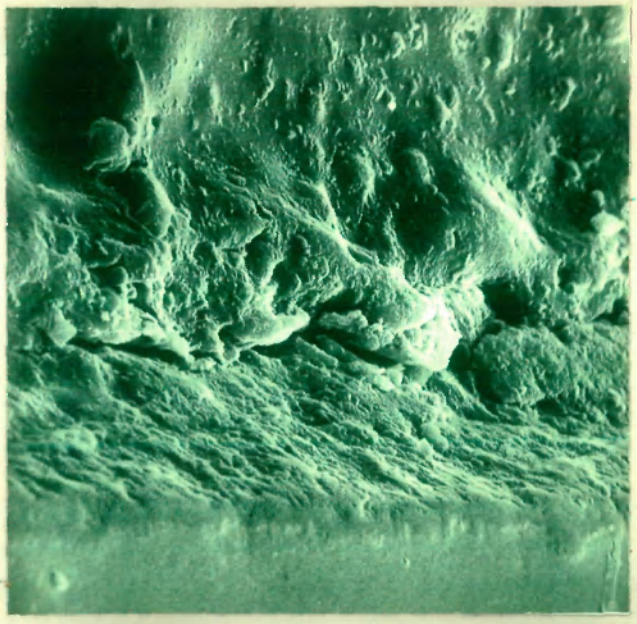

4.6

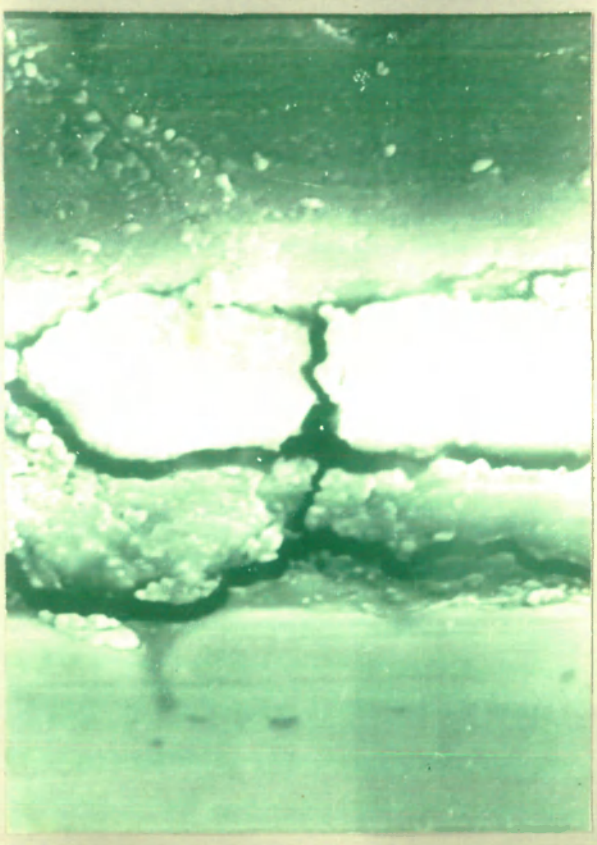

4.7

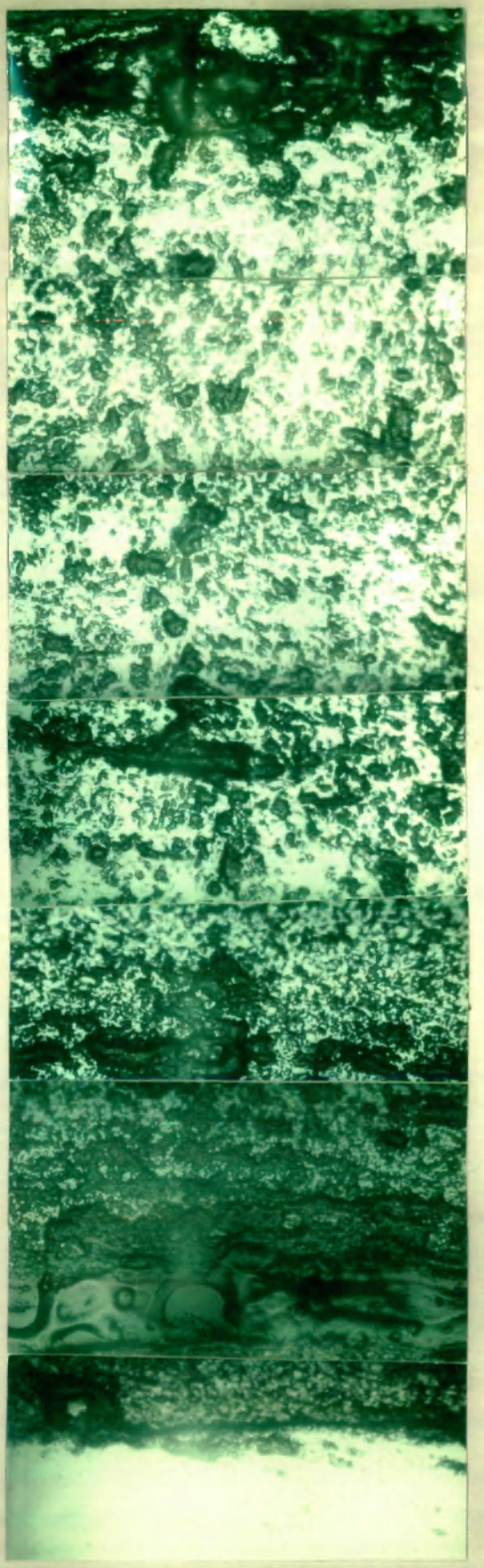

4.8

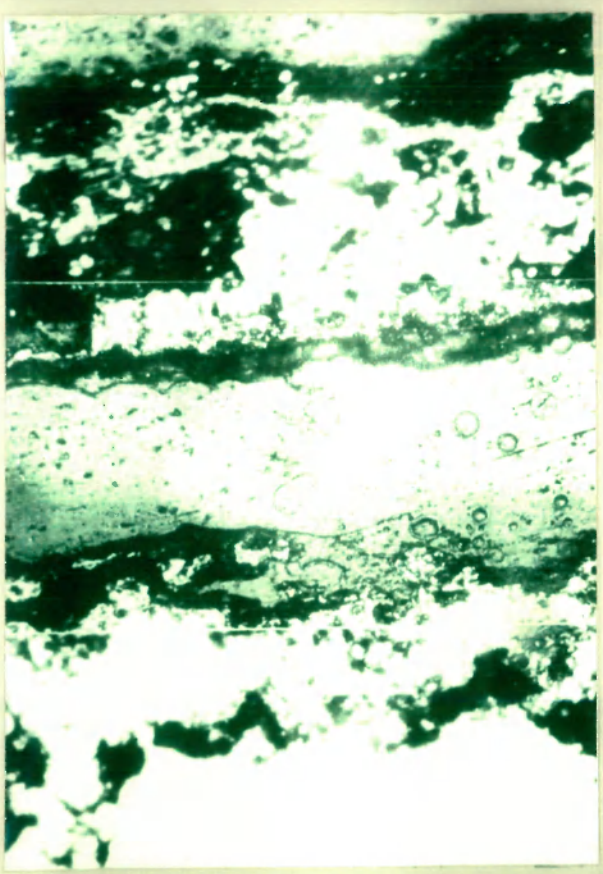

4.9

(a)

(b)

4.10

4.10

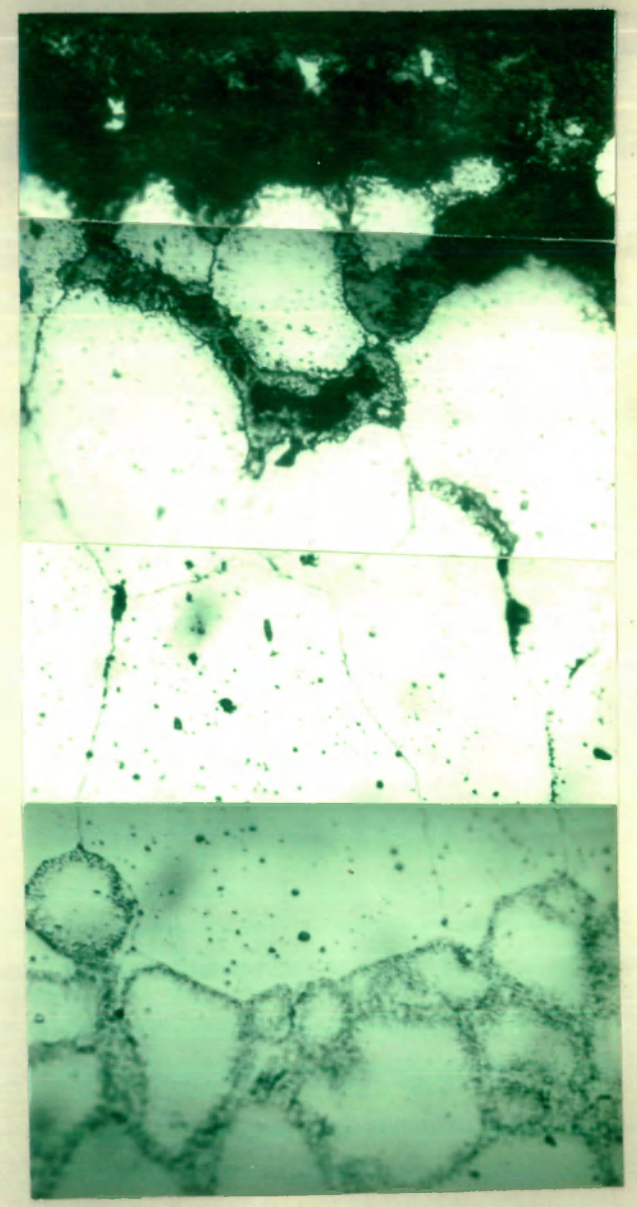

4.11

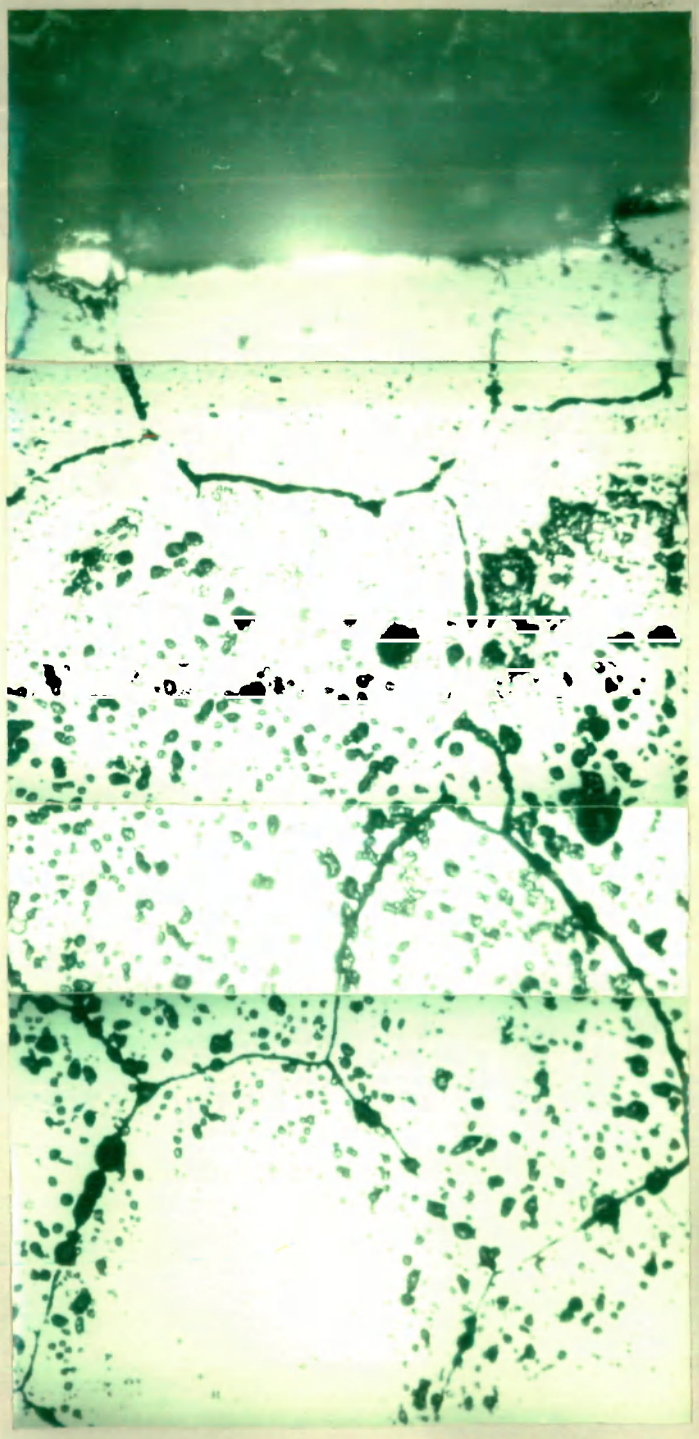

4. 12

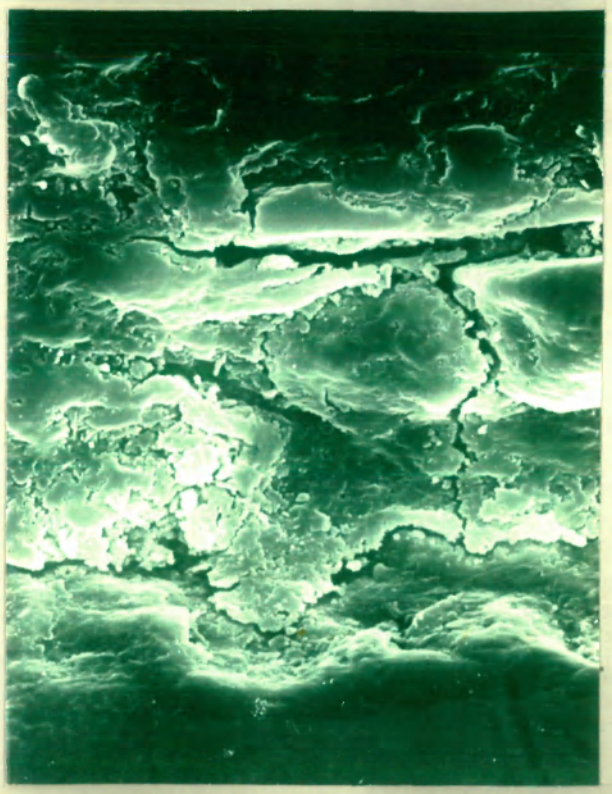

4.13

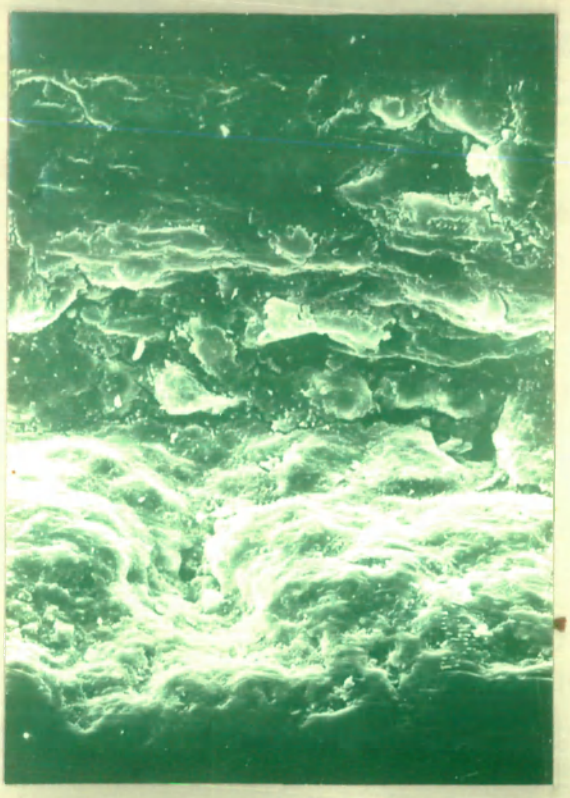

4.14

CAPTIONS OF EDAX

Fig. 4.15 X-ray profiles of NiK , CrK and FeK of uncoated Inconel-600 oxidised at 1000°C for 12 hours.

Fig. 4.16 X-ray profiles of NiK , CrK and FeK of Inconel-600 coated with Na_2SO_4 and oxidised at 1000°C for 12 hours.

Fig. 4.17 X-ray profiles of NiK , CrK and FeK of Inconel-600 coated with Na_2SO_4 and oxidised at 1000°C for 12 hours.

Fig. 4.18 X-ray profiles of NiK and CuK of Monel-400 coated with Na_2SO_4 and oxidised at 850°C for 12 hours.

Fig. 4.19 X-ray profiles of NiK and CuK of Monel-400 coated with Na_2SO_4 and oxidised at 1000°C for 12 hours.

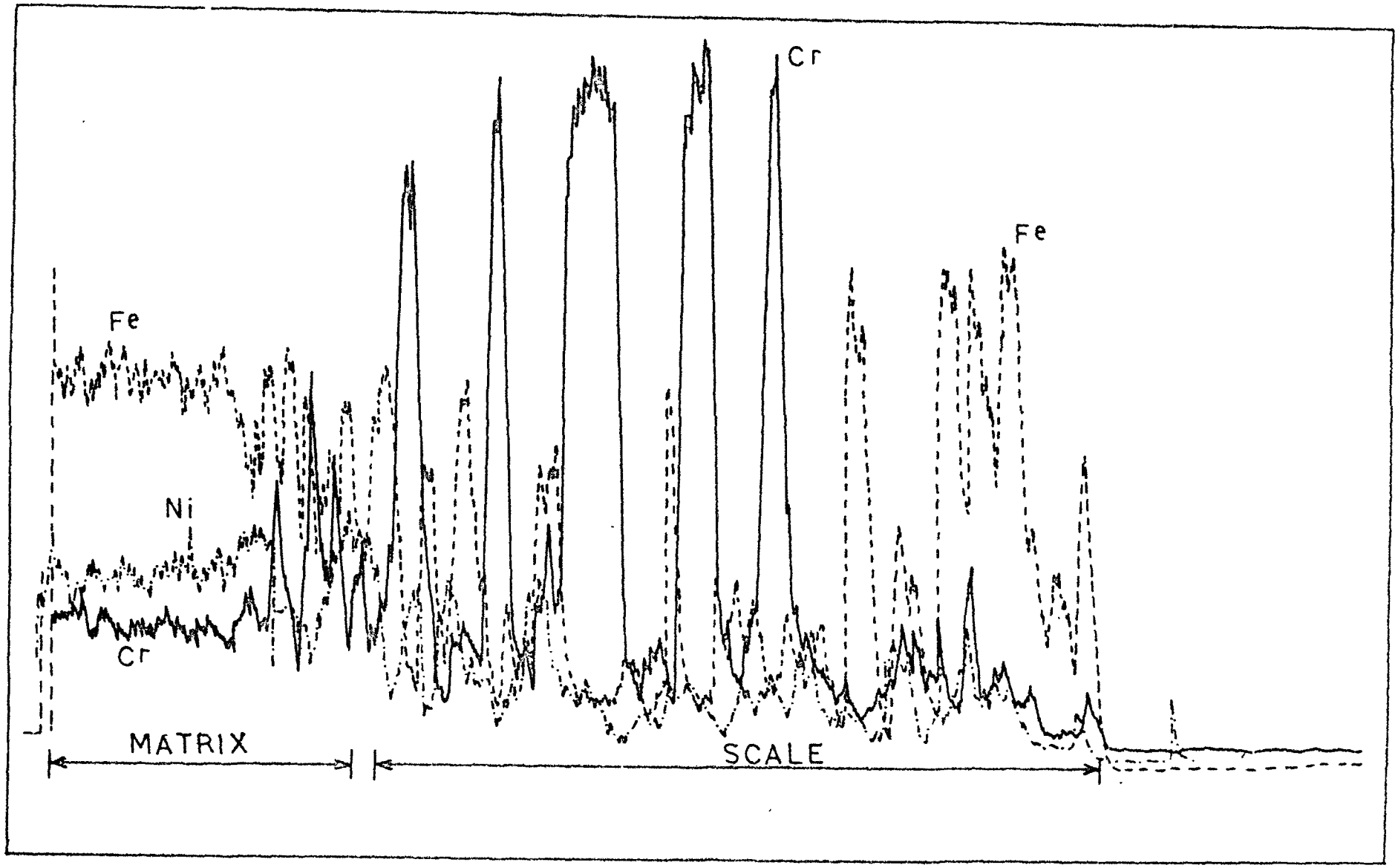

FIG. 4.15

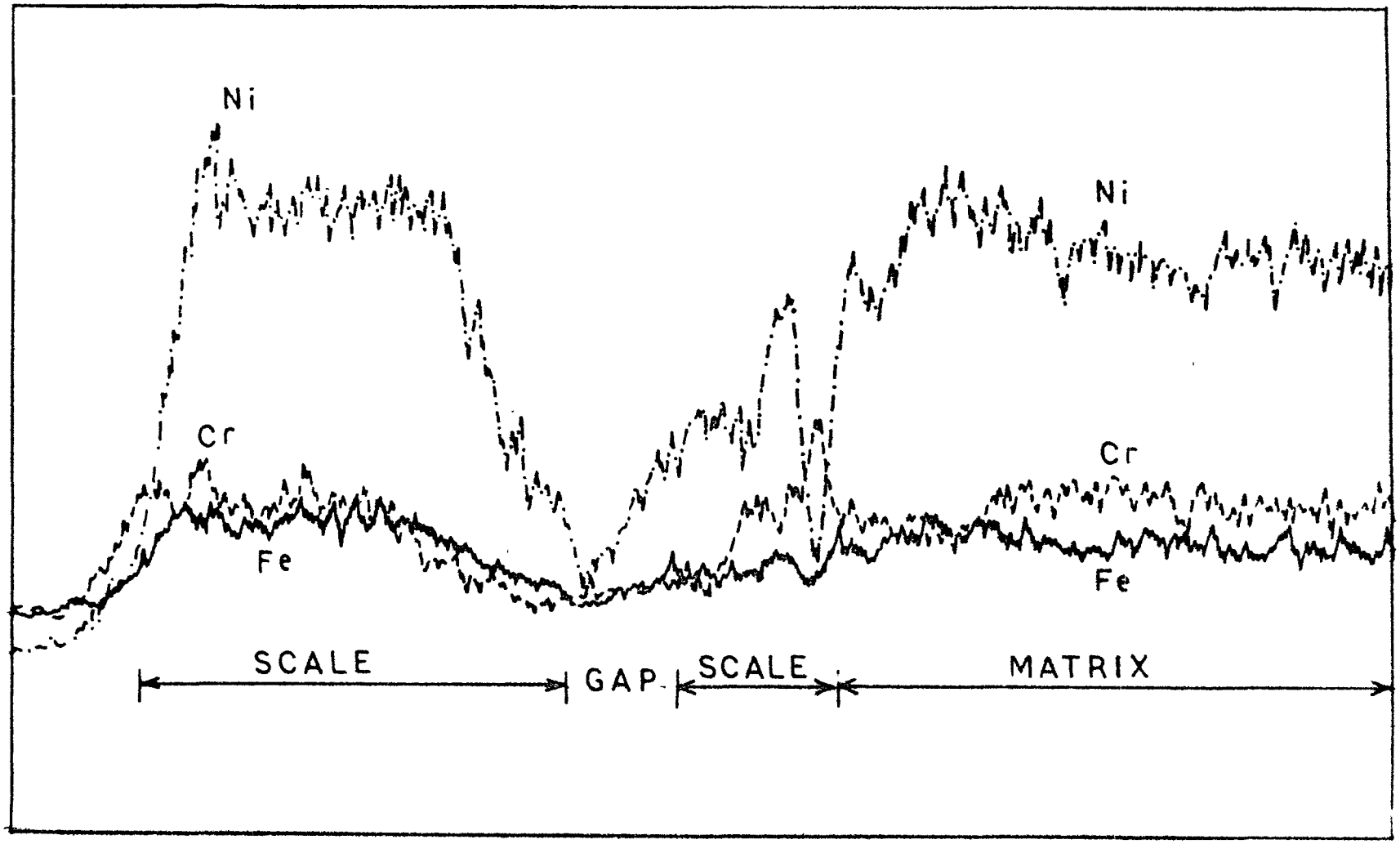

FIG 4.16

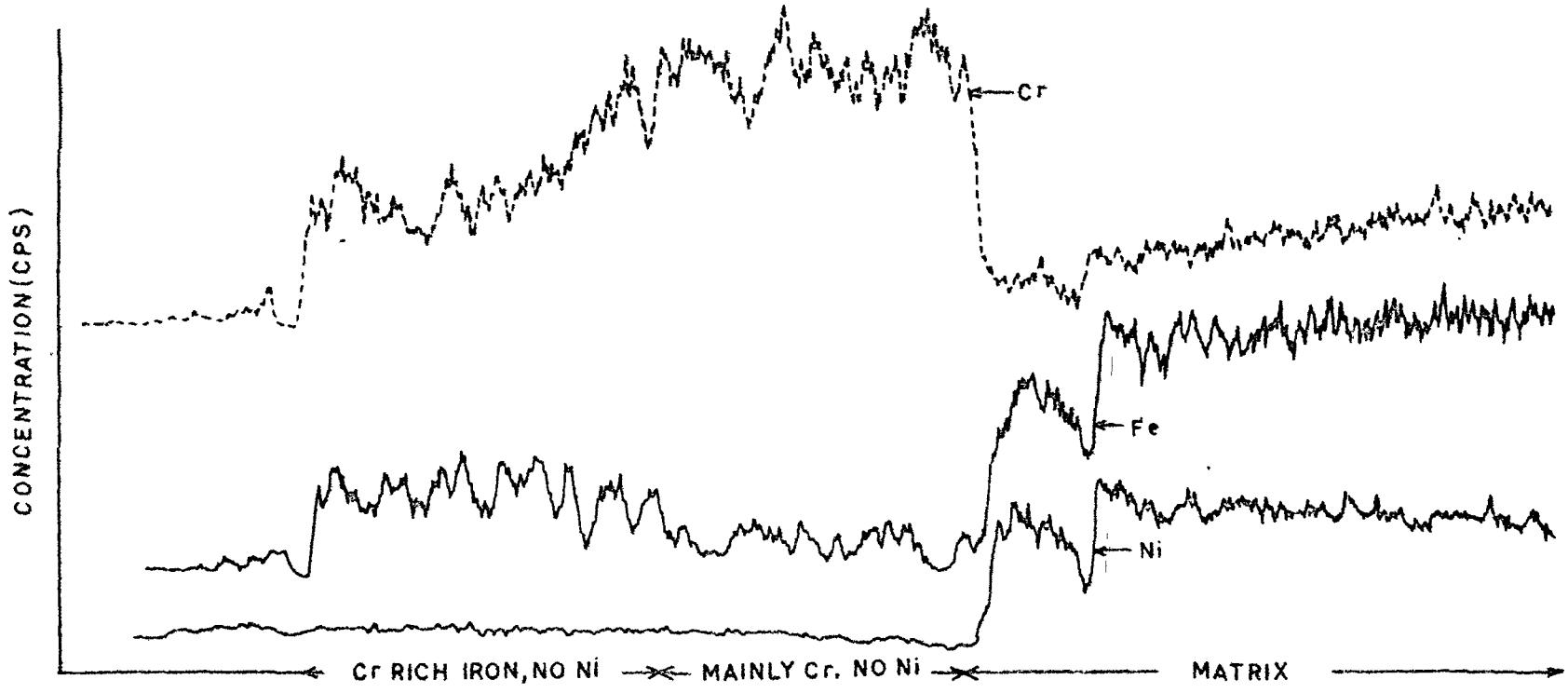
CONCENTRATION (CPS)
Cr
Fe
Ni
Cr RICH IRON, NO Ni
MAINLY Cr. NO Ni
MATRIX

FIG.4.17

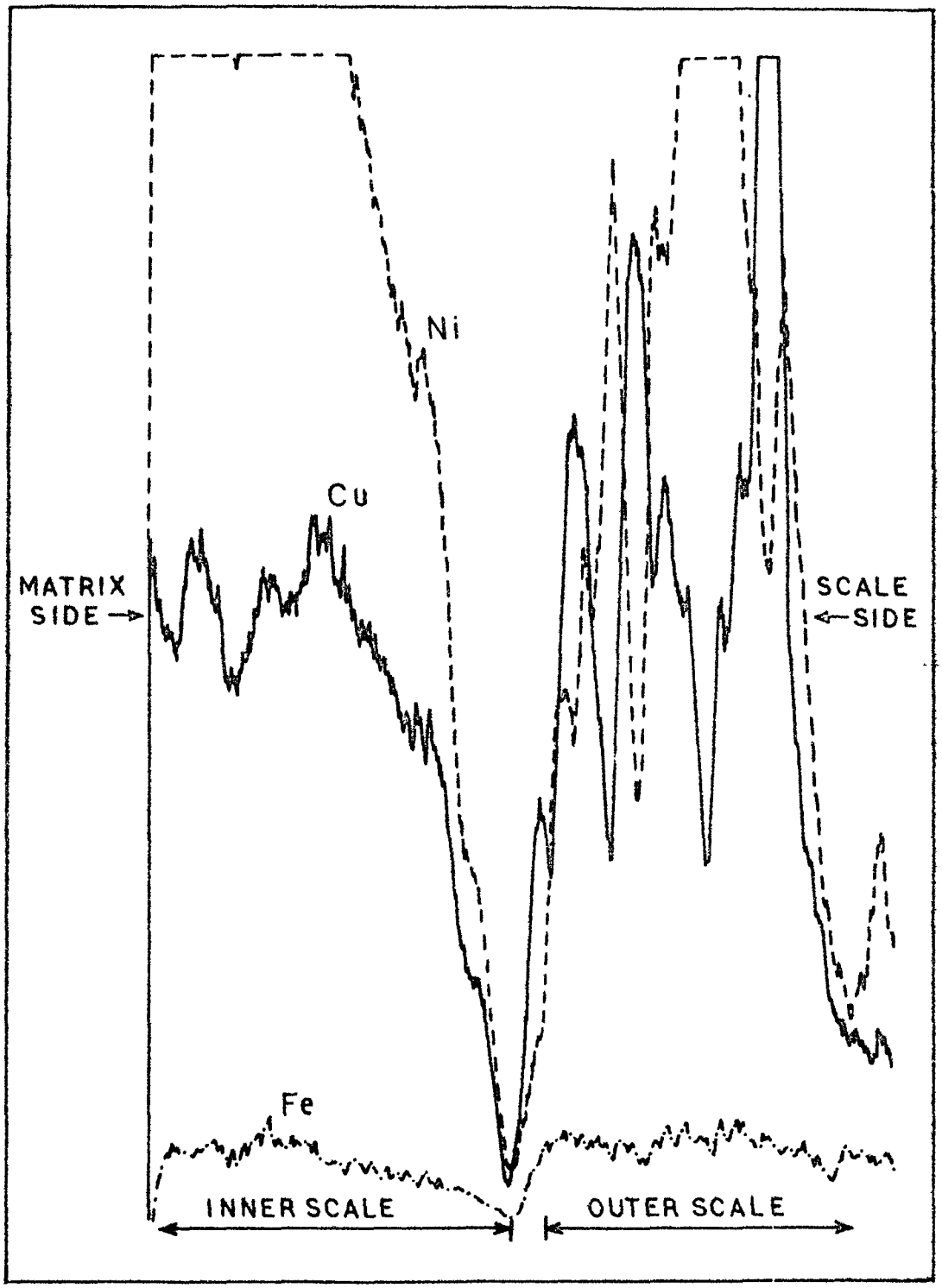

FIG. 4.18

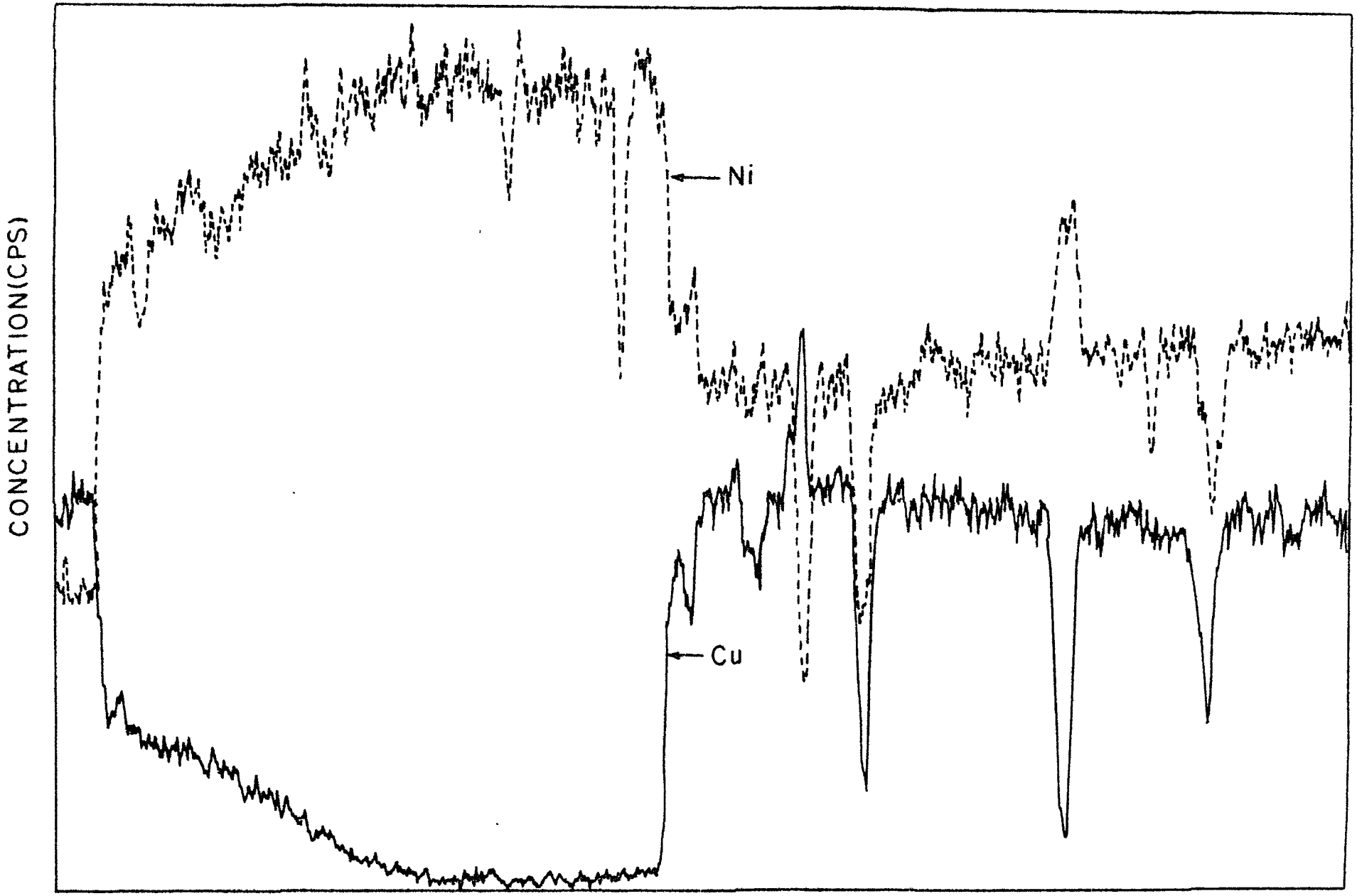

FIG.4.19

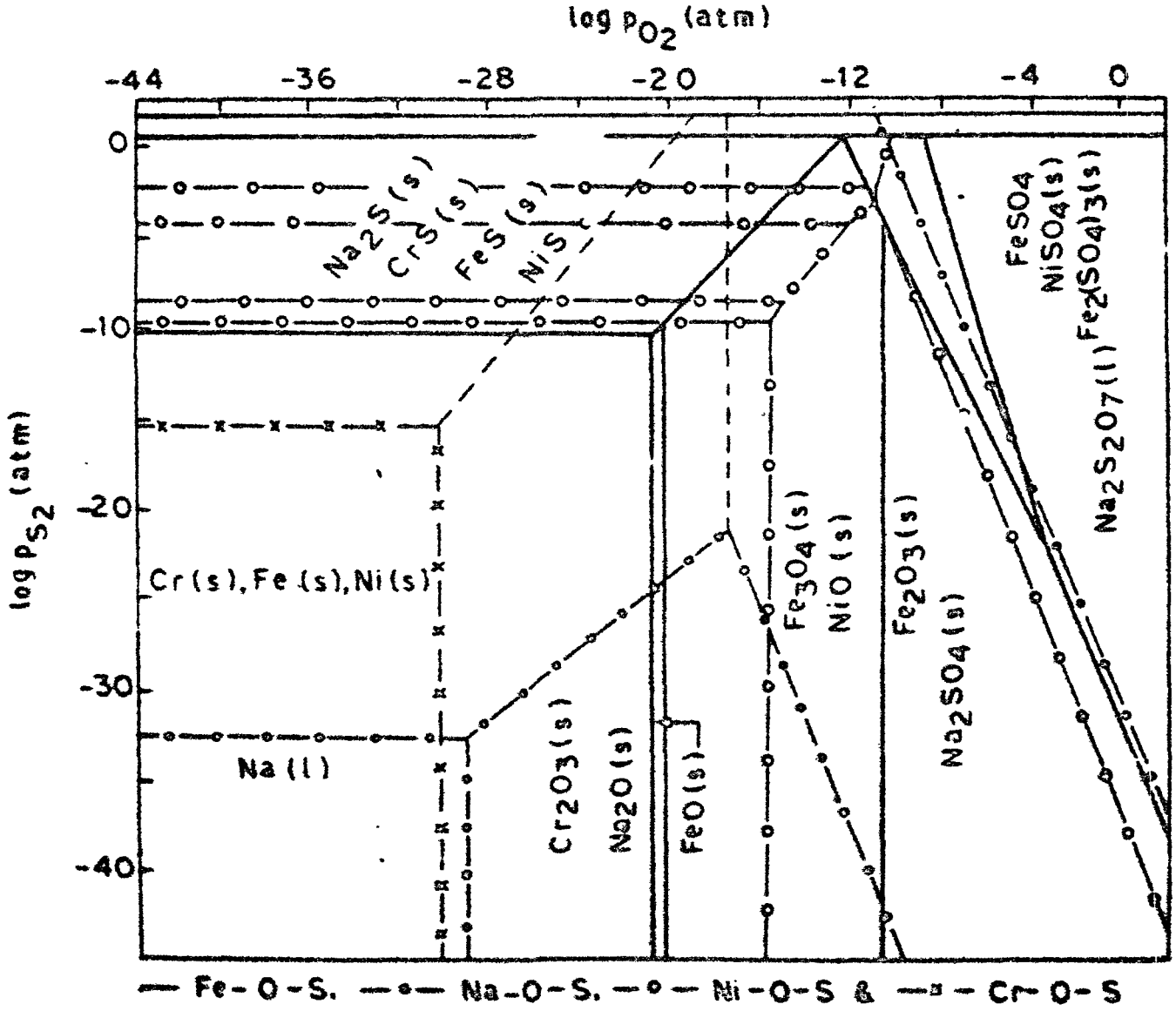

FIG. 4.20 M-O-S THERMOCHEMICAL PHASE DIAGRAM AT 1000°K

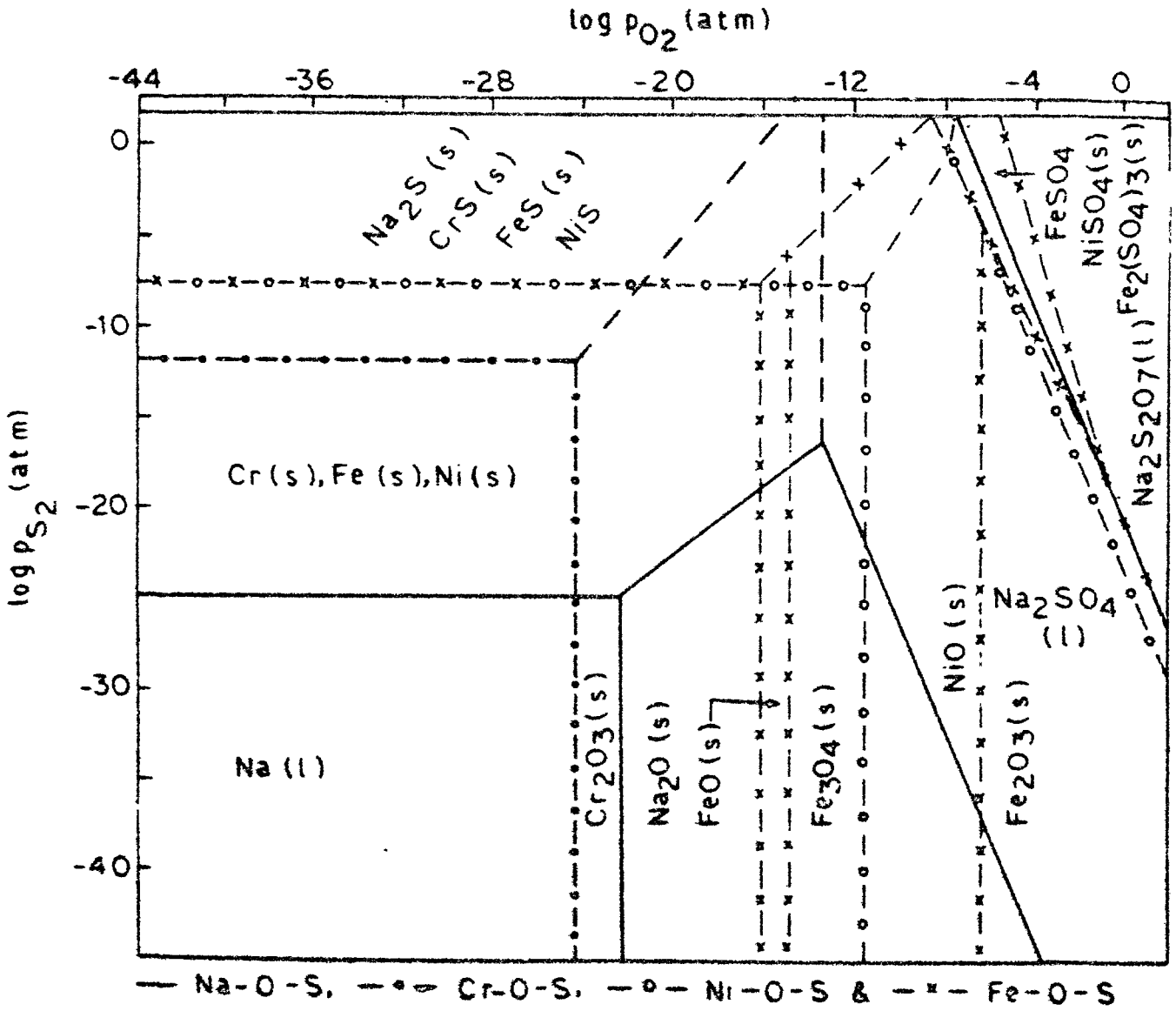

FIG 4.21 M-O-S THERMOCHEMICAL PHASE DIAGRAM AT 1200°K

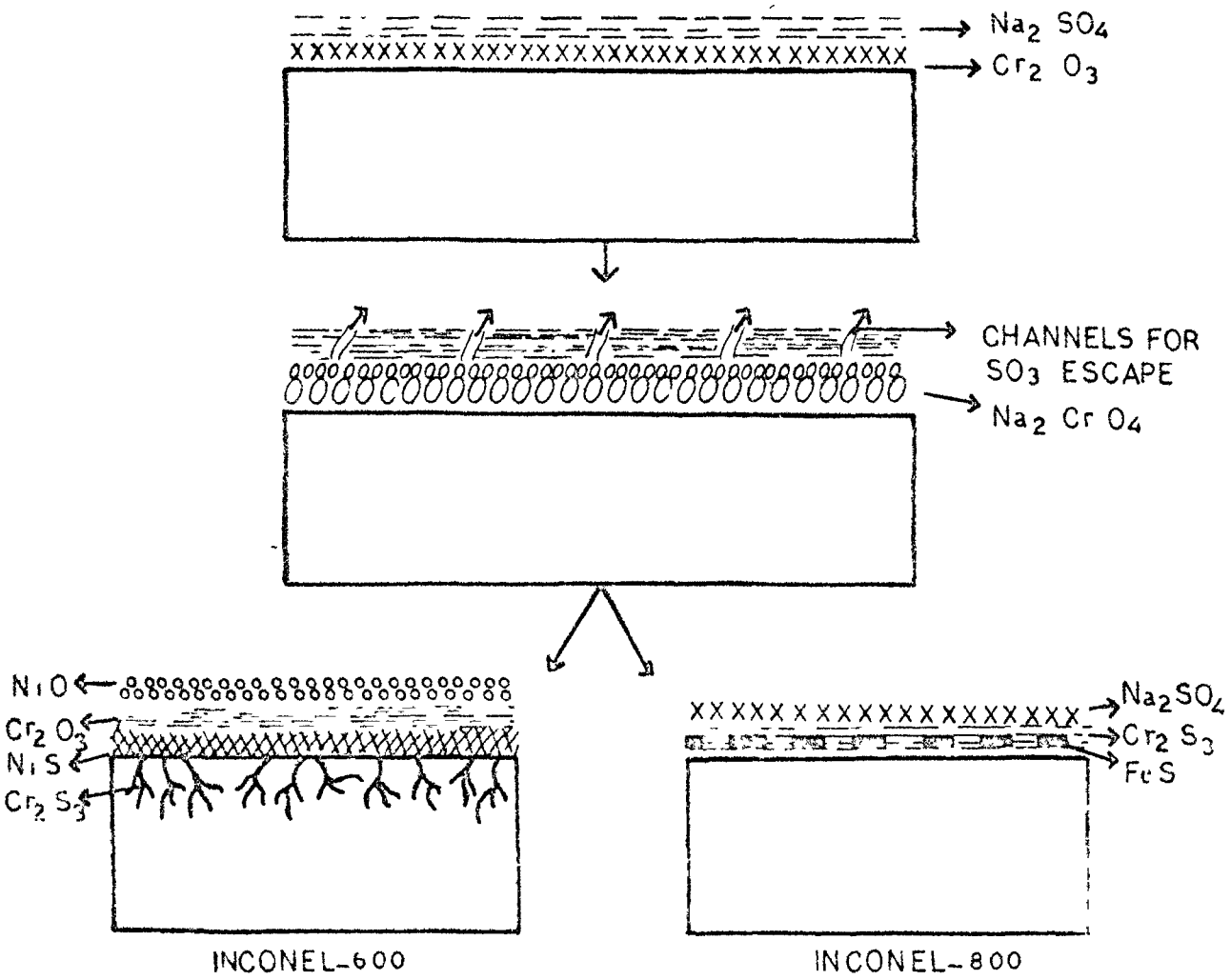

FIG. 4.22

SCHEMATIC REPRSESENTATION OF CORROSION ATTACK BY $Na_2 SO_4$ IN CHROMIA FORMING ALLOYS

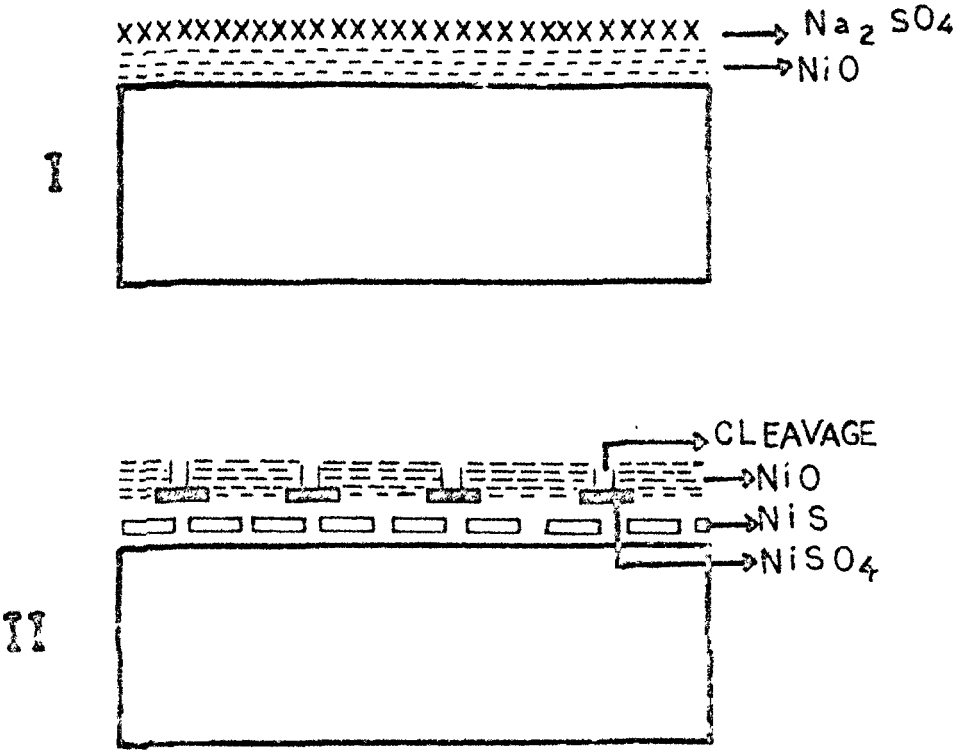

FIG.4.23 SCHEMATIC DIAGRAM SHOWING Na_2SO_4-INDUCED HOT CORROSION OF NICKEL-200

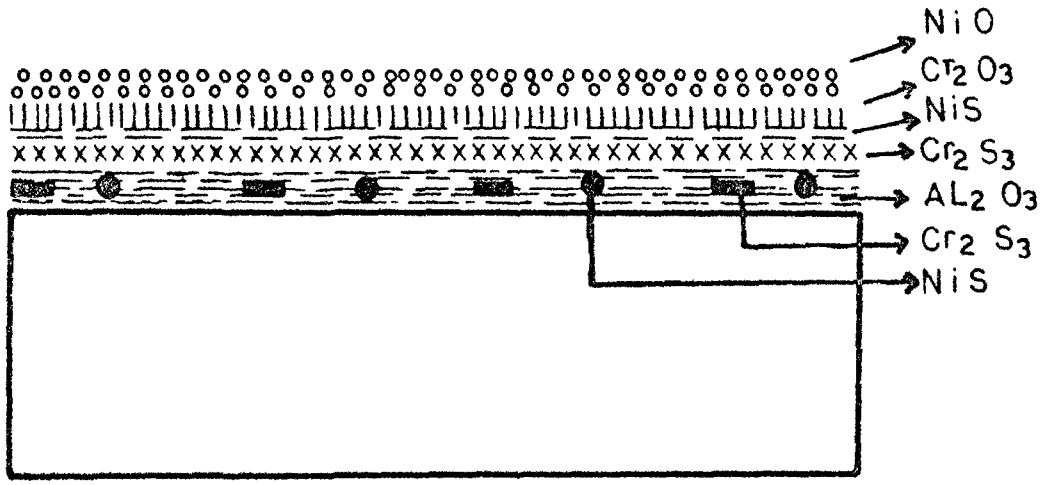

FIG. 4.24

DIAGRAMATIC REPRESENTATION OF THE SCALES FORMED ON NIMONIC-105 DURING Na_2SO_4 INDUCED HOT CORROSION

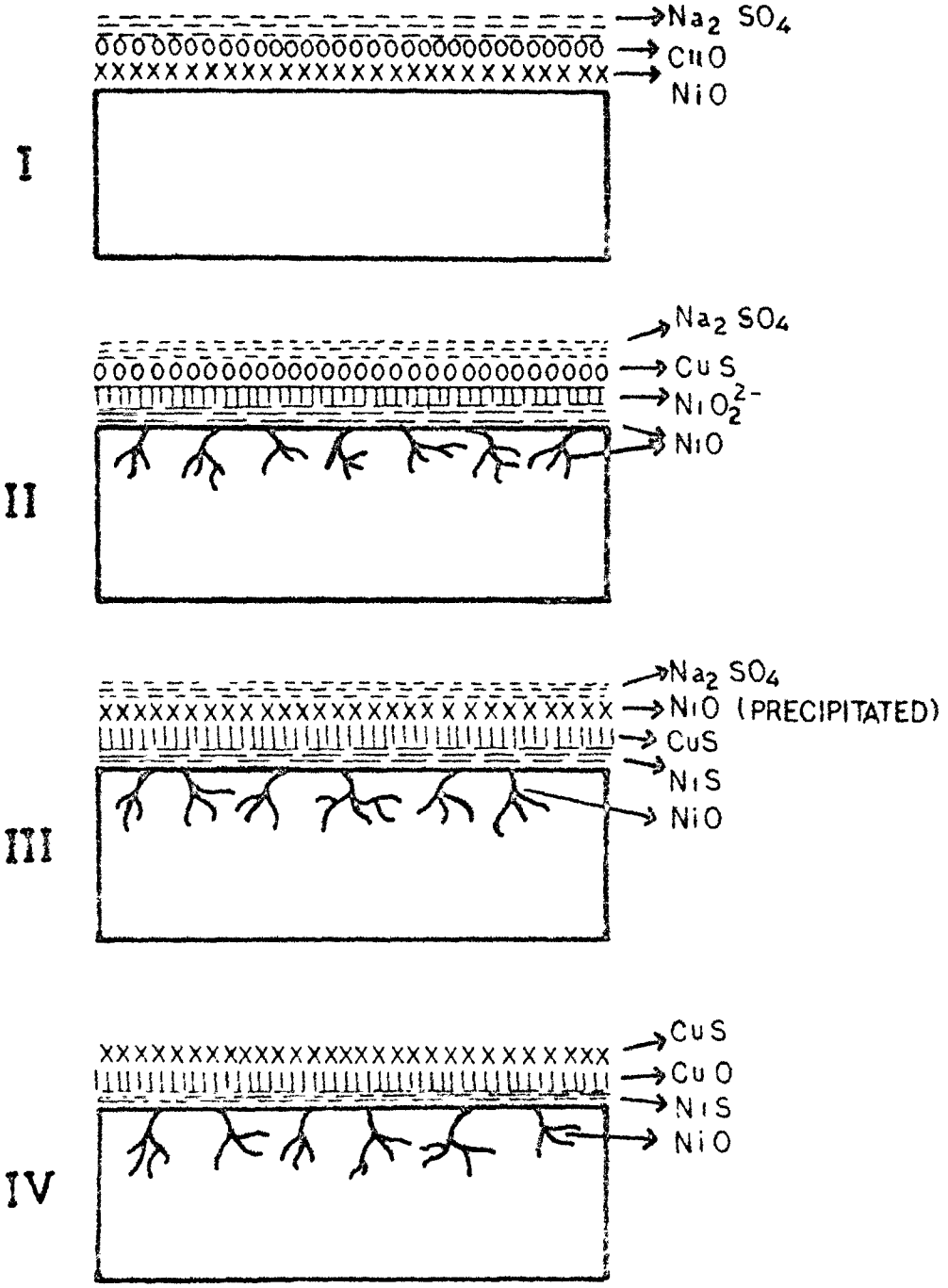

FIG. 4.25 SCHEMATIC REPRESENTATION OF THE $Na_2 SO_4$ - INDUCED HOT CORROSION OF MONEL 400

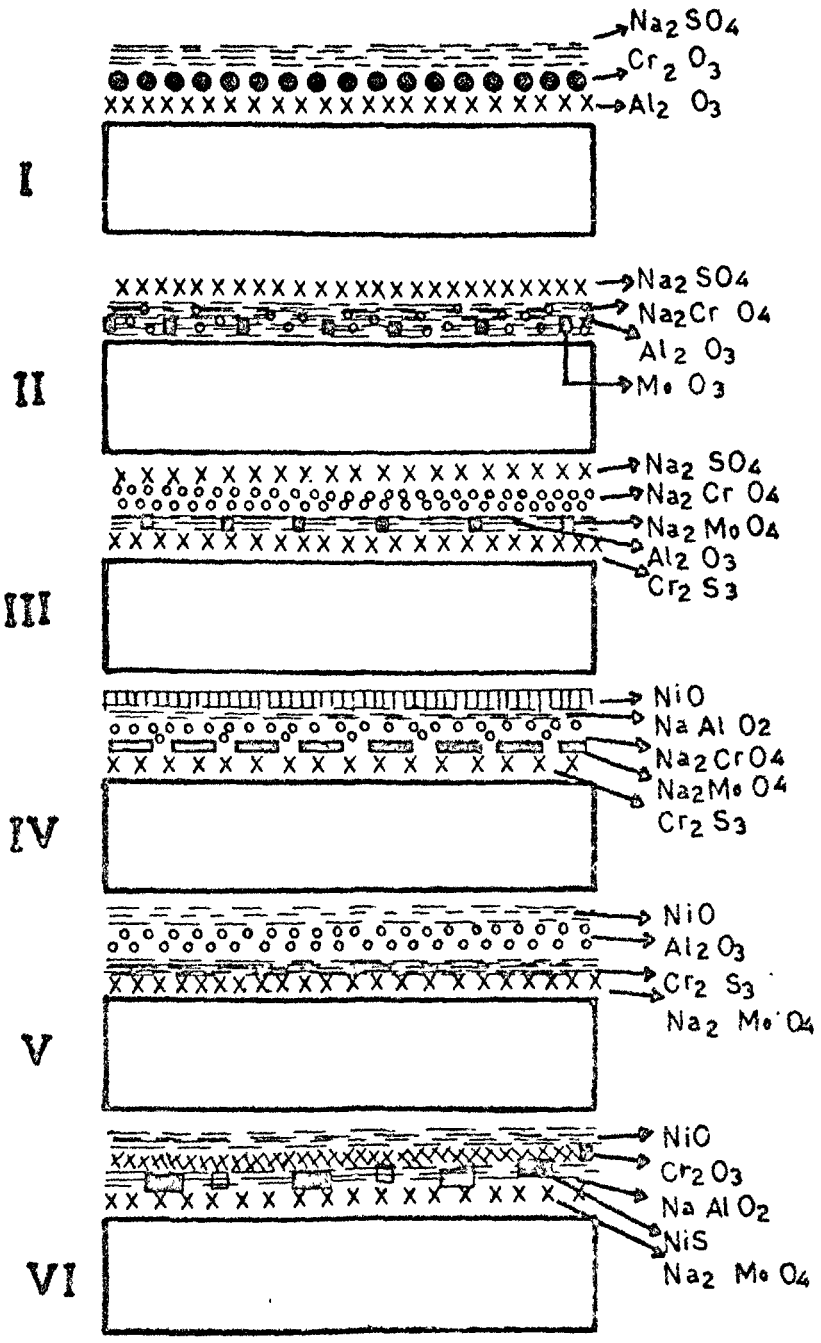

FIG.4.26

SCHEMATIC REPRESENTATION OF Na_2SO_4-INDUCED HOT CORROSION OF B-1900

CHAPTER - V

HOT CORROSION BEHAVIOUR OF NICKEL-BASE ALLOYS IN PRESENCE OF NaCl

EXPERIMENTAL

5.1.1 Selection of alloys

Six commercially based Ni-containing alloys, e.g. Inconel-600, Inconel-800, Nickel-200, Nimonic-105, Monel-400 and B-1900 were used during high temperature oxidation experiments conducted in presence of NaCl. The nominal composition of the alloys is referred in table 4.1.

5.1.2 Preparation of the salt coated specimen

Coupons of 1.5 cm x 0.5 cm x 0.1 cm size or circular specimens of 1.5 cm diameter x 0.2 cm thickness were cut either from sheets or rods of the alloys, respectively. The coupons were abraded sequentially with 180, 320 and 600 grade SiC papers, washed with water and were degreased with CCl_4. The specimens were coated with a thin film of NaCl of~6.0 μm thickness (about 1.0 mg/cm^2). This was done by spraying a concentrated solution of NaCl on a specimen heated upto about 300°C. Coated samples were dried by keeping them in a hot air oven maintained at 150°C for overnight.

5.1.3 Hot corrosion studies

NaCl coated specimens were suspended to the helics of a quarts helical thermal balance. The hot corrosion studies were carried out at 850 and 1000°C for 12 hours in flowing air. Weight changes were measured at an interval of 1 hour.

For a particular oxidation run, three samples were corroded under nearly identical conditions.

5.1.4 X-ray diffraction analysis

X-ray diffractograms of the scales on corroded samples were obtained by a X-ray diffractometer assembly using $CoK\alpha$, $CuK\alpha$, or $FeK\alpha$ radiations and an appropriate filter. The constituents as identified in the scales are listed in table 5.1.

5.1.5 Morphological studies

5.1.5.1 Optical metallography:

Oxidized samples were mounted in paper moulds of cylindrical shape, using Araldite as a cold setting compound. The mounted samples were polished sequentially on 180, 320, and 600 grade SiC papers using Kerosene oil as a lapping liquid. The abraded specimens were subsequently polished on 1 μ alumina powder. Samples were washed with alcohol and CCl_4 and were examined under a photometallurgical microscope. The polished samples were either etched in 1% acidic solution of $FeCl_3$ or etched electrolytically in a 2% HNO_3 solution for 2-3 minutes. Samples alternatively polished and etched were found to reveal greater details of matrix structure.

The polished and etched samples were examined under a Leitz Photometallurgical microscope and the portions of the

microstructures providing details were photographed.

5.1.5.2 Scanning Electron Microscopy (SEM):

Cambridge Scanning Electron Microscope Model S4-10 were used for the SEM studies. The samples were coated with colloidal solution or gold emulsion, prior to scanning through microscope.

5.1.6 Energy Dispersion X-ray Analysis (EDAX)

Elements distribution within the scale and the matrix were obtained from the EDAX concentration profile. Cambridge Scanning Electron Microscope Model S4-10 was also used for EDAX studies.

RESULTS

5.2.1 Kinetic studies

The kinetic of oxidation of Inconel-600, Inconel-800, Monel-400, Nimonic-105, B-1900 and Nickel-200 has been studied in presence of NaCl at 850 and 1000°C for 12 hours. The weight change/time plots have been given in figures 5.1 and 5.2.

Inconel-600:

At 1000°C, after initial loss of about 0.5 mg/cm^2 the NaCl coated alloy does not show any change in weight during 12 hour oxidation run. However, the same alloy shows a parabolic behaviour upto 8 hours at 850°C, this is followed by a relatively rapid weight gain with increasing oxidation time.

Inconel-800:

The NaCl coated Inconel-800 on oxidation shows a nearly parabolic behaviour at 850 and 1000°C. The total weight gains are 19.5 and 32.0 mg/cm^2 at 850 and 1000°C, respectively.

Monel-400:

At 850°C, the coated alloy shows a nearly parabolic behaviour upto about 6 hours, this is followed by a fast rate of oxidation. However, at 1000°C alloys obey parabolic rate law. The oxidation rates at 1000°C are much higher than at 850°C.

Nimonic-105:

Nimonic-105 shows relatively small weight gains of 1.5 mg/cm^2 and 3.0 mg/cm^2 at 850 and 1000°C, respectively. The curves seem to be parabolic at both the temperatures.

B-1900:

The NaCl coated alloy shows weight losses at both the temperatures, though weight losses are relatively small - 0.5 mg/cm^2 and 2.1 mg/cm^2 at 850 and 1000°C, respectively. Initially during periods upto 4 hours the weight losses continuously occur followed by virtually no further loss in weight.

Nickel-200:

NaCl coated Nickel-200 oxidises by a parabolic rate law at 850 and 1000°C. The alloy seem to oxidise at much slower rates than the Inconel-600 and 800 alloys under similar conditions. A 'linear rate' law seems to be operative soon after the culmination of parabolic oxidation.

5.2.2 Morphological studies

Inconel-600:

Figure 5.3 shows Scanning Electron micrograph of a cross section of NaCl coated alloy sample corroded at 850°C for 12 hours. The scales are separated from the substrate at some regions, possibly due to polishing artifacts. The

inner scales constitute magnetite (light phase) with NiO (light grey) inclusions. The outer scales are predominantly concentrated in NiO with Cr_2O_3 inclusions (dark grey). There is evidence of internal oxidation. Cr_2O_3 has not been found in the inner scales. This might be due to formation of an intermediate volatile species CrO_2Cl_2, some of which evaporates and get condensed on the wall of the reaction tube and some of it decomposes and accumulates at the alloy/salt interface in the form of Cr_2O_3.

Inconel-800:

Figure 5.4 shows an optical micrograph of a cross section of NaCl coated alloy at 850°C. The micrograph shows strong evidence of deep penetration of the salt along the grain boundaries and a profuse internal oxidation. Visual examination of the corroded alloy indicates the presence of brown coloured Fe_3O_4/Fe_2O_3 layered multiple scales which are too fragile and are easily detached from the alloy. The SEM picture (Fig. 5.5) of the alloy shows more details about the internal oxidation and deep penetration of the salt along the grain boundaries. The internal oxide network almost entirely comprises of Cr_2O_3.

Monel-400:

Optical micrograph of the sample corroded at 850°C in the presence of NaCl has been shown in figure 5.6. The micro-

graph shows the presence of a scale which contains 2-phases, the dark phase which is CuO and a light phase of NiO. There is evidence of some internal oxidations. NiO predominantly seems to form at the grain boundaries and CuO along the grains. The scales are perhaps detached from the alloy during polishing. Scanning Electron micrograph of the corroded alloy (Fig. 5.7) show similar structure but with much finer details. The picture indicates the formation of a copious scale of NiO with CuO inclusions. Outermost layer is rich in CuO.

Nickel-200:

Figure 5.8 shows the SEM picture of NaCl coated Ni-200 alloy corroded at 1000°C for 12 hours. The outer layers of the scales are mainly composed of NiO whereas the inner layers perhaps contain $NiCl_2$ in predominant concentrations.

5.2.3 X-ray diffraction analysis

Constituents as identified in the scales of NaCl coated alloys, are listed in the table 5.1.

5.2.4 Energy Dispersion X-ray Analysis (EDAX)

Nimonic-105:

Figure 5.9 represents X-ray concentration profiles of NaCl-coated Nimonic-105 alloy oxidised at 1000°C. The profiles indicate the presence of a multilayered scale. Cr_2O_3

forms an inner layer followed by a duplex scale of Cr_2O_3 and NiO and the outer scale primarily consists of CoO.

Monel-400:

Figure 5.10 shows NiKα and CuKα X-ray concentraion profiles of the NaCl-coated alloy oxidised at 1000°C. The scales seem to contain duplex NiO and CuO though the outer scales are rich in NiO. The Ni present in the matrix also appears to be affected by preferential oxidation of $NiCl_2$ to NiO.

Inconel-600:

Figure 5.11 shows FeKα, NiKα and CrKα X-ray concentration profile of the NaCl-coated alloy, oxidised at 850°C for 12 hours in air. The inner most layer is richer in iron followed by a Ni-enriched layer with inclusions of iron. The outermost layer of the scale is mainly composed of iron probably in the form of Fe_2O_3. It is noteworthy that chromium is absent in the scale region.

B-1900:

Figure 5.12 shows the X-ray concentration profiles of B-1900, coated with NaCl and oxidised at 1000°C for 12 hrs in air. The profile indicates that the scale is mainly composed of nickel with inclusions of chromium and cobalt in the outer region of the scale. Steep rise in Cl profile at the outer most region shows the presence of unreacted NaCl.

D I S C U S S I O N

The high temperature corrosion studies carried out on Ni-base alloys in presence of NaCl at 850 and 1000°C in air reveal that the corrosion behaviour can be divided into two groups:

(i) the oxidation rates of chromia forming alloys e.g., Inconel-600, Inconel-800, Nimonic-105 (forming mixed oxide scales with Al_2O_3) are much higher in presence of NaCl than in presence of Na_2SO_4 or air.

(ii) Al_2O_3 formers (e.g., B-1900) and NiO formers (Ni-200) which have much lower oxidation rates in presence of NaCl. Monel-400 which is a CuO-NiO former is severely attacked by NaCl.

It appears that if NaCl is deposited on the surface of a chromia forming alloy the breakdown of the protective oxide scale occurs. NaCl attacks the Cr_2O_3 film producing a volatile product, CrO_2Cl_2, which is subsequently converted into Na_2CrO_4 and condensed away from the specimen on some cooler part of the reaction tube. A yellow deposit which was identified as Na_2CrO_4 is invariably found in case of Inconel and Nimonic alloys.

$$\text{I} \qquad 4NaCl + Cr_2O_3 + \tfrac{5}{2}O_2 \longrightarrow 2CrO_2Cl_2 + 2Na_2O$$

$$\text{II} \qquad 2Na_2O + Cr_2O_3 + \tfrac{5}{2}O_2 \longrightarrow 2Na_2CrO_4$$

The melt adjacent to the alloy consists of: NaCl, Na_2CrO_4, CrO_2Cl_2 and Na_2O. NaCl (l) penetrates through this melt and reacts with alloy components as proposed in the following equations,

$$\text{III}^{*} \qquad 2NaCl + 2Ni + O_2 \longrightarrow Na_2NiO_2 + NiCl_2$$

$$\text{IV}^{**} \qquad 2NaCl + 2Fe + O_2 \longrightarrow Na_2FeO_2 + FeCl_2$$

$$\text{V}^{***} \qquad 2NaCl + Co + O \longrightarrow CoCl_2 + Na_2O$$

$$\text{VI}^{****} \qquad 3NaCl + 4Al + 3O_2 \longrightarrow AlCl_3 + 3NaAlO_2$$

* Inconel-600, Inconel-800, Nimonic-105

** Inconel-800

*** Nimonic-105

**** Nimonic-105

The sequence of the reactions III to VI depends upon the thermodynamic conditions. Table 5.2 shows the m.p., b.p. and v.p. of the chlorides of common elements[1,2].

As metallic chlorides (III to VI) move outward through the melt, oxygen activities are sufficiently high to convert metallic chlorides into metallic oxides,

VII $2FeCl_2 + \frac{3}{2}O_2 \longrightarrow Fe_2O_3 + 2Cl_2$

VIII $3FeCl_2 + 2O_2 \longrightarrow Fe_3O_4 + 3Cl_2$

IX $NiCl_2 + O \longrightarrow NiO + Cl_2$

X $CoCl_2 + O \longrightarrow CoO + Cl_2$

XI $2AlCl_3 + \frac{3}{2}O_2 \longrightarrow Al_2O_3 + 3Cl_2$

The chlorine is recycled to react with elements in the alloy,

XII $xCl_2 + 2M\ (alloy) \longrightarrow 2MCl_x$

Continuation of this process results in the development of discontinuous nonprotective and porous oxide scales. Reactions III, IV and VI indicating the formations of Na_2NiO_2, Na_2FeO_2 and $NaAlO_2$, respectively, proceed at the backward direction at the melt/salt interface due to depletion in P_{O_2} resulting in the precipitation of the oxide at the salt/gas interface. The dissociation of chlorides into oxides and precipitation of oxides at the salt/gas interface gives rise to a thick porous oxide scale.

Besides the active role played by Cr_2O_3 in enhancing the hot corrosion attack induced by NaCl, the role of metal chlorides cannot be underestimated in aggravating the situation. The boiling points of transition metal halides (Table 5.2) are quite low and at the alloy/scale interface

the volatile species could build up sufficient pressure to lift up the scales or break down the protective oxide layers[3].

The chromia oxide forming alloys show discontinuous oxidation curves, a linear kinetics is usually followed by a parabolic behaviour. This is again an evidence of breaking up oxide scales during aggressive action of NaCl. The scale morphologies are in consistent with the above mechanism which is schematically represented in Fig. 5.13.

The aggressive action of NaCl in enhancing the corrosion attack of Cr_2O_3 forming alloys has been reported by a number of investigators[3-5]. However, it has also been agreed that if sufficient Cr is present in the alloy then besides forming a protective scale, Cr_2O_3 will neutralise the aggressive action of NaCl. High Cr alloys will therefore be beneficial to NaCl corrosion if small amount of salt is present.

NaCl-coated B-1900 alloy shows much lower oxidation rates than Na_2SO_4-coated alloy. Little attack was observed with Al_2O_3 in NaCl upto a temperature of 1000°C. Continuous and smooth oxidation curves are obtained and scales seem to be adhered and protective in nature. It appears that the integrity of the Al_2O_3 film is maintained in presence of NaCl. Although the alloy is most severely attacked

either in presence of Na_2SO_4 or its mixture with NaCl (Chapter IV and VI).

Nickel-200 seems to be moderately attacked by NaCl in comparison to chromia forming alloys. The corrosion rates of the NaCl-coated alloys are much lower than the corresponding Na_2SO_4-coated alloy. Further, the oxidation rate at 850°C is much higher than at 1000°C. When NiO film on the alloy comes into contact with liquid NaCl, chloridising reaction occure.

XIII $\quad 2NiO + 2NaCl \longrightarrow NiCl_2 + Na_2NiO_2$

Liquid NaCl penetrates through the melt and comes into contact with the metal and reacts according to the reaction:

XIV $\quad 2NaCl + 2Ni + O_2 \longrightarrow NiCl_2 + Na_2NiO_2$

However, XIV may proceed to only a limited extent due to low oxygen potential gradient produced at the alloy/melt interface. In these circumstances the volatile $NiCl_2$ vapours break the oxide scale or pass through the melt and oxidise to NiO at salt/gas interface as according to IX. Further, Na_2NiO_2 as formed by XIII and XIV is dissociated and precipitated as NiO at the salt/gas interface. This results in the formation of porous and copious scales of NiO on the alloy surface. However, the inner layer of the scale seemed to retain some $NiCl_2$.

During corrosion of the alloy in presence of NaCl, two opposing factors affect the corrosion rates, with increasing temperature the increasing amount of liquid tends to accelerate the rate but at the same time the amount of Cl_2 decreases. The balance between these effects perhaps leads to the occurrence of maximum attack at an intermediate temperature. Inconel-600 and Nickel-200 are the materials which show this behaviour whereas other alloys do not show maximum corrosion at 850°C and corrosion rate increases with increasing temperature. According to Hancock[6], the integrity of the scales strongly influences the normal effect of temperature on corrosion rates of the alloys.

Monel-400 is most severely attacked by NaCl at high temperature, the intensity of the corrosion attack increases with increasing temperature.

At 1000°C, NaCl (l) attacks outer scales of CuO to form CuCl (XV), the liquid further penetrates and react with inner NiO film to form $NiCl_2$ and Na_2NiO_2 (XIII).

XV $\quad 2NaCl + 2CuO \longrightarrow 2CuCl + Na_2O + O$

NaCl (v) further attack the alloy forming CuCl, $NiCl_2$ and Na_2NiO_2.

CuCl and $NiCl_2$ formed from XV and XIV and from the substrate move outward and oxidise to CuO (XVII) and NiO

(IX), respectively, at the gas/salt interface.

XVI $2CuCl + O \longrightarrow Cu_2O + Cl_2$

XVII $Cu_2O + O \longrightarrow 2CuO$

At 1000°C, IX, XIII and XVII continue to provide a thick duplex oxide scale of CuO and NiO. The Cl_2 evolved during the oxidation is available for further corrosion along with NaCl(v), thus increasing the severity of corrosion with time. This is indicated by the onset of a linear kinetics shortly after the culmination of a parabolic kinetics. The scale morphology indicates the presence of a thick duplex oxide containing alternate layers of copper and nickel oxides.

At 850°C, NaCl(l) penetrates through the oxide scales and directly attack the alloy according to the reactions III and XVIII.

XVIII $2NaCl + 2Cu + O \longrightarrow 2CuCl + Na_2O$

CuCl and $NiCl_2$ volatilise off at this temperature and move outward through the melt and oxidise according to reactions XVI, XVII and IX. The weight gain/time plot indicates that the alloy oxidizes by a parabolic rate law at 850°C.

It appears that oxidation and chloridisation reactions (involving only NaCl) generally follow a parabolic rate law,

whereas, chloridation reactions (involving NaCl and $Cl_2(g)$) producing more serious attack are indicated by a linear rate law.

Fig. 5.14 presents schematic representation of NaCl-induced corrosion of Monel-400 alloy at 1000°C.

REFERENCES

1. P. L. Daniel and R. A. Rapp, 'Advances in Corrosion Science & Technology", 5, 55 (1976).

2. M. C. Ball and A. H. Norbury, "Physical Data for Inorganic Chemists", Longman Group Ltd. (1974).

3. D. W. McKee, D. A. Shores and K. L. Luthra, J. Electrochem Soc., 125, 412 (1978).

4. J. G. Smeggil and N. S. Bornstein, J. Electrochem Soc., 125, 1283 (1978).

5. R. C. Hurst, J. B. Jhonson, M. Davies and P. Hancock, Proc. C.E.G.B. Conf. on 'Corrosion and Deposition in Gas Turbines', London, (Dec., 1972).

6. P. Hancock, 'The Role of Halides in High Temperature Gas Corrosion', Presented at Electrochem Soc., 'High Temperature Metal Halide Chemistry' Symposium, Atlanta, U.S.A., (Oct., 1977).

Table 5.1: Constituents identified in scales of NaCl coated alloys using X-ray diffraction technique.

Alloys	Temp.°C	Constituents
IN-600	1000	Fe_2O_3, Fe_3O_4, NiO
IN-600	850	Fe_3O_4, NiO, Cr_2O_3
IN-800	1000	Fe_2O_3, Fe_3O_4, Cr_2O_3
IN-800	850	Fe_3O_4, Cr_2O_3
M-400	1000	CuO, NiO
Ni-200	850	NiO, $NiCl_2$
Nim-105	1000	NiO, Cr_2O_3, CoO
B-1900	1000	NiO, Al_2O_3

(IN = Inconel; M = Monel; Ni = Nickel; Nim = Nimonic)

Table 5.2: Melting point (T_m), Boiling point (T_b), Temperature at which the vapour pressure of the chloride is 10^{-4} atm (T_4) and Standard free energy of formation ΔH_{298}.

(All temperatures in degree Kelvin)

Chlorides	T_m	T_4	T_b	$-\Delta H_{298}$ KCal/mol
$FeCl_2$	949	809	1285	81.5±0.4
$FeCl_3$	576	340	592	95.7
$NiCl_2$	1305	880	-	73.0±0.5
$CoCl_2$	1013	860	1323	77.8±4.0
$CrCl_2$	1093	1014	1577	97.0±3.5
$CrCl_3$	1423	884	-	132.5±4.5
$AlCl_3$	463	345	720	166.8±0.8
NaCl	1074	1015	1738	98.6±0.2
CuCl	703	-	1963	32.5±0.75
$CuCl_2$	810	-	-	49.2±2.5

Table 5.3: Visual observations of NaCl-coated alloys after high temperature oxidation.

Alloys	Temperature (in degree Centigrade)	
	850	1000
Inconel-600	(i) Spalling of the scales. (ii) Outer layer of the scale is brown while the inner layer is grey in colour. (iii) Yellowish deposition on the wall of the bucket.	(i) Complete spalling of the scales. (ii) Nothing found deposited on the wall of the bucket.
Inconel-800	(i) Spalling of the scales. (ii) Outer layer of the scale is of grey colour, while the inner one is brown in colour.	(i) Three distinct layers observed in the scale: (a) outermost layer thick, smooth and black. (b) thin green layer. (c) Innermost layer - white and adhered with the alloy surface.

continued ...

Table 5.3: continued ...

Alloys	Temperature (in degree Centigrade)	
	850	1000
Monel-400	(i) Black scales with blisters. (ii) Poorly adhered scales.	(i) Scales are thick, smooth and of grey colour. (ii) Scales ruptured at the rim of the sample.
Nickel-200	(i) Dirty green scale. (ii) Scales poorly adhered to the samples.	Same as found at 850°C.
Nimonic-105	(i) Black scale with many blisters. (ii) Scale adherent to the sample.	(i) Three distinct layers observed in the scale: (a) Outer layer - thick and dark green in colour with blisters.

continued ...

Table 5.3: continued ...

Alloys	Temperature (in degree Centigrade)	
	850	1000
		(b) thin black layer. (c) inner layer - light grey in colour.
B-1900	Thin adherent scale of grey colour.	(i) An outer bluish green scale below which there is a thin grey scale. (ii) Bluish green deposition on the wall of the bucket.

CAPTIONS OF KINETIC STUDIES

Fig. 5.1 Weight change versus time plots of NaCl coated alloys oxidized at 850°C.

Fig. 5.2 Weight change versus time plots of NaCl coated alloys oxidized at 1000°C.

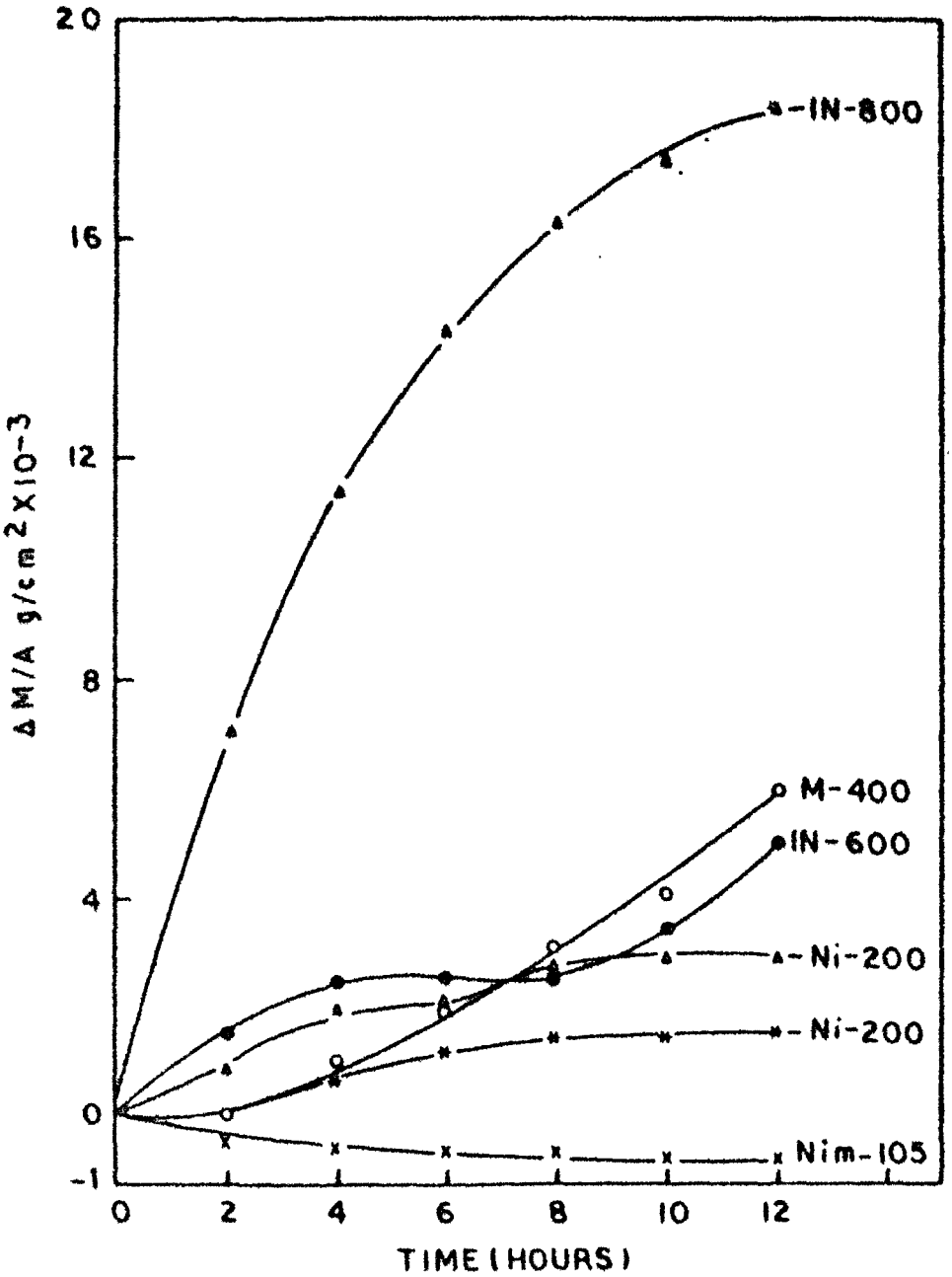
20
16
12
8
4
0
-1
ΔM/A g/cm²X10⁻³
0
2
4
6
8
10
12
TIME (HOURS)
IN-800
M-400
IN-600
Ni-200
Ni-200
Nim-105

FIG 5.1

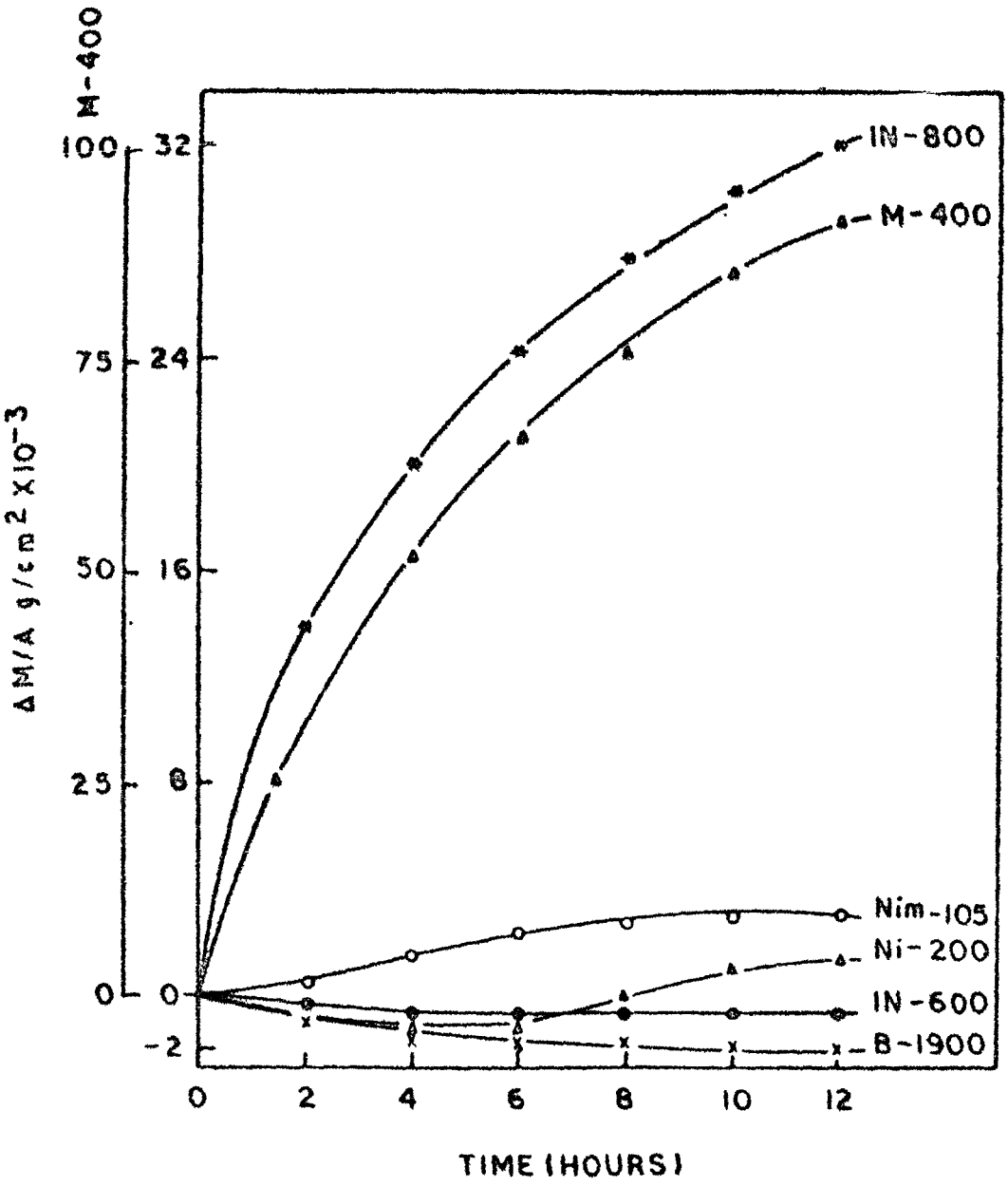
M-400
100
75
50
25
0
32
24
16
8
0
-2
ΔM/A g/cm² X10⁻³
IN-800
M-400
Nim-105
Ni-200
IN-600
B-1900
0
2
4
6
8
10
12
TIME (HOURS)

FIG. 5.2

CAPTIONS OF METALLOGRAPHS

Fig. 5.3 Scanning micrograph of Inconel-600 coated with NaCl and oxidized at 850°C for 12 hours. (2850x)

Fig. 5.4 Photomicrograph of Inconel-800 coated with NaCl and oxidized at 850°C for 12 hours. (400x)

Fig. 5.5 Scanning micrograph of Inconel-800 coated with NaCl and oxidized at 850°C for 12 hours. (1000x)

Fig. 5.6 Photomicrograph of Monel-400 coated with NaCl and oxidized at 850°C for 12 hours. (400x)

Fig. 5.7 Scanning electron micrograph of Monel-400 coated with NaCl and oxidized at 850°C for 12 hours. (600x)

Fig. 5.8 Scanning electron micrograph of Nickel-200 coated with NaCl and oxidized at 1000°C for 12 hours. (800x)

Fig. 5.9 Photomicrograph of Nimonic-105 coated with Na_2SO_4 and oxidized at 1000°C for 12 hours. (400x)

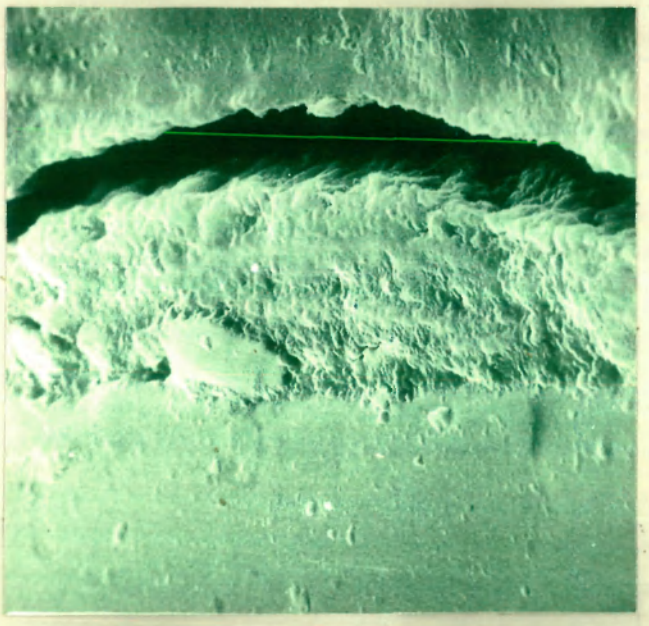

5.3

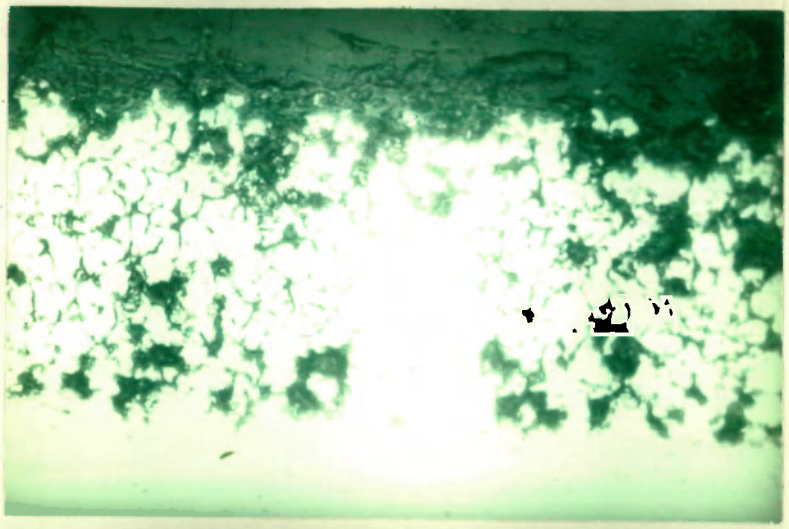

5.4

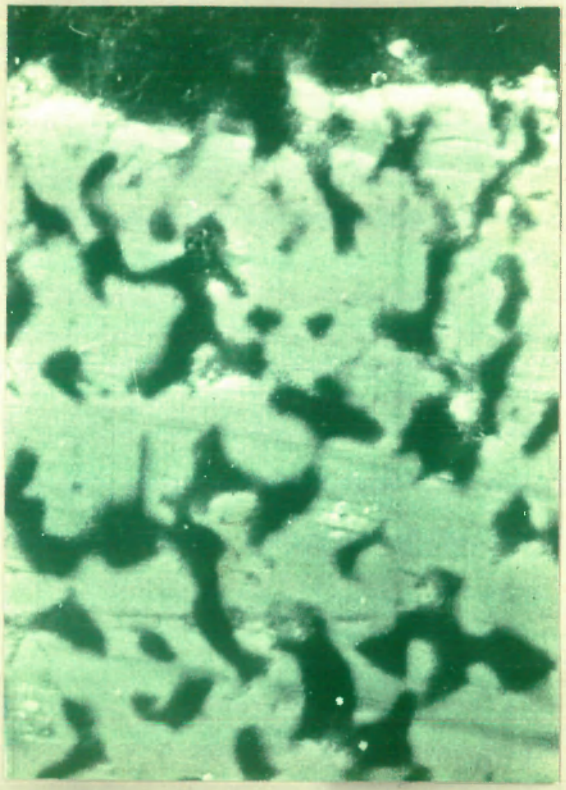

5.5

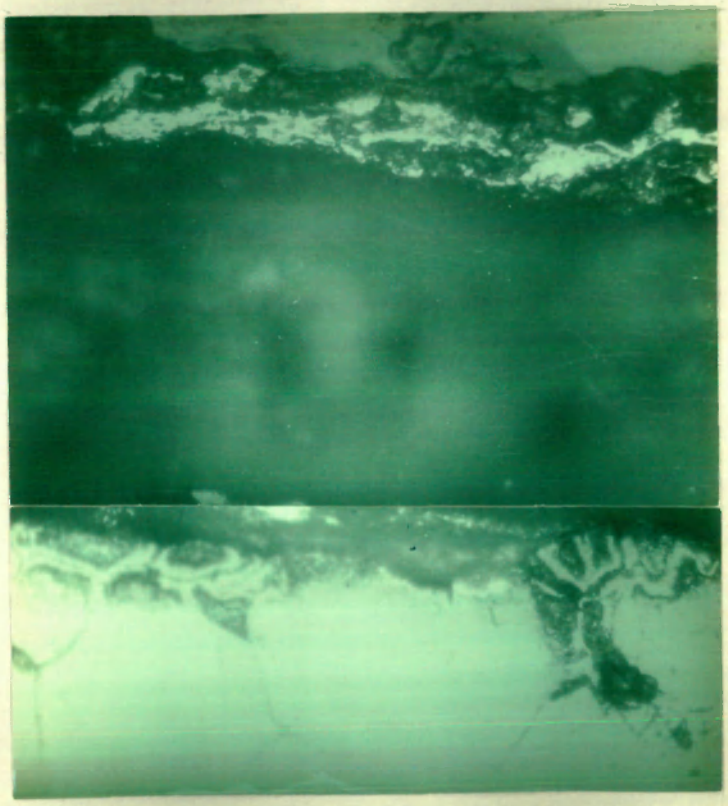

5.6

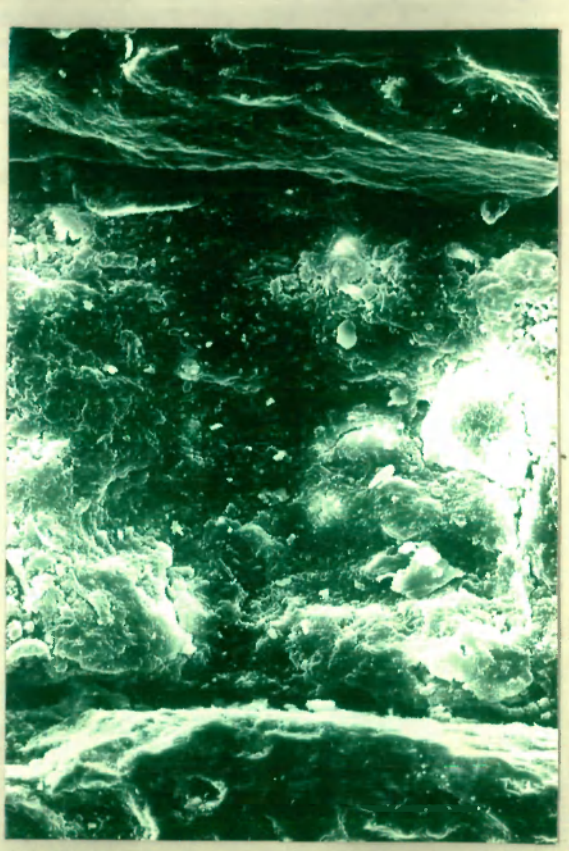

5.7

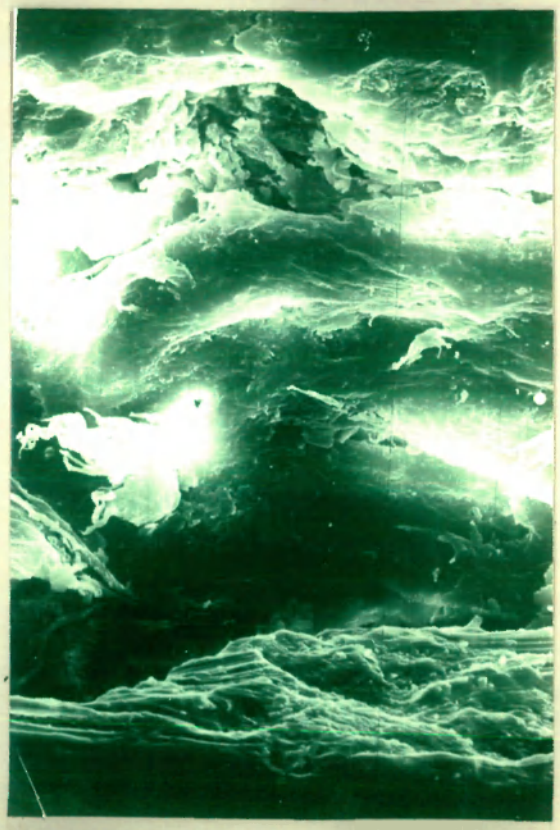

5.8

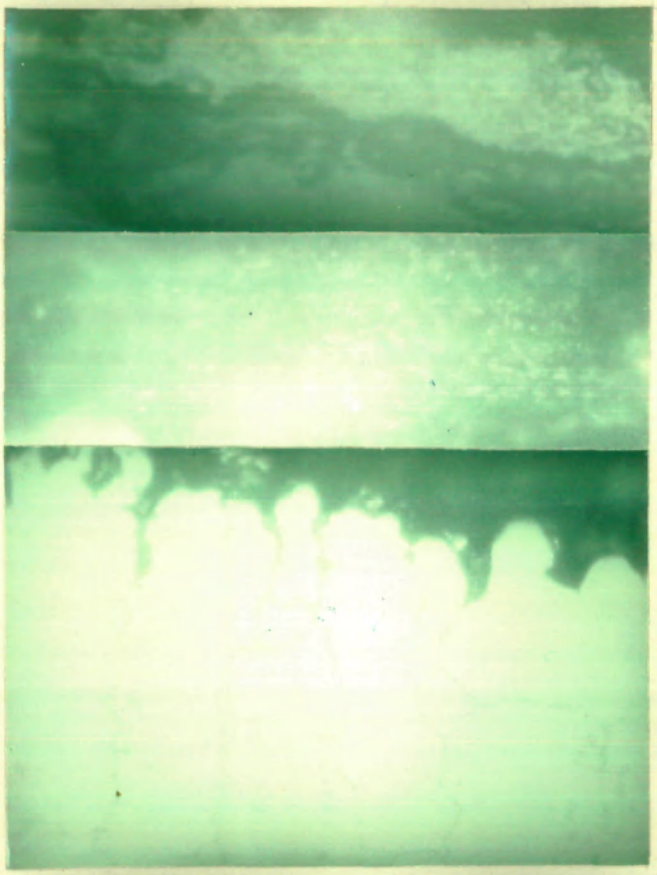

5.9

CAPTIONS OF EDAX RESULTS

Fig. 5.9 X-ray concentration profiles of NiKα , CoKα and CrKα of Nimonic-105 coated with NaCl and oxidized at 1000°C for 12 hrs.

Fig. 5.10 X-ray concentration profiles of NiKα and CuKα of Monel-400 coated with NaCl and oxidized at 1000°C for 12 hrs.

Fig. 5.11 X-ray concentration profiles of Ni Kα , Cr Kα and Fe Kα of Inconel-800 coated with NaCl and oxidized at 850°C for 12 hrs.

Fig. 5.12 X-ray concentration profiles of Ni Kα , Co Kα and Cr Kα of B-1900 coated with NaCl and oxidized at 1000°C for 12 hrs.

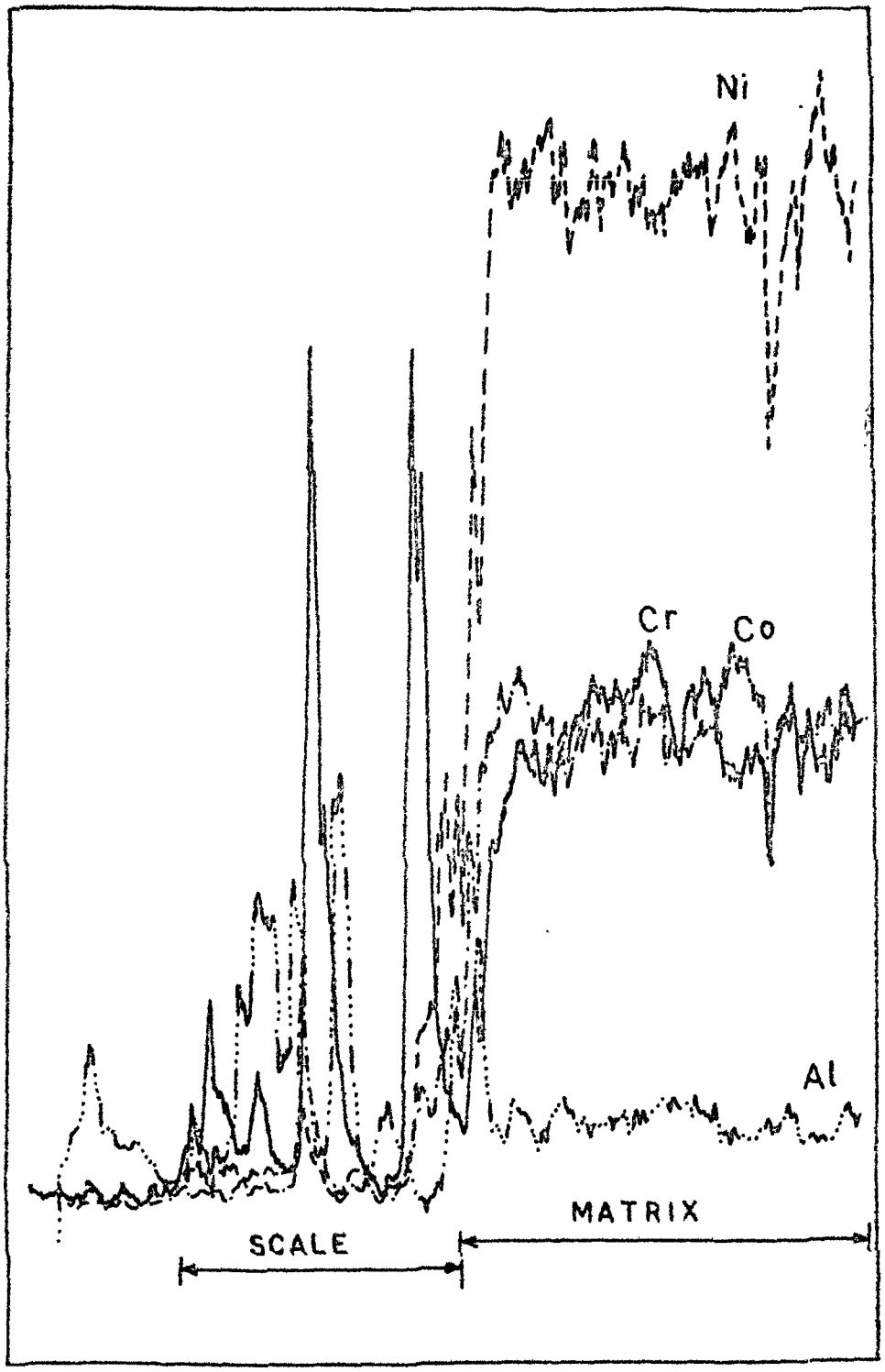

FIG. 5.9

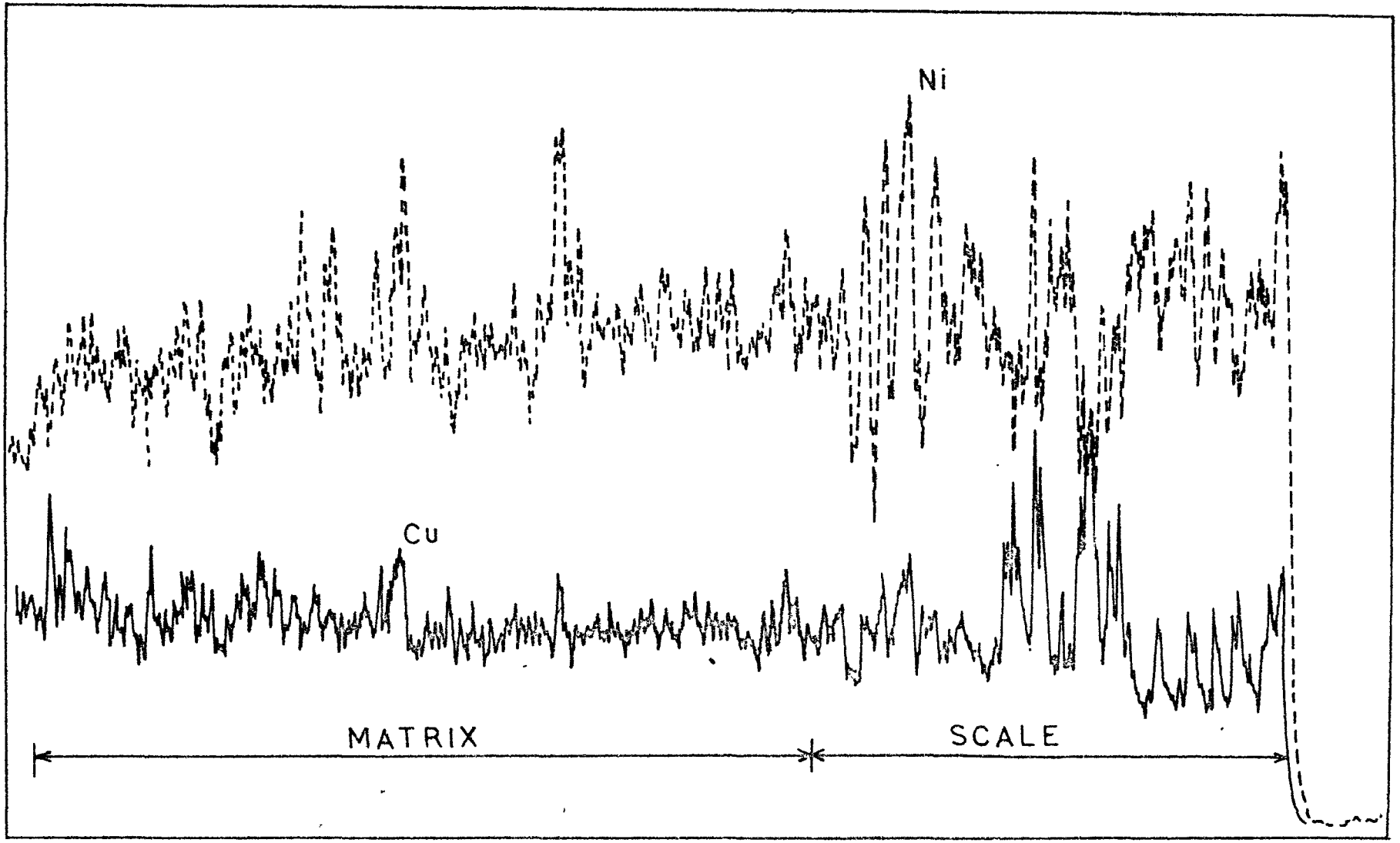

FIG. 5.10

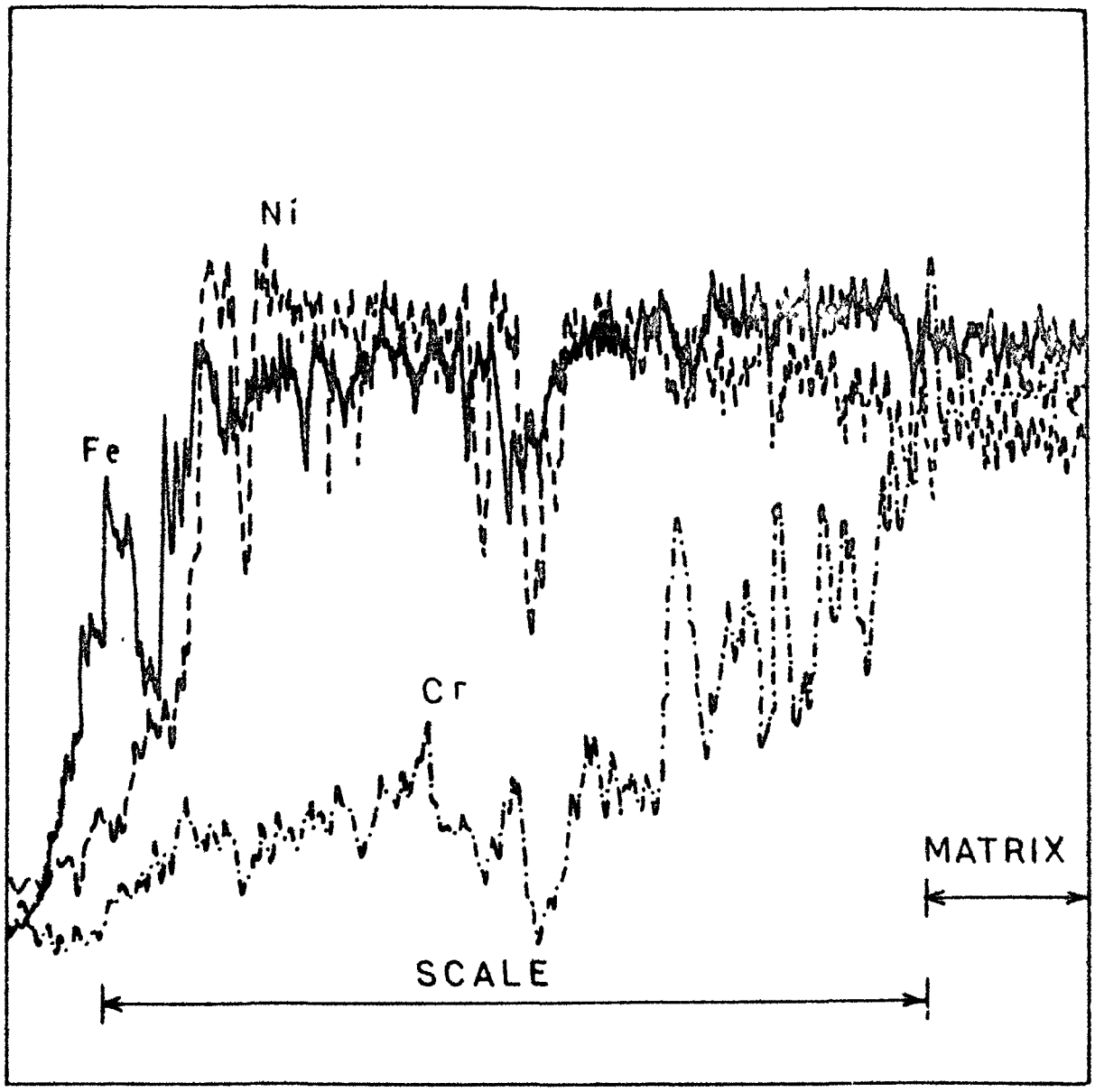

FIG. 5.11

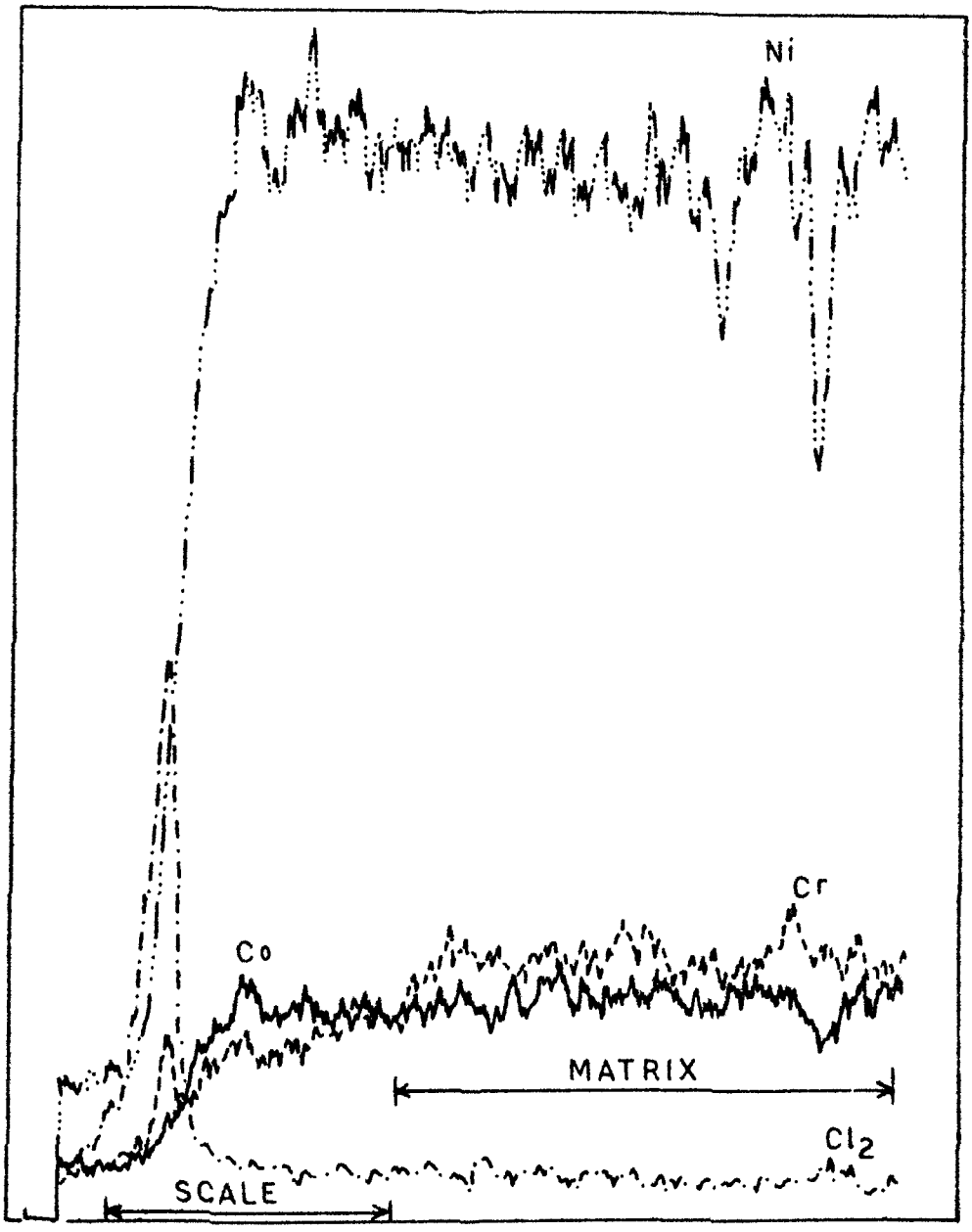

FIG 5.12

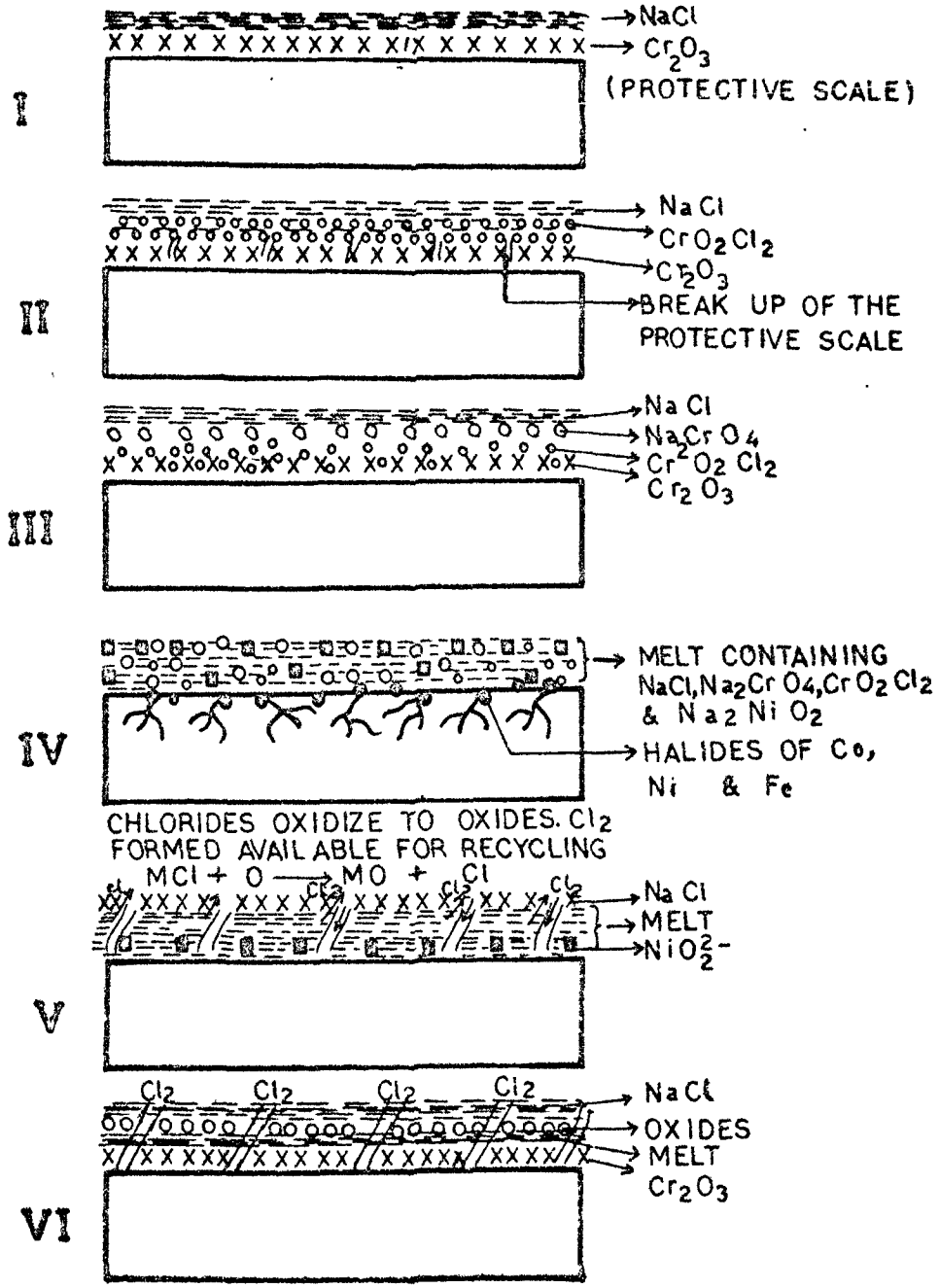

F16.5.13

SCHEMATIC REPRESENTATION OF CORROSION ATTACK BY NaCl IN CHROMIA FORMING ALLOYS

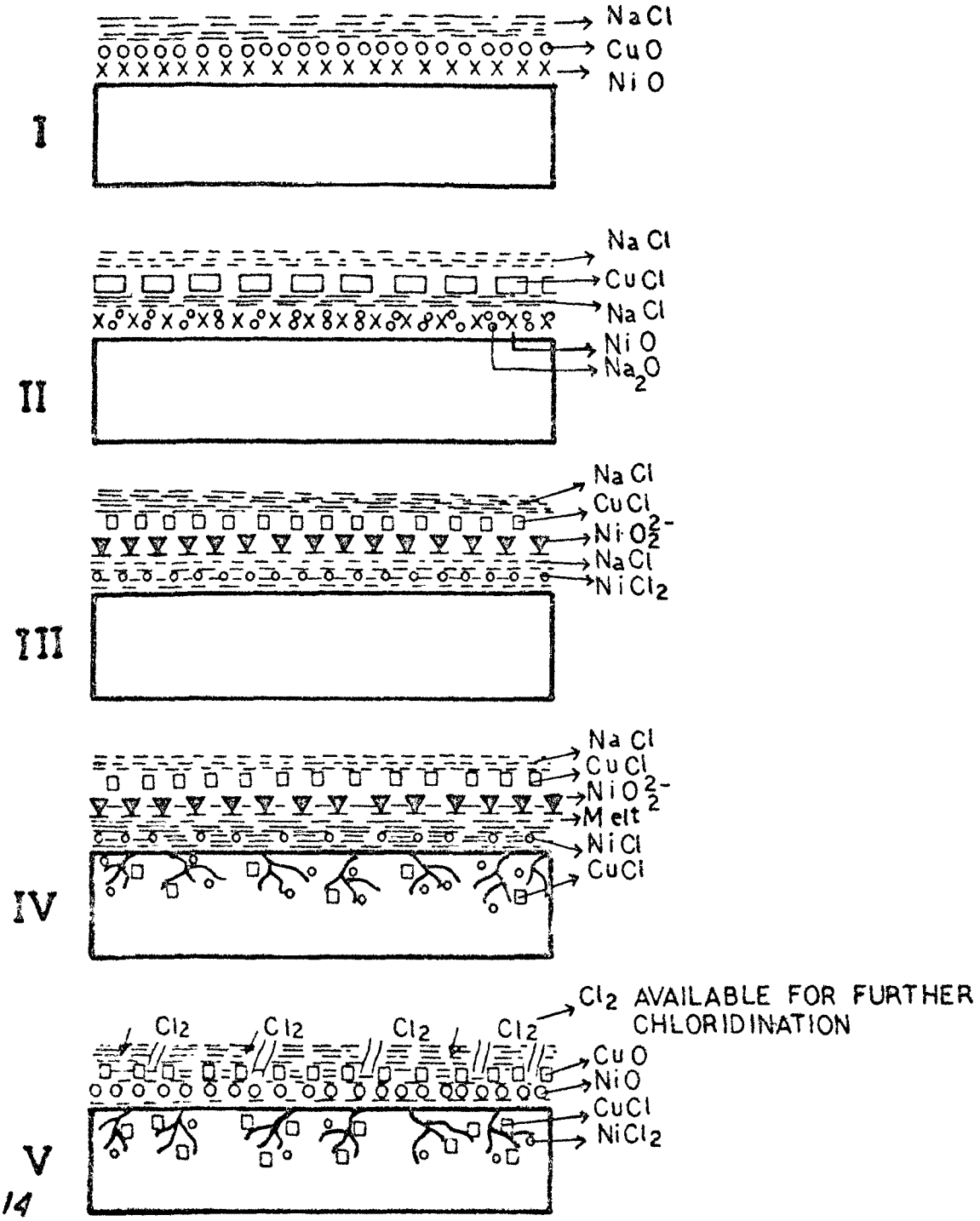

FIG.5.14

SCHEMATIC DIAGRAM SHOWING Na_2Cl-INDUCED HOT CORROSION OF MONEL 400 AT 1000°C

CHAPTER - VI

HOT CORROSION BEHAVIOUR OF NICKEL-BASE ALLOYS IN PRESENCE OF Na_2SO_4-NaCl MIXTURES

EXPERIMENTAL

6.1.1 Selection of alloys

Inconel-600, Inconel-800, Monel-400, Nickel-200 and B-1900 were employed during hot corrosion studies in presence of mixtures of Na_2SO_4 and NaCl. The nominal compositions of the alloys are referred in table 4.1.

6.1.2 Preparation of the salt mixture

Solutions of Na_2SO_4 and NaCl containing definite amounts of the salts were prepared. Solutions of the salts were mixed in proportions so as to provide mixture solutions containing Na_2SO_4 : NaCl in molar ratios of 1 : 5 and 5 : 1, respectively. Care was taken to use minimum amount of water in preparing the solutions.

6.1.3 Preparation of the salt mixture coated specimen

Rectangular coupons of 1.5 cm x 0.5 cm x 0.1 cm size or round specimens of dimensions 1.3 cm diameter x 0.2 cm thickness were either cut from the sheet or rod of the alloys respectively. These specimen samples were polished on a motor driven disc polisher using SiC papers of 180, 320 and 600 grades, respectively. The polished samples were washed with water and then degreased with CCl_4. The polished specimens were coated uniformly with salt mixture using spraying technique. A coating of about 6 μm salt thickness (1.5

mg/cm^2) was maintained during experiments. Coated specimens were dried for 12 hours in a hot air oven maintained at 150°C.

6.1.4 Hot corrosion studies

Salt mixture coated specimens were transfered in the quartz bucket and the bucket was suspended to the quartz helics of the helical thermal balance attached with a cathetometer. The balance was surrounded by a vertical type furnace. For kinetic measurements weight changes were measured after each one hour. The hot corrosion experiments were carried out at 850 and 1000°C in a current of air.

Three specimens were oxidized in nearly identical conditions for a particular oxidation experiment. The first specimen was utilised for chemical identifications of corrosion products in the scales, the other one was used for X-ray identification and the third was retained for metallographic examinations.

6.1.5 Morphological studies

6.1.5.1 Optical Metallography

Oxidised samples were mounted in paper pile boxes using Araldite as a cold setting compound. Mounted samples were abraded on disc polisher using SiC papers of 180, 320 and 600 grades and on a hand polisher using 0/4 grade emery

paper. Fine polishing of these samples were carried out on selvyt cloth using 1 μ grade alumina powder. Kerosene oil has been used as lapping liquid during the entire polishing operation. Samples were washed with alcohol and CCl_4 and were then etched either with 1% acidic solution of $FeCl_3$ or etched electrolytically in 2% HNO_3 for 2-3 minutes.

The polished and etched samples were examined under the Leitz photometallurgical microscope attached with a 35 mm camera and relevent portions of the microstructures were photographed.

6.1.5.2 Scanning Electron Microscopy

Polished specimens were coated with colloidal silver or gold emulsions and examined under a Cambridge Scanning Electron Microscope Model S4-10. Microstructures giving relevent details were photographed at a desired magnification.

6.1.6 Energy Dispersion X-ray Analysis

Elemental distribution within the scales and matrix was determined from EDAX by obtaining Kα concentration profiles.

6.1.7 X-ray Diffraction Analysis

X-ray diffraction patterns of the scales on the corroded alloys were obtained by a X-ray diffractometer

assembly, using CoKα , CuKα or FeKα radiations and an appropriate filter. The constituents identified in the scales are listed in table 6.1.

RESULTS

6.2.1 Kinetic studies

High temperature hot corrosion behaviour of Ni-base superalloys, e.g. Inconel-600, Inconel-800, Monel-400, Nimonic-105, B-1900 and Nickel-200 has been studied in the presence of Na_2SO_4-NaCl mixtures prepared in the molar ratios of 1:5 and 5:1. These studies have been carried out at 850 and 1000°C in flowing air. The corrosion runs were of 12 hours durations. Figures 6.1 and 6.2 show the weight change/time at 850 and 1000°C, respectively in the presence of the mixture prepared in 1:5 molar ratio, while figures 6.3 and 6.4 show the weight change/time in the presence of the mixture prepared in 5:1 molar ratio, at 850 and 1000°C, respectively.

Inconel-600:

The Na_2SO_4-NaCl (1:5) coated alloy oxidises by a parabolic rate law at 850 and 1000°C. In both cases the alloy oxidises at a relatively slow rate and the oxidation rates are similar in magnitude.

At 850°C, the Na_2SO_4-NaCl (5:1) coated alloy too oxidizes slowly following a parabolic rate law showing a total weight gain of about 0.5 mg/cm^2 in a 12 hour oxidation run. At 1000°C, the 5:1 mixture coated alloy initially

oxidises by a weight gain. However, after about 4 hours the alloy starts loosing weight with a total loss of about 1.0 mg/cm^2 after 12 hours of oxidation run.

Inconel-600:

At 850°C, the 1:5 mixture coated alloy oxidises at an abnormally high oxidation rate, perhaps by a linear rate law, while, at this temperature 5:1 mixture coated alloy oxidises by a parabolic rate law and shows comparatively low oxidation rate.

At 1000°C, the 1:5 mixture coated alloy oxidises at a much slow rate and follows a parabolic law. However, in the presence of 5:1 mixture alloy shows weight losses upto 6 hours followed by small weight gains. A weight gain of about 1.5 mg/cm^2 is obtained at the end of the oxidation run.

Monel-400:

At 850°C, 1:5 mixture coated alloy oxidises by a parabolic rate law and the oxidation rates are lower than those in uncoated conditions or in presence of NaCl or Na_2SO_4. However, at 1000°C the coated alloy oxidises at much faster rate perhaps by a parabolic rate law and the oxidation rates are similar to those observed during uncoated condition or in presence of NaCl.

In the presence of 5:1 mixture alloy oxidises by a parabolic rate law at both the temperatures. The oxidation rate is much higher at 1000°C than at 850°C.

In comparison to the normal oxidation, the oxidation rate does not seem to be altered effectively by the presence of higher concentration of NaCl. But the salt mixture containing higher amount of Na_2SO_4 (i.e. 5:1 mixture) diminishes the rate of the oxidation at 1000°C.

Nimonic-105:

1:5 mixture coated Nimonic-105 shows a relatively slow rate of oxidation at both the temperatures (850 and 1000°C) and by a parabolic rate law. The weight gains of 0.8 mg/cm^2 and 2.0 mg/cm^2 have been observed at 850 and 1000°C, respectively during 12 hour oxidation run.

Unlike the oxidation behaviour observed at 850°C in the presence of salts mixture containing high amount of NaCl (1:5 mixture), alloy coated with salt mixture containing higher amount of Na_2SO_4 (5:1 mixture) shows weight losses to the extent of 1.0 mg/cm^2 in a 12 hour oxidation run. However, at 1000°C in the presence of 5:1 mixture the alloy oxidises slowly showing a weight gain of about 1.0 mg/cm^2 at the end of the oxidation run.

B-1900:

At 850 and 1000°C Na_2SO_4-NaCl (1:5) mixture coated B-1900 shows small weight losses during oxidation. The weight losses are 0.8 and 1.8 mg/cm^2 at 850 and 1000°C, respectively.

At 850°C and 1000°C, the 5:1 mixture coated alloys oxidise at a rapid rate by a parabolic rate law. However, at 1000°C, 5:1 mixture coated alloy shows a higher weight gain of about 32 mg/cm^2 at the end of run, in comparison to the 15.0 mg/cm^2 weight gain observed at 850°C. This behaviour is contrary to the oxidation behaviour observed in the presence of mixture containing higher amount of NaCl (1:5), where small weight losses have been observed at both the temperatures.

Nickel-200:

At 850°C the 1:5 mixture coated alloy oxidises at a relatively slow rate and follows a parabolic rate law. However, at 1000°C the alloy oxidizes at a very slow rate upto 5 hours, this is followed by a high oxidation rate indicated by rapid weight gains.

In the presence of a mixture containing higher amounts of Na_2SO_4 (5:1 mixture) Ni-200 obeys a parabolic rate law during oxidation at both the temperatures, viz. 850 and 1000°C.

6.2.2 X-ray diffraction analysis

Constituents identified in the scales of the samples corroded in the presence of Na_2SO_4-NaCl mixtures at 850 and 1000°C are listed in the table 6.1.

6.2.3 Morphological studies

Inconel-600:

Figures 6.5 and 6.6 show the SEM pictures of the scales formed on a sample of Inconel-600 coated with Na_2SO_4 + NaCl (1:5) and corroded at 1000°C for 12 hours. The inner layers of the scales largely contain Cr_2S_3 and the outer layers are rich in NiO with Cr_2O_3 inclusions. The scales are continuous, compact and reasonably adherent to the alloy. At 1000°C, due to selective sulfidation of Cr, copious internal and grainboundary sulfidation has occurred which can be seen in the optical micrograph (figure 6.7).

Figure 6.8 shows the SEM picture of the scale of Na_2SO_4 + NaCl mixture (in the molar ratio of 5:1) coated IN-600 alloy sample corroded at 850°C for 12 hours. The scales are strongly adhered to the alloy surface. The outer layer is mainly comprised of NiO (light) with Cr_2O_3 inclusions. The inner scales contain some pockets of Cr_2S_3 (grey). At 1000°C in the presence of this salt mixture (5:1) the samples show similar features in the microstructure, as that observed at 850°C, but the scales are denser,

less adherent, more porous and Cr_2S_3 is present in the larger concentration in the inner scales (figure 6.9).

Inconel-800:

In the presence of 1:5 mixture of Na_2SO_4-NaCl, thick and uniform scales are formed at both the temperatures (850 and 1000°C). These scales are very poorly adhered to the alloy and therefore easily detached away from the alloy. Micrograph of the sample corroded at 1000°C shows the copious internal sulfidation which may be due to formation of $(Fe,Cr)S_x$ or Cr_2S_3 at the grainboundaries (figure 6.10). Fe and Ni in the alloy are preferentially oxidised and are present as internal oxide particles. NiO, Fe_2O_3 and Fe_3O_4 are identified in the scales by X-ray diffraction.

Monel-400:

Figure 6.11 shows the SEM picture of the M-400 alloy sample corroded at 1000°C in the presence of the mixture of Na_2SO_4 + NaCl (1:5). The scales largely consist of NiO with NiS or (Cu,Ni)S inclusions, this is followed by a thick porous scale of NiO with the inclusions of CuO.

Figure 6.12 shows the optical micrograph of a cross section of M-400 alloy corroded at 850°C in presence of mixture of Na_2SO_4 + NaCl (5:1). The micrograph indicates the presence of internal sulfide particles and penetration of the salt into the alloy matrix. The inner scales are richer

in Ni_3S_2 and the outer thicker scales contain duplex scale of NiO and CuO.

Nimonic-105:

Figure 6.13 shows the SEM picture of the cross section of a sample of Nim-105 at 1000°C in the presence of a mixture of Na_2SO_4 + NaCl (1:5). The picture shows the formation of a uniform and compact scale with poor adherence. The inner-most scale contains Al_2O_3 (light) with inclusions of Cr_2O_3 (grey) in the form of a thin layer, while the outer scales are comprised of Cr_2O_3 (grey) and CoO (light grey) with NiO (light) inclusions in the form of stratified layers. The oxide scales contain blisters, as has been observed in the samples of the same alloy corroded in the presence of only NaCl. Figure 6.14 shows the SEM picture of a single blister. This blister mainly comprises of Cr_2O_3 with uneven inclusions of CoO and NiO. The blisters are most probably formed during fluxing of oxide/scales by $NaCl/Na_2SO_4$ resulting in the release of SO_2 and Cl_2 gases which penetrates through the scales and escape during cooling of the scales.

Figure 6.15 shows the SEM picture of Nim-105 sample coated with Na_2SO_4-NaCl mixture of 5:1 molar ratio and corroded at 1000°C for 12 hours in flowing air. The micrograph shows the presence of an inner layer of Al_2O_3 which is disrupted due to the presence of NaCl. Some of the frag-

nents of Al_2O_3 scales can be located in the middle zone of the scale which is much thicker and comprises of CoO (light grey), Cr_2O_3 (dark grey) and NiO forming the outer scales. Chromium present in the substrate is preferentially sulfidised and is present as internal sulfide particles.

B-1900:

Figure 6.16 shows SEM picture of a cross section of B-1900 alloy oxidised in presence of Na_2SO_4-NaCl mixture (1:5) at 850°C. The multilayered scales contain a well adhered inner layer which is comprised of Al_2O_3 containing inclusions of MoO_3, the next outer layers of the scales contain Cr_2O_3 with inclusions of Mo, Ti and Ta and the outermost layers contain NiO with inclusions of CoO. The scales contain crystallcits of oxides. The uncompactness of the scales perhaps results due to the release of $Cl_2(g)$ which escape through oxide scale providing voids in between the oxide crystallcits.

Figure 6.17 shows a SEM picture of cross section of B-1900 alloy coated with a mixture of Na_2SO_4 + NaCl (5:1) and oxidised at 850°C for 12 hours. The micrograph shows the presence of a scale predominently concentrated in Al_2O_3 in the form of crystallcits with inclusions of TiO_2, MoO_3 and Ta_2O_5. The matrix shows indication of internal sulfidation, Cr_2S_3 particles are present at the alloy/scale interface.

Nickel-200:

Figures 6.18 and 6.19 represent typical photographs of Na_2SO_4 + NaCl (1:5) coated Ni-200 alloy, oxidised at 1000°C for 12 hours. Due to presence of NaCl, the otherwise compact scales are disrupted. The outer scales appear in the form of a nearly uniform layer of NiO. The inner scales are largely comprised of NiS (grey) with NiO inclusions. The NiO seems to be precipitated during decomposition of $NiCl_2$ and subsequently oxidation of NiO. The $Cl_2(g)$ released produces blisters and voids in the middle section of the scales.

Figure 6.20 shows the photograph of a cross section of Ni-200, coated with Na_2SO_4-NaCl (1:5) mixture and oxidised at 850°C for 12 hours. The outermost layer seems to be comprised of Ni_3S_2 (grey) and NiO (white), while the inner compact continuous grey coloured band is of Ni_3S_2. Accumulation of the NiS along the grainboundaries may be clearly seen in the matrix region of the micrograph.

Figure 6.21 shows the optical micrograph of cross section of a sample of Ni-200 alloy, coated with Na_2SO_4 + NaCl mixture (5:1) and corroded at 1000°C for 12 hours. The outer layer is composed of NiO with NiS inclusions but at the alloy/scale interface intense sulfidation occurs which causes the fragmentation of the matrix. The (Ni + Ni_3S_2)

eutectic which was liquid at the oxidation temperature solidifies and is concentrated at some regions in the matrix.

6.2.4 Energy Dispersion X-ray Analysis (EDAX)

Inconel-600 in the presence of Na_2SO_4-NaCl (1:5) mixture:

Figure 6.22 shows EDAX profiles of Inconel-600 oxidized in presence of Na_2SO_4-NaCl mixture (1:5) at 1000°C. The profiles indicate the presence of Cr_2S_3 in the innermost layer. This is followed by Ni-rich layers probably containing NiS the outer layers are rich in Cr_2O_3 and outermost layers form duplex scales of Cr_2O_3 and NiO.

Inconel-800 in presence of Na_2SO_4-NaCl (5:1) mixture:

Figure 6.23 represents Fe, Ni and Cr Kα X-ray concentration profiles of Na_2SO_4 + NaCl (5:1) coated Inconel-800 oxidised at 1000°C. The presence of iron-rich layer in the inner scale is indicated, this is followed by chromium rich layers forming outer scales. There is little iron or nickel in the outer scale.

Monel-400 in presence of Na_2SO_4-NaCl (5:1) mixture:

Figure 6.24 shows X-ray concentration profiles for Monel-400 coated with 5:1 mixture of Na_2SO_4-NaCl and oxidised at 1000°C. The inner scales appear to be rich in nickel (perhaps in the form of Ni_3S_2) followed by duplex scales of (Ni,Cu)S. The outer scales contain NiO in pre-

dominant concentrations while the outermost scales comprise mainly of copper (in the form of CuO). The profiles indicate the presence of Ni-rich zone in the matrix at the alloy/scale interface. Perhaps preferential sulfidation of Ni in the substrate has occurred.

B-1900 in presence of Na_2SO_4-NaCl (5:1) mixture:

Figure 6.25 shows the X-ray concentration profile of B-1900 alloy sample coated with Na_2SO_4-NaCl (5:1)mixture and oxidised at 850°C. Profile shows a Ni-rich scale with inclusions of chromium. Aluminium and cobalt may also be seen distributed throughout the scale but in comparatively low concentrations.

D I S C U S S I O N

The high temperature oxidation behaviour of some Ni-base alloys has been studied in presence of Na_2SO_4 and NaCl (5:1 and 1:5 molar ratios) at 650 and 1000°C in a current of air.

The weight gain/time curves indicate that chromia forming alloys, e.g. Inconel-600 and 800 and Nimonic-105 show increasing corrosion rates with increasing amount of NaCl in Na_2SO_4 whereas Al_2O_3 former (B-1900) and NiO former (Ni-200) show decreasing oxidation rates with increasing amount of NaCl in Na_2SO_4, although small amount of NaCl in Na_2SO_4 enhances the oxidation rates initially. Monel-400 (NiO/CuO former) behaves similar to chromia forming alloys.

The corrosion sequences (in order of decreasing corrosion rates) for different Ni-base alloys are as follows:

Inconel-600:

650°C:

$NaCl\text{-}Na_2SO_4$ (5:1) > $NaCl\text{-}Na_2SO_4$ (1:5) > NaCl > Na_2SO_4> uncoated.

1000°C:

NaCl > $NaCl\text{-}Na_2SO_4$ (5:1) > $NaCl\text{-}Na_2SO_4$ (1:5) > Na_2SO_4> uncoated.

Inconel-600:

850°C:

NaCl > NaCl-Na_2SO_4 (5:1) > NaCl-Na_2SO_4 (1:5) > uncoated > Na_2SO_4.

1000°C:

NaCl > NaCl-Na_2SO_4 (5:1) > NaCl-Na_2SO_4 (1:5) > uncoated > Na_2SO_4.

Nimonic-105:

850°C:

NaCl > NaCl-Na_2SO_4 (5:1) > NaCl-Na_2SO_4 (1:5) > Na_2SO_4 > uncoated.

1000°C:

NaCl-Na_2SO_4 (5:1) > NaCl-Na_2SO_4 (1:5) > uncoated > Na_2SO_4 ~ NaCl.

B-1900:

850°C:

NaCl-Na_2SO_4 (1:5) > Na_2SO_4 > NaCl-Na_2SO_4 (5:1) > uncoated.

1000°C:

NaCl-Na_2SO_4 (1:5) > Na_2SO_4 > uncoated ~ NaCl-Na_2SO_4 (5:1) > NaCl.

Nickel-200:

850°C:

$NaCl-Na_2SO_4$ (1:5) > Na_2SO_4 > NaCl > $NaCl-Na_2SO_4$ (5:1) > uncoated.

1000°C:

$NaCl-Na_2SO_4$ (1:5) > $NaCl-Na_2SO_4$ (5:1) > Na_2SO_4 > uncoated > NaCl.

Monel-400:

850°C:

Uncoated ~ NaCl > $NaCl-Na_2SO_4$ (1:5) > Na_2SO_4 > $NaCl-Na_2SO_4$ (5:1).

1000°C:

$NaCl-Na_2SO_4$ (5:1) > NaCl > uncoated > $NaCl-Na_2SO_4$ (1:5) > Na_2SO_4.

Oxidation of chromia forming alloys with Na_2SO_4-NaCl mixtures (5:1 and 1:5 molar ratios) results in the development of degradation microstructures. The degradation is more pronounced in alloys coated with higher amounts of NaCl. Inconel-600 is most severely attacked and Nimonic-105 is least affected.

Inconel-600 alloy coated with 5:1 mixtures (NaCl:

Na_2SO_4) shows NiO with Cr_2O_3 inclusions in the outer scales, beneath the oxide scales chromium sulfide is present containing some NiS. The same alloy shows relatively less corrosion attack in presence of NaCl:Na_2SO_4 (1:5) although a sulfide layer is present. Inconel-600 which is more severely attacked shows similar morphology beneath the oxide scales which are comprised of oxides of all the elements in the alloy with predominent concentration of Ni, Cr and Fe oxides, a sulfide front is present in the form of a zone which extended into the alloy much as if internal corrosion product has been formed. The microstructures of Na_2SO_4-NaCl corroded Nimonic-105 alloy show the disruption of otherwise protective scales. The disruption is more distinct in alloy coated with Na_2SO_4-NaCl (1:5) mixture where deep penetration of the salt and alloy fragmentation are also observed.

Considering Na_2SO_4-induced hot corrosion chromia former Ni-base alloys in air, it is found that the alloys are extremely resistant to this form of degradation at least for short exposures (Chapter IV). Upon exposure to Na_2SO_4 in air, Cr_2O_3 scales are developed between the alloy and the salt. This condition persists for extremely long periods of time. Eventually chromium depletion followed by nickel depletion reaches levels where oxides of elements other than Cr or Ni are formed and substantial amounts of sulfur are

introduced into the alloy from Na_2SO_4 for sulfidation. Subsequent degradation then occur by oxidation of these sulfides resulting in the release of sulfur which is available for the formation of more sulfides in the alloy beneath the nonprotective scales.

When NaCl is present in Na_2SO_4, the chromia scales which were initially protective in presence of Na_2SO_4 are attacked by NaCl. The corrosion rates are enhanced by several magnitude due to the formation of volatile CrO_2Cl_2 and subsequent conversion to yellow Na_2CrO_4 which is deposited on the cooler end of the reaction tube. The presence of this deposit has indeed been observed in all the alloys. The function of chloride is to remove chromium preferentially thus producing chromium depletion in the alloy. It has two important bearings; NaCl(l) creeps through the melt and meets the alloy directly, the alloying elements undergo chloridination reactions and form chlorides according to their thermodynamic stabilities. These chlorides which are volatile move outward in the form of vapours and getting oxidised at the salt/air interface to respective oxides, the chlorine given off recycles and induces chlorination reactions (Chapter V). Secondly, due to removal of chromium by chloride the sulfur from Na_2SO_4 begins to sulfidise the alloy much earlier. The combined effect of the two factors

results in much higher corrosion rates in NaCl-Na_2SO_4 coated alloys than in Na_2SO_4 coated alloy. In those cases where the deposits contain mostly NaCl as in case of 5:1 NaCl: Na_2SO_4 mixture the effects produced by sulfur will become less important. In this case NaCl will cause rapid depletion of the alloy of chromium, nickel and other elements along with the development of a porous network in the alloy.

Inconel-800 coated with NaCl-Na_2SO_4 (5:1) has much higher oxidation rate at 850°C than 1000°C; similar behaviour although not so markedly has been shown by the same alloy coated with 1:5 mixture. An explanation is offing which is based upon the fact that two opposing factors act during hot corrosion attack: the one involving the formation of increasing amount of liquid with increasing temperature tends to accelerate the rate, but at the same time the declining activities of Cl_2 tend to lower the rate approaching that in Cl_2-free environments above 900°C. The activity of Cl_2 at the alloy surface may be further limited by diffusion when the sample is covered by a continuous film of liquid salt or is submerged in a melt. Chlorine transport through a liquid salt is likely to be slow and therefore, at high temperatures the liquid may effectively shield the specimen from Cl_2 and thereby further contribute to a reduction in corrosion rate.

The alumina forming B-1900 shows high corrosion rates in presence of a mixture consisting of NaCl and Na_2SO_4 in the molar ratio of 1:5 and lowest in presence of pure NaCl. Addition of little amount of NaCl in Na_2SO_4 enhances the oxidation rates of alloy enormously.

Al_2O_3 scales seem to remain intact in presence of NaCl upto 1000°C (Chapter V) and further, increasing amounts of NaCl in Na_2SO_4 decrease the aggressiveness of Na_2SO_4.

It has been shown that the presence of Mo in B-1900 is responsible for catastrophic oxidation when this alloy is corroded in presence of Na_2SO_4 at 850 and 1000°C (Chapter IV). It appears that the small amount of NaCl which is added enhances the corrosion rates by decreasing the induction periods (2 hrs at 850°C and about 1 hr at 1000°C) and onset of degradation reactions starts much earlier. This degradation is caused by rapid removal of Al from alloy. With the culmination of reactions (I to V) involving oxygen and sulfur removal from the salt deposit the sulfur and oxygen activities are reduced at melt/oxide interface, and NaCl from the deposit will react with Al_2O_3 and later Al in the substrate to form $AlCl_3$. Removal of Al from alloy by NaCl occurs via development of internal network of pores. The pores act as active centres for enrichment of liquid NaCl. As the $AlCl_3$ moves outward in the pore, higher oxygen

activities exist in the liquid because oxygen is being supplied by air. Consequently, the $AlCl_3$ is converted to Al_2O_3 and chlorine is free to react again with the alloy. In such a process, a small amount of NaCl can produce a substantial effect because it is recycled.

I $\quad \gamma 2Cr_2O_3(s) + Na_2SO_4(l) + \gamma 4\, O_2(g) \longrightarrow Na_2CrO_4(l) + SO_2(g)$

II $\quad Ni + SO_4^{2-} \longrightarrow NiS(l) + \frac{3}{2}O_2 + O^{2-}$

III $\quad 2Al + 3SO_4^{2-} \longrightarrow Al_2O_3 + 3SO_2(g) + 3O^{2-}$

IV $\quad 2Cr + 3SO_4^{2-} \longrightarrow Cr_2O_3 + 3SO_2(g) + 3O^{2-}$

V $\quad Al_2O_3 + O^{2-} \longrightarrow 2AlO_2^-$

VI $\quad Al_2O_3 + 6NaCl \longrightarrow 2AlCl_3 + 3Na_2O$

VII $\quad 2Al + 6NaCl + \frac{3}{2}O_2 \longrightarrow 2AlCl_3 + 3Na_2O$

VIII $\quad 2AlCl_3 + \frac{3}{2}O_2 \longrightarrow Al_2O_3 + 3Cl_2$

IX $\quad 3Na_2O + 3Cl_2 \longrightarrow 6NaCl + \frac{3}{2}O_2$

The presence of relatively larger proportions of NaCl in Na_2SO_4 greatly suppress the corrosion rates as indicated by the lowest oxidation rates of B-1900 coated with NaCl-Na_2SO_4 (5:1) mixture. There does not appear to be a simple

and plausible explanation of the role of NaCl in decelerating the corrosion rate of B-1900 alloy. In this regard, two important factors are to be considered which were found responsible for the accelerated/catastrophic corrosion of Na_2SO_4-coated B-1900 alloy: the basic fluxing of protective Al_2O_3 scales and deleterious effect of MoO_3 by forming a low melting phase (Na_2MoO_4/MoO_3) that removes the protective scale by acid fluxing (Chapter IV). NaCl seems to protect the integrity of the protective scales and also chemically deactivates the influence of Mo by unknown mechanisms. A detailed study of the influence of NaCl in Na_2SO_4-induced hot corrosion of B-1900 is required to investigate the mechanism. A comparative study of the scale morphologies of B-1900 alloy corroded in presence of Na_2SO_4-low NaCl and Na_2SO_4-high NaCl indicates that in the former the scales are almost completely perturbed whereas in the latter case the protective Al_2O_3 scales are only marginally ruptured (Fig. 6.16). It is reported that NaCl attacks Cr_2O_3 but not Al_2O_3, but the integrity of alumina scales is much inferior to Cr_2O_3 scales. This means that the contaminant has easier access to the underlying metal in alloys which depends upon Al_2O_3 rather than Cr_2O_3. However, the present results lead to the opposite conclusions. Stroud and Rapp[14] showed that the introduction of 10% NaCl into the Na_2SO_4 did not alter the solubility of Al_2O_3 in the Na_2SO_4 melt, suggesting that

the accelerating influence of NaCl on the hot corrosion experienced by many alloys must be due to other factors.

Nickel-200 which forms a NiO scale oxidises at a much lower rate in presence of higher concentrations of NaCl in Na_2SO_4 than the salt mixture containing small concentrations of NaCl in Na_2SO_4. Alloy coated with NaCl-Na_2SO_4 (1:5) oxidises at a higher rate at 850°C than at 1000°C whereas alloy coated with mixture (5:1) shows higher corrosion rate at 1000°C.

The small amount of NaCl in Na_2SO_4 is perhaps helpful in breaking the protective NiO scales and consequently induction time is greatly reduced. Following basic fluxing and sulfidation reactions in which O^{2-} and S are used up the chloridination reaction proceeds involving conversion of NiO and Ni metal into $NiCl_2$. $NiCl_2$ decomposes at salt/air interface into NiO, chlorine released is available for recycling. The NiO_2^{2-} formed during fluxing end up as NiO by precipitation at the salt/gas interface. This provides a porous NiO scale on the alloy. The observed morphology supports this mechanism. For the higher corrosion rates of the alloy at lower temperature (850°C) the same reasoning is applicable as in case of Inconel-800 alloy coated with 1:5 Na_2SO_4-NaCl mixture. The lower corrosion rates of 1:5 Na_2SO_4-NaCl coated Ni-200 alloy could perhaps be explained on the

basis of retention of protectiveness by the NiO at 850°C. At 1000°C, a large induction period is observed. By the end of this period sufficient S-activities are developed to sulfidise metal to NiS and sequentially NiO is basically fluxed to NiO_2^{2-}. The reactions perhaps continue till entire Na_2SO_4 is consumed. NaCl(l) creeps inward to carry out chloridation reactions with NiS and Ni metal.

X $\quad NiS + 2NaCl \longrightarrow NiCl_2 + Na_2S$

XI $\quad Ni + 2NaCl + O \longrightarrow NiCl_2 + Na_2O$

XII $\quad Na_2O + Ni + O \longrightarrow Na_2NiO_2$

XIII $\quad Na_2S + 2O_2 \longrightarrow Na_2SO_4$

The $NiCl_2$ formed moved outward to get oxidise to NiO at the salt/air interface and similarly Na_2NiO_2 is precipitated as NiO. Na_2SO_4 formed by XIII penetrates into the alloy to carry out internal sulfidation. The amount of Cl_2 available after oxidation of $NiCl_2$ will decline ultimately to nearly zero level at 1000°C and hot corrosion reactions are ceased to proceed further. In the present study, the 12 hour exposure presumably represent sulfidation-basic fluxing and partly chloridation reaction. The optical micrograph of the corroded alloy shows the presence of a relatively thick porous and adherent oxide scale and evidence of extensive internal sulfidation. The observed

morphology is in consistent with the proposed mechanism.

Like chromia formers, the corrosion rates of Monel-400 (CuO/NiO former) increase with increasing amounts of NaCl in Na_2SO_4. The effect is more pronounced at 1000°C. NaCl breaks the protective outer scales of CuO and inner scales of NiO. This results in a series of sulfidation, fluxing and chloridation reactions (Chapters IV and V) which contribute to enhanced corrosion rates. The corrosion rates at 1000°C are much higher than at 850°C, this is presumably due to the increase in aggressiveness of the melt inspite of the expected fall in chlorine activity.

The important role of NaCl in enhancing the aggressiveness of Na_2SO_4-induced hot corrosion attack in chromia forming alloys and its equal important role in suppressing the corrosion rates of alumina forming alloys has been emphasized in a large number of studies[1-6,9,10]. In the present studies chromia forming alloys, Inconel-600 and 800 and Nimonic-105 and CuO forming Monel-400 show profound degradation in presence of NaCl either alone or in Na_2SO_4 and the severity of corrosion attack increases with increasing NaCl concentration. On the other hand, Al_2O_3 forming B-1900 and NiO forming Ni-200 alloys, which are subjected to severe corrosion by Na_2SO_4 show decreasing corrosion rates with increasing NaCl content in Na_2SO_4. These results

are consistent with the reported results on the studies on hot corrosion of Ni-base alloys in presence of $NaCl-Na_2SO_4$ mixtures[7,8,11-13]

REFERENCES

1. H. T. Shirley, J. Iron and Steel Inst., 182, 144 (1956).
2. R. W. Archdale, Paper to Inter-Service Metal Res. Counc. Heat Resist. Met. Comm. ISMET 2805 HR 558 (1961).
3. H. Lewis and R. A. Smith, Roc. 1st Int. Conf. on Metallic Corrosion, London, 202, (1965).
4. W. T. Reid, "External Corrosion and Deposits", American Elsvier Publishing Co., New York, N.Y. (1971).
5. R. C. Hurst, J. B. Johnson, M. Davies and P. Hancock, "Deposition and Corrosion in Gas Turbines", A. B. Hart and A. J. B. Cutler, eds., pp. 143-57, John Wiley and Sons, New York (1973).
6. J. A. Goebel, F. S. Pettit and G. W. Goward, "Deposition and Corrosion in Gas Turbines", A. B. Hart and A. J. B. Cutler, eds., pp. 96-114, John Wiley and Sons, New York (1973).
7. D. M. Johnson, D. P. Whittle and J. Stringer, Corros. Sci., 15, 721 (1975).
8. J. Stringer, 'Hot Corrosion of High Temperature Alloys', Ann. Rev. Mater. Sci., 7, 477-509 (1977).
9. J. Stringer, V. Nagrajan and D. P. Whittle,'High Temperature Metal Halid Chemistry', ed., D. L. Hildebrand D. D. Cubicciotti, The Electrochem. Soc., Princeton, p. 509 (1978).

10. Peter Hancock, 'The Role of Halides in High Temperature Gas Corrosion', Proc. Electrochem. Soc., Symposium on 'High Temperature Metal Halide Chemistry', eds., D. L. Hildebrand and D. D. Cubicciotti, The Electrochem. Soc., Princeton (1978).

11. C. S. Giggins and F. S. Pettit, 'Hot Corrosion Degradation of Metals and Alloys' —'A Unified Theory', Pralt and Whitney Air Craft Group, Final Scientific Report FR-11545 (June, 1979).

12. T. K. Glasgow and G. J. Santoro, Oxid. Met., 15, 251 (1981).

13. Y. Shinata and Y. Nishi, 'High Temperature Corrosion of Metals and Alloys', Proc. 'High Temperature Corrosion of Metals and Alloys', (JIMIS-3), Mt. Fuji, Japan, p. 385 (Nov., 1982).

14. W. P. Stroud and R. A. Rapp, Proc. of the Symp. on "High Temperature Metal Halide Chemistry", D. L. Hildebrand and D. D. Cubicciotti, eds., The Electrochem. Soc., Inc., Princeton, N.J., 574-594 (1978).

Table 6.1: Constituents identified in corrosion products of Na_2SO_4-NaCl mixture coated alloys.

Alloy	Molar ratio of Na_2SO_4-NaCl mixtures	Temp. ^oC	Constituents
IN-600	1:5	1000	Fe_2O_3, Fe_3O_4, NiO, Cr_2S_3
IN-600	1:5	850	Fe_3O_4, Cr_2S_3, Cr_2O_3
IN-600	5:1	1000	NiO, Cr_2O_3, Cr_2S_3
IN-800	1:5	1000	Fe_2O_3, Fe_3O_4, NiO
IN-800	5:1	850	Fe_2O_3, Cr_2O_3, NiO
M-400	1:5	1000	NiO, NiS, CuO
M-400	5:1	1000	Ni_3S_2, NiO, CuO
Nim-105	1:5	1000	NiO, Cr_2O_3, CoO
Nim-105	5:1	1000	$NiMoO_4$, Cr_2O_3, CoO, Al_2O_3
B-1900	1:5	850	NiO, Cr_2O_3, CoO
B-1900	5:1	1000	NiO, Al_2O_3, Cr_2O_3, CoO
Ni-200	1:5	850	NiO
Ni-200	5:1	1000	NiO, NiS

(IN = Inconel; M = Monel; Nim = Nimonic; Ni = Nickel)

Table 6.2: Some visual observations of Na_2SO_4-NaCl mixture coated alloys after high temperature oxidation.

Alloy	Temperature (°C)	
	850	1000
Inconel-600	<u>1:5 Na_2SO_4-NaCl Mixture</u>	
	(i) Spalling of the scales. (ii) Yellow coloured compound deposited on the wall of the reaction tube.	(i) Spalling of the scales. (ii) Outer layer of the scale is black while the inner one is grass green in colour. (iii) Greenish yellow compound deposited on the wall of the reaction tube.
	<u>5:1 Na_2SO_4-NaCl Mixture</u>	
	Same as found in the case of 1:5 mixture coated alloy.	(i) Scales adherent in nature. (ii) Greenish yellow compound deposited on the wall of the reaction tube.

continued ..

Table 6.2: continued ..

Alloy	Temperature (°C)	
	850	1000
Inconel-800	1:5 Na_2SO_4-NaCl Mixture	
	(i) Complete spalling of the scales.	(i) Poorly adherent, thick, smooth scale of grey colour.
	(ii) Scale formed is thick, smooth, compact and of grey colour.	
	5:1 Na_2SO_4-NaCl Mixture	
	(i) Spalling of the powder like scales.	(i) Poorly adherent scale of black colour.
Monel-400	1:5 Na_2SO_4-NaCl Mixture	
	(i) Black scale formed on the alloy surface.	(i) Very thick grey coloured scale formed on the alloy surface
	(ii) Some dirty blue dots have been found on the wall of the reaction tube.	

continued ..

Table 6.2: continued ..

Alloy	Temperature (°C)	
	850	1000
Monel-400	5:1 Na_2SO_4-NaCl Mixture	
	(i) Grey adherent scale formed on the alloy surface.	(i) Very thick grey scale formed on the alloy surface.
Nickel-200	1:5 Na_2SO_4-NaCl Mixture	
	(i) Poorly adherent scales, which have two layers: outermost soil coloured layer with black blisters and an inner greenish oxide layer. Inner layer is quite adherent to the alloy surface.	(i) Dirty green scale formed on the alloy surface.
	5:1 Na_2SO_4-NaCl Mixture	
	(i) There is an outer green coloured scale below which thin black scale is formed.	Same as found on the sample oxidized at 850°C.
	(ii) Scales are adherent in nature.	

continued ..

Table 6.2: continued ..

Alloy	Temperature (°C)	
	850	1000
Nimonic-105	1:5 Na_2SO_4-NaCl Mixture	
	(i) Double layered scale formed: outer layer black and inner layer green in colour.	(i) Inner scale adherent and of grey colour while the outer layer is bluish green in colour.
	5:1 Na_2SO_4-NaCl Mixture	
	(i) Thin adherent green scale.	(i) Outer green coloured layer of the scale spalled while the inner grey scale remained intact with the alloy surface.
B-1900	1:5 Na_2SO_4-NaCl Mixture	
	(i) Thin adherent scale of green colour. (ii) Some greenish deposition on the wall of the reaction tube.	(i) Outer green layer of the scale spalled while the inner grey layer remained intact to the sample.

continued ..

Table 6.2: continued ..

Alloy	Temperature (°C)	
	850	1000
B-1900	5:1 Na_2SO_4-NaCl Mixture	
	(i) Outer layer of the scale is of grey colour while the inner one is green in colour. (ii) Scale is poorly adherent to the alloy surface.	(i) Scale is comprised of three layers: Outer layer is grey in colour, middle layer is bluish green and the inner one is thick green layer. (ii) Scales spalled during cooling.

CAPTIONS OF KINETIC RESULTS

Fig. 6.1 Weight change versus time plots of Na_2SO_4-NaCl (1:5) mixture coated alloys oxidized at 850°C for 12 hours.

Fig. 6.2 Weight change versus time plots of Na_2SO_4-NaCl (1:5) mixture coated alloys oxidized at 1000°C for 12 hours.

Fig. 6.3 Weight change versus time plots of Na_2SO_4-NaCl (5:1) mixture coated alloys oxidized at 850°C for 12 hours.

Fig. 6.4 Weight change versus time plots of Na_2SO_4-NaCl (5:1) mixture coated alloys oxidized at 1000°C for 12 hours.

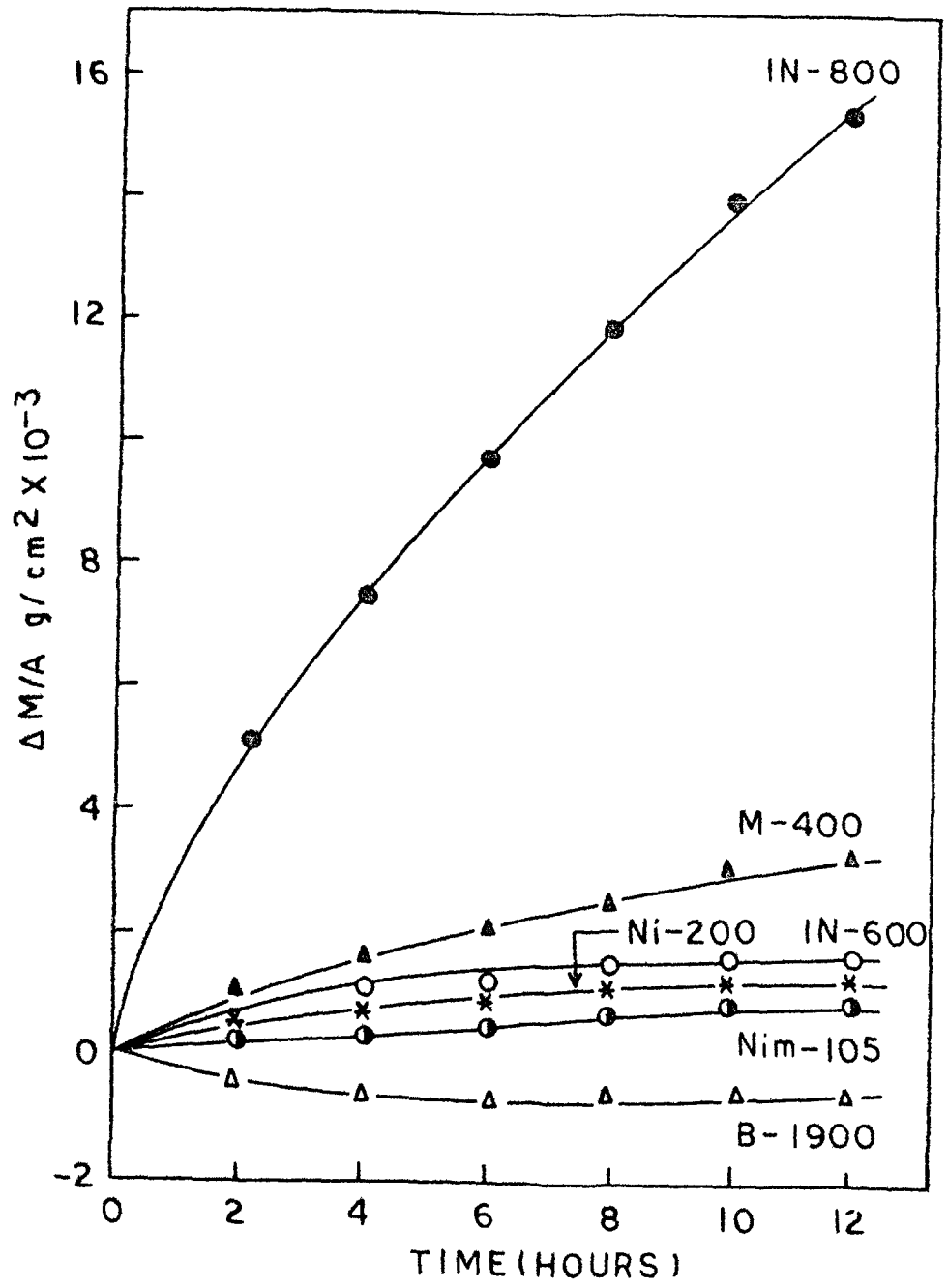
IN-800
M-400
Ni-200
IN-600
Nim-105
B-1900
16
12
8
4
0
-2
0
2
4
6
8
10
12
ΔM/A g/cm² X 10⁻³
TIME (HOURS)

FIG. 6.1

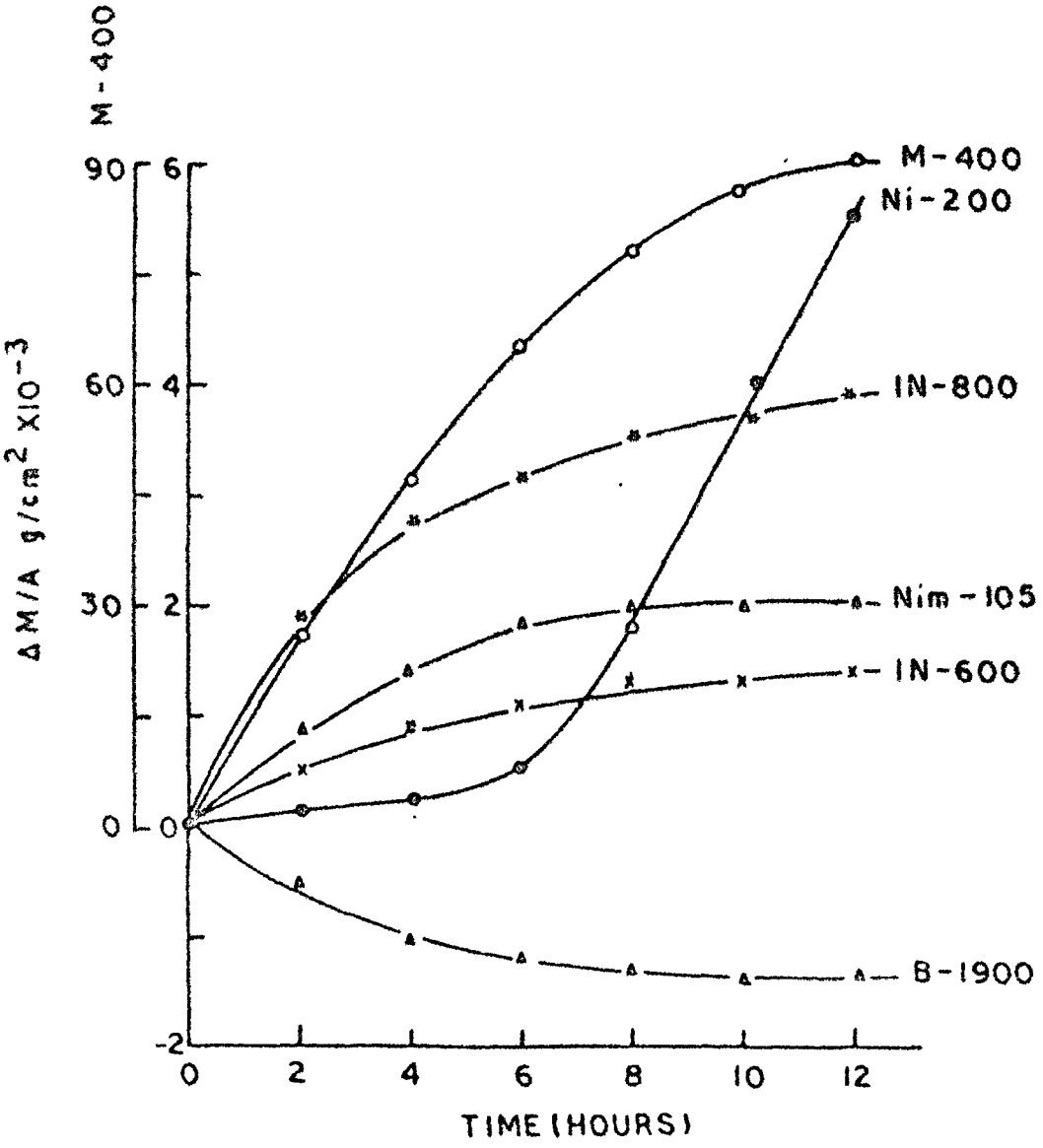
M-400
90
6
60
4
30
2
0
0
-2
ΔM/A g/cm² X10⁻³
M-400
Ni-200
IN-800
Nim-105
IN-600
B-1900
0
2
4
6
8
10
12
TIME (HOURS)

FIG. 6 2

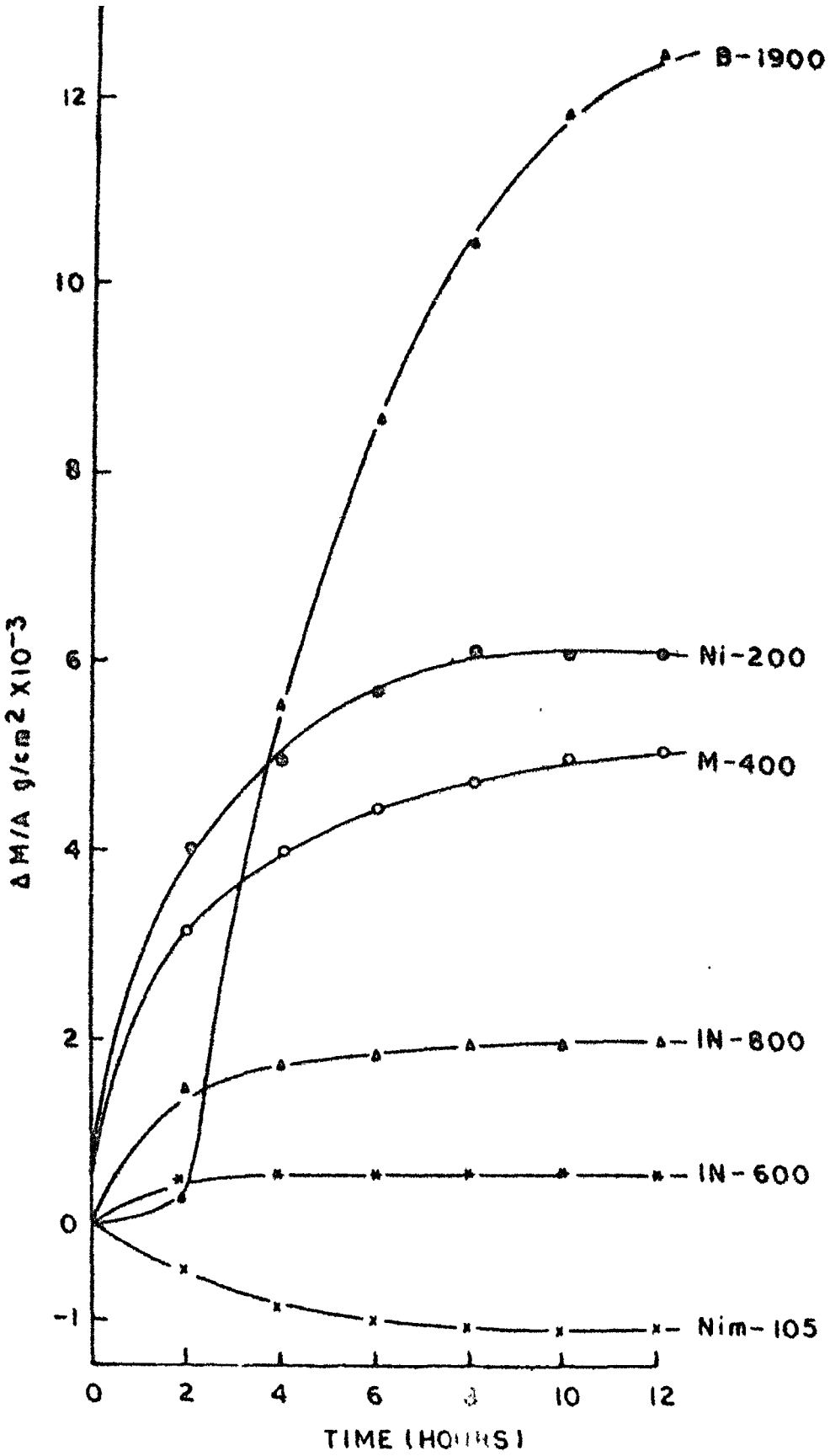
B-1900
Ni-200
M-400
IN-800
IN-600
Nim-105
ΔM/A g/cm² X10⁻³
TIME (HOURS)
12
10
8
6
4
2
0
-1
0
2
4
6
8
10
12

FIG. 6 3

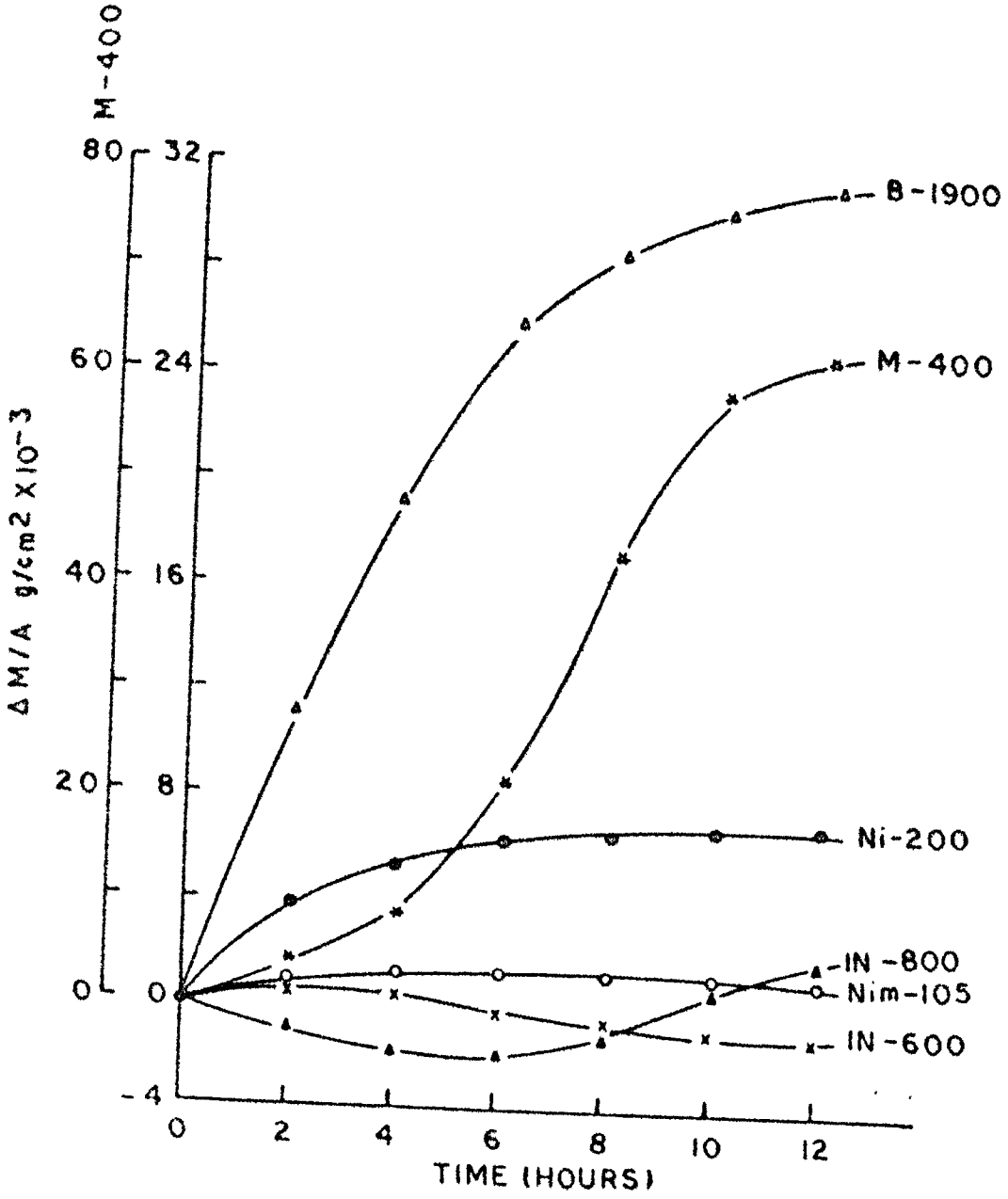
M-400
80
32
60
24
40
16
20
8
0
0
-4
ΔM/A g/cm2 X10-3
B-1900
M-400
Ni-200
IN-800
Nim-105
IN-600
0
2
4
6
8
10
12
TIME (HOURS)

FIG 6 4

CAPTIONS OF METALLOGRAPHS

Fig. 6.5 & 6.6 Scanning electron micrograph of cross section of Inconel-600 in presence of Na_2SO_4-NaCl (1:5) mixture at 1000°C for 12 hours at lower and higher magnifications, respectively.

(x550; x1100)

Fig. 6.7 Photomicrograph of cross section of Inconel-600 oxidized at 1000°C for 12 hours in presence of Na_2SO_4-NaCl (1:5) mixture.

(x400)

Fig. 6.8 Scanning electron micrograph of cross section of Inconel-600 oxidized at 850°C for 12 hours in presence of Na_2SO_4-NaCl (5:1) mixture.

(x1800)

Fig. 6.9 Scanning electron micrograph of cross section of Inconel-600 oxidized at 1000°C for 12 hours in presence of Na_2SO_4-$NiSO_4$ (5:1) mixture.

(x650)

Fig. 6.10 Photomicrograph of cross section of Inconel-800 oxidized at 1000°C for 12 hours in presence of Na_2SO_4-NaCl (1:5) mixture.
(x400)

Fig. 6.11 a & b Scanning electron micrograph of cross section of Monel-400 oxidized at 1000°C for 12 hours in presence of Na_2SO_4-NaCl (1:5) mixture.
(a. x500; b. x1500)

Fig. 6.12 Photomicrograph of cross section of Monel-400 oxidized at 850°C for 12 hours in presence of Na_2SO_4-NaCl (5:1) mixture.
(x400)

Fig. 6.13(a) Scanning electron micrograph of cross section of Nimonic-105 oxidized at 1000°C for 12 hours in presence of Na_2SO_4-NaCl (1:5) mixture.
(x500)

Fig. 6.13(b) Photomicrograph of sample in fig. 6.13(a)
(x400)

Fig. 6.14 Scanning electron micrograph of a blister formed on the outermost scale of Nimonic-105 oxidized at 1000°C in presence of Na_2SO_4-NaCl (1:5) mixture for 12 hours.
(x300)

Fig. 6.15 Scanning electron micrograph of cross section of Nimonic-105 oxidized at 1000°C for 12 hours in presence of Na_2SO_4-NaCl (5:1) mixture.
(x500)

Fig. 6.16 Scanning electron micrograph of cross section of B-1900 oxidized at 850°C for 12 hours in presence of Na_2SO_4-NaCl (1:5) mixture.
(x1000)

Fig. 6.17 Scanning electron micrograph of cross section of B-1900 oxidized at 850°C for 12 hours in presence of Na_2SO_4-NaCl (5:1) mixture.
(x650)

Fig. 6.18 Scanning electron micrograph of Nickel-200 oxidized at 1000°C for 12 hours in presence of Na_2SO_4-NaCl (1:5) mixture.
(x1000)

Fig. 6.19 & 6.20 Photomicrograph of cross section of Nickel-200 oxidized at 1000° & 850°C, respectively, for 12 hours in presence of Na_2SO_4-NaCl (1:5) mixture.
(x400)

Fig. 6.21 Photomicrograph of cross section of Nickel-200 oxidised at 1000°C for 12 hours in presence of Na_2SO_4-NaCl (5:1) mixture. (x400)

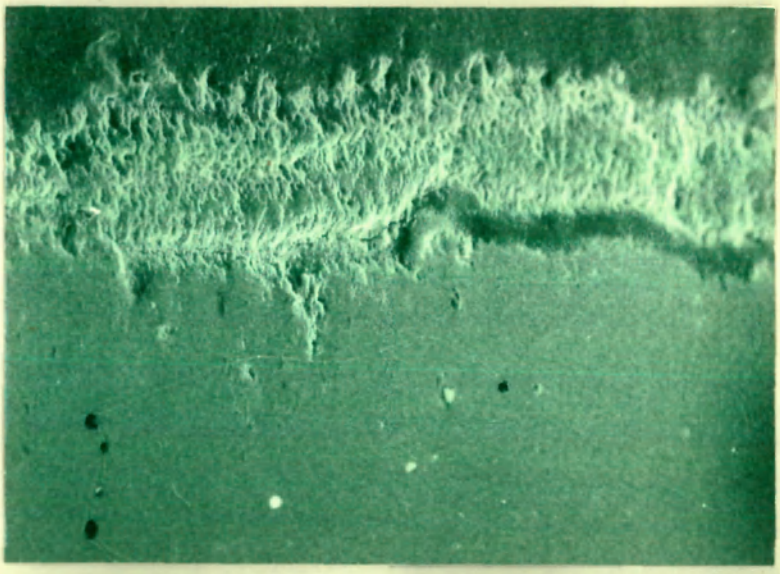

6.5

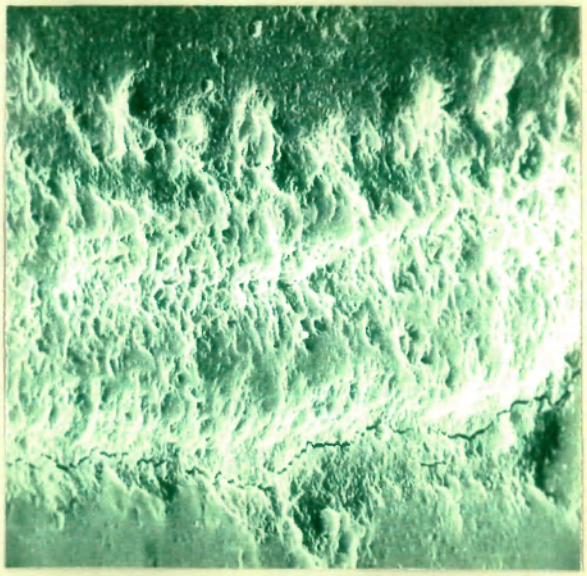

6.6

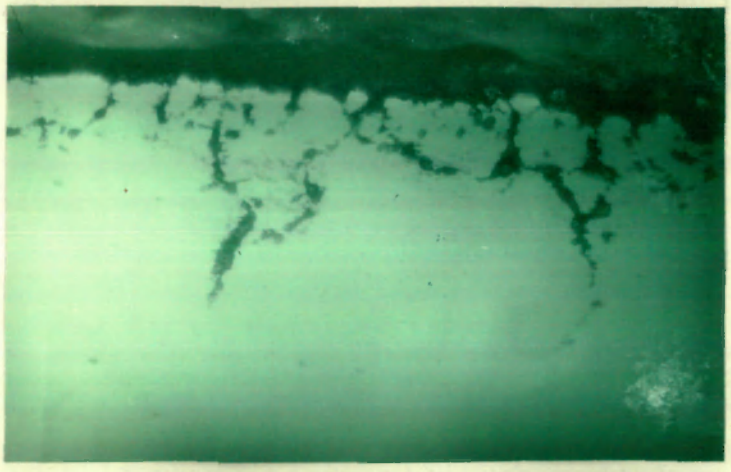

6.7

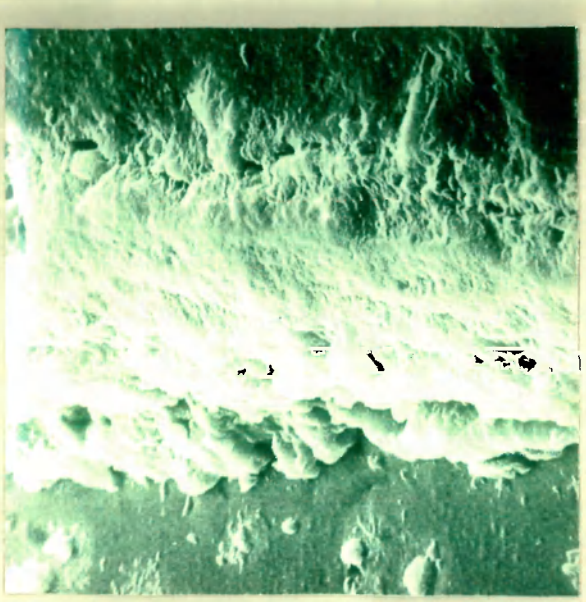

6.8

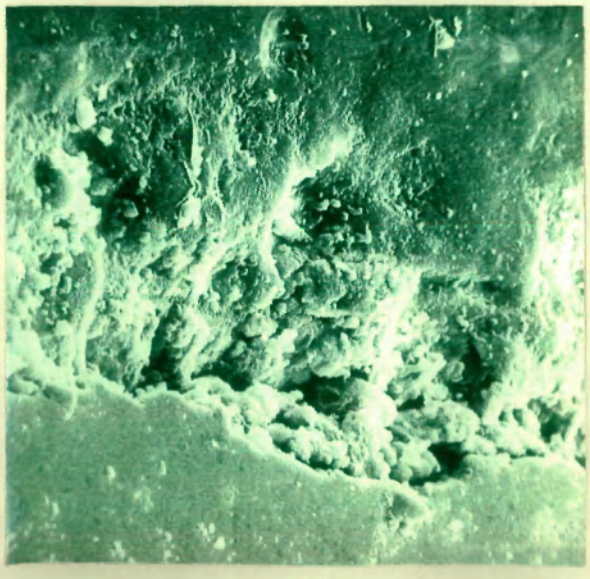

6.9

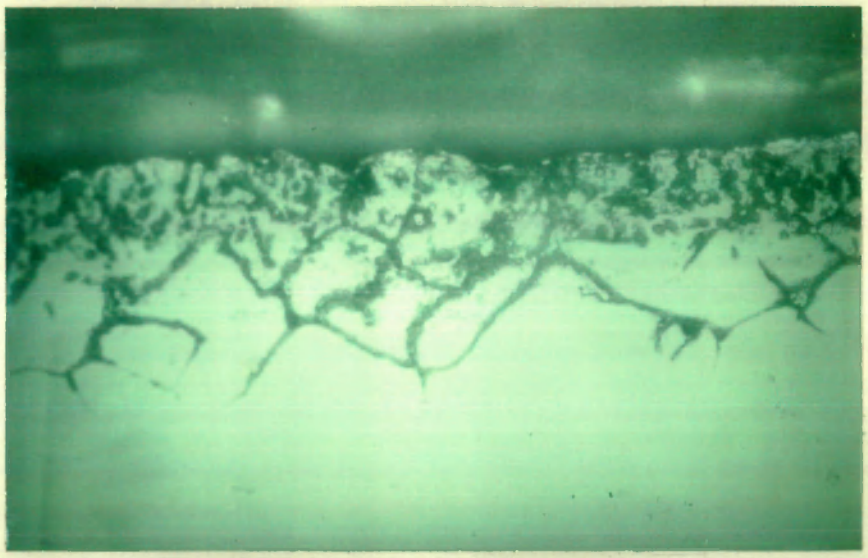

6.10

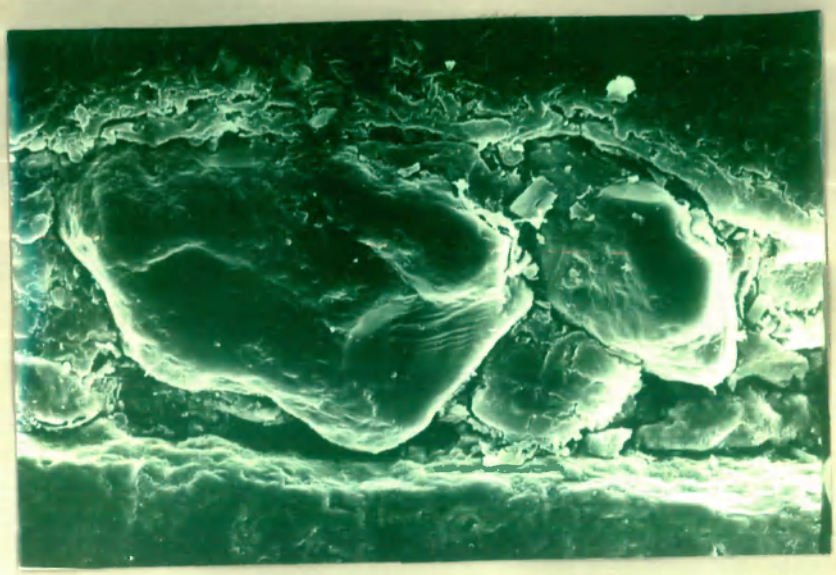

(a)

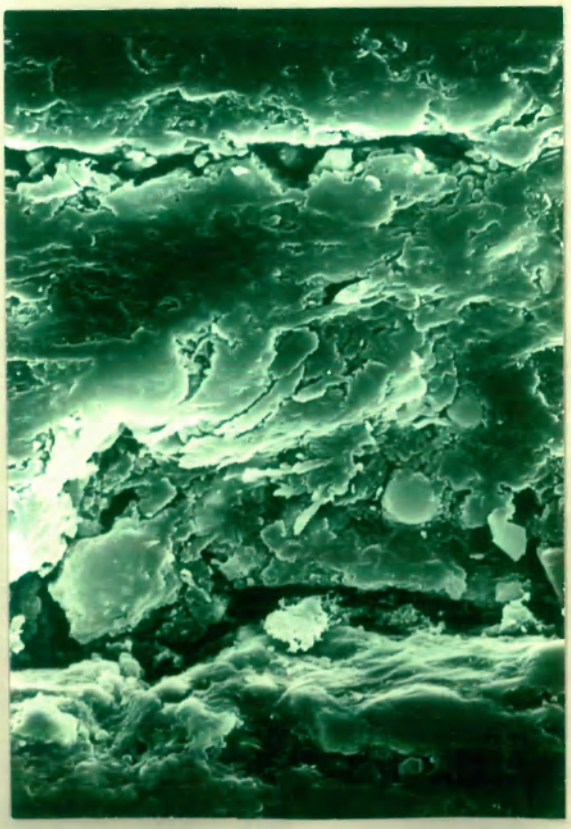

(b)

6.11

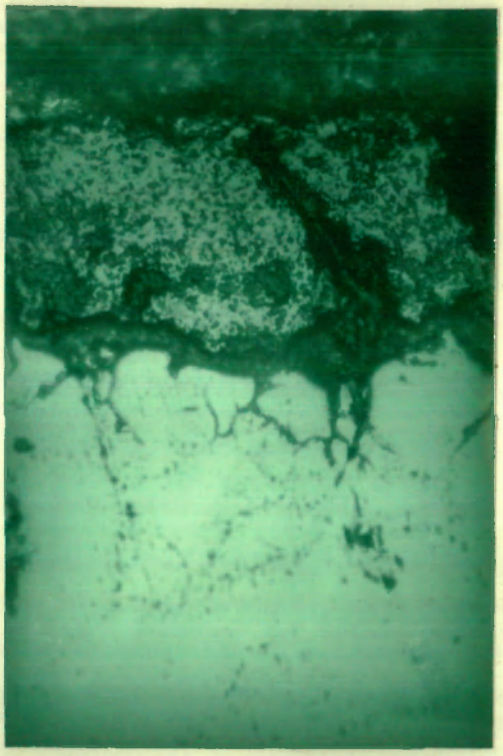

6.12

6.13

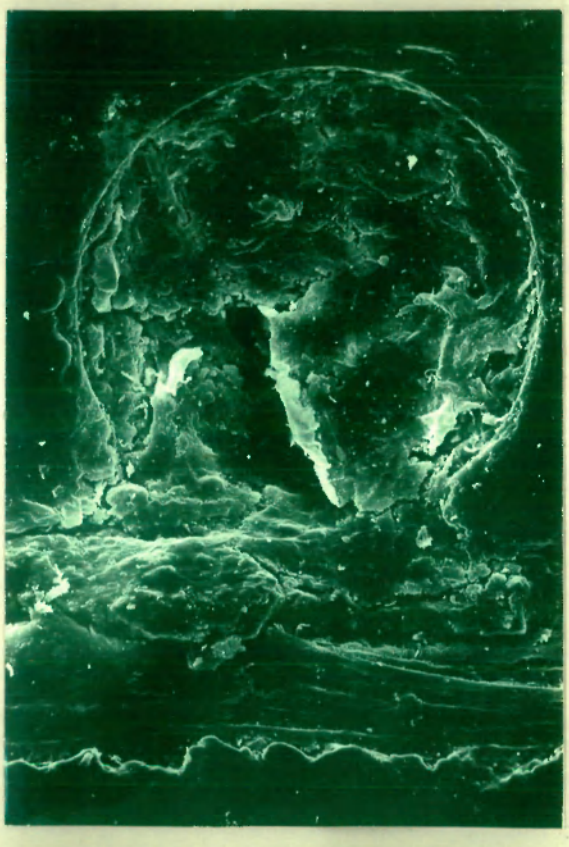

6.14

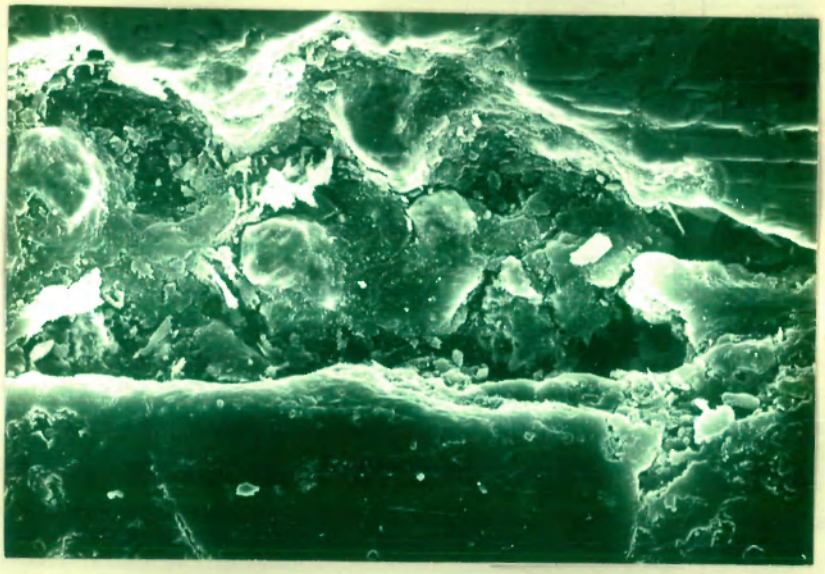

6.15

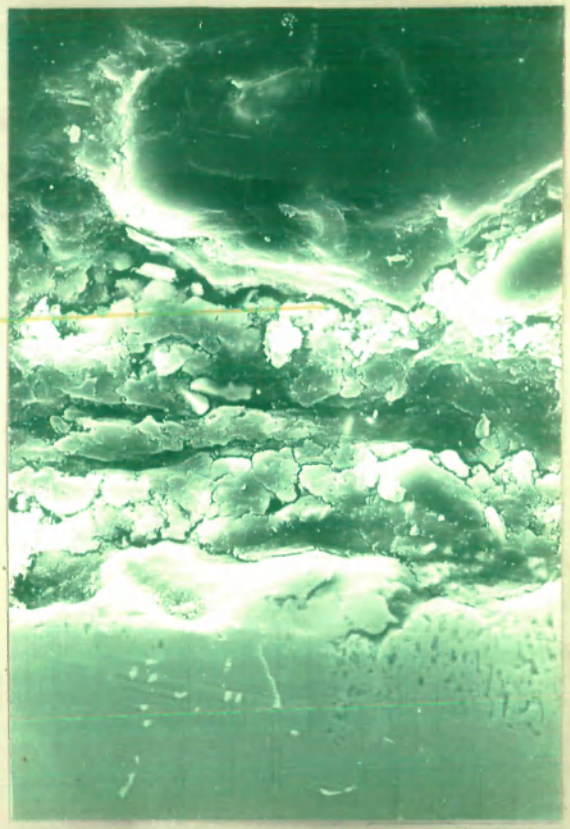

6.16

6.17

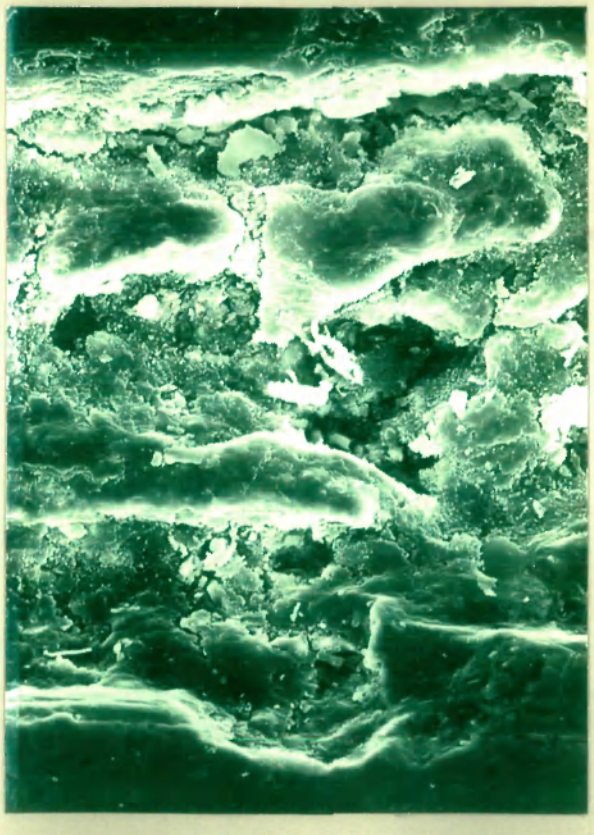

6.18

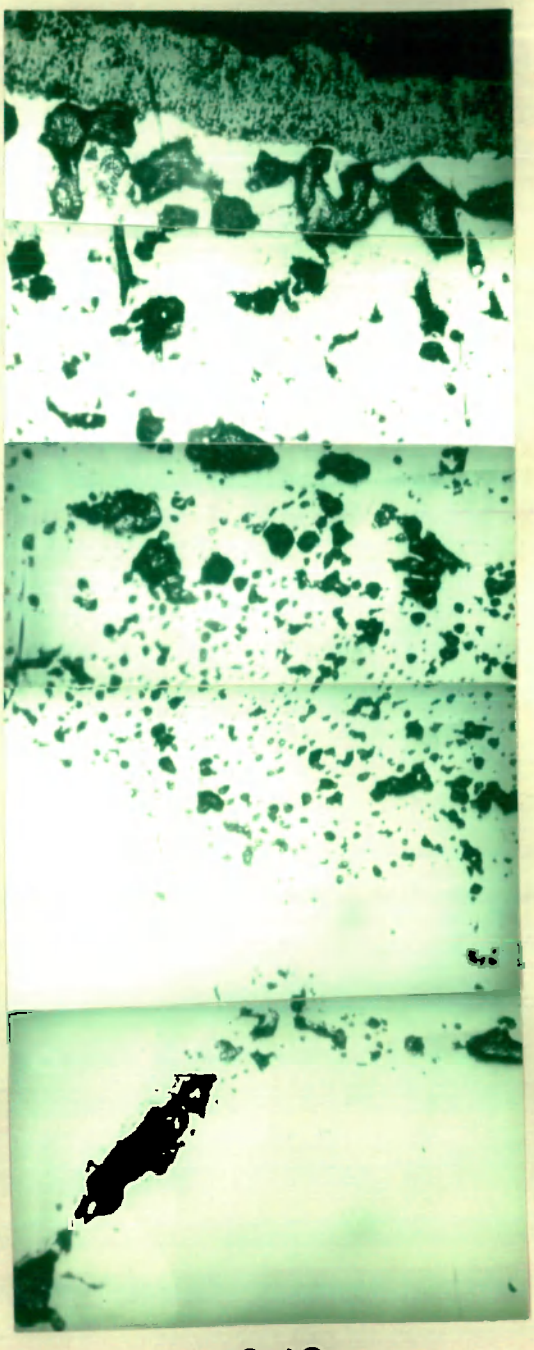

6.19

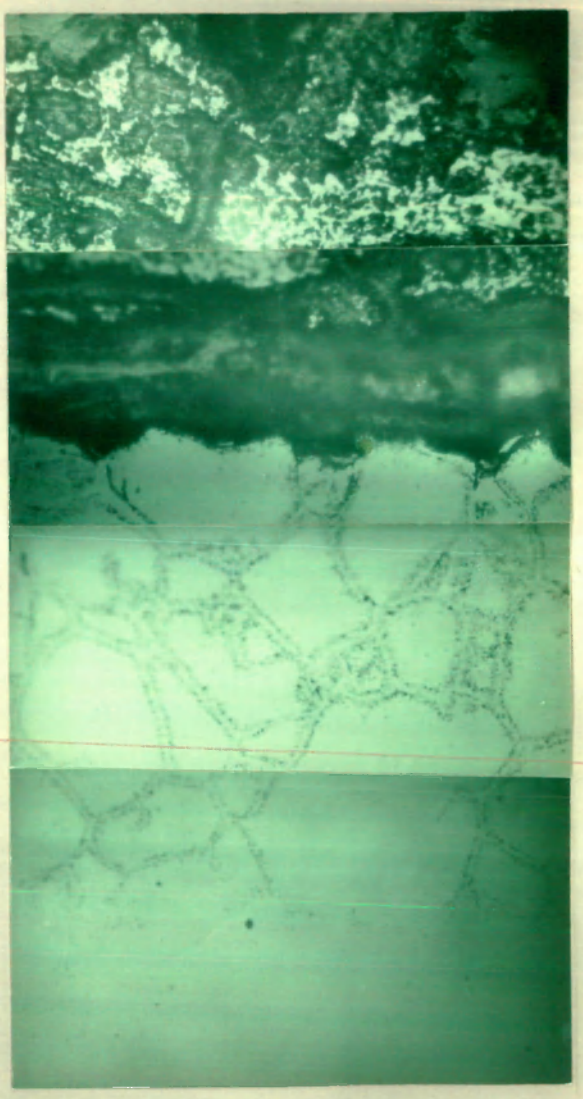

6.20

6.21

CAPTIONS OF EDAX

Fig. 6.22 X-ray concentration profiles of NiK , CrK and FeK of Inconel-600 oxidised at 1000°C for 12 hours in presence of Na_2SO_4-NaCl (1:5) mixture.

Fig. 6.23 X-ray concentration profiles of NiK , FeK and CrK of Inconel-800 oxidised at 1000°C for 12 hours in presence of Na_2SO_4-NaCl (5:1) mixture.

Fig. 6.24 X-ray concentration profiles of NiK and CuK of Monel-400 oxidised at 1000°C for 12 hours in presence of Na_2SO_4-NaCl (5:1) mixture.

Fig. 6.25 X-ray concentration profiles of NiK , CoK and CrK of B-1900 oxidised at 850°C in presence of Na_2SO_4-NaCl (5:1) mixture.

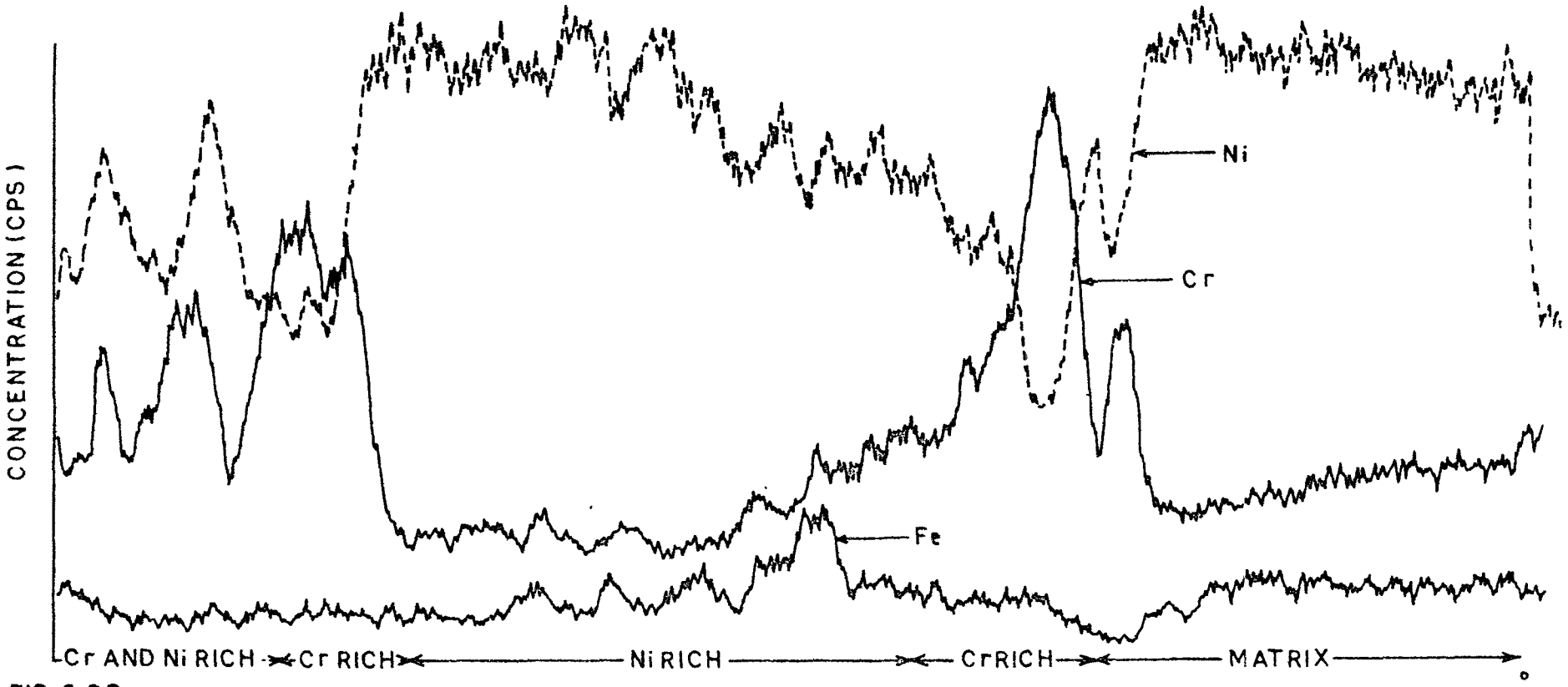
CONCENTRATION (CPS)
Ni
Cr
Fe
Cr AND Ni RICH
Cr RICH
Ni RICH
Cr RICH
MATRIX

FIG. 6.22

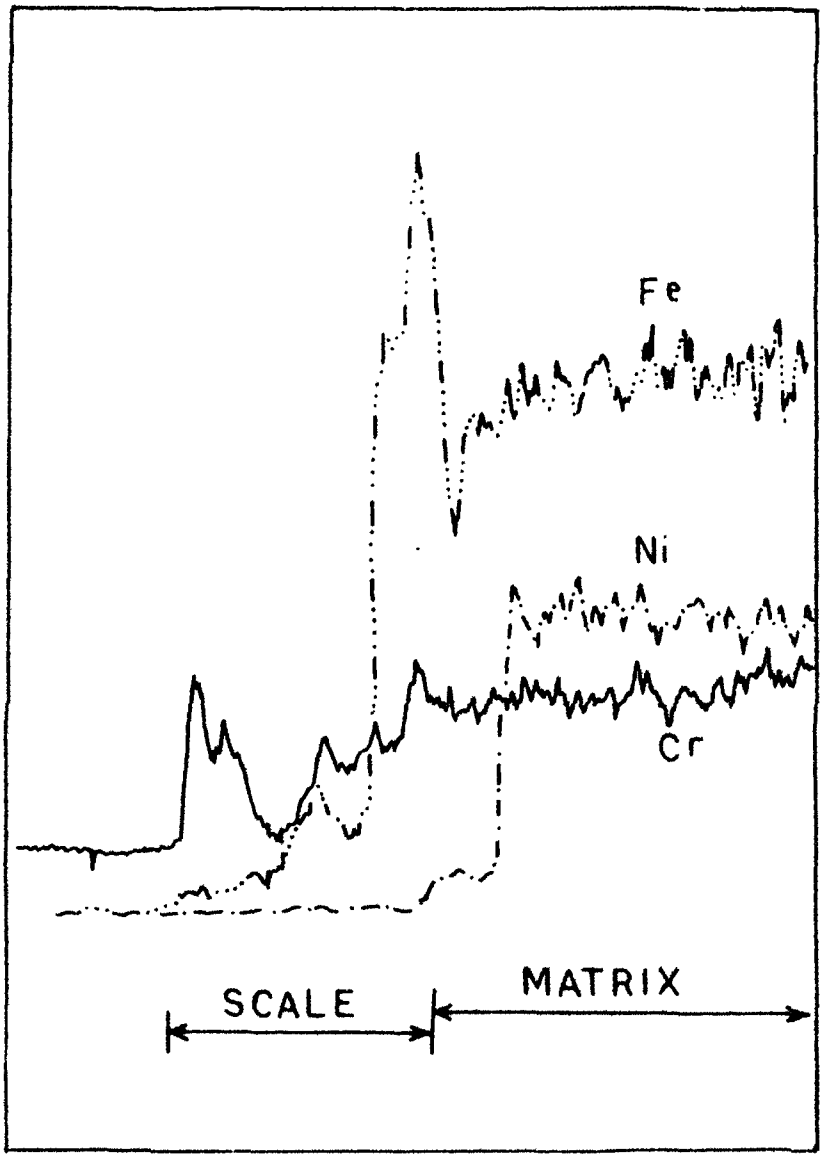

FIG. 6.23

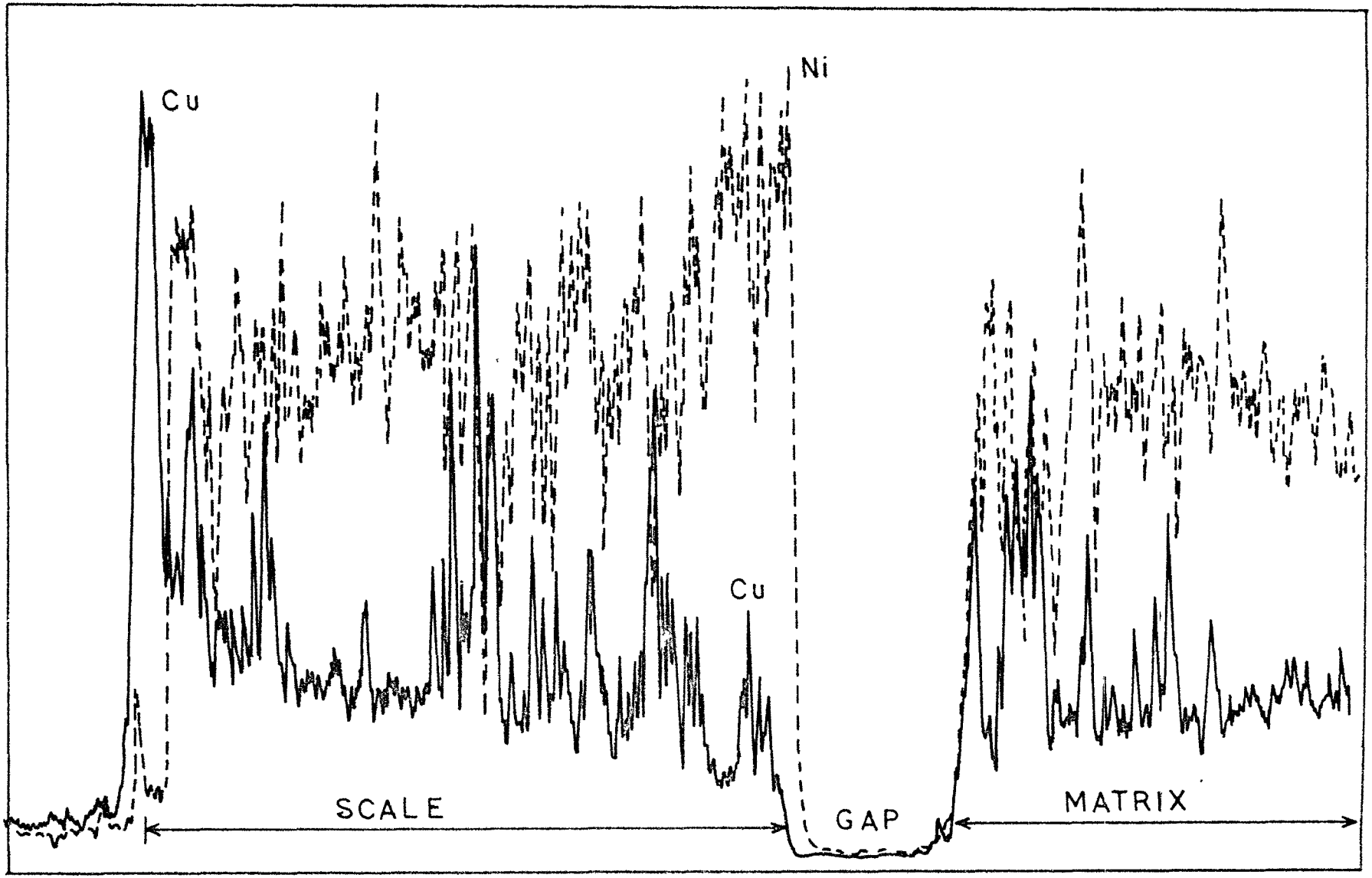

FIG. 6.24

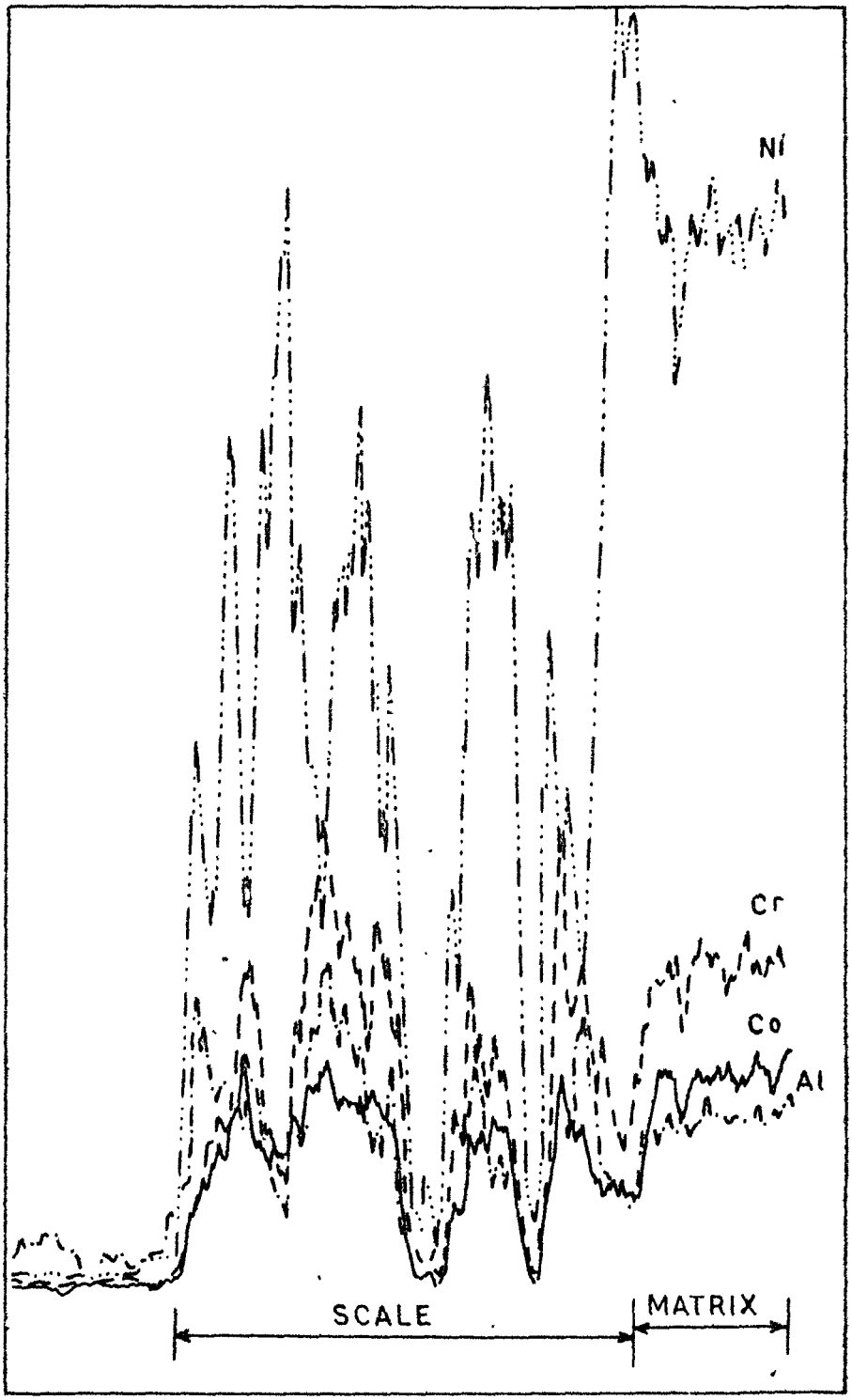

FIG. 6.25

CHAPTER VII

LOW TEMPERATURE HOT CORROSION OF NICKEL-BASE ALLOYS IN PRESENCE OF Na_2SO_4-$NiSO_4$ MIXTURE

EXPERIMENTAL

7.1.1 Selection of the alloys

Nickel-base alloys, e.g. Inconel-600, Inconel-800, Monel-400, Nimonic-105 and Nickel-200 were used for the low temperature corrosion studies in the presence of mixture of Na_2SO_4 and $NiSO_4$. The nominal composition of the alloys are given in the table 4.1.

7.1.2 Preparation of the salt mixture

A 1:1 molar Na_2SO_4:$NiSO_4$ solution was prepared by mixing equal volumes of equimolar solutions of Na_2SO_4 and $NiSO_4$. This solution was used for coating purpose.

7.1.3 Preparation of the specimen

Specimens of 1.3 cm x 0.2 cm size were cut from the rods of the alloys and polished on motor driven disc polisher using sequentially 180, 320 and 600 grade SiC papers. Polished samples were washed with water and then degreased with CCl_4.

7.1.4 Preparation of the preoxidised specimens

Some of the alloy specimens were oxidised in air at 650 and 750°C for 20 hours. These preoxidised samples were used for subsequent studies.

7.1.5 Preparation of the coated specimen

The unoxidized and preoxidized specimens were coated with 1:1 molar mixture of Na_2SO_4 and $NiSO_4$ by spraying technique. The specimens were heated to about 300°C with a hot air blower and were then subjected to spray of the salt solution. The spraying was carried out till a nearly uniform thin coating of the mixture was obtained on all the faces of the specimen. A salt coating of about 1 mg/cm^2 (corresponding salt thickness of ~ 5 μm) was maintained.

7.1.6 Hot corrosion studies

The alloy specimen coated with the salt mixture was placed in a quartz bucket which was suspended through quartz helics of a helical thermal balance. The oxidation kinetics were studied in air at 650 and 750°C for 20 hours. Weight changes were recorded after an interval of one hour duration till the end of 20 hour oxidation run.

7.1.7 Morphological studies

Oxidized samples were mounted in paper moulds using Araldite as a cold setting compound. The mounted samples were abraded sequentially on 180, 320 and 600 grade SiC papers followed by 0/4 grade emery paper. Samples were finally polished on selvyt cloth using 1 μ grade alumina powder. Kerosene oil was used as a lapping liquid. Polished samples were washed with alcohol, degreased with CCl_4, and

were then etched either with 1% acidic solution of $FeCl_3$ or electrolytically in a 2% HNO_3 solution for 2-3 minutes.

7.1.8 Scanning Electron Microscopy (SEM)

Cambridge Scanning Electron Microscope Model S4-10 were used for SEM studies. Samples were coated with colloidal gold emulsion prior to scanning operation.

7.1.9 X-ray diffraction analysis

The X-ray diffraction patterns of the corroded samples of the alloys were obtained using a diffractometer assembly. Table 7.1 lists the different constituents identified in the scale of corroded alloys by X-ray diffraction analysis.

RESULTS

7.2.1 Kinetic studies

The influence of Na_2SO_4-$NiSO_4$ mixture on the oxidation behaviour of some Ni-base alloys, viz. Inconel-600, Inconel-800, Monel-400, Nimonic-105 and Nickel-200 has been studied at 650 and 750°C. The duration of the oxidation runs was 20 hours. Two sets of kinetics experiments were carried out. In one set the alloy specimens were preoxidised and coated with Na_2SO_4-$NiSO_4$ mixture and in another set the specimens were not preoxidised but directly coated with the salt mixture.

Nimonic-105:

At 750°C, the alloy coated with Na_2SO_4-$NiSO_4$ mixture shows weight losses in preoxidised and unoxidised conditions. However, at 650°C, the preoxidised specimen shows small weight losses but the unoxidised specimen after initial losses shows weight gains and the behaviour seems to be nearly parablic (figure 7.1).

Inconel-600:

At 750°C, both the preoxidised and unoxidised samples coated with the Na_2SO_4-$NiSO_4$ mixture show weight losses as observed in the case of Nim-105. But contrary to the behaviour of Nim-105 at 650°C, the preoxidised sample shows

weight gain, while weight losses are observed in case of unoxidised sample though the rate of the weight losses is extremely slow (figure 7.2).

Inconel-800:

The behaviour is similar to that observed in case of Inconel-600. Except preoxidised coated alloy which shows weight gains at 650°C, the coated alloy in preoxidised and unoxidised conditions at 750°C and unoxidised alloy at 650°C show weight losses. The weight losses in case of Inconel-800 are higher than those observed in Inconel-600 (figure 7.3).

Monel-400:

At 750°C, both the preoxidised and unoxidised specimens show a weight gain and the weight gain/time curves are nearly parabolic. The oxidation rate of the Na_2SO_4-$NiSO_4$ mixture coated preoxidised alloy is higher than the unoxidised coated alloy at 750°C. At 650°C, the unoxidised and preoxidised alloy specimens show small weight gains and weight losses of about 1.0 mg/cm^2, respectively (figure 7.4).

Nickel-200:

As observed in the case of M-400 at 750°C, the preoxidised Na_2SO_4-$NiSO_4$ coated specimen of Ni-200 shows weight gains with increasing exposure time. The weight gain/time

plots are parabolic. After initial weight losses, the unoxidised coated alloy specimens at 650 and 750°C, and pre-oxidised specimens at 650°C, show weight gains (figure 7.5).

6.2.1 Morphological studies:

Inconel-600:

Figure 7.6 represents a SEM photomicrograph of unoxidised Na_2SO_4-$NiSO_4$ coated Inconel-600 oxidised at 750°C for 18 hours. The molten eutectic seemed to penetrate deeply into the alloy substrate and produced sulfidation at the edges and in the vicinity of the cleavages. The inner scales largely contain NiO with grey inclusions of Cr_2S_3 and FeS, and the outer scales perhaps contain coating with NiO. The micrograph indicate comparatively little disruption of the oxide scales whereas matrix is deeply affected by salt penetration.

Monel-400:

Figure 7.7 presents a SEM micrograph of Na_2SO_4-$NiSO_4$ coated preoxidised Monel-400 alloy specimen oxidised at 750°C for 18 hours. The molten salt mixture has splitted the oxide scales at the alloy/scale interface. Sulfidised NiO and CuO can be noticed in the form of disrupted aggromelarations. The outer scales contain NiO in the form of relatively thick and compact oxide layer. In preoxidised sample the matrix is not much affected but the scales are

greatly disrupted perhaps due to fluxing of the scales with the molten salt.

Nimonic-105:

The SEM micrograph of a cross section of Na_2SO_4-$NiSO_4$ coated preoxidised Nimonic-105 alloy and oxidised at 750°C shows disruption of Al_2O_3/Cr_2O_3 scales (figure 7.8).

DISCUSSION

Figure 7.9 presents $NiSO_4$-Na_2SO_4 phase diagram due to Bel'shakov and Fedorov. Depending upon $NiSO_4$ concentration, Na_2SO_4 forms a series of mixed sulfates as solids upto about 500°C followed by the formation of solid solution and liquid phases. A 1:1 mixture will correspond to the formation of a double salt $Na_2SO_4.NiSO_4$. At 650°C, a solid solution phase is present and at 750°C a liquid phase is expected.

The hot corrosion studies have been carried out at 650 and 750°C on Inconel-600, Inconel-800, Nimonic-105 (chromia formers), Nickel-200 and Monel-400 (NiO formers) in presence of 1:1 molar ratio of $NiSO_4$ and Na_2SO_4. The studies have been carried out under two different conditions: in one condition the alloys are preoxidised for about 20 hours, subsequently coated with $NiSO_4$-Na_2SO_4 mixture followed by hot corrosion and under the other condition the alloys are directly coated with salt mixture and corroded.

It can be derived from the following discussion that the alloys exhibit extensive corrosion in presence of Na_2SO_4-$NiSO_4$ and the corrosion rates are highest at 750°C. These results are consistent with the low temperature hot corrosion studies carried out by Luthra et al[1,2] and Jones et al[3]

on Co- and Ni- base alloys which show the aggressive action of Na_2SO_4-$NiSO_4$ and Na_2SO_4-$CoSO_4$.

Some important generalisation could be made from the hot corrosion studies carried out on Ni-base alloys:

In general the chromia forming alloys (Inconel-600 & 800 and Nimonic-105) show weight losses in presence of salt mixture at 650 and 750°C. In contrary, NiO forming alloys (Nickel-200 and Monel-400) after initial weight losses show weight gains and oxidized by a parabolic rate law. With a few exceptions, the preoxidized alloys have higher corrosion rates than unoxidized alloys. The preoxidized alloys when corroded in presence of Na_2SO_4-$NiSO_4$ show morphologies in which scales are greatly disrupted and the substrate is relatively less affected. On the other hand, alloys which were directly corroded in presence of Na_2SO_4-$NiSO_4$ show a morphology in which substrate is deleteriously attacked by the salt mixture.

Considering the hot corrosion of preoxidized Inconel-600, 800 and Nimonic-105 in presence of $NiSO_4$-Na_2SO_4 mixture, the outer nickel oxide scales are expected to get thickened due to the presence of residual NiO of the decomposed $NiSO_4$ plus NiO produced by nickel migration from the metal zone.

I $\quad NiSO_4 \longrightarrow NiO + SO_2 + \frac{1}{2}O_2$

The liquid salt mixture will penetrate through NiO scale and will attack the Cr_2O_3 scale and following reactions are expected at the salt/oxide interface.

II $\quad Cr_2O_3 + \frac{1}{2}O_2 + 2Na_2SO_4(l) \longrightarrow 2Na_2CrO_4 + 2SO_2(g)$

III $\quad FeO + Na_2SO_4 \longrightarrow Na_2FeO_2 + SO_3$

IV $\quad 2Cr_2O_3 + 3NiSO_4 + 2Na_2SO_4 \longrightarrow$

$$Cr_2S_3 + Ni_3S_2 + 2Na_2CrO_4 + 18O$$

Reaction I to III will result in the expulsion of sulfurous gases and subsequently loss in weight. The release of oxygen in IV will result in rapid oxidation of the alloy by Cr/Ni diffusion and thickening of the scales. CrO_4^{2-} and FeO_2^{2-} formed move outward to the salt interface and precipitate as FeO (or Fe_2O_3) and Cr_2O_3 at some distance from the gas/salt interface and beneath NiO scale due to fall off in Na_2O. Reactions II to IV will terminate when the salt is consumed.

In NiO-forming Nickel-200 and Monel-400 alloys under preoxidised conditions, reactions II to IV are not possible but in Monel-400, the liquid salt extrudes through outer CuO scales and attacks NiO scales:

V $\quad NiO + 2NiSO_4 \longrightarrow Ni_3S_2 + \frac{9}{2}O_2$

VI $\quad 4NiO + 2Na_2SO_4 \longrightarrow 2Na_2NiO_2 + Ni_3S_2 + 4O_2$

The oxygen evolved during V and VI will react with diffusing Ni and Cu (from the metal) to form copious oxide scales. Some Ni_3S_2 formed in V and VI may also get oxidized and consequently release sulfur which produces internal sulfidation by forming Ni_3S_2 and Cu_2S in the matrix. In Nickel-200 similar reactions are expected. NiO_2^{2-} formed in VI moves outward and precipitates as NiO at the gas/salt interface.

Considering the hot corrosion of unoxidized alloys, the liquid salts penetrate the thin oxide film and directly attack the underlying metal:

VII $\quad 9Ni + 2NiSO_4 \rightleftharpoons 8NiO + Ni_3S_2$ (G° = -77 Kcal)

The $Ni-Ni_3S_2$ eutectic which forms below the surface oxide seems primarily responsible for the hot corrosion attack.

Since only a thin oxide (Cr_2O_3) film is formed on the alloy prior to degradation reaction, II and IV are expected to proceed only to a limited extent during hot corrosion of unoxidized chromia forming alloys.

The oxidation kinetic curves show that preoxidized alloys usually have smaller induction periods whereas unoxidized alloys show relatively larger period of inductions.

This is perhaps one of the important reasons that preoxidised alloys have comparatively higher oxidation rates. The induction periods are relatively longer in chromia formers than the NiO former.

Fig. 7.10 to 7.13 present schematic diagrams of hot corrosion of alloys under preoxidised and unoxidised conditions in presence of $NiSO_4$ and Na_2SO_4.

REFERENCES

1. K. L. Luthra and D. A. Shores, J. Electrochem. Soc., 127, 2202 (1980).

2. K. L. Luthra, 'Mechanism of Low Temperature Corrosion', Proc. of MACE Int. Conf. on "High Temperature Corrosion" San Diego, California (March 1981).

3. R. L. Jones and S. T. Godomski, J. Electrochem. Soc., 129, 1613 (1982).

Table 7.1: Low temperature hot corrosion products of alloys in presence of Na_2SO_4-$NiSO_4$ mixture.

Alloys	Temp. ^oC	Hot corrosion products
Inconel-800 (Unoxidized)	750	NiO, Cr_2S_3, FeS
Inconel-800 (Preoxidized)	750	Cr_2O_3, FeO, NiO, Cr_2S_3
Inconel-600 (Preoxidized)	750	Cr_2O_3, NiO, Cr_2S_3
Monel-400 (Preoxidized)	650	NiO, CuO, NiS
Monel-400 (Preoxidized)	750	NiO, CuS, NiS
Nimonic-105 (Unoxidized)	750	NiO, Al_2O_3, Cr_2S_3
Nimonic-105 (Unoxidized)	650	NiO, NiS, Cr_2S_3, Al_2O_3
Nickel-200 (Preoxidized)	750	NiO, Ni_3S_2

CAPTIONS OF PLOTS OF KINETIC RESULT

Fig. 7.1 Weight change versus time plots of Nimonic-105 in presence of Na_2SO_4-$NiSO_4$ (1:1 molar) mixture at at 650 and 750°C.

Fig. 7.2 Weight change versus time plots of Inconel-600 in presence of Na_2SO_4-$NiSO_4$ (1:1 molar) mixture at 650 and 750°C.

Fig. 7.3 Weight change versus time plots of Inconel-800 in presence of Na_2SO_4-$NiSO_4$ (1:1 molar) mixture at 650 and 750°C.

Fig. 7.4 Weight change versus time plots of Monel-400 in presence of Na_2SO_4-$NiSO_4$ (1:1 molar) mixture at 650 and 750°C.

Fig. 7.5 Weight change versus time plots of Nickel-200 in presence of Na_2SO_4-$NiSO_4$ (1:1 molar) mixture at 650 and 750°C.

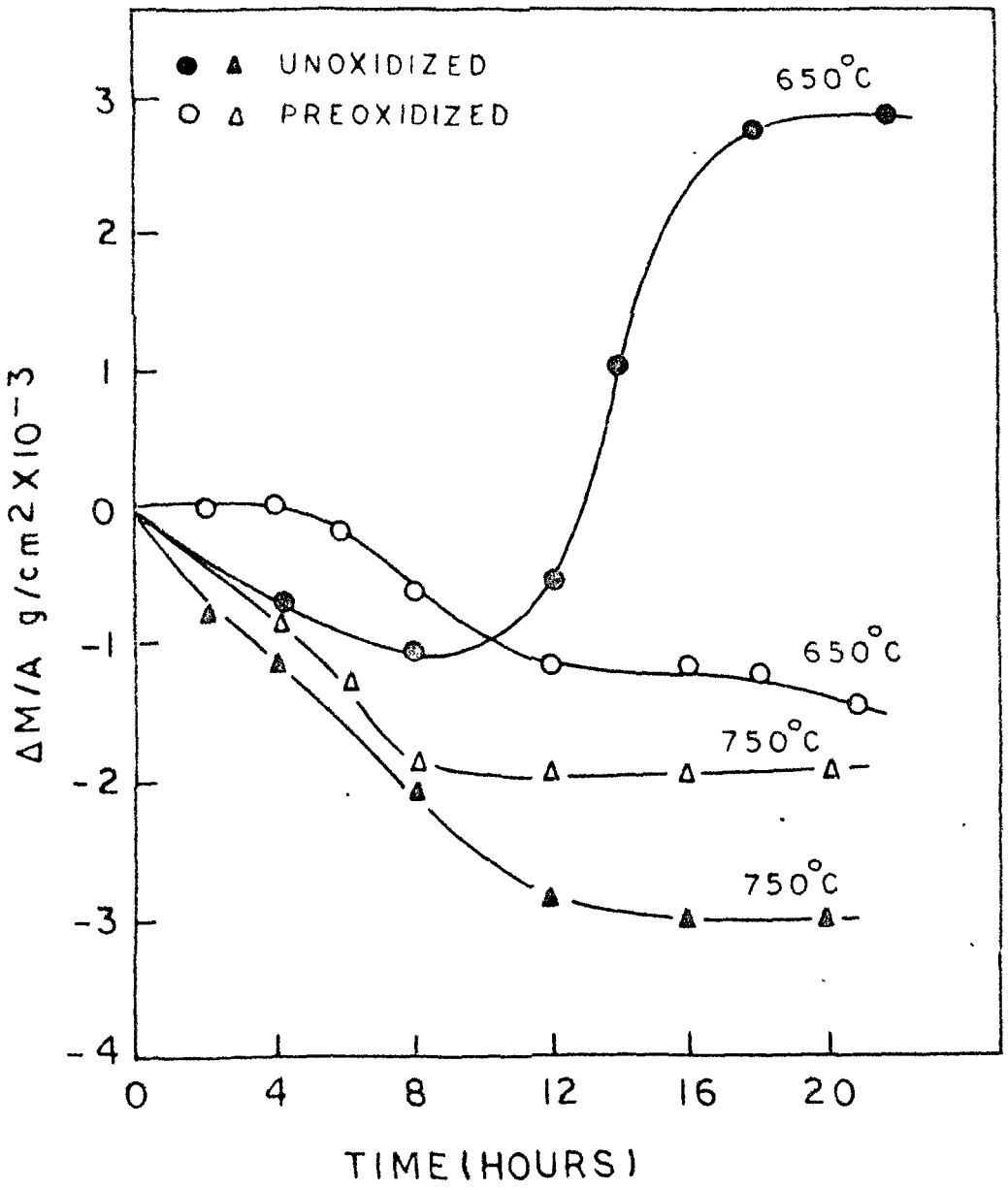
UNOXIDIZED
PREOXIDIZED
650°C
650°C
750°C
750°C
ΔM/A g/cm2 X10⁻³
TIME (HOURS)
3
2
1
0
-1
-2
-3
-4
0
4
8
12
16
20

FIG. 7.1

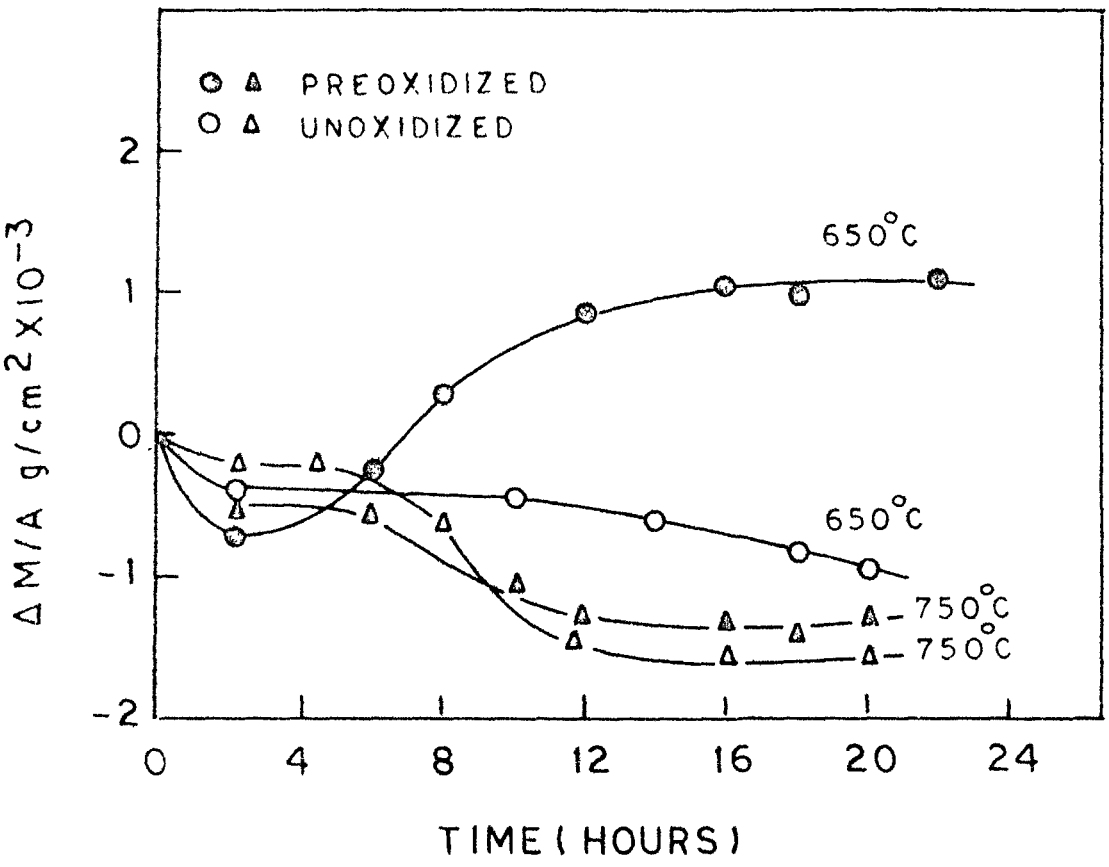
PREOXIDIZED
UNOXIDIZED
650°C
650°C
750°C
750°C
ΔM/A g/cm² X10⁻³
2
1
0
-1
-2
0
4
8
12
16
20
24
TIME (HOURS)

FIG 7 2

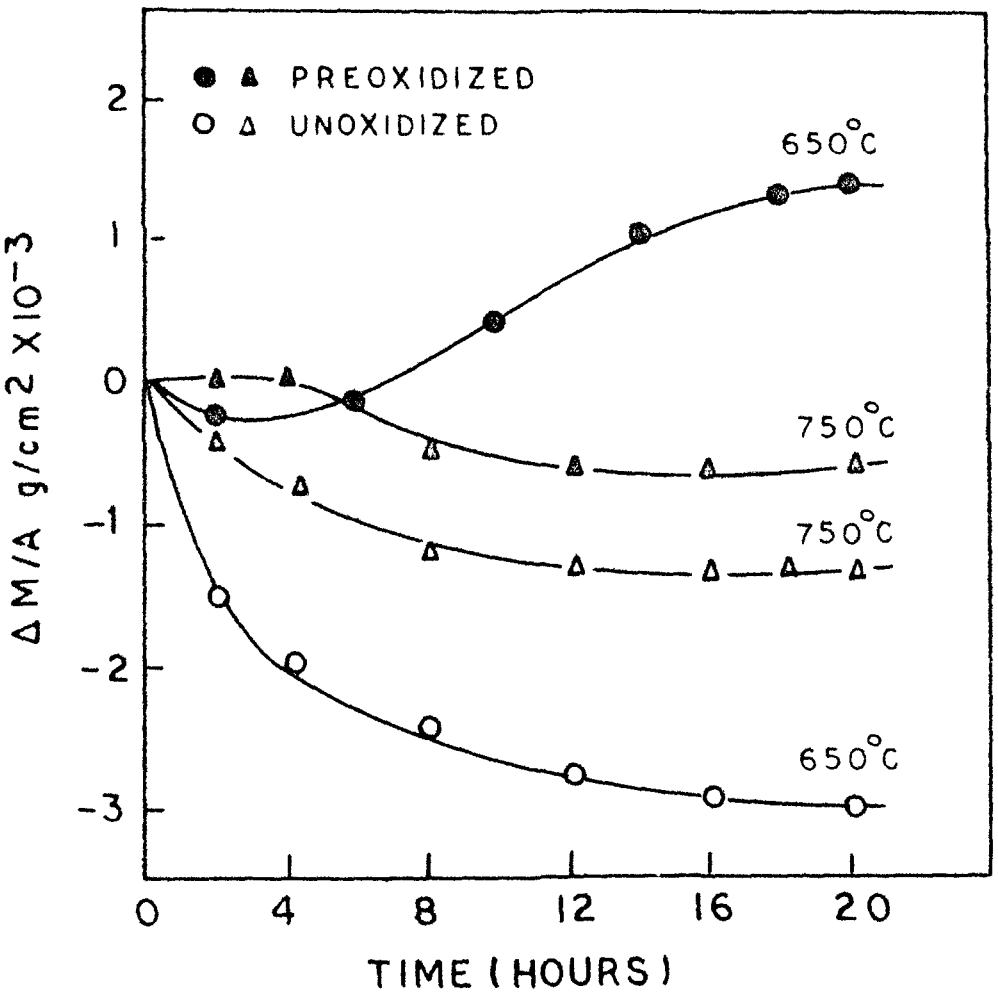
● ▲ PREOXIDIZED
○ △ UNOXIDIZED
650°C
750°C
750°C
650°C
ΔM/A g/cm2 X10⁻³
2
1
0
-1
-2
-3
0
4
8
12
16
20
TIME (HOURS)

FIG. 7.3

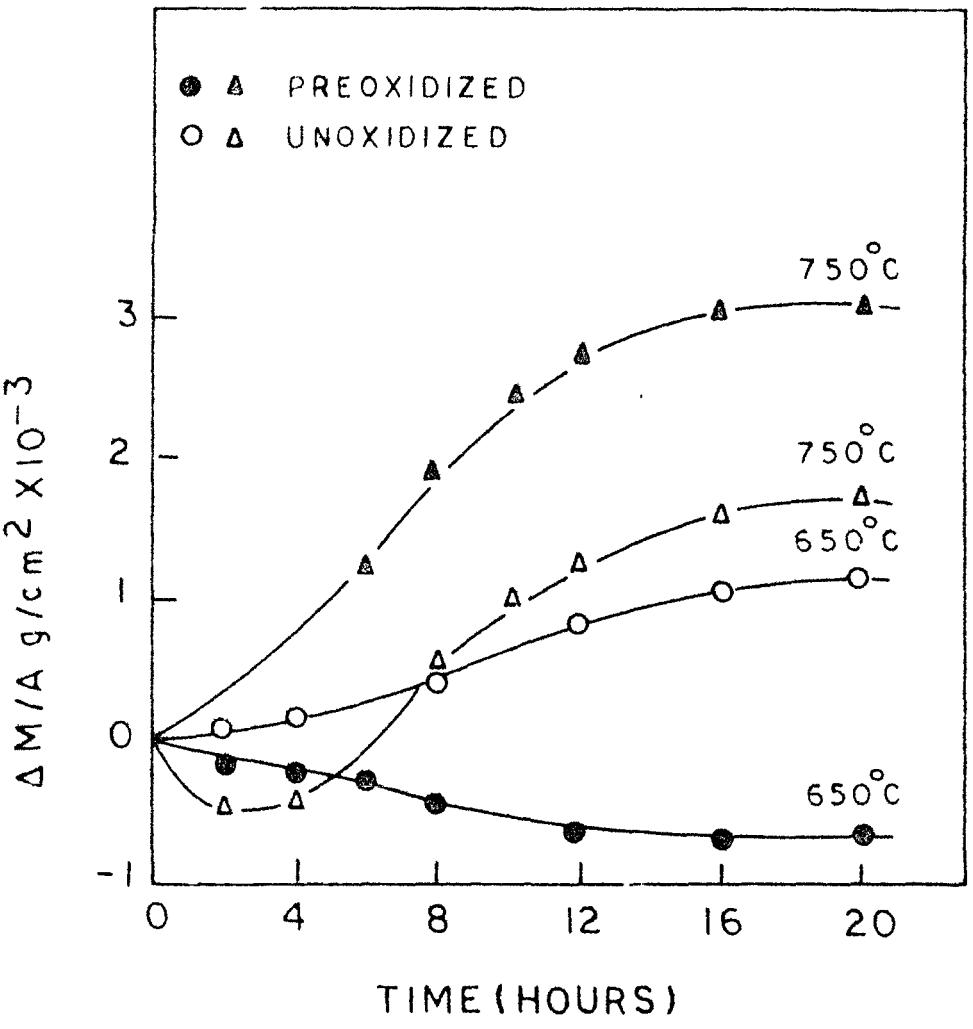
PREOXIDIZED
UNOXIDIZED
750°C
750°C
650°C
650°C
ΔM/A g/cm² X10⁻³
3
2
1
0
-1
0
4
8
12
16
20
TIME (HOURS)

FIG 7 4

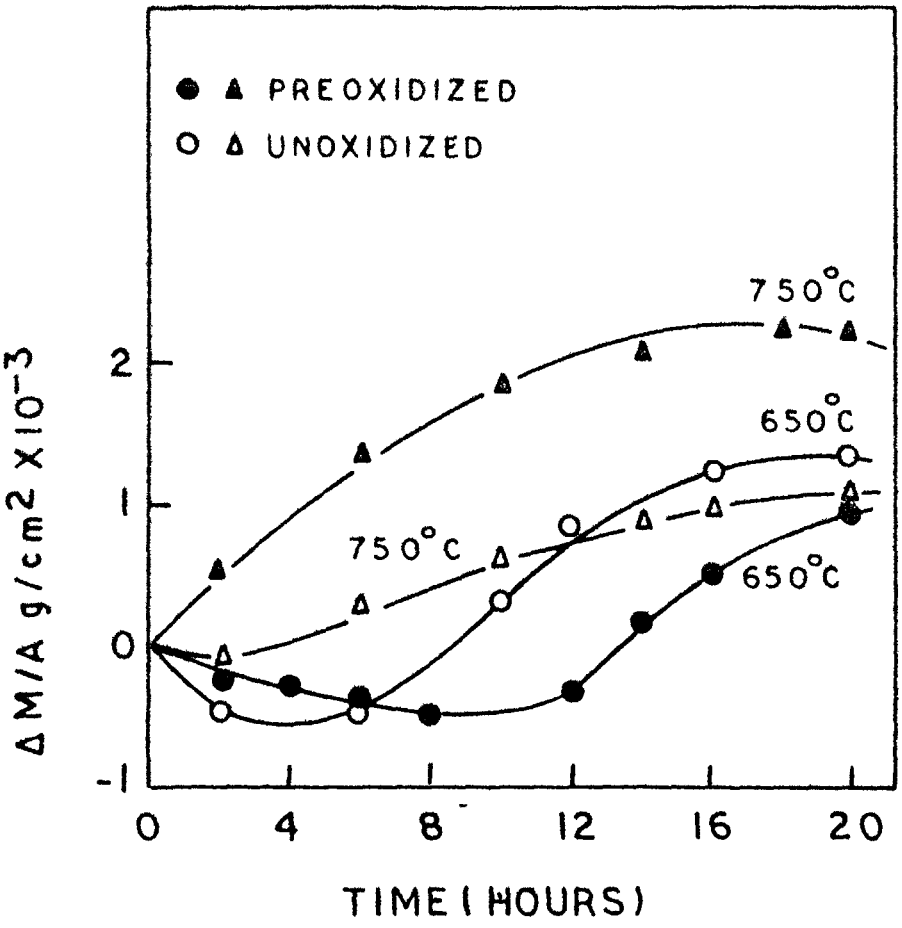
● ▲ PREOXIDIZED
○ △ UNOXIDIZED
750°C
650°C
750°C
650°C
ΔM/A g/cm² X10⁻³
2
1
0
-1
0
4
8
12
16
20
TIME (HOURS)

FIG. 7.5

CAPTIONS OF METALLOGRAPHS

Fig. 7.6 Scanning electron micrograph showing cross section of Inconel-800 in presence of Na_2SO_4-$NiSO_4$ (1:1 molar) mixture and oxidized at 750°C for 20 hours.

Fig. 7.7 Scanning electron micrograph showing cross section of Monel-400 (preoxidized for 20 hours) in presence of Na_2SO_4-$NiSO_4$ (1:1 molar) mixture and reoxidized at 750°C for 20 hours.

Fig. 7.8 Scanning electron micrograph showing cross section of Nimonic-105 (preoxidized for 20 hours) in presence of Na_2SO_4-$NiSO_4$ (1:1 molar) mixture and reoxidized at 750°C for 20 hours.

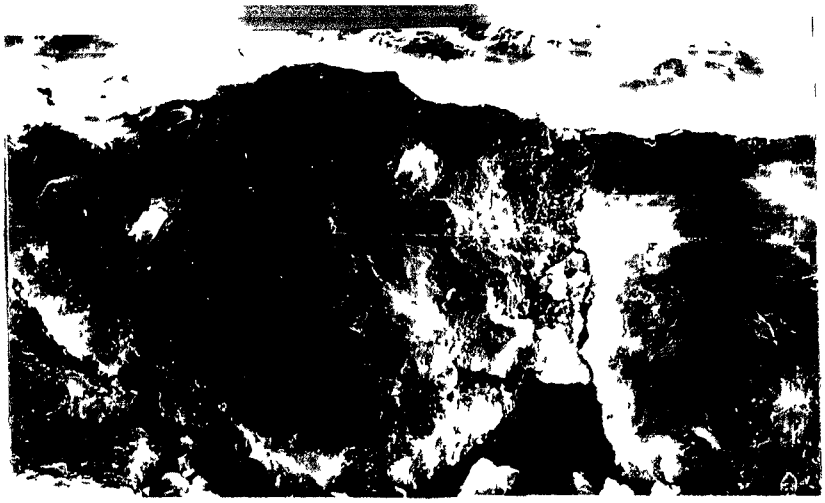

(a)

(b)

7.6

7. 7

(a)

(b)

7. 8

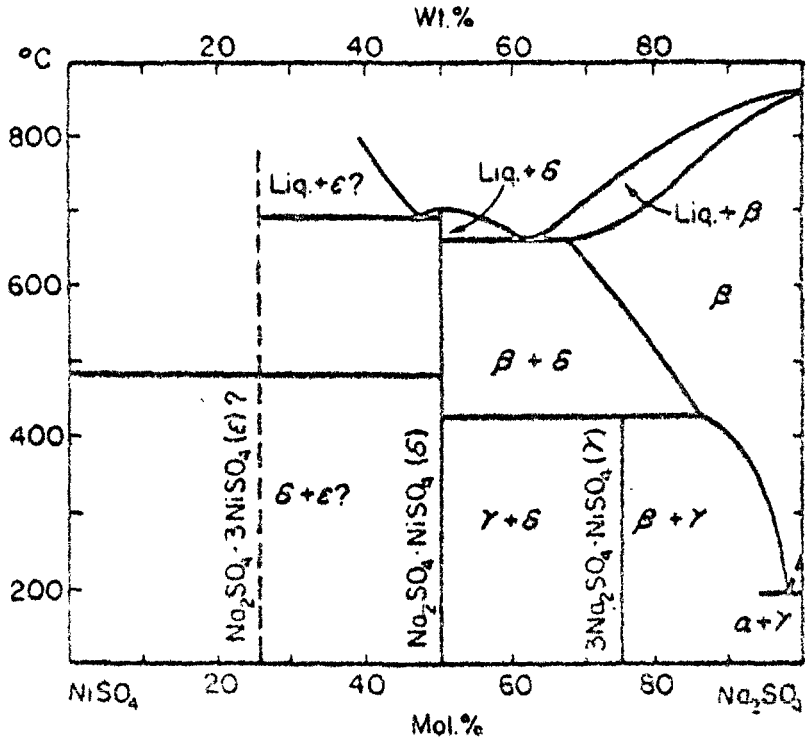

FIG. 7.9. $NiSO_4$-Na_2SO_4 PHASE DIAGRAM

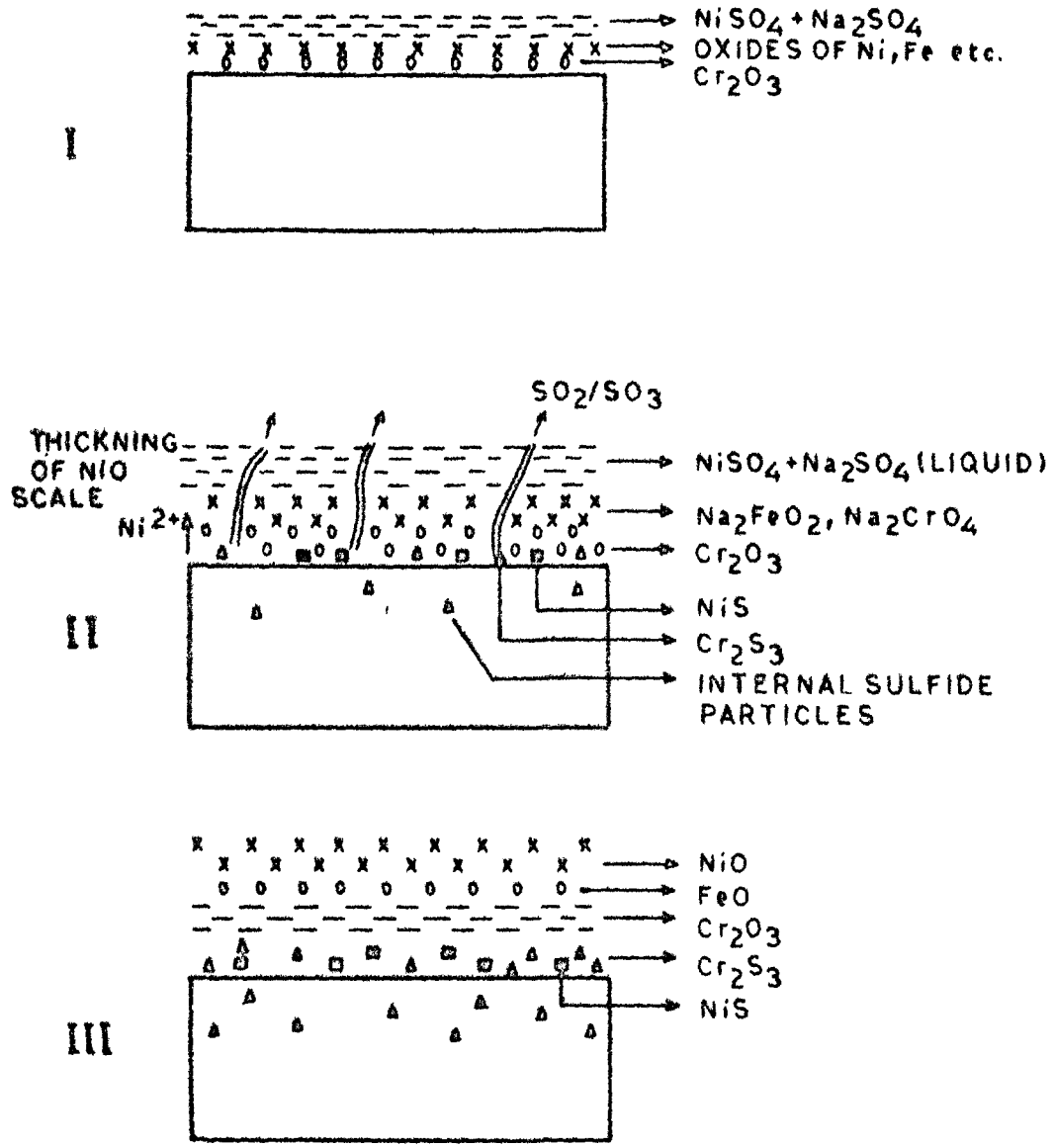

FIG. 7.10 HOT CORROSION OF $Na_2SO_4 + NiSO_4$ MIXTURE (1:1) COATED PREOXIDIZED CHROMIA FORMING ALLOYS REOXIDIZED AT 750°C FOR 20 Hrs.

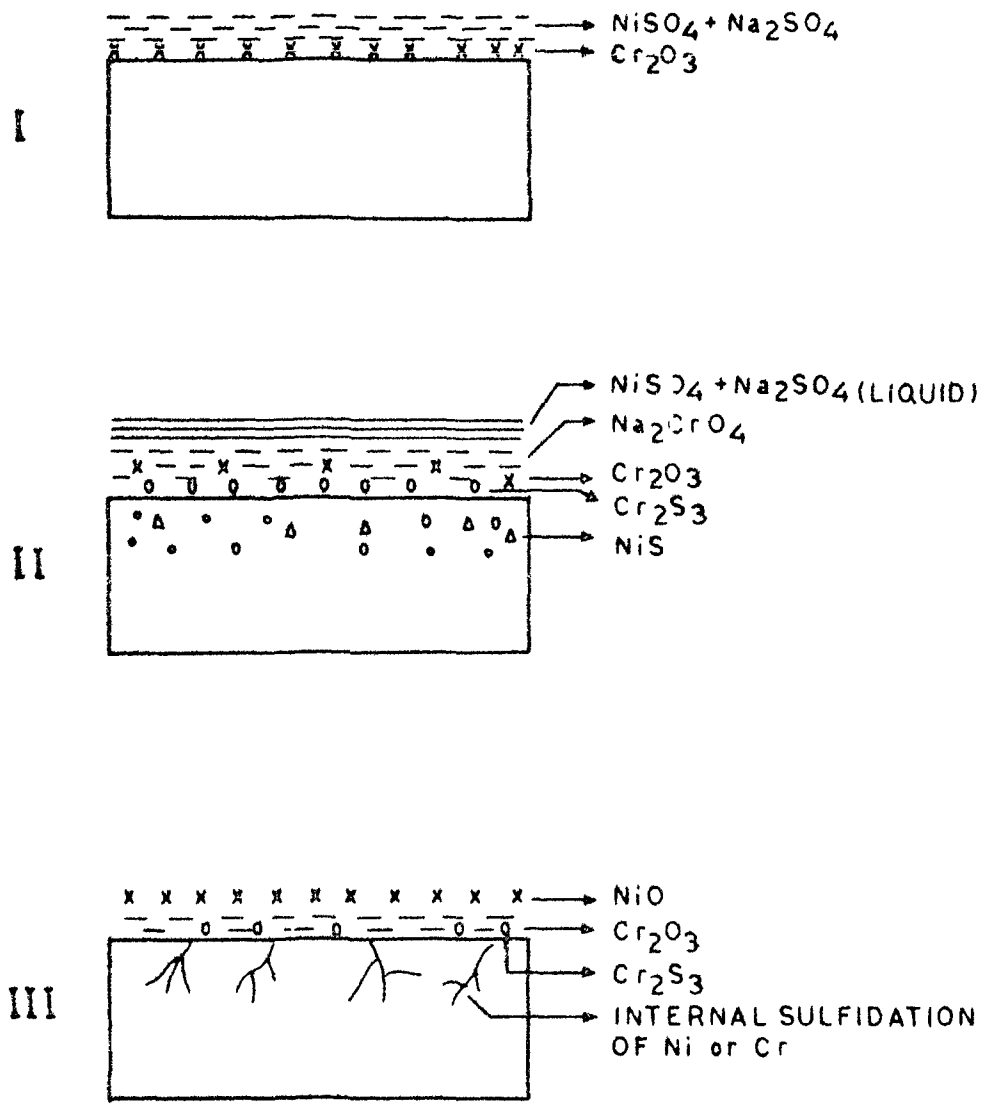

FIG. 7.11 HOT CORROSION OF $Na_2SO_4 + NiSO_4$ MIXTURE (1:1) COATED CHROMIA FORMING ALLOYS AT 750°C FOR 20 Hrs.

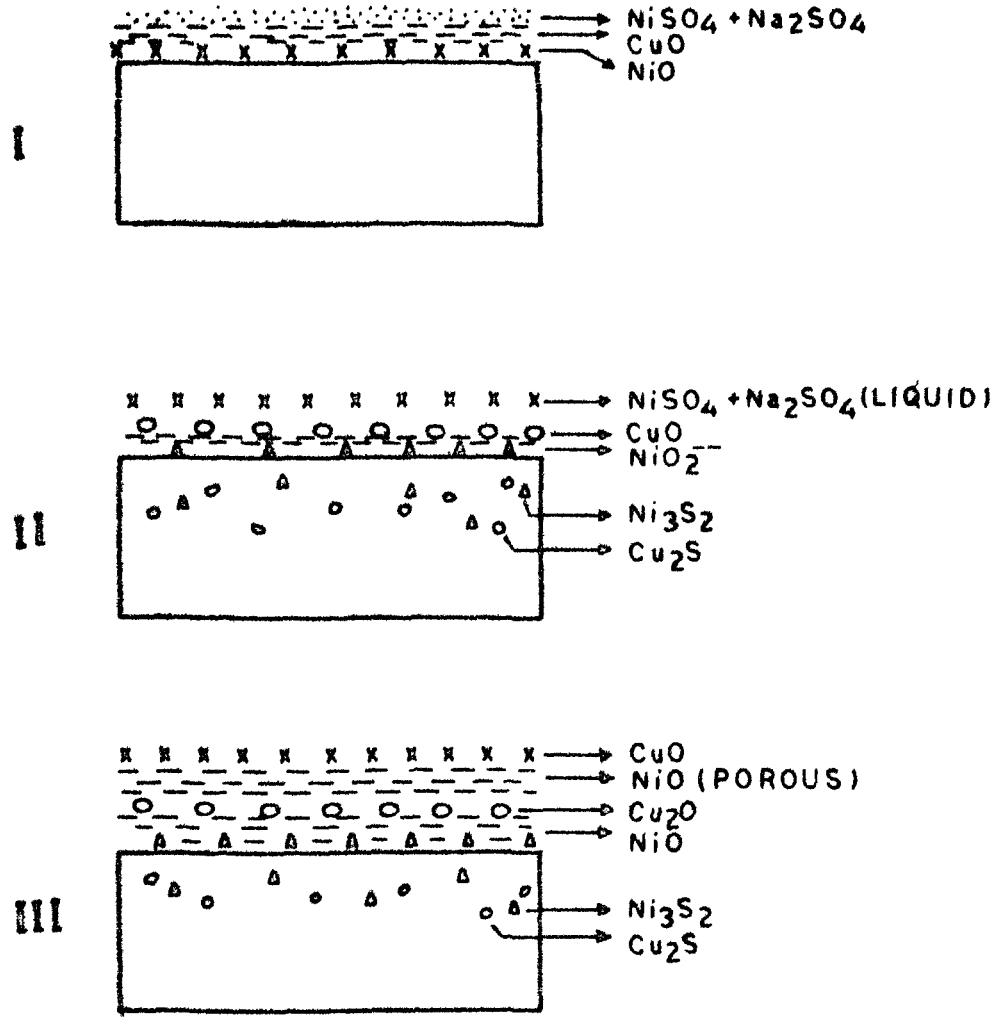

FIG. 7.12 HOT CORROSION OF MONEL-400 (PREOXIDIZED) COATED WITH $Na_2SO_4 + NiSO_4$ MIXTURE (1:1) AND REOXIDIZED AT 750°C FOR 20 Hrs.

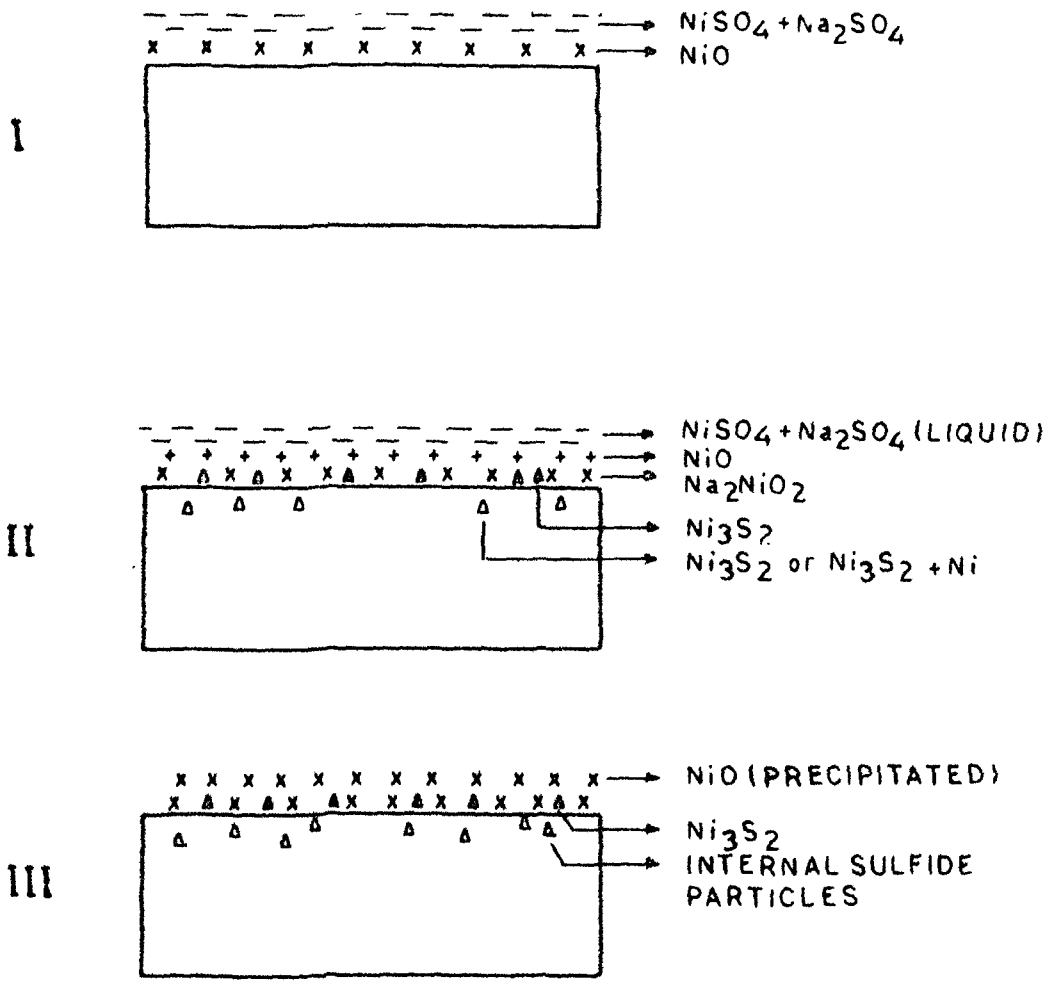

FIG. 7.13 HOT CORROSION OF NICKEL-200 (PREOXIDIZED) COATED WITH $Na_2SO_4 + NiSO_4$ MIXTURE (1:1) AND REOXIDIZED AT 750°C FOR 20 Hrs.

SUMMARY AND CONCLUSIONS

SUMMARY

The studies presented in this thesis deal with the hot corrosion behaviour of stainless steels (viz. AISI 303 and 321) and nickel-base superalloys (viz. Inconel-600, Inconel-800, Monel-400, Nimonic-105, Nickel-200 and B-1900). Low temperature hot corrosion behaviour of some of the nickel-base superalloys have also been studied in presence of Na_2SO_4-$NiSO_4$ mixture.

Chapter I, part I describes some aspects of hot corrosion. Recent studies carried out on hot corrosion of nickel and cobalt-superalloys, and iron-base alloys with special reference to the effect of salt and alloy compositions, have been referred. Various mechanisms, proposed to explain hot corrosion attack, are discussed in reasonable details.

Chapter I, part II presents a literature survey pertaining to oxidation behaviour of iron and iron-base alloys and discusses important contributions made to the oxidation chemistry of iron-base alloys.

Chapter II describes hot corrosion behaviour of sensitized and unsensitized steels in presence of Na_2SO_4.

Hot corrosion behaviour of sensitized (AISI 321) and

unsensitized (AISI 303) steels has been studied in presence of Na_2SO_4 of varying thicknesses at 800 and 1000°C. At 800°C, both the steels show highest oxidation rates at a certain salt concentration which is 4.0 and 9.5 mg/cm^2 for AISI 321 and AISI 303 steels, respectively followed by a gradual decrease in oxidation rates with increasing salt concentration.

At 1000°C, there is a linear relationship existing between amount of salt deposited and oxidation rate — the oxidation rate increases with increasing salt deposition. Initially unsensitized steel has higher oxidation rate than the sensitized steel but when the salt deposition exceeds by 3.5 mg/cm^2 the oxidation rate of sensitized steel becomes higher than the unsensitized steel.

Initially a sulfidation reaction is favoured. With the consumption of sulfur, there is an increase in oxygen activity; Cr_2O_3 is converted into chromate, Na_2CrO_4 dissolves in the melt and precipitated as Cr_2O_3 at the salt/gas interface due to low Na_2O. The sulfidation and fluxing reactions are represented as follows:

$$\text{I} \quad Cr_2O_3 + 3Na_2SO_4 \longrightarrow Cr_2S_3 + 3Na_2O + 6\,O_2$$

$$\text{II} \quad Cr_2O_3 + 2Na_2O + \tfrac{3}{2}O_2 \longrightarrow 2Na_2CrO_4$$

III $FeO + Na_2SO_4 \longrightarrow FeS + Na_2O + 2O_2$

IV $Na_2O + FeO \longrightarrow Na_2FeO_2$

V $NiO + Na_2SO_4 \longrightarrow NiS + Na_2O + 2O_2$

VI $Na_2O + NiO \longrightarrow Na_2NiO_2$

VII $2FeO + \frac{1}{2}O_2 \longrightarrow Fe_2O_3$

At lower temperature (800°C) reactions I to VII proceed only to a limited extent and once a compact oxide layer is formed beneath the Na_2SO_4 coating the oxidation rate falls gradually and Na_2SO_4 acts only as a protective barrier.

At higher temperature (1000°C) same mechanism will be followed but the aggressiveness of the melt increases with increasing salt deposition. In addition, the following reactions are likely to occur, the complex species NiO_2^{--}, CrO_4^{--} and FeO_2^{--} are likely to be precipitated as NiO, Cr_2O_3 and FeO, respectively at the salt/air interface.

VIII $4Cr + 3Na_2SO_4(l) \longrightarrow Cr_2O_3 + 3Na_2O + Cr_2S_3 + 3O_2$

IX $Cr + Na_2O + 3O \longrightarrow Na_2CrO_4$

X $4Fe + Na_2SO_4 \longrightarrow FeS + 2FeO + Na_2FeO_2$

Sensitised AISI 321 steel oxidises at a much faster rate than unsensitised AISI 303 steel when relatively large

amount of salt is deposited on the alloy. Due to rapid oxidation at this temperature a Cr-depleted zone is established in the matrix and TiC is now subjected to be attacked by Na_2SO_4:

XI $\quad TiC + Na_2SO_4 \longrightarrow TiO_2 + Na_2O + S + CO$

TiO_2 is either concentrated at the alloy/oxide interface or present as oxide dispersion in the matrix. Release of sulfur, CO and Na_2O further enhances the oxidation rates.

The observed scale morphologies are consistent with the proposed mechanism. Sulfides or sulfospinels form inner scales and oxides forming outer scales. Internal sulfidation is invariably observed. The sensitized steels are more aggressively attacked as indicated by the presence of thicker porous scales and more intense penetration of the salt into the matrix.

Chapter III contains the results of a hot corrosion study carried out on AISI 303 and AISI 321 steels in presence of Na_2SO_4 or transition metal sulfates, viz. $NiSO_4$, $CoSO_4$ and $Cr_2(SO_4)_3$ or their mixtures, at 800 and 1000°C.

At 800°C, steels coated either with transition metal salt or its mixture with Na_2SO_4 show relatively heavy weight losses with increasing salt deposition. The weight losses

are usually higher in steels coated with salt mixture than coated with bare salt. The continuing weight losses with increasing transition metal salt on the steel can be attributed to the fact that inner chromium oxide scales initially formed on the alloy remain intact and probably do not interact with decomposition products of metallic sulfates, e.g. oxide(s), SO_2(g) and O_2(g). The gaseous products escape resulting in weight losses:

XII $\quad NiSO_4 \longrightarrow NiO + SO_2 + \frac{1}{2}O_2$

XIII $\quad CoSO_4 \longrightarrow CoO + SO_2 + \frac{1}{2}O_2$

XIV $\quad Cr_2(SO_4)_3 \longrightarrow Cr_2O_3 + 3SO_2 + \frac{3}{2}O_2$

At 800°C, the Na_2SO_4-$CoSO_4$ and Na_2SO_4-$NiSO_4$ coated steels show much higher oxidation rates than the corresponding Na_2SO_4-$Cr_2(SO_4)_3$ coated steel due to the formation of low temperature eutectics (Na_2SO_4-$CoSO_4$: 575°C and Na_2SO_4-$NiSO_4$: 671°C). The liquidus phase breaks the protective chromia film and the alloy oxidizes at a much higher oxidation rate.

The weight losses in Na_2SO_4-$Cr_2(SO_4)_3$ coated steel may be attributed to the following reactions:

XV $\quad Cr_2O_3(s) + 2Na_2SO_4(l) + \frac{1}{2}O_2 \longrightarrow$

$$2Na_2CrO_4(l) + 2SO_2(g)$$

XVI $FeO(s) + Na_2SO_4(l) \longrightarrow Na_2FeO_2(l) + SO_2(g) + \frac{1}{2}O_2(g)$

At 1000°C, both steels show increasing oxidation rates with increasing salt/mixture deposition till a maxima is reached, this is followed by weight losses on further increase in salt deposition. The transition metal sulfate coated on the steel at this temperature is likely to decompose into oxide (XII to XIV) and sulfide (XVII to XIX) at the air/salt and oxide/salt interfaces, respectively.

XVII $Cr_2(SO_4)_3 \longrightarrow Cr_2S_3 + 6\,O_2$

XVIII $CoSO_4 \longrightarrow CoS + 2\,O_2$

XIX $NiSO_4 \longrightarrow NiS + 2\,O_2$

In case of $Cr_2(SO_4)_3$ coated steel reaction XVII seems to proceed only to a limited extent and XIV is likely to be predominant throughout the oxidation. This is shown by relatively lower oxidation rates and the presence of compact and adhered chromia scales. In $CoSO_4$ coated steels, CoS formed at the oxide/salt interface (XVIII) may undergo following reactions which are thermodynamically feasible:

XX $CoS + Cr_2O_3 \longrightarrow 3CoO + Cr_2S_3$

XXI $CoS + FeO \longrightarrow CoO + FeS$

XXII $FeS.Cr_2S_3 \longrightarrow FeS + Cr_2S_3$

} oxide/salt interface

XXIII $CoS + 2O_2 \longrightarrow CoSO_4$) gas/salt interface

No CoS was detected in the scales and observed morphology is consistent with the proposed reactions.

In $NiSO_4$ coated steel, NiS formed (XIX) accumulates beneath the Cr_2O_3 scales and may undergo the following reaction:

XXIV $3NiS + Cr_2O_3 \longrightarrow 3NiO + Cr_2S_3$

There is a possibility of penetration of NiS through oxide scale and its interaction with Ni in the substrate to form low melting Ni-NiS eutectic. When the S-activity at the oxide/salt interface is sufficiently lowered due to formation of sulfide, the sulfides get oxidised to NiO and Cr_2O_3 and sulfur thus released produces internal sulfidation. Cr_2S_3 as internal sulfide particles along with NiS were actually found in the matrix.

During oxidation of $Cr_2(SO_4)_3 + Na_2SO_4$ coated steels at 1000°C reactions XIV and XXV will undergo at the air/salt interface in the initial stages.

XXV $Na_2SO_4 \longrightarrow Na_2O + S + \frac{3}{2}O_2$

In the propagation stage, there will be sufficient S potential to form FeS and Cr_2S_3. The culmination of

sulfidation reactions at the oxide/salt interface will increase the oxygen activity and resulting in the oxidation of sulfides into respective oxides and the sulfur released is available for internal sulfidation. The oxides are likely to get fluxed forming Na_2O_3(IV)/$Na_2Fe_2O_4$(XXVI) and Na_2CrO_4(II)/$Na_2Cr_2O_4$(XXVII).

XXVI $Fe_2O_3 + Na_2O \longrightarrow Na_2Fe_2O_4$

XXVII $Cr_2O_3 + Na_2O \longrightarrow Na_2Cr_2O_4$

The reactions are thermodynamically feasible and are likely to continue till entire Na_2O is exhausted. At air/salt interface Na_2O is considerably low and in consequence the complex species present in the melt will ultimately reprecipitate as oxides, e.g. Cr_2O_3, FeO or Fe_2O_3 etc.

In Na_2SO_4 + $NiSO_4$ coated steels, NiS is formed at the oxide/salt interface and Ni-NiS eutectic are responsible for aggressiveness of the mixture. In presence of Na_2SO_4-$CoSO_4$, reactions XVIII, XX to XXIII are likely to go along with XV and XVI. The relatively lower weight gains in Na_2SO_4-$CoSO_4$ coated steels are probably due to the reactions XV and XVI which proceed with the evolution and expulsion of SO_2.

Chapter IV deals with the studies on high temperature oxidation behaviour of Ni-base alloys in presence of Na_2SO_4.

The oxidation behaviour of some Ni-base alloys, viz. Inconel-600, Inconel-800, Monel-400, Nimonic-105, B-1900 and Nickel-200 has been studied in presence of Na_2SO_4 at 850 and 1000°C in flowing air. While the chromia former alloys, e.g. Inconel-600, Inconel-800 and Nimonic-105 show relatively small weight losses at 850 and 1000°C (to the extent of about 3 mg/cm^2 in 10 hrs); B-1900 (alumina former), Nickel-200 and Monel-400 (NiO former) oxidize appreciably following a parabolic and/or linear kinetic.

It appears that Na_2SO_4-coated Inconel-600, 800 and Nimonic-105 form chromia film at the very early stage of oxidation. This film reacts with Na_2SO_4 to undergo the following types of reactions at 850 and 1000°C:

XXVIII $$Cr_2O_3 + \tfrac{3}{2}O_2 + 2Na_2SO_4(l) \longrightarrow 2Na_2CrO_4(l) + 2SO_3(g)$$

The evidences for XXVIII are overwhelming such as (i) weight losses during oxidation, (ii) deposition of a yellow product on the walls of the reaction vessel which was identified chemically or by X-ray diffraction analysis as chromates, (iii) detection of SO_2/SO_3 in the reaction product gases, (iv) slightly basic nature of the melt. At the end of the induction period when molten Na_2SO_4 comes into contact with the alloy, the following reactions are

possible:

XXIX $Ni + SO_4^{2-} \longrightarrow NiS(l) + \frac{3}{2}O_2 + O^{2-}$

XXX $2Cr + 3SO_4^{2-} \longrightarrow Cr_2O_3 + 3SO_2(g) + 3O^{2-}$

XXXI $2Cr + 3SO_4^{2-} \longrightarrow Cr_2S_3 + \frac{9}{2}O_2 + 3O^{2-}$

XXXII $2Al + 3SO_4^{2-} \longrightarrow Al_2O_3 + 3SO_2 + 3O^{2-}$

XXXIII $Fe + SO_4^{2-} \longrightarrow FeS + \frac{3}{2}O_2 + O^{2-}$

Reactions XXIX to XXXI are feasible in Inconel-600, XXIX to XXXI and XXXIII in Inconel-800 and XXIX to XXXII in Nimonic-105. Sulfidation reactions (XXIX, XXXI and XXXIII) are possible when partial pressure of oxygen is substantially lowered and consequently P_{S_2} is increased. This situation can arise at the oxide/salt interface. Isolated pockets of Cr_2S_3 have indeed been found in the oxidised alloys.

The higher oxidation rates of Inconel-800 in presence of Na_2SO_4 in comparison to Inconel-600 have been explained on the basis of high Cr- low Ni contents of Inconel-800 which promotes reaction XXVIII. On the other hand, in Inconel-600 alloy the accumulation of NbC and/or TaC at the grain boundaries restricts the flux of Cr^{3+} ions which results in the discontinuation of reaction XXVIII. In Inconel-600, FeO will be fluxed according to reaction XXXIV.

XXXIV $FeO + Na_2SO_4 \longrightarrow Na_2FeO_2(l) + SO_2 + \frac{1}{2}O_2$

Reaction XXXIV may continue till all the Na_2SO_4 is exhausted or a decrease in P_{O_2} at the salt/gas interface may result in the precipitation of FeO.

During oxidation of Na_2SO_4-coated Nimonic 105 Cr_2O_3 and Al_2O_3 inner scales are formed with NiS inclusions through reactions XXIX, XXX and XXXII. At the oxide/salt interface the oxygen activity is dropped to such a level that sulfidation reactions commence resulting in the formation of NiS and Cr_2S_3. Due to fragile nature of the sulfidized scales the contact between scale and alloy is lost at some sites and fresh salt directly comes into contact with the alloy surface at these sites. The fragmentation of the alloy surface during hot corrosion supports this view point. Molybdenum is present in appreciable concentrations (about 5.5%) in Nimonic 105 and forms MoO_3 which is present in the inner scales. Although there is evidence of the formation of Na_2MoO_4 (XXXV) in the scales, acidic fluxing reactions XXXVI and XXXVII do not seem to undergo due to high chromium contents of the alloy.

XXXV $MoO_3 + Na_2SO_4 \longrightarrow Na_2MoO_4(l) + SO_3(g)$

XXXVI $Cr_2O_3 + 3MoO_3 \longrightarrow 2Cr^{3+} + 3MoO_4^{2-}$

XXXVII $Al_2O_3 + 3MoO_3 \longrightarrow 2Al^{3+} + 3MoO_4^{2-}$

During corrosion of Nickel-200 in presence of Na_2SO_4, NiO is basically fluxed with Na_2SO_4 and S is released:

XXXVIII $NiO + Na_2SO_4 \longrightarrow Na_2NiO_2 + S + \frac{3}{2}O_2$

The sulfur thus released penetrates through the alloy along the grain boundaries to produce profuse sulfidation. NiS may also form through XXIX and accumulates in the inner layers of the scales. Again with a decrease in Na_2O at the salt/gas interface NiO is precipitated and appears in the form of stratified layers as the outer scales. At the regions where cracking or disruption of scales occurred Ni_3S_2 is oxidized to $NiSO_4$ due to passage of air through cleavages. The Na-Ni-S-O superimposed diagram shows the possibility of $NiSO_4$ existence at the regions of higher oxygen activities.

In presence of Na_2SO_4, B-1900 exhibits a linear kinetic at 850°C and a parabolic kinetic at 1000°C. The coated alloy in the initial stages shows induction periods lasting about 4 hours and 1 hour at 850 and 1000°C, respectively. The oxidation rates of Na_2SO_4 coated B-1900 are much higher than the nimonic and Inconel alloys under corresponding conditions.

At 850°C, during the induction period, Cr_2O_3 formed on the alloy reacts with oxide ion in Na_2SO_4 (XXV) forming soluble chromate and liberating SO_3 (XXVIII). In the later stages of induction period, MoO_3 that has formed under Na_2SO_4 layer by oxidation of surface carbides reacts with the sulfate (XXXV). The occurrence of XXXV is supported by the presence of a soluble molybdate ion in the scale. This reaction proceeds more vigorously at 1000°C. The formation of MoO_4^{2-} and CrO_4^{2-} is resulted by the consumption of oxide ions thus increasing the acidity of Na_2SO_4. The reduction in oxide ion concentration increases the sulfur activity (XXXIX and XL) as a result S is able to diffuse through Al_2O_3 scale into the alloy forming chromium or aluminium sulfides. However, internal sulfides were found to be chromium sulfide because Al_2S_3 formation requires a much lower partial pressure of oxygen. Near the end of induction period, due to breaching of the scales at some localized spots, the underlying nickel will be exposed to Na_2SO_4 and NiS will be formed (XXIX) along with Cr_2O_3 (XXX) and Al_2O_3 (XXXII). This will increase the oxide ion concentration above 10^{-8} atm making Na_2SO_4 melt markedly basic. Consequently, basic fluxing of protective Al_2O_3 occurs (XLI)

XXXIX $\quad SO_4^{2-} \longleftarrow O^{2-} + SO_3$

XL $\quad SO_4^{2-} \rightleftharpoons S^{2-} + 2O_2$

XLI $Al_2O_3 + O^{2-} \rightleftharpoons 2AlO_2^-$

The reaction proceeds actively with rapid increase in the rate of oxidation. However, as the oxide ion is used up the attack slows down which is indicated by a 'parabolic foot' in the hot corrosion curve. Since the corrosion studies were restricted to 12 hours the oxidation kinetic curves represent only induction and parabolic regions and there is no evidence for intermediate or linear region.

The monel 400 is markedly corroded in presence of Na_2SO_4, the intensity of attack increases with increasing temperature.

Initially a NiO film is formed beneath a CuO film. When molten Na_2SO_4 comes into contact with the CuO film the following reaction is feasible:

XLII $CuO + SO_4^{2-} \longrightarrow CuS + O^{2-} + 2O_2$

O^{2-} is consumed by fluxing with NiO present in the inner scales (XXXVIII). $O_2(g)$ penetrates through the scale and preferentially oxidises Ni to NiO. With the depletion of oxygen activity at the oxide/salt interface NiO is sulfidised to NiS due to corresponding increase in S-activity. The depletion in O^{2-} at the salt/gas interface will result in the precipitation of NiO as a porous scale ahead of CuS

scale formed initially (XLII). Again fused Na_2SO_4 will react with NiO to carry out sulfidation reaction forming NiS:

XLIII $\quad NiO + SO_4^{2-} \longrightarrow NiS + O^{2-} + 2\,O_2$

When XLIII is completed a fall in S-activity will result in the oxidation of underneath copper sulfide layer. In consequence S is released which will penetrate through the alloy to sulfidize Ni. This process of alternate sulfidation and oxidation will continue till all the Na_2SO_4 is consumed. The morphology of the scales consisting of alternate Ni- and Cu- enriched layers is in conformity with the above mechanism.

Chapter V deals with the studies on high temperature corrosion behaviour of Ni-base alloys in presence of NaCl.

The high temperature corrosion behaviour of Ni-base alloys in presence of NaCl can be divided into two categories:

(i) Chromia forming alloys, viz. Inconel-600, Inconel-800 and Nimonic 105 which show much higher oxidation rates than those in presence of Na_2SO_4 or air.

(ii) Al_2O_3 formers (B-1900) and NiO formers (Ni-200) which

have much lower oxidation rates than in presence of Na_2SO_4.

Monel 400 which is CuO-NiO former is severely attacked by NaCl.

NaCl breaks down the protective oxide scale by attacking the Cr_2O_3 film formed on the category (1) alloy producing a volatile product CrO_2Cl_2 (XLIV) which is subsequently converted into Na_2CrO_4 and condensed on the cooler part of the reaction tube in the form of a yellow deposit:

XLIV $\quad 4NaCl + Cr_2O_3 + \frac{3}{2}O_2 \longrightarrow 2CrO_2Cl_2 + 2Na_2O$

The melt adjacent to the alloy consists of NaCl, Na_2CrO_4, CrO_2Cl_2 and Na_2O. NaCl(l) penetrates through the melt and reacts with the alloy components as suggested in the following equations:

XLV* $\quad 2NaCl + 2Ni + O_2 \longrightarrow Na_2NiO_2 + NiCl_2$

XLVI** $\quad 2NaCl + 2Fe + O_2 \longrightarrow Na_2FeO_2 + FeCl_2$

XLVII*** $\quad 2NaCl + Co + \frac{1}{2}O_2 \longrightarrow CoCl_2 + Na_2O$

XLVIII**** $\quad 3NaCl + 4Al + 3O_2 \longrightarrow AlCl_3 + 3NaAlO_2$

* Inconel-600, Inconel-800, Nimonic 105

** Inconel-800

*** Nimonic 105

**** Nimonic 105

The sequence of reactions XLV to XLVIII depends upon the thermodynamic conditions. As metallic chlorides move outward through the melt, oxygen activities are sufficiently high to convert metallic chlorides into metallic oxides:

XLIX $2FeCl_2 + \frac{3}{2}O_2 \longrightarrow Fe_2O_3 + 2Cl_2$

L $3FeCl_2 + 2O_2 \longrightarrow Fe_3O_4 + 3Cl_2$

LI $NiCl_2 + O \longrightarrow NiO + Cl_2$

LII $CoCl_2 + O \longrightarrow CoO + Cl_2$

LIII $2AlCl_3 + \frac{3}{2}O_2 \longrightarrow Al_2O_3 + 3Cl_2$

The chlorine is recycled to react with elements in the alloy.

LIV $xCl_2 + 2M(alloy) \longrightarrow 2MCl_x$

Continuation of this process results in the development of discontinuous, nonprotective and porous oxide scales. Reactions XLV, XLVI and XLVIII indicating the formation of NiO_2^{--}, FeO_2^{--} and AlO_2^{-}, respectively proceed at the backward direction due to the depletion in O^{--} at the melt/salt interface and consequently precipitating corresponding oxides at the salt/gas interface. The conversion of chlo-

rides into oxides (XLIX to LIII) and precipitation of the oxides at the salt/gas interface gives rise to thick porous scales. Another factor responsible for high oxidation rates in presence of NaCl is the low boiling points of transition metal halides which develop sufficient vapour pressure at the alloy/scale interface to lift up the scales or break down the protective oxide layers.

NaCl-coated B 1900 shows much lower oxidation rates than Na_2SO_4-coated alloy. Little attack was observed with Al_2O_3 in NaCl upto a temperature of 1000°C. Continuous and smooth oxidation curves are obtained and scales seem to be adhered. It appears that the integrity of the Al_2O_3 film is maintained in presence of NaCl.

Nickel-200 seems to be moderately attacked by NaCl in comparison to chromia forming alloys. The corrosion rates of NaCl-coated alloys are much lower than the corresponding Na_2SO_4-coated alloys. Further the oxidation rate at 850°C is much higher than at 1000°C.

When NiO films come into contact with liquid NaCl, chloridisation reaction occurs

LV $\quad 2NiO + 2NaCl \longrightarrow NiCl_2 + Na_2NiO_2$

Liquid NaCl penetrates through the melt and comes into

contact with the metal and reacts according to the reaction

LVI $2NaCl + 2Ni + O_2 \longrightarrow NiCl_2 + Na_2NiO_2$

However, LVI may proceed to only a limited extent due to low oxygen potential produced at the alloy/melt interface. In these circumstances the volatile $NiCl_2$ vapours break the oxide scale or pass through the melt and oxidized to NiO at the salt/gas interface (LI). Further, NiO_2^{--} as formed by LV or LVI is dissociated and precipitated as NiO at the salt/gas interface. This results in the formation of porous and copious scales of NiO on the alloy surface. However, the inner layer of the scales seemed to retain some $NiCl_2$.

During corrosion of Nickel 200 in presence of NaCl, two opposing factors affect the corrosion rates; with increasing temperature the increasing amount of liquid tends to accelerate the rate but at the same time the amount of chlorine decreases. The balance between these effects perhaps leads to the occurrence of maximum attack at an intermediate temperature; this is possibly the reason of higher corrosion rates of the alloy at 850°C than at 1000°C.

Monel 400 is severely attacked by NaCl, the intensity of attack increases with increasing temperature. At 1000°C, liquidus NaCl attacks outer scales of CuO to form CuCl (LVII), the liquid further penetrates and reacts with inner

NiO film to form $NiCl_2$ and Na_2NiO_2 (LV).

LVII $2NaCl + 2CuO \longrightarrow 2CuCl + Na_2O + O$

CuCl (LVII) and $NiCl_2$ (LVI) formed in the substrate move outward to oxidise to CuO (LIX) and NiO (LI) at the gas/salt interface:

LVIII $2CuCl + O \longrightarrow Cu_2O + Cl_2$

LIX $Cu_2O + O \longrightarrow 2CuO$

At 1000°C, LI, LV and LIX continue to provide a thick duplex scale of CuO and NiO. The Cl_2 evolved during the oxidation is available for further corrosion along with NaCl(v) thus increasing the severity of corrosion with time. This is indicated by the onset of a linear kinetic shortly after the culmination of a parabolic kinetic. The scale morphology indicates the presence of a thick duplex scales containing alternate layers of CuO and NiO.

It appears that oxidation and chloridisation reactions (involving O_2 and NaCl) generally follow a parabolic rate law whereas chloridation reactions (involving NaCl and Cl_2 (g)) producing more severe attack follow a linear rate law.

Chapter VI describes hot corrosion behaviour of some nickel-base alloys in presence of $NaCl-Na_2SO_4$ mixtures.

The high temperature oxidation behaviour of Inconel-600, Inconel-800, Nimonic 105, Nickel 200, B-1900 and Monel-400 has been studied in presence of mixtures of Na_2SO_4 and NaCl (5:1 and 1:5 molar ratios) at 850 and 1000°C in a current of air.

The weight gain/time curves indicate that chromia forming alloys, e.g. Inconel-600 and 800 and Nimonic 105 show increasing corrosion rates with increasing amount of NaCl in Na_2SO_4 whereas Al_2O_3 former (B-1900) and NiO former (Nickel-200) show decreasing oxidation rates with increasing amount of NaCl in Na_2SO_4 although small amount of NaCl in Na_2SO_4 enhances the oxidation rate initially. Monel-400 (NiO/CuO former) behaves similar to chromia forming alloys.

Oxidation of chromia forming alloys with Na_2SO_4-NaCl mixtures results in the development of degraded microstructure. The degradation is more pronounced in alloys coated with higher amounts of NaCl. Inconel-800 is most severely attacked and Nimonic-105 is least affected.

Inconel-600 coated with 5:1 NaCl:Na_2SO_4 mixture on corrosion shows NiO with Cr_2O_3 inclusions in the outer scales, beneath the oxide scales Cr_2S_3 is present containing some NiS. The same alloy shows less severe attack in presence of 1:5 NaCl:Na_2SO_4 mixture although a sulfide layer is

present. Inconel-800 which is more severely attacked shows similar morphology beneath the oxide scales which are comprised of oxides of all elements present in the alloy with predominent concentration of Ni, Cr and Fe oxides, a sulfide front is present in the form of a zone which extended into the alloy as if internal corrosion product has been formed. The microstructures of Na_2SO_4-NaCl corroded Nimonic 105 show the disruption of otherwise protective scales. The disruption is more distinct in alloy coated with 1:5 Na_2SO_4:NaCl mixture where deep penetration of the salt and fragmentation are observed.

In Na_2SO_4-NaCl coated chromia forming alloys, the chromia scales which were initially protective in presence of Na_2SO_4 are attacked by NaCl. The corrosion rates are enhanced by several magnitude due to the formation of volatile CrO_2Cl_2 (XLIV) and subsequent conversion to yellow Na_2CrO_4 which is deposited on the cooler end of the reaction tube. The function of chloride is to remove chromium preferentially thus producing chromium depletion in the alloy. It has two important bearings: NaCl(l) creeps through the melt and attacks the alloy directly, the alloying elements undergo chloridination reactions and form chlorides according to their thermodynamic stabilities. Those chlorides which are volatile move outward in the form of vapours and

get oxidized at the salt/air interface to respective oxides, the chlorine gas given off recycles and induces chlorination reactions. Secondly, due to removal of chromium by chloride the sulfur from Na_2SO_4 begins to sulfidize the alloy much earlier. The combined effect of two factors results in much higher corrosion rates in Na_2SO_4-NaCl coated alloy than Na_2SO_4-coated alloy. In those cases where the deposits contain mostly NaCl as in 1:5 Na_2SO_4:NaCl mixture the effects due to sulfur will be less pronounced. In this case NaCl will cause rapid depletion of Cr,Ni and other elements in the alloy and in consequence thick and porous scales are developed on the alloy.

The alumina forming B-1900 shows highest corrosion rates in presence of a mixture consisting of Na_2SO_4 and NaCl in the molar ratio of 5:1 and lowest in pure NaCl. Addition of a small amount of NaCl in Na_2SO_4 enhances the oxidation rates of the alloy enormously. It appears that a small amount of NaCl enhances the corrosion rates by decreasing the induction periods (2 hr at 850°C and about 1 hr at 1000°C) and thus on setting of degradation reactions much earlier. This degradation is caused by rapid removal of Al from alloy. With the culmination of reactions LX to LXIV involving oxygen and sulfur removal from the salt deposit, the oxygen and S-activities are consequently reduced at

melt/oxide interface, and NaCl from the deposit will react with Al_2O_3 and later Al in substrate to form $AlCl_3$ (LXV and LXVI). As $AlCl_3$ moves outward in the pores, higher oxygen activities exist in the liquid because oxygen is supplied by air. Consequently, $AlCl_3$ is converted into Al_2O_3 and chlorine is free to react again with the alloy (LXII and LXVII). In such a process, a small amount of NaCl can produce a substantial effect because it is recycled.

LX $\quad Cr_2O_3(s) + 2Na_2SO_4(l) + \frac{1}{2}O_2(g) \longrightarrow 2Na_2CrO_4(l) + 2SO_2(g)$

LXI $\quad Ni + SO_4^{2-} \longrightarrow NiS(l) + \frac{3}{2}O_2 + O^{2-}$

LXII $\quad 2Al + 3SO_4^{2-} \longrightarrow Al_2O_3 + 3SO_2(g) + 3O^{2-}$

LXIII $\quad 2Cr + 3SO_4^{2-} \longrightarrow Cr_2O_3 + 3SO_2(g) + 3O^{2-}$

LXIV $\quad Al_2O_3 + O^{2-} \longrightarrow 2AlO_2^-$

LXV $\quad Al_2O_3 + 6NaCl \longrightarrow 2AlCl_3 + 3Na_2O$

LXVI $\quad 2Al + 6NaCl + \frac{3}{2}O_2 \longrightarrow 2AlCl_3 + 3Na_2O$

LXVII $\quad 3Na_2O + 3Cl_2 \longrightarrow 6NaCl + \frac{3}{2}O_2$

Nickel-200 which forms a NiO scale oxidises at a much lower rate in presence of higher concentrations of NaCl in Na_2SO_4 than the salt mixture containing smaller concentrations of

NaCl. Alloy coated with NaCl-Na_2SO_4 (1:5) oxidizes at a higher rate at 850°C than at 1000°C whereas alloy coated with 5:1 mixture shows higher corrosion rate at 1000°C.

The small amount of NaCl in Na_2SO_4 is perhaps helpful in breaking the protective NiO scales and consequently induction period is greatly reduced. Following sulfidation and basic fluxing reactions in which S and O^{2-} are used up the chloridination reaction proceeds involving conversion of NiO and Ni metal into $NiCl_2$. $NiCl_2$ decomposes at salt/air interface into NiO, chlorine released is available for recycling. The NiO_2^{2-} formed during fluxing ends up as NiO by precipitation at the salt/gas interface. This provides a porous NiO scale on the alloy. The observed morphology supports this mechanism.

The lower corrosion rates of 1:5 Na_2SO_4:NaCl coated Nickel-200 alloy could perhaps be explained on the basis of retention of protectiveness by the NiO at 850°C. At 1000°C, a relatively large induction period is observed. By the end of this period sufficient S-activity is developed to sulfidise nickel metal to NiS and sequentially NiO is basically fluxed to NiO_2^{2-}. These reactions perhaps continue till entire Na_2SO_4 is consumed. NaCl(l) creeps inward to carry out the chloridation reactions with NiS and Ni metal (LXVIII to LXXI).

LXVIII $NiS + 2NaCl \longrightarrow NiCl_2 + Na_2S$

LXIX $Ni + 2NaCl + \frac{1}{2}O_2 \longrightarrow NiCl_2 + Na_2O$

LXX $Na_2O + Ni + \frac{1}{2}O_2 \longrightarrow Na_2NiO_2$

LXXI $Na_2S + 2O_2 \longrightarrow Na_2SO_4$

The $NiCl_2$ formed move outward to get oxidise to NiO at the salt/air interface and similarly Na_2NiO_2 is precipitated as NiO. Na_2SO_4 formed by LXXI penetrates into the alloy to carry out internal sulfidation. The amount of Cl_2 available after oxidation of $NiCl_2$ will decline ultimately to nearly zero level at 1000°C and hot corrosion reactions are ceased to proceed further.

Like chromia formers, the corrosion rates of Monel-400 (CuO/NiO former) increase with increasing concentration of NaCl in Na_2SO_4. The effect is more pronounced at 1000°C. NaCl breaks the protective outer scales of CuO and inner scales of NiO. This results in a series of sulfidation, fluxing and chloridation reactions which contribute to enhanced corrosion rates. The corrosion rates at 1000°C are much higher them at 850°C, this is presumably due to increase in aggressiveness of the melt inspite of the expected fall in chlorine activity.

Chapter VII describes studies on low temperature hot corrosion in presence of Na_2SO_4-$NiSO_4$ mixture.

The hot corrosion studies have been carried out at 650 and 750°C on Inconel 600, Inconel 800, Nimonic 105, Nickel 200 and Monel 400 in presence of 1:1 molar ratio of $NiSO_4$ and Na_2SO_4. The studies have been carried out under two different conditions: under one condition the alloys are preoxidized for 20 hours subsequently coated with $NiSO_4$-Na_2SO_4 mixture followed by hot corrosion and under the other condition the alloys are directly coated with the mixture and are then corroded.

In general, the chromia forming alloys (Inconel 600 and 800 and Nimonic 105) show weight losses in presence of salt mixture at 650 and 750°C. In contrary, NiO forming alloys (Nickel 200 and Monel 400) after initial weight losses show weight gains and oxidised by a parabolic rate law. With a few exceptions, the preoxidised alloys have higher corrosion rates than unoxidised alloys. The preoxidised alloys when corroded in presence of Na_2SO_4-$NiSO_4$ mixture show morphologies in which scales are greatly disrupted and the substrate is relatively less affected. On the other hand, alloys which were directly corroded in presence of salt mixture show a morphology in which substrate is deleteriously attacked.

During hot corrosion of preoxidised Inconel 600 and 800 and Nimonic 105 in presence of $NiSO_4$-Na_2SO_4 mixture, the outer scales are expected to get thickened due to the presence of NiO of the decomposed $NiSO_4$ (XII) plus NiO produced by nickel migration from the metal zone.

The liquid salt mixture will penetrate through NiO scale and will attack inner Cr_2O_3 scales and reactions XV, XVI and LXXII are expected at the salt/oxide interface.

LXXII $\quad 2Cr_2O_3 + 3NiSO_4 + 2Na_2SO_4 \longrightarrow$

$$Cr_2S_3 + Ni_3S_2 + 2Na_2CrO_4 + 9O_2$$

Reactions XII, XV and XVI will result in the expulsion of sulfurous gases and subsequently loss in weight. The release of oxygen by LXXII will result in rapid oxidation of the alloy by Cr/Ni diffusion and thickening of the oxide scales. CrO_4^{2-} and FeO_2^{2-} formed moved outward to the salt interface and precipitate as Cr_2O_3 and FeO (or Fe_2O_3) at some distance from the gas/salt interface and beneath NiO scale due to fall off in Na_2O. Reactions XV, XVI and LXXII will terminate when the salt is consumed.

In NiO forming Nickel 200 and Monel 400 alloys under preoxidised conditions, reactions XV, XVI and LXXII are not possible but in Monel 400, the liquid salt extrudes through

outer CuO and attacks NiO scales (LXXIII and LXXIV).

LXXIII $NiO + 2NiSO_4 \longrightarrow Ni_3S_2 + \frac{9}{2}O_2$

LXXIV $5NiO + 2Na_2SO_4 \longrightarrow 2Na_2NiO_2 + Ni_3S_2 + \frac{9}{2}O_2$

The oxygen released during LXXIII and LXXIV will react with diffusing Ni and Cu (from the metal) to form copious oxide scales. Some Ni_3S_2 formed may also get oxidized and consequently sulfur released produces internal sulfidation by forming Ni_3S_2 and Cu_2S in the matrix. In Nickel-200 similar reactions are expected; NiO_2 formed in LXXIV moves outward and precipitated as NiO at the gas/salt interface. During hot corrosion of unoxidised NiO forming alloys, the liquid salt penetrates the thin oxide film and directly attacks the underlying metal:

LXXV $9Ni + 2NiSO_4 \rightleftharpoons 8NiO + Ni_3S_2$ ($G^\circ = -77$ Kcal)

The $Ni-Ni_3S_2$ eutectic which forms below the surface oxide seems primarily responsible for the hot corrosion attack.

During corrosion of unoxidised $Na_2SO_4-NiSO_4$ coated chromia forming alloys initially a chromia film is formed on the alloy. Reactions XV and LXXII are expected to proceed only to a limited extent. The oxidation kinetic curves show that preoxidised alloys have usually shorter induction periods whereas unoxidised alloys show relatively longer

induction periods. This is perhaps one of the important reasons that preoxidized alloys have comparatively higher oxidation rates. The induction periods are relatively longer in chromia former than NiO former.

CONCLUSIONS

The following conclusions may be drawn from the hot corrosion studies:

Chapter II

(i) At 800°C, Na_2SO_4 coated sensitized (AISI 321) and unsensitised (AISI 303) steels show highest oxidation rates at a certain concentration which is 4.0 and 9.0 mg/cm^2, respectively followed by a gradual decrease in oxidation rate with increasing salt concentration.

(ii) At 1000°C, a linear relationship exists between amount of salt deposition and oxidation rate.

(iii) At 1000°C, with relatively large amount of Na_2SO_4, sensitized 321 steel oxidises at a much faster rate than the unsensitized 303 steel. During corrosion a Cr-depleted zone is established in the matrix and TiC which is present on the grainboundaries is now subjected to be attacked by Na_2SO_4

$$TiC + Na_2SO_4 \longrightarrow TiO_2 + Na_2O + CO + S$$

Release of S and Na_2O enhances the degradation of the alloy.

Chapter III

(i) At 800°C, 303 and 321 steels coated either with tran-

sition metal salt or its mixture with Na_2SO_4 show relatively heavy weight losses and the weight loss increases with increasing salt deposition. This can be attributed to the fact that inner chromium oxide scales initially formed on the alloy remain intact and perhaps do not interact with decomposition products of metallic sulfates, e.g. oxides, SO_2 and O_2. The gaseous product escape resulting in weight losses.

(ii) At 800°C, the Na_2SO_4-$CoSO_4$ and Na_2SO_4-$NiSO_4$ coated steels show much severe corrosion due to the formation of low temperature eutectics (Na_2SO_4-$CoSO_4$: 575°C and Na_2SO_4-$NiSO_4$: 671°C). The liquidus phase breaks the protective oxide film and the alloy oxidizes at a much faster rate.

(iii) At 1000°C, both steels show increasing oxidation rates with increasing salt/mixture deposition till a maxima is reached, this is followed by weight losses on further increase in salt deposition.

(iv) Higher corrosion rates of $NiSO_4$ coated steels at 1000°C are attributed to the formation of NiS which accumulates beneath the Cr_2O_3 scales and undergo the following or similar type of reaction:

$$3NiS + Cr_2O_3 \longrightarrow 3NiO + Cr_2S_3$$

NiS also penetrates through the oxide scales and interact with nickel in the substrate to form low melting Ni-NiS eutectic.

(v) The Na_2SO_4 and transition metal sulfate coated steels undergo severe corrosion at 1000°C due to sequential progress of sulfidation and fluxing reactions.

Chapter IV

(i) Chromia forming Inconel 600, Inconel 800 and Nimonic 105 oxidize slowly in presence of Na_2SO_4 whereas alumina former B-1900 and NiO former Nickel-200 oxidise at a faster rates following a parabolic and/or linear kinetic.

(ii) In presence of Na_2SO_4, the chromia forming alloys show well defined induction periods indicated by weight losses.

(iii) The aggressive action of Na_2SO_4 on B-1900 is due to the presence of MoO_3 in the alloy which is formed under Na_2SO_4 layer and undergo following or similar types of acid fluxing reactions:

$$MoO_3 + Na_2SO_4 \longrightarrow Na_2MoO_4(l) + SO_3(g)$$

$$Cr_2O_3 + 3MoO_3 \longrightarrow 2Cr^{3+} + 3MoO_4^{2-}$$

$$Al_2O_3 + 3MoO_3 \longrightarrow 2Al^{3+} + 3MoO_4^{2-}$$

The reduction in oxide ion concentration increases the acidity of the melt and as a result sulfur is able to diffuse through Al_2O_3 scale into the alloy forming internal sulfides.

(iv) Monel-400 is appreciably corroded in presence of Na_2SO_4 and a mechanism involving alternate sulfidation and oxidation reactions seems responsible for development of a scale morphology consisting of alternate Ni and Cu enriched layers.

Chapter V

(i) Chromia forming nickel-base alloys show much higher oxidation rates in presence of NaCl than in presence of Na_2SO_4 or air.

(ii) Al_2O_3 or NiO forming alloys show much lower oxidation rates than in presence of Na_2SO_4.

(iii) Molten NaCl attacks the protective chromia scales forming volatile product CrO_2Cl_2 which is subsequently converted to Na_2CrO_4. NaCl then penetrates through the chromate melt and reacts with alloy components to form respective chlorides. As metallic chlorides move outward through the melt, oxygen activity is sufficiently high to convert metallic chlorides into metallic oxides. The chlorine is recycled to react with elements in the alloy.

(iv) Integrity of Al_2O_3 is maintained in B-1900 in presence of NaCl at 850 and 1000°C.

(v) During corrosion of Nickel-200 formation of volatile $NiCl_2$ and Na_2NiO_2 at the alloy/melt interface and subsequent dissociation and precipitation into NiO, respectively result in the formation of porous and copious scales on the alloy.

(vi) In Monel-400, oxidation and chloridization reactions (involving O_2 and NaCl) generally follow a parabolic rate law whereas chloridation and chlorination reactions (involving NaCl and Cl_2) producing more serious attack follow a linear rate law.

Chapter VI

(i) Chromia forming Inconel 600 and 800 and Nimonic 105 show increasing corrosion rates with increasing amount of NaCl in Na_2SO_4.

(ii) Al_2O_3 former (B-1900) and NiO former (Nickel-200) show decreasing oxidation rates with increasing amount of NaCl in Na_2SO_4 although a small amount of NaCl in Na_2SO_4 enhances the oxidation rate initially.

(iii) During corrosion of chromia forming alloys in presence of Na_2SO_4 and NaCl mixture, NaCl creeps through the melt and duplicates the reactions which occur in presence of NaCl

alone. Due to the removal of chromium by NaCl the sulfur from Na_2SO_4 begins to sulfidize the alloy much earlier. The combined effect of two factors results in much higher corrosion rates in Na_2SO_4-NaCl coated alloy than Na_2SO_4-coated alloy.

(iv) Al_2O_3 former (B-1900) shows highest corrosion rates in presence of a mixture consisting Na_2SO_4:NaCl in the molar ratio of 5:1 and lowest in the pure NaCl. Addition of a small amount of NaCl in Na_2SO_4 enhances the corrosion attack enormously. This is perhaps due to a reduction in induction period and an early on set of degradation reactions. The degradation is caused by rapid removal of Al from the alloy.

(v) The corrosion rate of Monel-400 increases with increasing NaCl concentration in Na_2SO_4. A sequel of sulfidation, fluxing and chloridation reactions are responsible for high corrosion rates.

Chapter VII

(i) At 650 and 750°C, the preoxidised and Na_2SO_4-$NiSO_4$ coated Ni-base alloys have higher oxidation rates than the corresponding unoxidised Na_2SO_4-$NiSO_4$ coated alloys.

(ii) The preoxidised alloys when corroded in presence of Na_2SO_4-$NiSO_4$ mixture show morphologies in which scales are

greatly disrupted and are relatively less affected. On the other hand, alloys which were directly corroded in presence of a salt mixture show a morphology in which substrate is deleteriously attacked.

(iii) Preoxidized alloys have usually shorter induction periods whereas unoxidized alloys show relatively longer induction periods. This is perhaps on account of the important reasons that preoxidized alloys have comparatively higher oxidation rates. The induction periods are relatively longer in chromia former than NiO former.

(iv) In NiO formers, the Ni-Ni3 eutectic which forms below the surface oxide seems primarily responsible for the hot corrosion attack.

In Cr_2O_3 formers, the sulfidation involving formation of Cr_2S_3 and Ni_3S_2 and fluxing reactions are responsible for high corrosion rates.